Proteomic Investigation of the Class IA Phosphoinositide 3-Kinase Signalling Pathway

PhD Thesis of Luisa Beltran

Principal Supervisor: Dr. Pedro R. Cutillas

Second Supervisor: Prof. Bart Vanhaesebroeck

Acknowledgments

First and foremost I would first like to thank Pedro Cutillas for giving me the great opportunity to complete my PhD under his supervision. It was a privilege to work on such an interesting project and to learn so much from him and receive invaluable guidance and encouragement. I would also like to thank my second supervisor Bart Vanhaesebroeck for all of his advice and support throughout my PhD.

It was a great experience to work within the growing Analytical Cell Signalling Group and to be part of its development over the years. It was also a wonderful opportunity to work within the Centre for Cell Signalling and to be able to witness such diverse and exciting work. I want to thank all my colleagues from the lab, past and present, for everything they taught me but most importantly for their support and all the fun we shared over the years. I particularly want to thank fellow PhD students Maria and Ellie whose support and shared experience prevented me from giving up at the hardest times. I want to thank all the post-docs for their help but especially Pilar, J.C., Pedro, Claire, Khaled, Inma, Salma, Samira and Ezra for the knowledge and guidance that helped my project along its way. I am also very grateful to Alex Montoya; his assistance, hard work and dedication to the Mass Spec was invaluable for this work.

I would like to thank the Medical Research Council for the funding that enabled my PhD. I am also grateful to Subham Basu for his donation of a cell line that facilitated part of this project. I would also like to thank Simon Joel and the other graduate tutors who advised me along my way. I remain grateful to Mike Fahie-Wilson whose knowledge, support and enthusiasm encouraged me to have the confidence to do this PhD.

Finally, my deepest thanks go to my parents, Dean and all other family and friends for their love, belief, encouragement, support and patience.

Statement

The work presented in this thesis represents my own original work with the exception of the following experiments:

- Fig. 4.3. and 4.6.: PI3K activity assays performed and analyzed in collaboration with Dr Claire Chaussade.
- Fig. 4.15. and 4.16.: FACS analysis performed and analyzed in collaboration with Dr Khaled Ali.
- Appendix 7: Experiment performed by Nuzhat F. Razavi-Hussain as part of her MSc research project under the supervision of Luisa Beltran and Dr Pedro Cutillas.

The work presented in Chapters 3 and 4 of this thesis has been previously published:

- **Calpain interacts with class IA phosphoinositide 3-kinases regulating their stability and signalling activity (2011) Beltran L, Chaussade C, Vanhaesebroeck B and Cutillas PR. Proc Natl Acad Sci U S A. 2011 Sep 27; 108 (39):16217-22.**

Other work performed in the course of this research has also been published:

- **Characterization of a TiO_2 enrichment method for label-free quantitative phosphoproteomics (2011) Montoya A, Beltran L, Casado P, Rodríguez-Prados JC, Cutillas PR. Methods; 54(4): 370-378.**
- **Advances in Phosphopeptide Enrichment Techniques for Phosphoproteomics (2012) Beltran L & Cutillas PR. Amino Acids; 43(3): 1009-1024.**
- **Global profiling of protein kinase activities in cancer cells by mass spectrometry (2012) Beltran L[1], Casado P[1], Rodríguez-Prados JC, Cutillas PR. Journal of Proteomics (in press).**

Abstract

Class IA phosphoinositide 3-kinases (PI3Ks) are a family of enzymes with key roles in the regulation of signalling pathways, many of which are mediated through Akt. The PI3K/Akt pathway has a critical role in the regulation of key cellular functions such as cell survival, growth, proliferation, migration and metabolism and is involved in several diseases.

Advances in mass spectrometry and separation sciences have revolutionized the field of proteomics. Techniques based on mass spectrometry are now the first choice for protein identification and are increasingly important for their quantitative analysis. The development of phosphoproteomics has also permitted the global quantitative analysis of signalling activity.

The aim of this project was to contribute to our understanding of the activity and regulation of the PI3K/Akt signalling pathway from a proteomics perspective. Novel approaches based on mass spectrometry were designed, developed and applied to the investigation of this signalling pathway.

Firstly, we investigated the hypothesis that PI3K activity may be regulated by dynamic protein interactions. We designed an affinity purification mass spectrometry strategy to identify proteins interacting dynamically with PI3K. Our study revealed that calpain small subunit 1 interacts dynamically with PI3K. Further investigation demonstrated that active calpain heterodimers associate dynamically with PI3K, thereby regulating PI3K stability and activity.

Secondly, we characterized phosphorylation events downstream of Akt, a major downstream effector of PI3K. We used global shotgun phosphoproteomics of a cell line expressing an inducible construct encoding constitutively active Akt to identify phosphorylation events downstream of Akt *in vivo*. In addition, we also developed an *in vitro* kinase assay which, when coupled to global shotgun phosphoproteomics, enables the quantification of Akt1 activity in addition to the identification of downstream phosphorylation sites. Furthermore, we found that this *in vitro* approach may be used as a method suitable for the global profiling of endogenous kinase activities.

Table of Contents

Abbreviations

4-OHT	4-hydroxytamoxifen
ACN	Acetonitrile
AmBic	Ammonium Bicarbonate
AML	Acute myeloid leukaemia
AP	Affinity purification
AP-MS	Affinity purification – mass spectrometry
APEX	Absolute protein expression
ATP	Adenosine-5'-triphosphate
AUC	Area under the curve
BSA	Bovine serum albumin
CID	Collision-induced disassociation
DDA	Data-directed acquisition
DMEM	Dulbecco's modified Eagle's medium
DMSO	Dimethyl sulfoxide
DTT	Dithiothreitol
ECL	Enhanced chemiluminescence
EDTA	Ethylenediamine tetra-acetic acid
EGTA	Ethyleneglycol tetra-acetic acid
EGF	Epidermal growth factor
ESI	Electrospray ionization
EtOH	Ethanol
FACS	Fluorescence-activated cell sorting
FASP	Filter-assisted sample preparation
FBS	Foetal bovine serum
FA	Formic acid
FT-ICR	Fourier-transform ion cyclotron resonance
GAP	GTPase activating protein
GEF	Guanine nucleotide exchange factor
GPCR	G protein coupled receptor
IAM	Iodoacetamide
ICAT	Isotope-coded affinity tag
IgG	Immunoglobin G
IMAC	Immobilized metal affinity chromatography
IP	Immunoprecipitation
IPI	International protein index
IS	Internal Standard
i-TRAQ	Isobaric tag for relative and absolute quantitation
kDa	Kilodalton
KESTREL	Kinase substrate tracking and elucidation

LC	Liquid chromatography
LC-MS	Liquid chromatography mass spectrometry
LC-MS/MS	Liquid chromatography tandem mass spectrometry
LTQ	Linear triple quadrupole
m/z	Mass-to-charge ratio
MALDI	Matrix-assisted laser desorption ionization
MOAC	Metal oxide affinity chromatography
MS	Mass spectrometry
MS/MS	Tandem mass spectrometry
mAb	Monoclonal antibody
mTOR	Mammalian target of rapamycin
mTORC	Mammalian target of rapamycin complex
myrAktER	Myristoylated Akt and oestrogen receptor fusion protein
pAb	Polyclonal antibody
PAGE	Polyacrylamide gel electrophoresis
PBS	Phosphate-buffered saline
PCA	Principle component analysis
PDK1	Phosphoinositide-dependent kinase-1
PESCAL	Peak Statistic Calculator
PHLPP	PH domain and leucine-rich repeat protein phosphatase
PI3K	Phosphoinositide 3-Kinase
PI	Phosphoinositide
PI_4P	Phosphatidylinositol 4'-monophosphate
PIP_2	Phosphatidylinositol 4,5 -bisphosphate
PIP_3	Phosphatidylinositol 3,4,5 -triphosphate
PKC	Protein kinase C
Poly-HEMA	Poly(hydroxyethyl methacrylic) acid
PRAS40	Proline-rich Akt substrate of 40 kilodaltons
PTEN	Phosphatase and tensin homology
PVDF	Polyvinylidene fluoride
Q-TOF	Quadrupole time-of-flight
RPMI	Roswell Park Memorial Institute medium
RT	Retention time
RTK	Receptor Tyrosine Kinase
S6K	p70 ribosomal S6 kinase
SDS	Sodium dodecyl sulphate
SEM	Standard error of the mean
SH2	Src homology 2
SHIP	SH2-domain-containing inositol 5-phosphatase
SILAC	Stable isotope labelling of amino acids in cell culture
SIMAC	Sequential elution from IMAC
SRM	Selective reaction monitoring

TBS	Tris-buffered saline
TCL	Total cell lysate
TEMED	Tetramethylethylenediamine
TFA	Trifluoroacetic acid
TMT	Tandem mass tag
TOF	Time of flight
TRIS	Tris(hydroxymethyl)aminomethane
TSC	Tuberous sclerosis protein
UPLC	Ultra-performance liquid chromatography
WB	Western blot
XIC	Extracted ion chromatogram
Y2H	Yeast two-hybrid

1. Introduction

1.1. Phosphoinositide 3-kinases (PI3Ks)

The phosphoinositide 3-kinases (PI3Ks) are a family of enzymes with key roles in cell signalling, regulating essential cellular functions including survival, growth, migration and metabolism. Their major biological roles are carried out through their lipid kinase activity by which PI3Ks phosphorylate the 3-hydroxyl group on phosphatidylinositol lipids, which act as membrane docks for downstream effector signalling proteins.

1.1.1. Classification of PI3Ks

PI3Ks can be broadly classified into 3 groups based on their structure and lipid substrate specificity: class I, II & III (Fig. 1.1.) [1, 2].

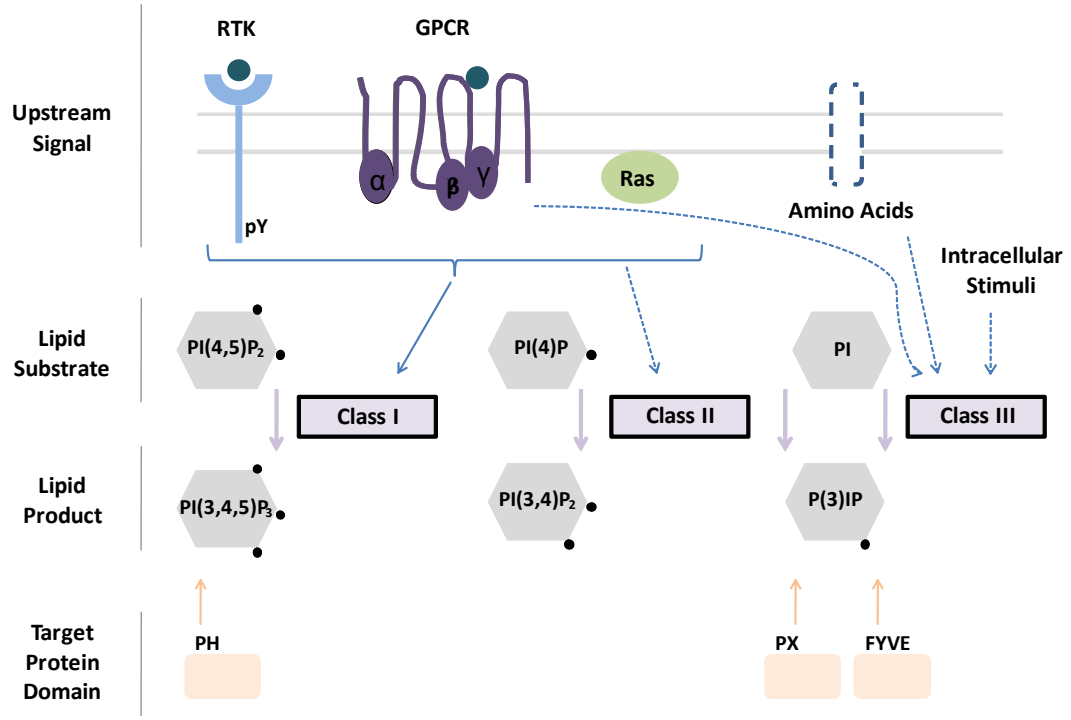

Figure 1.1. Summary of PI3K activity. Adapted from [2]. Upstream activating signals are relatively well-characterized for class I PI3K but are less well-understood for classes II and III. The three PI3K classes utilise distinct lipid substrates and, thus, generate different lipid products, all phosphorylated on position 3 of the inositol ring. Each lipid product recruits proteins with specific lipid-binding domains.

Yeast express solely the class III isoform but higher eukaryotes express at least one representation of each of the other classes [1, 2]. Class I PI3K is relatively well-characterized, however much remains to be discovered about classes II and III.

1.1.1.1. Class I PI3K

The ubiquitously expressed class I PI3Ks signal downstream of receptor tyrosine kinases (RTKs), G-protein coupled receptors (GPCRs) and Ras small GTPases (Ras) [2, 3]. They phosphorylate the lipid substrate phosphatidylinositol 4, 5-bisphosphate (PIP_2) to generate phosphatidylinositol 3, 4, 5-triphosphate (PIP_3) *in vivo* [4] and have been shown to have key roles in the regulation of cellular functions such as cell survival, growth, proliferation, migration and metabolism [2, 3].

This project will be focusing on the signalling downstream of Class I PI3K therefore this group will subsequently be discussed in further detail.

1.1.1.2. Class II PI3K

Class II PI3Ks are widely but not ubiquitously expressed in mammalian tissues and can be further subdivided into 3 isoforms: PI3K-C2α, PI3K-C2β and PI3K-C2γ [2]. All isoforms are composed of a single catalytic subunit and their activity is thought to be modulated through the N- or C- terminal domains, which are extended compared to other PI3K classes [2].

Although the mechanism remains unclear, class II PI3Ks have been shown to be activated downstream of RTKs and GPCRs, possibly due to compartment re-localization caused by recruitment to the membrane [5, 6]. Interaction partners that have been identified for class II PI3K, e.g. epidermal growth factor receptor (EGFR), clathrin and GRB2, may mediate this re-localization [2].

The *in vivo* lipid substrate of class II PI3K is thought to be phosphoinositide (PI) [7, 8], however it has been shown to additionally phosphorylate phosphatidylinositol 4-phosphate (PI_4P) *in vitro* [9]. The phosphatidylinositol 3-phosphate (PI_3P) product thought to be generated by class II PI3K is mainly found in endosomes [10] and recruits proteins containing PX or FYVE domains, e.g. protein kinase SGK3 [11]. Such proteins are highly conserved and have been found to have roles in endocytic membrane trafficking, phagosome maturation, signalling and microbial killing [11].

Class II PI3Ks were discovered through their homology to classes I and III PI3K and much remains to be discovered about their functional physiological roles and downstream effectors. They have, however, been implicated through cell and knockout animal studies in the regulation of apoptosis, migration, metabolism, exocytosis and smooth muscle contraction [2, 6].

1.1.1.3. Class III PI3K

Class III PI3K is comprised of a single isoform, Vps34, and is highly conserved from yeast through to mammals [2]. Vps34 is generally found in the endosomal compartment and it binds constitutively to Vps15 with which it forms 3 distinct multi-protein complexes in yeast [12] and a further 3 in mammals [13]. The composition of multi-protein Vps34 complexes determines biological output [2].

Vps15 is myristyolated, i.e. contains a hydrophobic myristyol group on the N-terminus, therefore it permanently tethers the Vps15-Vps34 complex to the intracellular membrane [2, 13]. There is some evidence that Vps34 is additionally regulated downstream of amino acid stimulation [14] and activated GPCRs [12], however the mechanisms for these activities remain unclear.

Class III PI3K phosphorylates PI to generate PI_3P [15]. Thus it recruits effector proteins containing PX or FYVE domains although it is unclear if these downstream substrates overlap with those of class II PI3K [2]. Vps34 also interacts with other proteins that do not carry these characteristic domains, suggesting that class III PI3K may also have a scaffold function [2].

Vps34 regulates essential cellular functions and homozygous deletion of the gene is lethal in yeast and flies [2]. The biological functions of class III PI3K are mediated through regulation of vesicular trafficking and include regulation of autophagy, endocytosis and phagocytosis [2, 13].

1.1.2. Structure and characterization of class I PI3Ks

Class I PI3Ks catalyze the formation of the second messenger phosphatidylinositol 3, 4, 5-triphosphate (PIP_3) from phosphatidylinositol 4, 5-bisphosphate (PIP_2) *in vivo* [4]. This class

of heterodimeric proteins can be further subdivided into class IA and class IB, depending on the type of regulatory subunit that associates with the p110 catalytic subunit (Fig 1.2.).

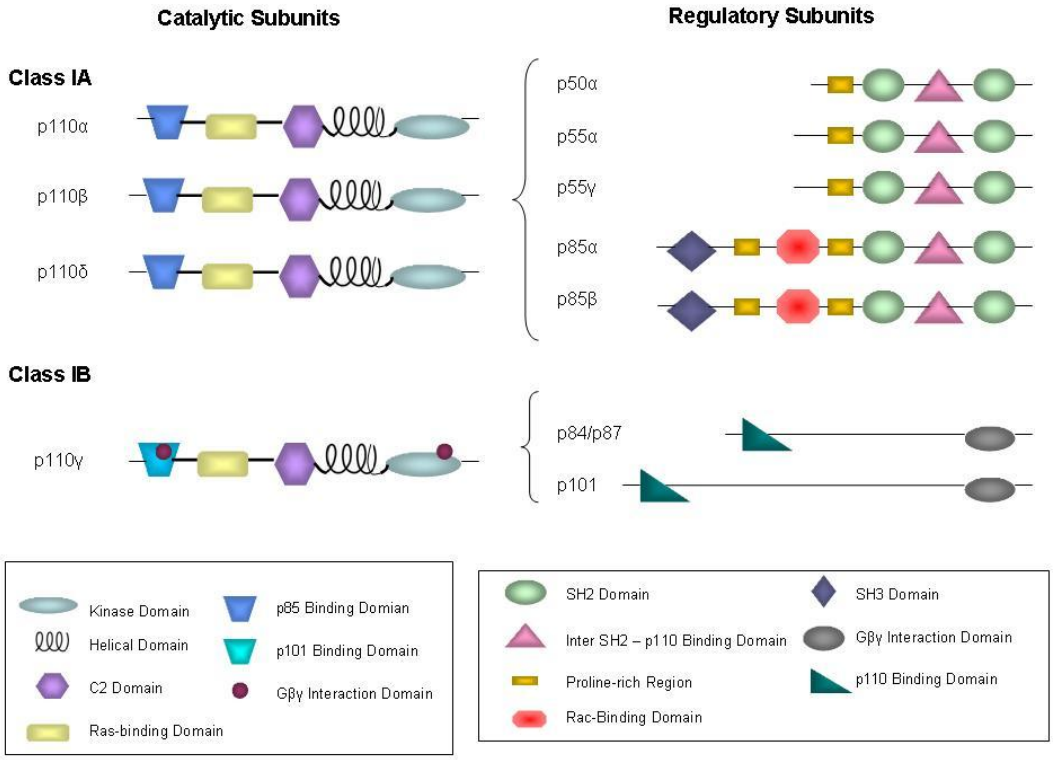

Figure 1.2. Summary of the structure of Class I PI3K subunits. Each class I p110 catalytic subunit forms a heterodimer with a regulatory subunit, the type of which further subdivides class I into class IA and class IB. The structure of p110 isoforms is highly conserved. Figure adapted from [16].

The p110 catalytic subunits are comprised of a C2 domain, a helical domain and a catalytic domain, which form the core of all PI3K proteins [16]. The p110 subunits in addition have a regulatory subunit-binding domain and a Ras-binding domain, indicating that all PI3K subunits have the potential to be activated by Ras. The p85 regulatory subunits of class IA PI3K contain Src homology (SH2) domains, which bind phosphorylated tyrosine. In addition, they have proline-rich domains and may also have BCR homology (BH) and SH3 domains, all of which may contribute to additional regulation of class IA PI3K activity although mechanisms remain unclear [17, 18]. Class IB regulatory subunits are poorly understood and have no known homology to other proteins or recognizable domain structures [2].

Class I PI3Ks form stable heterodimers *in vivo* [19]. The various class IA p85 regulatory subunits, which have no known preference for the different p110 isoforms, act to inhibit p110 catalytic activity and to stabilize the p110 protein when the complex is free in the cytosol [20]. The X-ray crystal structure for p85-bound p110α has been resolved and shows that there are multiple interaction sites between the two proteins [21]. The structure of the p110β-p85β complex also revealed multiple interaction sites between the subunits, revealing a dual mechanism for inhibition of p110β catalytic activity [22]. Studies of p110δ structure have recently revealed that overall p110δ most closely resembles p110α structurally, although it is more flexible upon the binding of inhibitors [23]. Investigations into the crystal structure of p110γ revealed that interaction of p110 with the membrane is likely to be mediated by the C2 domain [24] but the binding to regulatory subunits was unclear.

Class IA PI3Ks have been shown by absolute quantification to be present only as heterodimers under basal conditions [19]. Furthermore, both the p110 catalytic subunit and p85 regulatory subunit have been shown to be unstable when free as monomers [20, 25]. However, some groups suggest that free p85 exists and has a role in the regulation of insulin signalling as it acts as a competitive inhibitor of PI3K [26]. The possibility that the expression of either the p85 or the p110 subunit could be transiently regulated cannot be excluded.

Within the class I PI3Ks, p110α and p110β are ubiquitously expressed, whereas p110δ and p110γ are enriched in leukocytes [27] and isoform-specific roles have been determined for the various p110 catalytic subunits (discussed further below). Within the p85 subunits, p85α and β are ubiquitously expressed whereas the other isoforms appear to show more restricted distributions [27]. Detailed investigation of the relative tissue distribution levels of the different isoforms have been hampered so far by the lack of high specificity tools, such as isoform-specific antibodies suitable for immunohistochemistry [27].

1.1.3. Activation of class I PI3K

Class I PI3Ks are activated by a variety of mechanisms (Fig. 1.3.). All p110 isoforms have a Ras-binding domain and activation of class I PI3K by Ras has been demonstrated in a variety of *in vitro* studies and is thought to be an ancient mechanism for PI3K activation [2].

However, a high degree of variability has been demonstrated in the response depending on the Ras GTPase and p110 isoform investigated [28] and the contribution of Ras in PI3K regulation remains unclear. *In vivo* studies have however demonstrated that the interaction between Ras and p110α is essential for normal response to growth factors and Ras-driven tumourogenesis [29, 30].

Class IA PI3Ks are also activated in response to receptor tyrosine kinase (RTK) stimulation by extracellular stimuli, such as growth factors, hormones and inflammatory mediators. The SH2 domain of the p85 regulatory subunit is recruited by the dimerized, phosphorylated receptor producing a conformational change in the PI3K complex, which leads to the release of p85's inhibitory effect on catalytic p110. The single class IB PI3K is activated in response to G protein-coupled receptor (GPCR) stimulation by chemokines, which results in the release of the Gβγ subunit from the receptor. This mechanism of PI3K activation is less well characterized but it is known that Gβγ mediates the recruitment of the PI3K heterodimer to the membrane via interaction with p101/p84 [31]. p110γ thereby becomes active, although it is not clear whether Gβγ interacts with p101/p84 alone or with both p101/p84 and p110γ to mediate this [31, 32]. Recent work has also demonstrated that p110β signals downstream of GPCRs, through mechanisms which remain unclear, and that this class IA isoform has only a minor role in signalling in response to tyrosine kinase stimulation [33, 34]. Furthermore, GPCRs have been shown to transactivate RTKs which may represent an indirect method for PI3K activation by GPCRs [35].

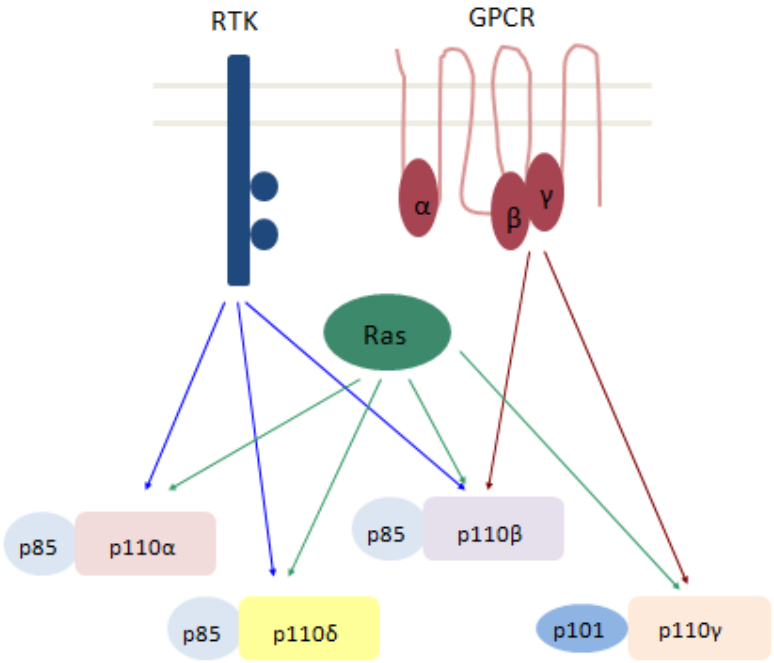

Figure 1.3. Summary of the upstream activation of class I PI3Ks. Class IA PI3Ks are recruited and activated by phosphorylated receptor tyrosine kinases (RTK). Class IA p110β and class IB p110γ have also been shown to be activated downstream of G-protein coupled receptors (GPCRs). All class I p110 isoforms have Ras-binding domains and are thought to be regulated by this protein.

1.1.4. Regulation of class IA PI3K

p85 has a key role in the regulation of PI3K through inhibition of the catalytic activity of p110. This conformational inhibition is mediated by the binding of p85 to the N-terminal of p110 and abrogated by the binding of p85 to phosphorylated residues on tyrosine kinase receptors [20]. In addition, p85 binding stabilizes the p110 protein and protects it from thermal stress when the complex is free in the cytosol [20]. Furthermore, it has been shown that p85 binding to p110 prevents its activation by Ras and that this inhibitory role is relieved by the binding of p85 to tyrosine kinases [36]. Thus, p85 has a dual inhibitory role on p110 activity.

It has been reported that the efficiency of p110 inhibition varies between p85 isoforms therefore expression levels of the distinct p85 isoforms may regulate PI3K activity [37]. It has also been proposed that free, non-p110 associated p85 may negatively regulate PI3K activity by competing for docking sites on phosphorylated tyrosine kinases [38, 39]. However, absolute quantitation of all isoforms of p85 and p110 by mass spectrometry found them to be present in equimolar ratios and therefore argues against this theory [19].

A further key mechanism for the regulation of PI3K is the activity of lipid phosphatases that de-phosphorylate the PIP_3 lipid product of PI3K. Phosphatase and tensin homolog deleted on chromosome 10 (PTEN) de-phosphorylates 3-phosphorylated phophatidylinositols [4] and therefore acts as a PIP_3 phosphatase [40]. PTEN is a ubiquitously expressed protein that has both protein and lipid phosphatase properties [41] and its high level of lipid phosphatase activity is thought to be regulated through membrane translocation [42]. Interestingly, it has been shown that p110δ negatively regulates PTEN activity via the inhibition of RhoA and therefore negatively controls itself via this feedback loop [43].

Another type of lipid phosphatase, SH2 domain containing inositol phosphatase (SHIP), de-phosphorylates 5-phosphoryated phosphatidylinositols and preferentially uses PIP_3 as a substrate [4]. SHIPs are also thought to be regulated by subcellular localization [44]. The activities of these different phosphatases will result in the generation of distinct lipid products, which may have implications for further regulation of signalling activity.

Another mechanism important for the regulation of PI3K is the activation of negative feedback loops. Negative feedback loops result from the activity of signalling proteins that are activated downstream of PI3K and that act to terminate the activation signal. The most well-characterized example of such a regulatory mechanism is the activation of mammalian target of rapamycin (mTOR) downstream of PI3K, the activity of which results in phosphorylation and subsequent degradation of insulin receptor substrate 1 (IRS1), resulting in impaired insulin signalling [45, 46]. mTOR activity has also been shown to down-regulate RTK levels, such as the PDGF receptor [47].

PI3K signalling can also be regulated by cross-talk from other pathways. For example, over-expression of mutant Ras represses PTEN transcription through the activation of mitogen-activated protein (MAP) kinase [48]. Similarly, PTEN expression was down-regulated by over-expression of MAP kinase 4 [49].

Another potential mechanism of kinase regulation, which has not been extensively investigated for PI3K, is regulation by interaction with binding partners. In addition to transient interactions with proteins that regulate PI3K activity through known mechanisms, such as RTKs, phosphatases and Ras, there are reports of other proteins binding PI3K and regulating activity through alternative mechanisms. For example, X-box binding protein-1

has been reported to bind p85, thus increasing its nuclear translocation and regulating the unfolded protein response [50, 51]. p85α has also been reported to bind directly with PTEN, enhancing its lipid phosphatase activity, thus regulating PI3K activity through negative feedback [52]. $G\alpha_{16}$ was also found to bind class IA PI3K complexes inhibiting EGF-induced Akt phosphorylation [53]. However, despite these studies the roles of interaction partners in the regulation of class I PI3K signalling remains poorly understood and under-explored.

1.1.5. Signalling downstream of class IA PI3K

The PIP_3 second messenger generated by class I PI3K activity recruits signalling proteins with plekstrin homology (PH) domains, which interact with phospholipids [54], to the cell membrane. Such proteins include protein kinases, such as Akt and PDK1; adaptor and scaffold proteins, such as Gab1, Dos, myosinX, and Sbf1 [55], and small GTPase regulators (GEFs and GAPs) [56, 57]. Membrane recruitment and cellular re-localisation regulates the activity of these downstream signalling proteins.

One of the most well characterized signalling molecules downstream of class I PI3K is the serine/threonine kinase Akt, also known as protein kinase B (PKB). Translocation of Akt to the cell membrane permits its phosphorylation and activation, thereby initiating a cascade of downstream effects. The downstream signalling of this effector protein will subsequently be discussed in more detail.

In addition, it has been proposed that PI3K may provide a scaffolding role for other proteins. p110γ has been shown to bind phosphodiesterase and some isoforms of protein kinase C forming an important component of their respective protein complexes and regulating their activity [58, 59]. It has also been proposed that other PI3K isoforms may have scaffolding roles but no specific binding partners have been identified to date [2].

The wide range of downstream effectors of PI3K contributes to the key role of this signalling pathway in essential functions such as cell growth, proliferation, survival, metabolism and migration [2, 60, 61].

1.1.6. Tools for the investigation of PI3K activity

The investigation of PI3K signalling and isoform-specific roles is not straightforward, however in recent decades a number of tools have become available to enable research in

this field. The first PI3K inhibitor identified was the microbial product wortmannin, which acts as a non-competitive, irreversible inhibitor of all isoforms of the PI3K family [62, 63]. Although this compound was a useful early resource its lack of specificity and poor stability mean that its use is now limited. The compound LY294002, a synthetic chromone, was found to reversibly inhibit PI3K but not PI4K or other tested protein and lipid kinases [64], thus providing a clear advantage over wortmannin. However, LY294002, like wortmannin, was later found to inhibit mTOR when used at doses nearly identical to those required to inhibit PI3K [65].

In time PI3K isoform-selective inhibitors were also developed. IC87114, a p110δ selective inhibitor was identified from a chemical library screen and shows relatively good specificity towards p110δ [66]. TGX221, a p110β selective inhibitor, was designed and developed working from the structure of LY294002 structure and exhibits good specificity towards p110β [67]. Inhibitors with dual specificity for p110δ and p110γ have also been designed for the specific targeting of immunological cells [68]. The development of p110α selective inhibitors has been more problematic and although compounds are available, such as PI103, their utility is limited by a lack of specificity.

Gene-targeted mice have been of great importance in the investigation of PI3K activity. There are two main strategies for kinase gene-targeting: the “knock-out” approach, where the gene is deleted and therefore the kinase is not expressed, and the “knock-in” approach, where single base pair changes result in inactivation of kinase activity but expression levels are largely unaffected. Where possible, the “knock-in” approach is preferable as complete lack of expression of a gene product may result in compensatory mechanisms that mask the true phenotype of the protein under investigation.

A number of p85 and p110 isoform selective “knock-out” models have been described (reviewed in [17]). Although a lot of useful information was obtained from the use of these models, our emerging understanding of compensatory mechanisms in signalling pathways means that results from these systems should be interpreted with caution. A number of “knock-in” mouse models were later developed for the investigation of PI3K activity. Mice that were homozygous for kinase-dead p110γ or kinase-dead p110δ, both isoforms of restricted expression, were found to be viable and fertile [69, 70]. Mice that are homozygous for kinase-dead p110α were found to be embryonic lethal but heterozygotes

were viable and fertile [34, 71]. Mice that were homozygous for inactive p110β were fertile, although partial lethality that has not yet been explained was observed [33]. All of these models have been successfully applied to investigate isoform-selective roles of PI3K.

1.1.7. Non-redundant roles of class IA PI3K isoforms

Genetic and pharmacological isoform-selective inhibition of PI3K showed that cell survival and proliferation can be sustained with minimal levels of PI3K activity produced by isoforms expressed at very low levels, indicating key redundant functions [72]. However, distinct biological roles have also been determined for the different class I PI3K isoforms.

Studies using mice heterozygous for kinase-dead p110α revealed that this isoform was critical for growth and normal glucose metabolism [71]. In addition, p110α has been demonstrated to be the PI3K isoform necessary for endothelial cell migration, in response to VEGF, during angiogenesis [34]. The use of the isoform-selective inhibitor TGX221 showed that p110β was critical for normal thrombus formation initiated by platelets [67].

Both p110δ and p110γ are enriched in leukocytes, however they demonstrate largely non-overlapping immune phenotypes [16]. The 110γ mouse model showed that this isoform was crucial for macrophage accumulation during inflammation [69]. Studies using the "knock-in" p110δ mice model showed that antigen receptor signalling in B and T cells was defective and that consequentially *in vivo* immune responses were attenuated [70]. Later, this model was also used to show p110δ to be the only PI3K isoform to mediate mast cell allergic response upon IgE receptor stimulation [73, 74]. IC87114, the p110δ selective inhibitor, was also used to show that this isoform was essential for directional chemotaxis [66].

It was also found that the different PI3K regulatory and catalytic isoforms have distinct roles in the regulation of cell motility [25, 61]. Different isoforms of p110 have been shown to regulate distinct functions in primary macrophages downstream of the same tyrosine kinase stimulation [75], suggesting that isoform-specific roles are not regulated solely by selective activation. In addition, different immortalised macrophage cell lines show variable dependence on the different isoforms of p110 downstream of CSF-1 receptor stimulation [75].

The basis for these distinct biological roles is unclear and various theories have been proposed. For example, differential tissue expression and activity levels of the different catalytic and regulatory isoforms may contribute to the reported variability of their biological effects [75]. It has also been suggested that subcellular localization of the PI3K complex may play an important role in the regulation of its activity [37]. Variable activity of PI3K in different cell types may be independent of the intrinsic lipid kinase activity of PI3K and therefore regulated by the cellular environment, such as small GTPase activity levels [75]. A further theory, which this project aims to investigate, is that unknown interaction partners may regulate PI3K activity, potentially in an isoform-specific manner [37].

1.2. Akt

Akt is a serine/threonine protein kinase that is activated downstream of class I PI3K activity. It is the most highly characterized downstream effector of class I PI3K and, as such, has been implicated in the regulation of key cellular functions including growth, survival, metabolism, proliferation and migration [60]. This kinase is thought to be one of the most important signalling nodes in higher eukaryotes [60].

There are 3 known isoforms of the protein kinase Akt: Akt1, Akt2 and Akt3, all of which are highly conserved and have extensive homology with other members of the AGC kinase family. Akt1 and Akt2 are ubiquitously expressed whereas Akt3 expression has a more selective distribution [60].

1.2.1. Activation of Akt

The key step in the activation of Akt is recruitment of the kinase to the cell membrane through the binding of its PH domain with PIP_3 [76, 77], produced from PIP_2 by the lipid kinase activity of PI3K. In fact, an intact PH domain was shown to be crucial for activation of Akt in response to PIP_3 levels [77].

The translocation of the kinase to the membrane enables the phosphorylation of Akt, at the residue Thr308, by PDK1 (phosphoinositide-dependent kinase 1) [78], which is also recruited and activated by PI3K activity [79]. It has recently been shown that interaction with membrane phosphatidylinositols is not necessary for Akt activation but it is likely to have a functional role in enabling the physical interaction between Akt and PDK1 [80].

Maximal activation of Akt requires further phosphorylation at Ser473, which was some years later found to be mediated by the mTORC2 complex [81]. Mutational analysis revealed that phosphorylation of the Thr308 site was crucial to enable Akt activity, however membrane-localized Akt that lacked Ser473 phosphorylation was still able to signal through mTOR [82].

PIP_3 levels, the direct product of PI3K activity, determine membrane association of Akt and correlate with phosphorylation of Akt at Thr308 [83]. Thus, Akt phosphorylation is widely used as a surrogate indirect measure of PI3K activity.

1.2.2. Regulation of Akt

The key regulatory factors of Akt activity are membrane localization and phosphorylation, which are determined by the balance of PIP_2 and PIP_3 at the cell membrane [83]. This is in turn regulated by the lipid kinase activity of PI3K and the lipid phosphatase activity of PTEN and SHIP.

Akt activity is also down-regulated by dephosphorylation of its activating phosphorylation sites. Protein phosphatase 2A (PP2A) dephosphorylates both the Thr308 and Ser473 sites [84, 85]. Furthermore, the Ser473 site is also dephosphorylated by PH domain leucine-rich repeat protein phosphatase (PHLPP).

In addition, it has recently been revealed that mTORC2 activity has a further role in the regulation of Akt. mTORC2 not only mediates the phosphorylation of Akt at Ser473, which enables full activation of the kinase [81], but furthermore promotes polyubiquitination and subsequent proteasomal degradation of Akt [86].

In addition to the regulatory processes described it is also likely that Akt activity is affected by specific stimuli, subcellular localization and substrate availability, mechanisms that are likely to affect the activity of all kinases although they may not be well characterized for specific cases [60].

1.2.3. Signalling downstream of Akt

Fully active Akt phosphorylates substrates at the consensus motif R-X-R-X-X-S/T-X, where X is any amino acid [87, 88]. The critical requirement for arginine residues at the -3 and -5 positions is the most distinctive feature of the motif. Phosphorylation of Akt

substrates can result in positive or negative regulation of protein activity and Akt substrates carry out a wide range of cellular functions, performing critical roles in the regulation of cell survival, growth, proliferation, metabolism and migration (Fig. 1.4.).

Cell survival is mediated by Akt through the negative regulation of pro-apoptotic proteins. For example, Akt directly phosphorylates, and thereby inactivates, the pro-apoptotic protein BAD [89]. Furthermore, Akt phosphorylates some transcription factors, such as FOXO and p53, which results in their translocation out of the nucleus and thereby reduces the expression of pro-apoptotic proteins [90]. A further indirect mechanism is the phosphorylation of MDM2 by Akt, which results in nuclear translocation and subsequent inhibition of p53-mediated transcription of pro-apoptotic proteins [91]. Akt also phosphorylates glycogen synthase kinase 3 (GSK3), resulting in inhibition of the pro-apoptotic protein MCL-1 [92].

mTOR complex 1 (mTORC1) has a critical role in cell growth, mediated through the control of translation initiation and ribosome biosynthesis, and is regulated by Akt. Akt phosphorylates tuberous sclerosis complex 2 (TSC2) thereby inhibiting its activity, which in turn enables the activation of mTORC1 by rheb-GTP, which is negatively regulated by TSC2 [93]. In an alternative mechanism, Akt phosphorylates proline-rich Akt substrate (PRAS40), resulting in activation of mTORC1 by this protein [94]. mTOR-independent mechanisms for control of cell growth downstream of Akt have also been described. Sterol-regulatory-element-binding-protein (SREBP) has been shown to have a role in transcriptional regulation of lipogenesis genes, downstream of Akt and GSK3, leading to control of cell and organ size *in vivo* [95].

Akt has a dual role in the regulation of cell proliferation as it promotes cell growth, through mTORC1, and regulates cell division. The major role of Akt in the control of cell proliferation is mediated through the negative regulation of p27, which represses cell cycle progression, by direct phosphorylation [96]. Akt also indirectly inhibits p27 through the phosphorylation and inhibition of FOXO transcription factors [97]. In addition, Akt regulates cyclin-dependent kinases, which control cell-cycle progression, through GSK3β-mediated regulation of cyclins [98].

Akt regulates metabolism by mediating the translocation of glucose-transporter 4 (Glut4) [99], although the mechanisms for this association remain unclear and may involve

the Rab-GAP AS160 [100]. Phosphorylation and inhibition of GSK3 results in the activation of glycogen synthase [101]. Akt also indirectly regulates metabolism through mTORC1 mediated transcription of Glut1 [102].

The exact mechanisms for the role of Akt in cell migration remain poorly understood but is thought to exhibit striking isoform-selectivity and to involve cross-talk with other signalling pathways [60].

There are many more reported substrates than those described here, some of which have not yet been fully validated *in vivo*.

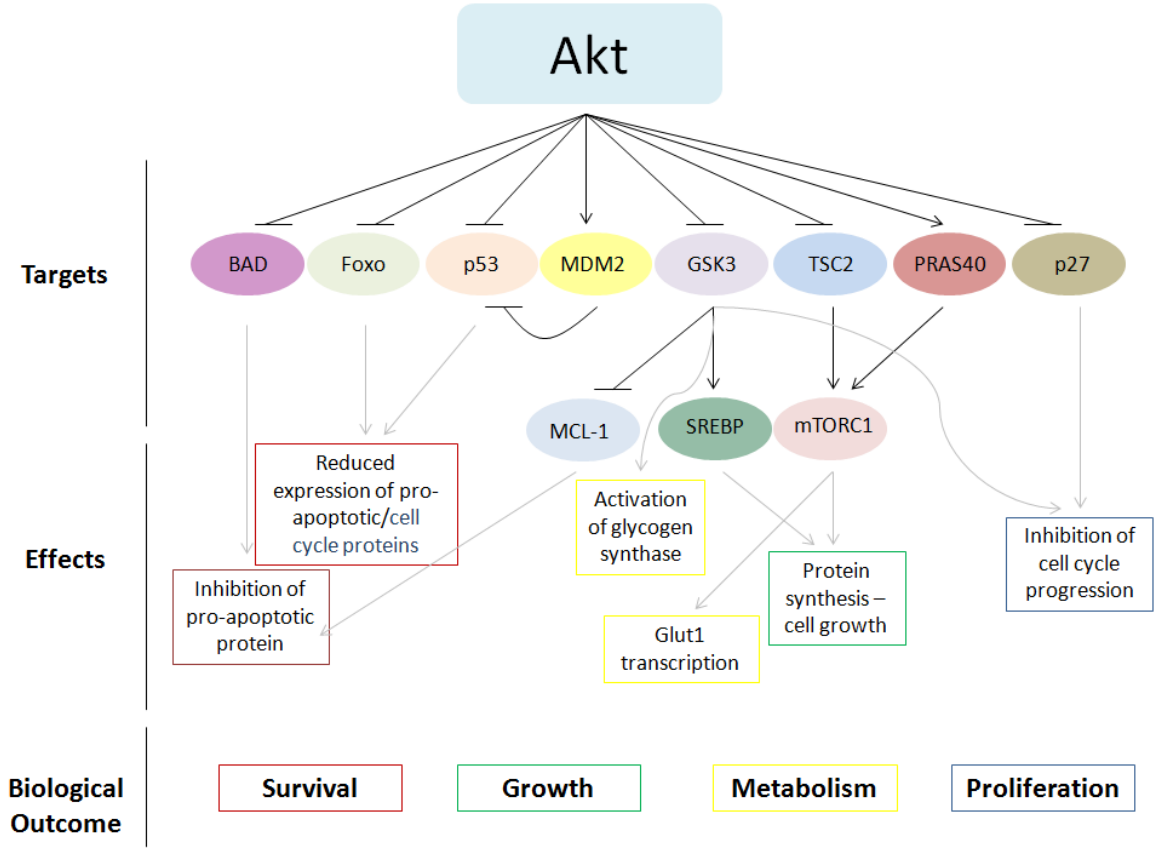

Figure 1.4. Overview of signalling downstream of Akt: targets and biological outcome. Phosphorylation of Akt substrates can result in positive or negative regulation of protein activity. Akt substrates carry out a wide range of cellular functions, performing critical roles in the regulation of cell survival, growth, proliferation, metabolism and migration through a complex signalling network. Some of the most well-characterized roles are illustrated in this figure.

1.2.4. Non-redundant isoform specific roles of Akt isoforms

The different isoforms of Akt are highly conserved, particularly in the kinase domain, thus it is unlikely that they have distinguishable substrate specificities [60]. Knockout models for the different Akt isoforms have demonstrated overlapping roles in key functions, such as growth [103]; however some isoform specific functions have been identified [104]. For example, Akt1, but not Akt2, is responsible for stimulating Glut4 translocation in adipocytes [105]. Isoform specific roles of Akt have been of particular interest in the investigation of cancer. It has been found that the different isoforms of Akt have distinct, complex roles in the regulation of cell transformation and metastasis in breast cancer. In one study, Akt1 was found to promote mammary tumour induction whereas Akt2 was found to have a key role in cell metastasis [106]. The actin-bundling protein palladin was identified as a substrate specific to Akt1 that may contribute towards these observed differences in breast cancer cell migration [107].

As for PI3K class IA, it is unclear how these isoform specific roles are regulated as the protein isoforms are extensively homologous. It has been suggested that expression levels and cytoplasmic location may regulate the activity of the different isoforms. It has also been proposed that regulation of Akt activity by PHLPP may produce isoform specific roles. PHLPP1 and PHLPP2 both dephosphorylate Akt at the same residue but PHLPP1 modulates Akt2 activity whereas PHLPP2 modulates Akt3 activity, therefore regulating distinct downstream substrates due to compartmentalization of the two complexes [108].

1.3. PI3K/Akt signalling in disease

Given the number of key cellular functions attributed to the PI3K/Akt pathway it is unsurprising that deregulation of this axis is implicated in a number of diseases. For example, the PI3K/Akt pathway is activated by inflammatory stimuli and thus has a role in the pathophysiology of inflammatory diseases, such as allergies [73].

PI3K/Akt activity is important in insulin signalling therefore this pathway is also implicated in metabolic diseases, such as diabetes mellitus. Elevated p85 levels have been detected in skeletal muscle from some patients with type 2 condition [109]. This is in line with *in vitro* data that proposed that free p85 down-regulates insulin-dependent PI3K signalling through competition with PI3K heterodimers [37]. Polymorphisms of the p85 gene

have also been found in patients, however the mechanisms for these genetic alterations on the development of disease have not been determined [110]. As a consequence of these alterations, attenuation of class IA PI3K signalling downstream of IRS-1 is known to be a significant feature of type 2 diabetes [111]. In addition, insulin-stimulated glucose uptake by the transporter Glut4 is impaired in adipocytes [105] and glucose production is increased in the liver [112] upon inhibition of PI3K signalling.

Despite interest in the diabetes field, the role of the PI3K/Akt pathway in cancer is the most comprehensive area of investigation of the effects of this signalling pathway on disease. PI3K/Akt signalling has key roles in cell proliferation, growth and survival, therefore upregulation of this pathway can contribute to uncontrolled cell growth and malignant transformation. Indeed, it is the most frequently mutated signalling pathway found in cancer [16, 113]. The role of PI3K/Akt in the regulation of cell motility also plays an important role in tumour cell invasion and metastasis. The role of PI3K/Akt signalling in inflammation is also important and can contribute to tumour inhibition or promotion.

1.3.1. Characterised mutations in the PI3K/Akt pathway

The investigation into PI3K/Akt pathway mutations has mostly been focused on the investigation of cancer. The most frequently encountered mutations in the PI3K/Akt pathway are loss of function or loss of expression of PTEN [16]. Such genetic alterations result in the accumulation of PIP_3 at the membrane and thus result in constitutive activation of the pathway. Recently, PTEN-deficient cancers were observed to be dependent on p110β signalling in PC3, BT549 and U87MG cancer cell lines [114]. This dependency has also been supported by a study that found p110β inhibition was important for the efficacy of PI3K inhibitors in inhibiting the PI3K/Akt pathway in PTEN-negative tumour xenografts [115]. Other authors have more recently suggested that p110δ activity is required, in addition to p110β, to mediate RTK-independent PI3K activity in PTEN-deficient prostate cancer cells [116].

Activating mutations were later identified in the PIK3CA gene, which encodes for the p110α catalytic isoform [117, 118]. Such mutations were shown to have little effect on the growth of colorectal cancer cells *in vitro*, however it was shown to reduce dependence on growth factors, attenuate apoptosis and facilitate invasion [119]. The effects of nine

different PIK3CA mutations were investigated in the transformation of MCF10A cells and found to have different effects on morphogenesis, invasion and inhibition of cell growth by LY294002 [120]. p110α is mutated in around 30% of prostate, breast, cervical and endometrium tumours, most frequently caused by a single amino acid change in the helical or kinase domain, which results in up-regulation of the pathway [121]. Helical domain mutant p110α activity is independent of p85 binding but requires interaction with Ras-GTP whereas catalytic domain mutant p110α activity is highly dependent on p85 association but does not require Ras-GTP binding [121].

Many of the mutations have been shown to occur at the p85-p110 interaction interface, which are likely to result in a loss of the regulatory effect of p85 or intrinsic changes to p110 catalytic activity, thus providing some clues into the mechanisms of such mutations [21, 122]. Indeed, sequence analysis has shown that the p110α mutant N345K is homologous to wild-type p110β and that this sequence in the C2 domain interface with p85 accounts for the oncogenic potential of over-expressed p110β [123]. Amplification mutations of PI3K genes have also been found in head and neck cancers, squamous cell lung carcinoma and cervical and gastric cancers [111].

In some PIK3CA mutants, where Akt has been shown to be minimally activated, PDK1 has been implicated in Akt-independent oncogenic events [124]. Mutations have not yet been identified in other class IA PI3K catalytic isoforms; however they are often differentially expressed in cancers [16, 121]. p110γ over-expression has recently been implicated in the progression of pancreatic cancer through mechanisms that remain unclear [125]. Mutations have also been identified in the inter-SH2 domain of the p85α regulatory subunit of PI3K, although at much lower frequency than other pathway aberrations [126, 127]. In this context, p85 retains its p110 stabilizing role but its inhibitory effect is abrogated therefore promoting anchorage-independent growth, potentially through all expressed p110 isoforms [127].

The E17K activating mutation of Akt1 has been found in a variety of solid tumours, including breast, lung, colorectal and ovarian cancers [128]. This mutation causes constitutive activation of Akt1 and has also been shown to induce the development of leukaemia in mice models [128]. Other mutations that upregulate the PI3K/Akt pathway include activating mutations on Ras [30] and RTKs, such as EGFR or HER2.

Multiple mutations often co-exist, which is in line with the widely held view that initial, transforming mutations, known as “driver” mutations, increase the propensity of cancer cells to develop further mutations, known as “passenger” mutations. The existence of mutations in multiple signalling pathways within a cancer cell may enable them to evade regulatory feedback responses induced by the primary mutation [129]. PI3KCA mutations have been found to frequently co-exist with other PI3K-pathway altering mutations, such as RAS or PTEN, in a variety of solid tumours [130] and with alterations in other signalling pathways [129].

1.3.2. Use of PI3K/Akt inhibitors in disease

Many kinds of PI3K inhibitors, both isoform-specific and pan-isoform, have been developed and evaluated with varying degrees of success in both *in vitro* and *in vivo* studies. Most of them are small molecule inhibitors, which act by binding competitively to the ATP-binding pocket of the p110 catalytic domain. Due to the highly conserved nature of this domain specificity problems are a challenge in the development of these drugs, however selectivity is achievable through the exploitation of differences in flexibility between isoforms and sequence divergence in residues around the ATP-binding pocket [23].

Mammalian cells can proliferate and survive with very low levels (<10%) of PI3K activity [72]. *In vitro* studies show that there is little correlation between PTEN status and inhibition of growth by PI3K inhibitors in human breast cancer cell lines [131]. Furthermore, it has been shown that PI3K activity levels in cancer cell lines do not correlate well with PIK3CA mutation status [132]. It is possible that constitutive PI3K pathway activation results in compensatory feedback loops that affect PI3K activity. Cross-talk between signalling pathways can also account for unexpected results on pathway activity. Full understanding of the signalling pathways that modulate PI3K activity may be key to the effectiveness of targeting this pathway. Most of the data in favour of the use of PI3K inhibitors in the treatment of disease is derived from cell line and xenograft studies; therefore it remains to be seen if such successes can be replicated *in vivo* in the much more complex and often multifactorial setting of disease.

Despite such uncertainty, at least 195 clinical trials targeting the PI3K/Akt pathway have been initiated [41]. A number of PI3K inhibitors have reached Phase I clinical trials, for

use as single agents or in combination with existing therapies for solid tumours in cancer [16, 122]. The high incidence of tumours with multiple mutations affecting the pathway suggests that the latter approach may be the most effective [133]. For example, in lung adenocarcinoma models, driven by a PI3KCA mutation, tumours were found to decrease upon treatment with a dual PI3K and mTOR inhibitor [133]. However, combination treatments should be approached with care as PI3K inhibitors have shown to induce chemo-resistance in various human cancer cell lines *in vitro* [134] and feedback loops and pathway cross-talk could result in undesirable activation of other pathway elements [46]. However, side-effects from PI3K inhibition treatment have thus far proven to be tolerable [122].

Isoform-selective p110δ inhibitors are in early trials for haematological malignancies and promising results have been reported for B-cell lymphoma patients [135]. These compounds have not yet been tested for allergy or inflammation, although in principle they show great promise in these applications.

In accordance with its role as an important downstream effector of PI3K, several Akt inhibitors have been developed. The compound perifosine has had little effect as a single agent; however other compounds, such as MK2206, are currently under clinical investigation as part of a combination therapy [136]. Nevertheless, our emerging understanding of compensatory mechanisms following Akt inhibition may raise concerns about further use of kinase inhibitors. It has recently been reported that Akt inhibition activates a recovery mechanism, through mTOR inhibition and consequent FOXO activation, that results in expression and phosphorylation of RTKs [137]. It has also been shown that the ATP-competitive Akt inhibitor A-443654 induces hyperphosphorylation of Akt at Thr308 and Ser473 through conformational changes that facilitate PH domain binding to PIP_3 and the reactivity of phosphorylation sites [138]. Worryingly, Akt was found to be extremely active following inhibitor disassociation. This is the first time such a phenomenon, termed “inhibitor hijacking”, has been described, however should it turn out to be a common phenomenon, it may have serious implications for the use of kinase inhibitors.

The mTOR inhibitor rapamycin, and more recent analogues, are the compounds that have advanced the furthest clinically to date [41, 136]. Clinical trials using these compounds, in single or combination therapies, for the treatment of solid tumours have shown encouraging results but a clear improvement in survival has not been found [136]. Our

emerging understanding of the importance of mTOR regulated feedback loops in the regulation of PI3K, by which inhibition of mTOR results in an activation of PI3K, may account for the disappointing results encountered so far.

Improved understanding of the PI3K/Akt pathway activity and regulation is necessary to predict the efficacy of inhibitors in the treatment of disease. Distinct, sometimes opposing roles, for elements of this pathway are continually emerging, thus demonstrating the need to be cautious when using these drugs. Inhibition of multiple pathways may also become an important strategy as the importance of cross-talk emerges [136]. The identification of the specific pathway deregulation or biomarker panel in each patient, using high-throughput methods, would permit most efficient use of targeted drug treatment [139].

1.4. Proteomics

1.4.1. Principles of proteomic analysis using mass spectrometry

Mass spectrometry is an analytical technique used to determine the chemical composition of a sample by measuring the mass to charge ratio (m/z) of constituent molecules, after they have been converted to gas-phase ions. The technique is extremely specific and provides unbiased analysis, permitting diverse applications in a wide variety of fields in biology and chemistry. All mass spectrometers have the same basic structure, although there are a variety of different types for each component depending on the application. The key components are as follows:

ION SOURCE → **MASS ANALYZER** → **DETECTOR**

The ion source produces gas-phase ions from the molecules in the sample, which are then separated by the mass analyzer according to their m/z, a physical property of great diagnostic value. The final component is the detector, which measures the relative abundance of the separated ions.

The relative intensity of the ions detected from a compound can be plotted against their m/z to generate a unique mass spectrum, which can be used for identification. The charge of each ion can be determined from the mass spectrum and therefore its mass can

be calculated from the m/z. This data can be used to identify the molecular composition of the sample and intensity of ion peaks can be used to generate quantitative data.

Mass spectrometry has been applied extensively to the field of proteomics over the last decade. The technique can be applied to identify and quantify proteins present in a sample, to identify post-translational modifications, to sequence newly identified proteins and to elucidate protein structure. The major advantage of mass spectrometry over other techniques is that it can be used to profile the protein composition of a sample in depth without the need for targeting; i.e. without having a prior preconception of what molecules may be present in the sample and at what abundance.

Proteomic analysis by mass spectrometry is becoming increasingly important through its application to large-scale, global studies. Traditionally, genomic approaches, such as mRNA microarray analysis and large-scale sequencing projects, have been used for global characterization of cells or disease states. However, the impact of multiple levels of post-transcriptional and post-translational regulation of gene expression cannot be fully taken into account using these approaches. Global proteomics can overcome these limitations and is key to the understanding of complex biological systems, such as signalling pathways.

1.4.2. Protein sample preparation for mass spectrometry analysis

Sample preparation for mass spectrometry is a critical stage for successful protein analysis. The majority of protein analysis using mass spectrometry is carried out on peptide solutions resulting from proteolytic digestion of the protein mixture, using the so-called “bottom-up” approach [140]. In this approach, qualitative and quantitative data is generated for the peptides and extrapolated to give information about the whole protein [140].

Many different approaches for proteolytic digestion of biological samples prior to “bottom up” mass spectrometry proteomic analysis have been described (reviewed in [141]). An important consideration of all such methods is that many detergents and reducing agents used in the harvesting of protein from cells or tissue can inhibit protease activity. Accordingly, one approach to proteolytic digestion is to first immobilize proteins in a solid support, for example using polyacrylamide gel electrophoresis (PAGE). Proteins embedded in gels can then be washed clean of interfering substances before digestion and

subsequent elution of resulting peptides. A variation of this approach is filter-assisted sample preparation (FASP), a technique in which proteins are immobilized on a solid filter support [142]. An alternative method that is also widely used is to carry out proteolytic digestion of proteins in solution. In such an approach, samples are diluted after protein extraction to reduce the impact of interfering substances on digestion.

Selection of the most appropriate protease for proteolytic digestion is also important in mass spectrometry based proteomics. Trypsin, which cleaves proteins at the carboxyl terminus of arginine and lysine residues, is the most widely used protease for this purpose [141]. Other proteases used include: chymotrypsin, which cleaves proteins at tyrosine, tryptophan or phenylalanine; Lys-C, which cleaves proteins at the carboxyl terminus of lysine; and Asp-N, which cleaves proteins at the N-terminal side of aspartic acid. Protease choice should be influenced by the type of experiment that is being performed and it should be noted that a combination of proteases is likely to result in more complete protein digestion. In addition, the use of multiple proteases in parallel experiments produces complementary sequences, resulting in greater coverage of the proteome.

In the so-called “top down” proteomic approach intact proteins are analyzed by the mass spectrometer. Using this method more information can in principle be obtained about a protein’s primary structure as sequence coverage can be very high, approaching 100% for proteins up to 30 kDa in size [143]. Precise information about isoform variations and post-translational modifications can also be obtained. The method can also be applied for the investigation of protein-protein interactions to estimate binding affinities of proteins in solution [144]. Due to the complexity of fragmentation patterns from whole proteins “top down” proteomics is not suitable for the analysis of complex mixtures, such as those present in typical biological samples. However, the development of high resolution hybrid instruments like FT-ICR and LTQ-Orbitrap has enabled advances in this field in recent years [143].

Regardless of the proteomic approach used, biological protein solutions are typically very complex mixtures and some degree of sample separation is often required prior to mass spectrometry analysis [141]. Mass spectrometry may be coupled to traditional protein analysis methods, such as electrophoresis or chromatography, to fractionate the proteins in the sample to yield less complex mixtures [141]. Alternatively, the sample may undergo a

purification step, such as affinity purification or phosphopeptide enrichment, to enrich the sample for proteins of analytical interest. After proteolytic digestion, peptide samples are often further separated prior to mass spectrometry analysis by high or ultra performance liquid chromatography [141]. This last step is usually carried out on chromatography systems which are coupled to the mass spectrometer, with column eluents feeding directly into the analyzer.

1.4.3. Types of mass spectrometer used for proteomic analysis

The development of ionization methods that facilitated the formation of charged, gas-phase ions from an aqueous peptide or protein solution was the major breakthrough that allowed progress in the field of protein analysis by mass spectrometry. The two ionization methods currently used in protein analysis are electrospray ionization (ESI) and matrix-assisted laser desorption/ionization (MALDI), although the former is most widely employed. In ESI, a high voltage is applied to the sample, in liquid phase, as it passes through a silica or metallic capillary, thereby dispersing it into a charged aerosol which rapidly evaporates, producing gas phase ions [145]. In MALDI, a laser beam is used to vaporize and ionize the sample, which is crystallized in the solid phase [146]. Both techniques are known as “soft” ionization methods, as the peptides molecules are unlikely to fragment, but differ in that ESI tends to produce more multiply charged ions than MALDI. Another difference is that ESI is more readily coupled with LC than MALDI. MALDI is also less suited to quantitative investigation as signal intensity is dependent on analyte-matrix crystallization conditions [147].

Commonly used mass analyzers for protein mass spectrometry include quadrupole, time of flight (TOF), 3D and linear ion traps, Fourier transform ion cyclotron resonance (FT-ICR) and orbitrap instruments. In quadrupole analyzers, radiofrequency and electrical fields are created through which ions move at a speed and trajectory determined by their m/z. The conditions of the fields are manipulated to filter the ions and select those required. In TOF analyzers, ions are initially accelerated by an electrical field and then left to drift in a free-field, wherein they separate according to m/z as this determines the speed at which they travel. Ion trap analyzers, 3D and linear, trap ions in an oscillating electrical field, which can then be manipulated to sequentially eject the ions from the trap according to their m/z.

In FT-ICR instruments, the ions are trapped within a magnetic field and excited by an electrical field. The speed and movement of the ions in the trap is determined by the m/z, which can be calculated by Fourier transformation from the measurement of ion motion. Orbitrap analyzers work in a similar way to FT-ICR instruments, trapping ions in an electrical field causing them to oscillate around a central electrode. The m/z is determined by Fourier transformation of the measured frequency of ion oscillations.

Ions separated by quadrupole, TOF and ion trap instruments are most frequently detected by the physical impact of the ion on a detector, such as a conversion dynode or a micro-channel plate. The signal detected is then amplified using an electron multiplier. In FT-ICR and orbitrap analyzers detection is carried out by a pair of metal plate detectors between which a weak current is produced by the movement of the ions.

TOF, ion trap, FT-ICR and orbitrap analyzers all offer a wide range for mass detection; however orbitrap and FT-ICR instruments offer greater mass accuracy and resolution. Many applications of mass spectrometry in protein analysis require the use of hybrid instruments, which are composed of two or three of the mass analyzers described coupled together, to permit more complex analysis.

1.4.4. Qualitative protein analysis

Qualitative mass spectrometry analysis can be applied in a targeted manner. One example of such an application is the identification of a protein that has been found to be differentially expressed using traditional methods, such as affinity purification and SDS-PAGE [81, 148, 149]. However, the greatest strength of proteomic analysis using mass spectrometry lies in its application to global approaches. Current technology enables the identification of thousands of peptides or proteins and their post-translational modifications within a relatively short period of analysis time.

Qualitative analysis for the identification of peptides and proteins is usually carried out using tandem mass spectrometry (MS/MS) analysis (Fig. 1.5.). In the first and second stages of MS/MS analysis, peptide ions are selected and fragmented, usually along peptide bonds, generating daughter, fragment ions that are separated and detected by the third stage of analysis. The mass spectra generated for the daughter ions enable peptide identification by comparison to reference databases or by *de novo* amino acid sequencing. MS/MS can be

carried out using hybrid instruments, with the various stages of analysis carried out in multiple mass analyzers (MS/MS in space), or in a single ion storage analyzer, with the various stages of analysis carried out using an appropriate series of conditions (MS/MS in time).

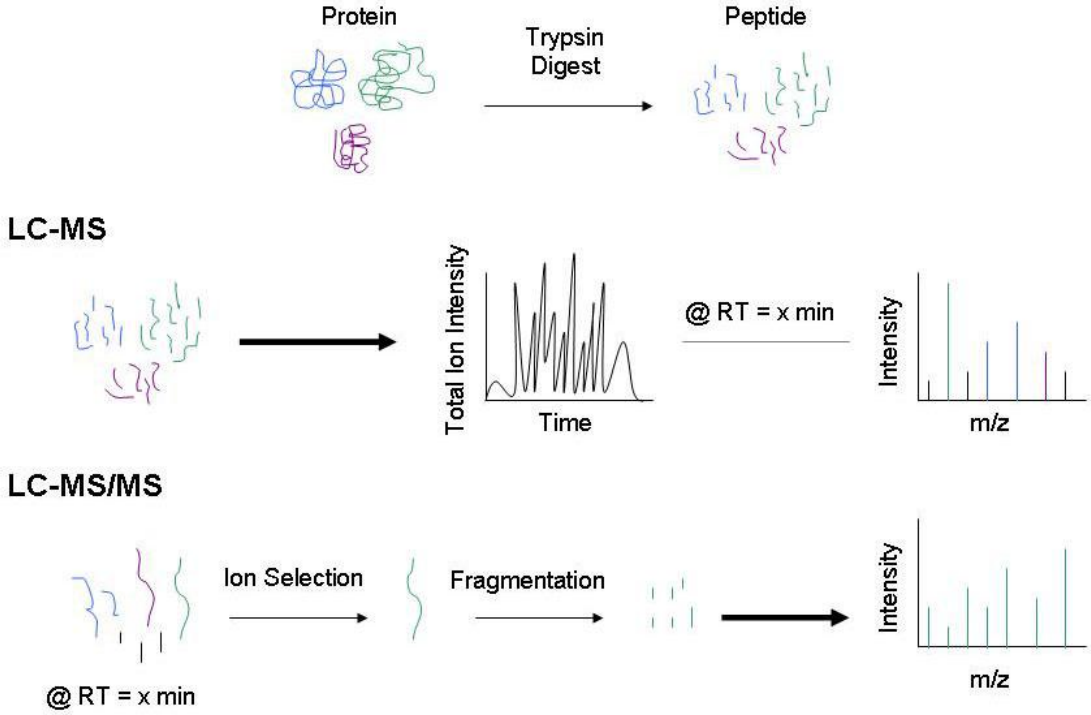

Figure 1.5. Illustration of the principles of MS and MS/MS proteomic analysis. In MS proteomic analysis the intensity of a peptide ion with a given m/z in detected (MS scan). In MS/MS analysis, peptide ions are selected and fragmented, usually along peptide bonds, generating daughter, fragment ions that are separated and detected by the third stage of analysis (MS/MS spectra).

Peptide fragmentation is typically induced by subjecting charged ions to collision with other particles. The kinetic energy of the collision is internalised and results in the rupture of the weakest bonds, which are typically the peptide backbone amide bonds. Thus, low-energy collision conditions result in fragmentation of peptides along the amino acid backbone [150-152]. However, peptide fragmentation patterns are complex and influenced by amino acid composition, molecule size and excitation method, amongst other factors [151]. Thus conditions must be optimized to ensure efficient fragmentation in order to obtain useful information.

Collision-induced dissociation (CID) is the most popular form of gas phase fragmentation. Charged peptides are accelerated within a vacuum in the collision cell and are bombarded with inert neutral gas, such as helium, nitrogen or argon and the resulting energy internalised. Higher energy collision dissociation (HCD) is similar in principle to CID carried out in quadrupoles but in hybrid linear ion trap-orbitrap instruments it is used to avoid the low mass cut-off typical of ion trap fragmentation and to enable the use of high resolution detection in the Orbitrap to improve resolution of fragments ions [153]. In electron-transfer dissociation (ETD) and electron-capture dissociation (ECD), peptides are fragmented by bombardment with electrons. In addition to MS/MS analysis of peptides, CID, ECD and ETD are also used for protein fragmentation in "top down" proteomic approaches [143].

MS/MS spectra resulting from peptide fragmentation can be used for *de novo* amino acid sequencing. As peptides fragment along the amino acid backbone they form structurally informative sequence ions (amino acid chains) and non-sequence small neutral ions, such as water and ammonia [154]. Fragments derived from the N-terminus of the peptide are designated as b ions and fragments derived from the C-terminus of the peptide are known as y ions [154]. In *de novo* sequencing, amino acid residues are identified by calculation of the mass difference between successive fragment ions of the same type i.e. b or y [151, 154]. Thus peptides, and by extrapolation proteins, can be sequenced with no prior knowledge of the sample. This process can be automated using software, however it remains a relatively time consuming method for routine peptide identification.

The mass spectra generated by daughter ion fragmentation can also be compared to databases of predicted fragments for known peptides generated by *in silico* digestion and fragmention of all known proteins present in databases to enable the identification of peptides and, by extrapolation, proteins. This process, more commonly used than *de novo* sequencing, can be highly automated using software programmes that are used as search engines, examples of which include MASCOT and SEQUEST. The major advantage of this approach is that peptide identifications in large-scale datasets can be obtained rapidly. However, there is a significant disadvantage associated with this approach in that false-positive matches are likely to occur by chance in a large dataset. It has been estimated that there are 3.8 million theoretical tryptic peptides in the widely used IPI human database, of

which 2 million are shared between 2 or more proteins thus potentially resulting in ambiguous protein identification [155]. Complex algorithms can be used to estimate the probability of an accurate identification [156] and thus the stringency of a match can be set by the user to generate low or high confidence results. Improved understanding of peptide fragmentation patterns would enable the generation of better *in silico* databases, resulting in more accurate results [151]. Improvements in this area are likely to occur as the method matures.

It should be noted that regardless of the peptide identification method used, the phenomenon of "under-sampling" remains a limitation of MS/MS analysis of complex samples. In MS/MS analysis, a limited number of high-abundance peptide ions are isolated for fragmentation; thus many low-abundance peptides in a complex mixture are not identified. This restricted analysis of complex mixtures is termed "under-sampling" and is a common phenomenon in MS/MS. The most influential factors on under-sampling are: target peptide ion intensity, sequencing speed (duty cycle), instrument sensitivity and precursor ion isolation [157]. It has been estimated that more than 100,000 peptide features can be eluted in a 100 min gradient elution using an LTQ Orbitrap Velos but only around 16% of these ions are selected for MS/MS [157]. One approach to combat this limitation is to analyze the same sample in multiple technical replicates as this has been demonstrated to increase the numbers of peptide identifications produced [158]. As the resolution and, more importantly, duty cycles of instruments improve the impact of under-sampling will gradually be reduced but it currently remains one of the greatest challenges for mass-spectrometry based proteomics.

1.4.5. Quantitative protein analysis

The capability for quantitative global analysis is the greatest strength of mass spectrometry in the field of proteomics. Qualitative proteomic analysis is an important tool in biological research, however the utility of the data obtained is limited as quantitative information is key to the understanding of biochemical processes. In quantitative analysis, mass spectrometry is unrivalled by any other proteomic tool, which are all reliant on the targeted analysis of a relatively small number of proteins. Current technology permits the

simultaneous identification and quantitation of hundreds or thousands of proteins per experiment [159-161].

1.4.5.1. Label-based approaches

One approach to quantitative proteomics is to label protein samples that are to be compared with tags of different isotopic mass. The samples can then be pooled, digested and analysed by LC-MS and LC-MS/MS. Proteins in the samples are identified and the relative abundance in the different samples can be obtained by comparing the peak heights for the different isotopic variants of the tag. The isotopic labelling of proteins can be carried out at various stages in the workflow process. In one approach, known as isotope-coded affinity tag (ICAT), the proteins are labelled after they have been harvested from cells. The ICAT has a cysteine reactive group, a "heavy" or "light" isotope linker and a biotin affinity tag [162]. Cell lysates are incubated with the ICAT reagent, digested and then the labelled peptides are isolated by affinity purification prior to LC-MS analysis [162]. Variations on this approach are isobaric tag for relative and absolute quantitation (iTRAQ) and tandem mass tag (TMT), which label amino groups with a tag that generates a specific reporter ion upon peptide fragmentation [163]. Limitations include variability of labelling efficiency between samples, isotopic impurities, e.g. from manufacturers, and interference of mixed MS/MS contributions during precursor ion selection [164]. Furthermore, it has recently been shown that isobarically labelled phosphopeptides result in significantly greater charging during ESI, which results in reduced fragmentation and identification efficiency [165]. This phenomenon was estimated to reduce phosphopeptide identification numbers by 50% even when using optimized MS/MS conditions [165].

An alternative labelling approach is to incorporate the isotopic tag *in vivo* during protein synthesis. The most widely used example of this approach, termed stable isotope labelling by amino acids in cell culture (SILAC), involves the addition of isotopically labelled amino acids to cell culture medium, thereby labelling the proteins more comprehensively and without affinity issues as may be encountered with alternative labelling approaches [166]. The cell lysates are then mixed prior to digestion and LC-MS and LC-MS/MS analysis. However, a key restriction of this approach is that *in vivo* labelling may be challenging, for

example if an animal tissue was under investigation, or indeed completely impracticable, for example if a human patient was under investigation.

The Mann group, which pioneered the SILAC method, have also developed solutions to overcome these limitations and broaden its applicability to more sample types or greater sample numbers. More recent work showed that *in vivo* isotopic labelling can be performed at the organism level by developing a SILAC-labelled mouse, thus enabling the use of tissue for proteomic studies [167]. Mice were labelled over 4 generations to obtain 100% labelling, although 93% labelling was obtained after a single generation [167]. Another strategy was also developed to enable the application of SILAC to human investigations. SILAC-labelled cell lines, termed "Super-SILAC" mix, were created to represent the proteome of the tissue type under investigation [168]. These lysates were then used as internal standards to enable the relative quantification peptides and phosphopeptides in cancer cell lines [169] and human tumour tissue samples [170]. This approach assumes that cell lines express the same repertoire of proteins and the same phosphorylation sites as primary tissues.

Despite the many advances in recent years, the major limitation of label-based proteomics is that only a small number of samples can be compared in any given experiment due to the limited number of isotopic labels available. These methods also tend to be more expensive due to the requirement for specific, labelled reagents. Despite these limitations, iTRAQ and SILAC quantitation methods are frequently used for global proteomic studies with great success.

1.4.5.2. "Label-free" approaches

Many label-free methods for the quantitation of proteins using mass spectrometry have also been developed. One approach, known as spectral counting, is to use the number of unique peptide spectra identified in a data-dependent LC-MS/MS experiment for a particular protein as an indicator of its abundance. Spectral counting has been reported to provide a simple and reliable index of protein abundance [171]. The number of peptides that are identified for a protein do indeed correlate with protein abundance, however the relationship between these measurements is complex as factors such as peptide size, ionization efficiency and sampling difference between runs are also implicated [147, 171, 172]. To overcome these limitations, labelled internal standards may be incorporated into

the samples or mathematical corrections can be used to take these factors into account. One example of the latter approach is absolute protein expression measurement (APEX), which corrects the observed spectral count using learned probabilities for sampling depth and confidence of peptide identification [172]. Although spectral counting has been successfully applied for many large scale proteomic studies [160, 172], it should be noted that extensive normalization and statistical analysis are required to obtain accurate and reliable quantification [171].

Alternative approaches use the measurement of ion peak area or height as a measure of peptide abundance, which can then be extrapolated as a measure of protein abundance. Selective reaction monitoring (SRM), also known as multiple reaction monitoring (MRM), uses the peak intensity of a small number (3-6) of the most abundant and proteotypic daughter ions from the MS/MS fragmentation of a peptide as a measure of abundance. SRM has been shown to be sensitive and specific [173], however the number of proteins that can be quantitated in a single analysis is limited by the duty cycle of the mass analyzer. Alternative strategies to SRM, which measure the intensity or area of the parent peptide ion, are not limited in this way and can quantitate a much larger number of proteins in each run. Thousands of peptides, and thus hundreds of proteins, can be easily quantified in a single experiment [159, 174].

Label-free methods for protein quantitation by mass spectrometry offer many advantages over labelling approaches. The most notable benefit is that a potentially unlimited number of samples can be compared in a single experiment. In addition, such methods tend to be cheaper, require less complex sample processing and can be applied to any sample type. The limitations are that mass spectrometry and data analysis can be more complex and the resolution and reproducibility of the analyzers can affect the quality of results. However, as the precision and resolution of mass spectrometry instruments continue to improve and data processing software is developed these issues are likely to become of limited impact. A study evaluating label-fee methods for quantitative proteomics found that linearity and reproducibility were within a 95% confidence limit for a spectral counting approach and for the measurement of peak area intensity [175]. The authors noted that spectral counting is the more sensitive method however peak area intensity provides more accurate quantitations [175]. Furthermore, peak areas and heights on

peptide elution profiles (extracted ion chromatograms - XICs) have been shown to correlate well with abundance across samples [159, 171, 176].

However, there are important factors to be considered when using peak measurement for peptide quantitation approaches. Some argue that quantitation of parent ion peaks requires confident assigned MS/MS spectra in each sample for peak matching, which, due to the phenomenon of "under-sampling", greatly reduces the number of quantifiable peptides in an experiment [147, 177]. However, modern high mass accuracy and resolution enables the confident identification of correct peaks using RT, m/z and isotopic distribution [159, 177]. A greater problem is that the XICs of different peptides within a protein may be very different, however the average of the three most abundant has been shown to provide an accurate estimate in most cases [171]. In addition, low resolution data may result in multiple or overlapping candidate peaks (pseudopeaks), however in such cases MS/MS can be used to identify the correct peak [175]. Experimental drifts in retention time (RT) and mass-to-charge ratio (m/z) can also complicate analysis and increase inaccuracy, however, again, improvements in the technology make this less relevant [171]. A rapid increase in the development of bioinformatic tools to assist label-free quantification has supported developments in this method [171].

Despite existing concerns, many validation studies have demonstrated the suitability of label-free ion peak measurement for peptide quantification. In a method termed "Serac", intensity of XICs was measured across multiple samples after normalization and background subtraction [175]. The data revealed that peak height exhibited a linear relationship with protein abundance and that reproducibility of quantification was within 95% confidence limits when more than three peptides were used [175]. Another approach, "SEMI" (sequence, elution time, mass-to-charge and internal standard) was applied to quantify peptides, identified in at least one but not every sample, across multiple samples [177]. This method used algorithms for retention time alignment and cross-referenced across multiple runs for confident peak assignment [177]. Further work with this method estimated quantitative accuracy at around 6% error and reproducibility at 34% relative SD [178].

Furthermore, work by this group has demonstrated the suitability of a label-free quantification method that uses a computer program named Pescal, which was developed in-house [159], for the quantification of peptides. Retention time, mass-to-charge ratio,

charge and isotopic distribution data, obtained from a single MS/MS event, is used to confidently identify peptide peaks in MS scans across multiple samples [159, 179]. Further work developed a validation method that demonstrated the ability of Pescal to quantitate peptides across a wide dynamic range with a mean accuracy variation of 22% for over 80% of the ions quantified [179].

1.4.5.3. Absolute quantification

Most investigations performed using both labelled and label-free mass-spectrometry based quantification are focused on the relative quantification of peptides or proteins between different experimental conditions. However, absolute quantification of peptides and proteins may also be of great interest and may be performed using either method.

Many methods for absolute quantification rely upon the use of labelled internal standards. The most straight-forward approach to absolute quantification of proteins is the so-called “Top 3 method”. In this approach, the average MS signal response of the three most intense tryptic peptides is measured per mole of internal standard protein [180]. This information is used to calculate a universal signal response factor that is then applied to quantify unknown proteins using the mean MS signal response of their three most intense tryptic peptides [180]. This method was shown to be applicable to complex mixtures [180] and to demonstrate a linearity of 0.98 across a wide dynamic range [181].

A similar approach identified proteotypic peptides representing an array of proteins across a wide dynamic range (40 – 15000 copies/cell) [182]. Absolute abundance levels were then determined for these proteins by measuring the median ion intensity for the three most abundant peptides using labelled reference standards [182]. These selected proteins were used as calibration points and the proteome of the pathogen *Leptospira interrogans* was quantified [182].

Although both of these methods make use of labelled internal standards these references serve primarily as calibration points and therefore extrapolation is necessary for the quantification of the thousands of proteins quantified in a proteome. An alternative approach, which aims to overcome this limitation is the QconCat method [183]. In QconCat technology, artificial genes that encode combinations of proteotypic tryptic fragments of multiple proteins are designed and expressed in bacteria using isotopic labelling [183, 184].

Known amounts of these artificial proteins are then used as internal standards for the absolute quantification of the selected proteins in a sample [183, 184]. This workflow is repeated to represent all the proteins in a proteome under investigation, providing high confidence absolute quantification of every protein using its own internal standard [184].

Alternative approaches for absolute quantification using label-free methods have also been developed in addition to the "top-three" method described above. In absolute protein expression profiling (APEX), spectral counting and mathematical algorithms based on learned probabilities are used to quantify proteins [172]. The abundance of a particular protein is quantified by measuring the spectral count and correcting for the prior expectation of observing each peptide, determined by *in silico* analysis [172]. Another label-free method, intensity based absolute quantification (iBAQ), uses the sum of peptide peak intensities divided by the number of theoretically observable tryptic peptides to quantify a protein [185].

Although absolute quantification of proteins is feasible but it remains a more complex, time-consuming and expensive method than relative quantification. Thus, its application is not as widespread as many questions in biology are often adequately addressed by the use of relative quantitation.

1.4.6. Affinity purification coupled to mass spectrometry: analysis of protein-protein interactions

One of the major applications of proteomics is in the field of mapping protein-protein interactions. The importance of protein-protein interactions and protein complexes in biological processes, such as cell signalling, is being increasingly recognized and mass spectrometry is facilitating such advances. Protein-protein interaction studies may be targeted, e.g. with the aim of identifying binding partners of a particular protein, or of a global, networked approach with the aim of characterizing the interaction network of an entire pathway or cell type.

The traditional proteomic approach for the identification of protein-protein interactions is the yeast 2-hybrid system (Y2H). This method, developed some decades ago, uses a "bait" protein and a "prey" protein, fused with a DNA binding domain and an activation domain of a reporter gene respectively, which are co-expressed in yeast [186].

Expression of the reporter gene indicates interaction between the "bait" and the "prey" in the yeast cell. This method has been used to identify thousands of stable and transient protein-protein interactions but the method is limited in that it can only identify binary interactions. Furthermore, Y2H has been shown to result in a high false positive rate and does not account for the influences of cellular localization, different cell environments, post-translational modifications and basal expression levels [187]. Despites its limitations, stringent, high-throughput Y2H strategies are suitable for the investigation of binary interactions cells [188] and have been used to begin to map the human interactome [189] and to comprehensively map those of *S. cerevisiae*, *C. elegans*, and *D. melanogaster* [190].

Affinity purification of protein complexes followed by proteomic analysis by mass spectrometry has more recently emerged as the method of choice for the identification of protein-protein interactions in protein complexes. In this technique the "bait" protein, which is the protein central to the complex of interest, is isolated from total cell lysate using affinity purification techniques, such as immunoprecipitation (IP) or epitope tag affinity chromatography. It is crucial that this affinity purification step is carried out under conditions that do not disrupt protein-protein interactions, for example low ionic strength solutions and mild detergents should be used. The isolated protein complex is then analyzed by mass spectrometry to facilitate the identification and quantitation of the constituent proteins, thus identifying interaction partners. This strategy has been successfully applied to a number of protein interaction studies in yeast and mammalian cells [191-193].

The advantages of affinity purification-mass spectrometry (AP-MS) are multiple and overcome many of the limitations of Y2H. Firstly, the technique can be applied to cells or tissues grown under physiological conditions, therefore permitting the study of dynamic changes in protein complexes by the manipulation of growth conditions. Another advantage of AP-MS is that post-translational modifications are not usually affected, thus providing further valuable information with regards to the regulation of protein complexes. Finally, AP-MS permits the identification of multi-protein complexes as it is not restricted by binary relationships. The inherent qualities of mass spectrometry are also important for making AP-MS the method of choice. Mass spectrometry analysis is sensitive and specific; it permits qualitative and quantitative analysis and permits the unbiased identification of proteins present in a sample.

The abundance of the "bait" protein is an important factor in the effectiveness of AP-MS as interacting partners may not be present in equimolar ratios. High amounts of "bait" protein may be required to ensure sufficient recovery of binding partners and the method can be biased towards high-abundance proteins [194].

However, the major consideration for AP-MS is that the technique is limited by the specificity of the affinity purification technique, as non-specific interactions will complicate the identification of true binding partners. A "one size fits all" AP-MS strategy is an unlikely proposition; it is necessary to optimize affinity-purification for the application required. Immunoprecipitation using monoclonal antibodies is an attractive approach as it is specific and does not require modification of the "bait" protein, however such tools are often unavailable [187]. An alternative approach, in which the "bait" protein is tagged is more widely used. Nonetheless, the use of artificially transfected "bait" proteins should be approached with care as expression levels of transfected proteins can be up to double basal concentrations [187] and it has also been shown that some tags, such as green fluorescent protein, can affect subcellular localization [194, 195], thereby increasing the likelihood of false-positives.

A consistent problem with AP-MS is the incidence of false-positives resulting from interactions of the "bait" with abundant house-keeping proteins that also have high affinity for purification reagents [194]. Tandem affinity purification approaches (TAP) were developed in an attempt to overcome such limitations [196]. In TAP, "bait" protein complexes are purified using two successive rounds of complimentary affinity purification [196]. This approach reduces the number of false positive results, however it can also result in decreased sensitivity due to sample losses during multiple rounds of purification [194, 197]. An innovative variation on this strategy, parallel affinity capture (iPAC), was more recently described [197]. In iPAC, cells are transfected with a transposable element that results in the production of endogenous proteins triple-tagged with FLAG-StrepII-YFP [197]. Parallel FLAG and StrepII purification steps are then performed, which results in lower protein losses than sequential purification steps [197]. Interactors are identified as proteins that are present in the complexes isolated using both purification systems but not found in the negative control wild type cell line purification products [197].

Computational methods have also been developing at an impressive pace to enable the advances in AP-MS that have been produced. Bioinformatic resources are crucial for managing the large datasets produced by this method and de-convoluting the data to identify protein-protein interactions within multi-protein complexes and larger networks [194]. Bioinformatics also has an important role in reducing the incidences of false-positive results in AP-MS studies. Control affinity purification samples can be used to generate a database of non-specific interactors with the affinity reagents; a so-called "beadome". *In silico* analysis can then be used to discard such data from experimental samples [193, 197].

Quantitative proteomics also has an important role in AP-MS. Quantitative strategies can be used to differentiate non-specific interactors from dynamic binding partners following AP-MS. In such an approach, unlabelled or SILAC-labelled cells were stimulated with EGF or left untreated prior to affinity purification against the phosphorylated EGF receptor [198]. Proteins interacting with the phosphorylated EGF receptor were then identified as those purified in different abundance under the two conditions [198]. There are several advantages to this approach for targeted studies, such as the reduced likelihood of false positives, due to the use of endogenous, untagged proteins, and the potential to investigate the dynamics of protein-protein interactions at multiple time points [198]. However, such an approach is unlikely to be practical for proteome-wide interaction studies.

The analysis of protein interactions requires further consideration of protein complex topology and structure, as well as composition [199]. Other emerging mass spectrometry methods, such as drift cell and travelling wave ion mobility, are likely to become increasingly important in this area.

1.4.7. Phosphoproteomics

Phosphoproteomics is the subfield of proteomics that is dedicated to the characterisation of protein phosphorylation. Phosphorylation is a reversible post-translational modification that has a key role in the regulation of protein function [200-202]. Phosphorylation occurs upon serine, threonine or tyrosine residues in eukaryotes [202] and has the potential to induce conformational changes in proteins, thereby enabling regulation of activity [203]. In addition, phosphorylation can also mediate recognition of proteins by interaction partners and affect subcellular localization. Protein phosphorylation is tightly

regulated by kinases, which phosphorylate proteins, and phosphatases, which dephosphorylate proteins [200, 204] and proteins may be phosphorylated on multiple sites, each event potentially resulting in a distinct biological output.

Protein phosphorylation has a fundamental role in signal transduction and, therefore, is a key regulator of essential cellular processes including metabolism, growth, cell cycle progression, migration and apoptosis [200-202]. As discussed in the previous section, the disruption of signalling pathways is associated with the pathology of many diseases including cancer, diabetes, autoimmune diseases and neurodegenerative conditions [200]. Hence, understanding the activity of signal transduction pathways can lead to the identification of novel therapeutic targets and biomarkers.

Phosphoproteins can be detected and quantified using immunochemical techniques. However, global mass spectrometry analysis of protein phosphorylation is emerging as a more powerful method for the investigation of signalling pathway activity [203, 205]. MS-based phosphoproteomic techniques enable the identification and quantification of thousands of phosphoproteins and phosphorylation sites in a single experiment. Thus, the method is inherently multiplexed (provides high content information) and a further advantage is that it is unbiased, requiring no prior knowledge of the proteins involved in the processes under investigation.

The mass spectrometry techniques previously described are all applicable to phosphoproteomic analysis although there are some additional considerations to be undertaken. Phosphorylation is a dynamic modification [200] and samples must be handled accordingly to prevent loss of phosphate groups due to phosphatase activity as these are efficient and robust enzymes [206, 207]. Therefore, cells or tissues must be lysed in the presence of phosphatase inhibitors to minimize phosphate hydrolysis [207, 208].

Mass spectrometry is a very sensitive technique, however its range of detection is limited due to the phenomenon of “under-sampling” discussed above. Large-scale proteomics experiments do not typically identify a significant number of phosphorylated peptides as phosphoproteins are usually present in very low stochiometry compared to their non-phosphorylated counterparts and are therefore less likely to be identified.

This issue is further compounded by the fact that MS/MS fragmentation methods frequently result in the neutral loss of the relatively labile phosphate and/or phosphoric acid

groups from phosphopeptides rather than backbone fragmentation, thereby reducing resulting sequence information [152, 209]. Another challenge is that phosphorylated peptides have been found to ionize less efficiently than non-phosphorylated peptides, using both ESI and MALDI [210].

Due to these phenomena, methods to enrich phosphorylated proteins prior to analysis are required in order to successfully perform MS-based phosphoproteomics experiments. A large number of techniques for the enrichment of phosphoproteins have emerged in recent years and been instrumental in the development and success of phosphoproteomics. These techniques can be divided into two groups: those that perform the enrichment at the protein level (Fig. 1.6.A) and those that enrich phosphopeptides after digestion of whole cell lysates by proteases (Fig. 1.6.B).

These methods will be subsequently discussed in detail and it should be noted that there are many different formats in which they may be applied. Methods for enriching phosphopeptides may be "on-line", where the enrichment method is coupled directly to the mass spectrometer, or "off-line". A wide range of affinity purification reagent solid phases is also available and includes beads, columns, tips and nanoparticles.

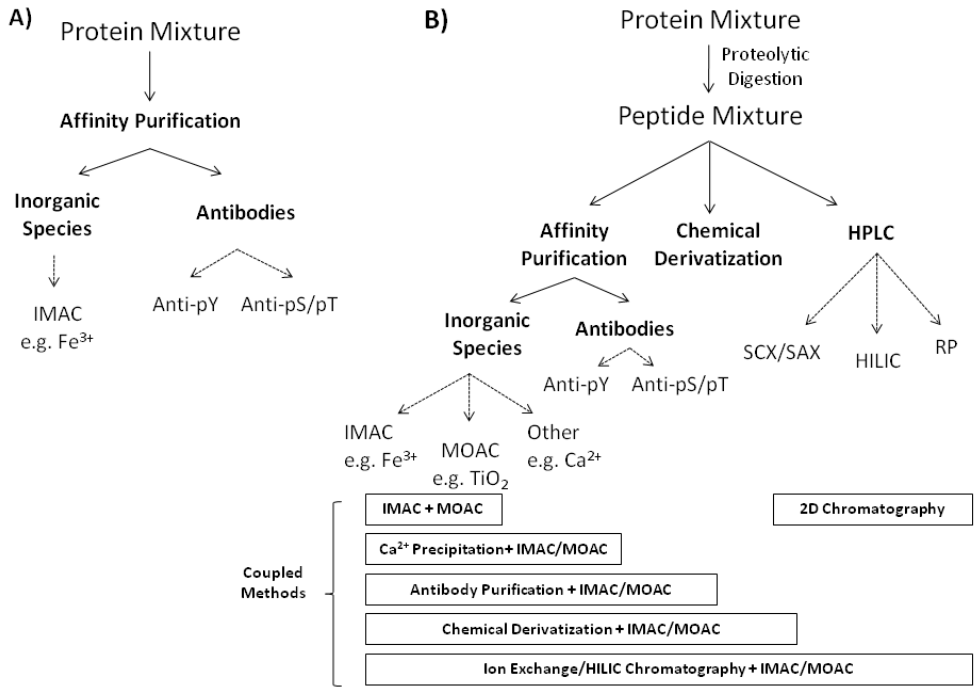

Figure 1.6. Summary of enrichment strategies commonly used for phosphoproteins (A) and phosphopeptides (B).

1.4.7.1. Affinity purification: inorganic species

Phosphorylated peptides or proteins can be purified by exploiting the affinity of negatively charged phosphate groups towards positively charged species bound to solid affinity matrices. The most widely used of these techniques are Immobilized Metal Affinity Chromatography (IMAC) and Metal Oxide Affinity Chromatography (MOAC) (Fig. 1.7. A).

IMAC exploits the affinity of phosphate groups for transition metal ions, which include Cu^{2+} (copper), Ni^{2+} (nickel), Zn^{2+} (zinc), Fe^{3+} (iron), Co^{2+} (cobalt), Al^{3+} (aluminium) and Ga^{2+} (gallium). The interaction occurs due to the formation of coordinate bonds between the electron donor groups of oxygen in the negatively charged phosphate group and positively charged metal ions [211]. Transition metals also have affinity for nitrogen and sulphur therefore many amino acids also bind metal ions, which reduces the specificity of IMAC for phospho enrichment. The binding efficiency of metal ions for each interaction species varies greatly; Fe^{3+} has a high affinity for phosphate groups [212] and thus is most frequently used for phosphopeptide enrichment [213].

IMAC can be used for the enrichment of both full length phosphoproteins and phosphopeptides and its use has been extensively demonstrated since the first application by Neville *et al.* [213-219].

The major limitation in the application of IMAC for phosphopeptide enrichment is that its specificity is limited by co-purification of acidic peptides. Solvent concentrations are an important factor in regulating specificity of IMAC and a higher concentration of acetonitrile was shown to improve the affinity and specificity of IMAC for phosphopeptides [220]. Interaction pH is also an important factor and acidic pH, between 2.5 and 3.5, has been shown to be optimal for phosphopeptide binding [221]. The choice of acid used is also influential and formic acid has been demonstrated to enhance IMAC specificity as it competes with non-phosphorylated peptides for binding [221, 222]. Elution conditions are another variable that can strongly influence efficiency and specificity. Phosphopeptides can be eluted from Fe^{3+} IMAC material under acidic or basic conditions [220, 222] and efficiency has been shown to be higher for mono- and multiply-phosphorylated peptides respectively [222]. Time is also an important factor and acidic and multiply-phosphorylated peptides have been demonstrated to elute more rapidly than non-acidic mono-phosphorylated

peptides [220]. Despite wide application, the characteristics of IMAC result in a systematic bias for multiply-phosphorylated peptides [220, 222].

An alternative method of affinity chromatography for phosphopeptide isolation exploits the interaction between phosphate groups and metal oxides, a method sometimes referred to as MOAC. This method is based on the affinity of negatively charged oxygen present in the phosphate group for metal atoms. Titanium dioxide (TiO_2) is the chemical species most frequently used for MOAC as it has the highest efficiency for this application [223]. TiO_2 affinity purification of phosphopeptides has been extensively demonstrated since its utility was first demonstrated by Pinkse *et al* [203, 223-226].

As with IMAC, the non-specific binding of acidic residues to TiO_2 reduces specificity for phosphopeptides. It has been shown that the addition of organic acids to solvents minimizes non-specific binding of acidic residues and improves specificity [223, 227]. Trifluoroacetic acid has been shown to be the best choice for reducing the binding of non-phosphorylated peptides [223]. Non-phosphopeptide excluders, acids that bind metal more weakly than phosphate groups but more strongly than carboxyl groups (e.g. glycolic acid), can also be used to improve the recovery of phosphopeptides [223, 228, 229]. Phosphopeptides are typically eluted using basic solutions, such as NH_4OH, as acidic eluents were found to be less efficient [223]. The recovery of phosphopeptides using MOAC has also been shown to be improved by applying multiple rounds of enrichment to a single sample [225, 230, 231]. TiO_2 affinity purification typically results in a bias towards mono-phosphorylated peptides as multiply-phosphorylated species bind with a very high affinity and are difficult to elute [223, 228, 229].

Despite their limitations, IMAC and MOAC are very efficient enrichment methods in phosphoproteomics and therefore they are widely used. It has been shown that TiO_2 MOAC is more selective and sensitive than IMAC in the enrichment of phosphopeptides, however more multiply phosphorylated peptides can be identified using the former [223, 228]. Our group has optimized the application of TiO_2 affinity chromatography for quantitative phosphoproteomics and demonstrated its suitability for this application [232].

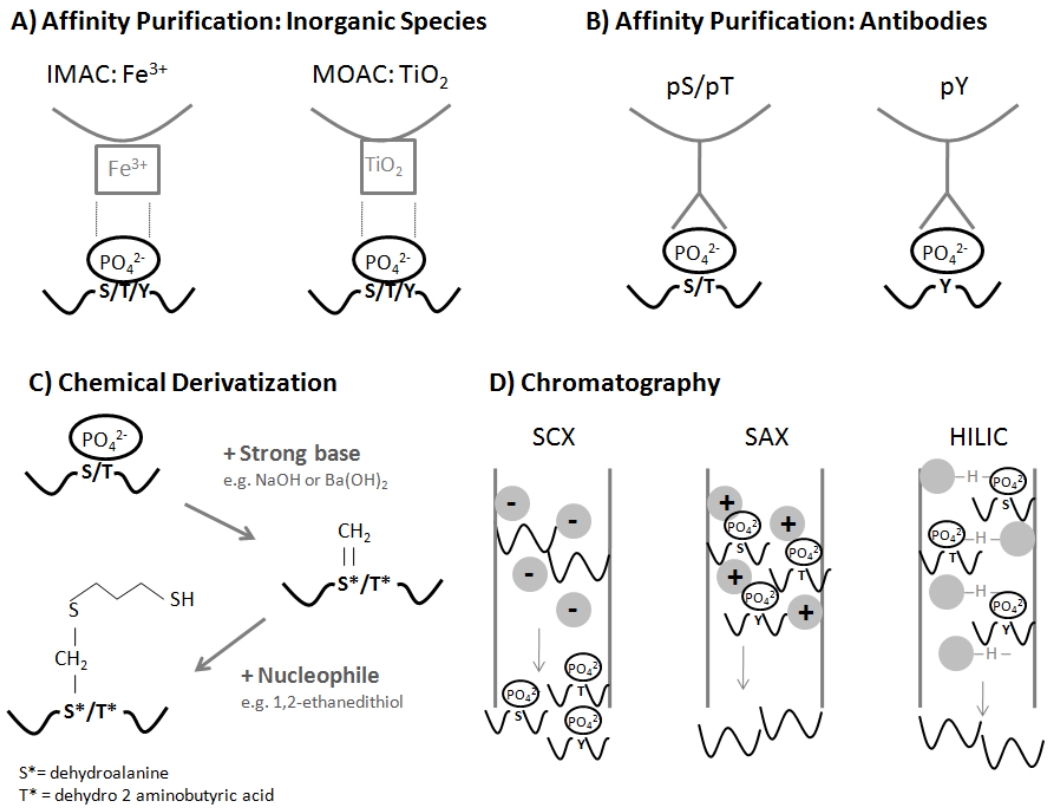

Figure 1.7. Principles of commonly used phosphopeptide enrichment methods.

1.4.7.2. Affinity purification: antibodies

Antibody-based affinity purification is based upon the selective enrichment of peptides or proteins that contain phosphorylated residues that are recognized by specific antibodies (Fig. 1.7.B). These methods are therefore limited by the specificity of the antibody tools available. There are many antibodies that claim specificity against phosphorylated serine (pS) and threonine (pT) residues, however few have been demonstrated to be suitable for phospho enrichment of peptides or proteins [233]. More success has been found for the enrichment of peptides and proteins phosphorylated on tyrosine residues, most likely because phosphorylation of this site is typically found at very low levels compared to serine and threonine. In fact, the distribution of phosphorylation sites has been estimated to be 86.4% on serine, 11.8% on threonine and 1.8% on tyrosine residues [203]. Thus, methods that are not specific for tyrosine-phosphorylation result in the enrichment of very low numbers of this modification relative to other phosphopeptides. Therefore, antibody purification methods specific for phosphorylated tyrosine have demonstrated better results than other methods. In addition, there are a number of available antibodies that are highly

efficient for the immunoprecipitation of peptides and proteins containing phosphorylated tyrosine [234], possibly because the aromatic ring of tyrosine is highly amenable to antibody recognition.

Antibody purification has been extensively used in global phosphoproteomic studies for the enrichment of peptides and proteins; most frequently in studies that are focused on tyrosine phosphorylation [160, 235-238].

1.4.7.3. Chemical derivatization

Phosphopeptide enrichment using chemical derivatization involves the selective modification of the phosphate group to enable selective enrichment of these peptides or proteins (Fig. 1.7.C). An important rationale of this method is that sensitivity and sequence coverage of phosphopeptides may be improved by removal of the phosphate group, which therefore results in greater fragmentation efficiency upon MS/MS. In addition, ionization efficiency is likely to be improved by the removal of negatively charged groups. The most common chemical derivatization method involves β-elimination of the phosphate group, using a reducing agent, followed by Michael addition with a stable chemical tag.

Limitations of this method include sample losses during multiple reaction steps and unavoidable side reactions. However, the method has been successfully applied for the enrichment of both phosphoproteins and phosphopeptides [239]. An additional feature of chemical derivitization is that sample labelling for quantification can be incorporated into the phosphopeptide enrichment workflow [219, 240].

1.4.7.4. Other chromatographic methods

Alternative forms of chromatography have also been applied for phosphopeptide enrichment. Strong cation exchange (SCX) chromatography separates molecules based on their charge (Fig. 1.7.D). The stationary phase is negatively charged and thus retains cations, which can be sequentially eluted by displacement using an increasing gradient of salt or pH. Strong anion exchange (SAX) chromatography is based on the same principles but the polarities of the reaction are reversed (Figure 1.7.D). SCX chromatography has been used under acidic conditions for the selective enrichment of phosphopeptides [241], however further studies have suggested that sensitivity and specificity is poor due to retention of

highly hydrophobic phosphopeptides and co-elution of acidic non-phosphorylated peptides [242, 243]. SAX chromatography was later proposed as a more suitable method for the enrichment of negatively charged phosphopeptides, providing greater scope for elution control. The method does enable the selective enrichment of phosphopeptides from a complex mixture [244], however sensitivity and specificity issues persist [243].

Hydrophilic interaction chromatography (HILIC) has also been applied to phosphopeptide enrichment (Figure 1.7.D). HILIC is based on the hydrogen-bonding interaction between charged ions and the neutral, hydrophilic stationary phase. The strength of this interaction increases with the degree of polarity and molecules can be eluted using an increasingly polar elution solvent. As phosphopeptides are more hydrophilic than non-phosphorylated peptides they are retained more strongly by the column and thus can be separated from a complex mixture. However, the sensitivity and specificity of this method are poor when used in isolation for the enrichment of phosphopeptides [245].

Accumulated data indicate that, on their own, HILIC, SCX and SAX are not suitable for phosphopeptide enrichment as they do not have sufficient specificity [243, 245-247], however they are powerful separation techniques and are useful in combination with other enrichment techniques in "coupled" approaches.

1.4.7.5. "Coupled" methods

Chromatography methods may be combined to provide multidimensional chromatographic separation for phosphopeptide enrichment. The rationale behind multidimensional chromatography is that the use of multiple orthogonal chromatographic methods (i.e. methods that produce non-overlapping separation) will result in comprehensive fractionation of a peptide mixture. Such strategies were not specifically designed for phosphopeptide enrichment, however comprehensive sample separation results in increased identification of low abundance peptides such as phosphopeptides.

In addition to SCX, SAX and HILIC, reverse phase (RP) chromatography has also been used for multidimensional chromatography. RP chromatography is based upon the interaction between charged molecules and the non-polar stationary phase, which can then be eluted according to polarity using a polar organic mobile phase. SCX, SAX and HILIC are orthogonal to RP, however HILIC and RP at high pH produce a more even fractionation of

peptides and thus are more useful for multidimensional chromatography [245, 248]. This technique has been applied for phosphoproteomic experiments [242, 249] and the major advantage of this strategy over other phosphopeptide enrichment techniques is that there is no loss of unmodified peptides, which provides additional informative data.

The combination of chromatographic separation with affinity purification methods can improve phospho enrichment efficiency as reduction of sample complexity can improve the sensitivity and specificity of affinity purification methods. Such approaches are reported to greatly enhance phosphoproteomic coverage [226, 243, 245, 246].

More specific phosphopeptide enrichment techniques have also been coupled to increase phosphopeptide enrichment efficiency. As discussed, MOAC and IMAC are complimentary methods with biases towards different populations of phosphopeptides. These methods have been coupled, in a method termed sequential elution from IMAC (SIMAC), to double the number of phosphopeptides identified using MOAC alone [222]. This method was further enhanced by combining it further with SCX [250]. In addition, antibody affinity purification and IMAC have been combined with chemical derivitization to improve specificity and sensitivity of phospho enrichment [251, 252].

1.4.7.6. Bioinformatic considerations

In addition to the use of phospho-enrichment methods prior to analysis in phosphoproteomics, there are important considerations to be made during mass spectrometry and bioinformatic analysis.

MS/MS analysis can be optimized to improve the likelihood and efficiency of phosphopeptide fragmentation using a method known as multi-stage activation. In this approach, collision energy conditions are selected to produce neutral loss of phosphoric acid, corresponding to losses of 80 or 98 kDa, and peptide backbone fragmentation [253]. Multi-stage activation increases the quantity and intensity of peptide fragment ions and therefore results in improved sequence coverage and confidence of identification [152, 254].

The fragmentation method used can also improve phosphopeptide fragmentation. ETD and HCD have been proposed as more suitable fragmentation methods for phosphoproteomics as they result in increased phosphopeptide sequence coverage than the

more widely used CID method [153, 209, 255]. The type of instrument used can also affect phosphopeptide fragmentation. It has been shown that CID performed in quadrupoles and linear ion traps produce complementary information and therefore the combination of datasets enhances phosphopeptide identification [158].

Additional consideration must be given during bioinformatic analysis in phosphoproteomic experiments. Such studies not only aim to identify the presence of phosphorylation but also the exact location within the peptide, which is not a trivial task [152, 177]. Serine, threonine or tyrosine account for 16% of the amino acids in the NCBI peptide database, therefore the potential for multiple candidate phosphorylation sites in a single peptide is high [152]. The confident localization of a phosphosite requires the identification of specific diagnostic backbone fragments; i.e. residues with intact phosphate ion and unmodified residues must both be present [152, 256]. When proton mobility is low, i.e. neutral loss most likely, some phosphopeptides may induce a charge-remote cleavage pathway that results in a higher than expected intensity for the C-terminal y-ion of the phosphorylated residue, therefore making it easier to detect [257]. However, during gas phase in MS/MS phosphate groups may be re-arranged and transferred prior to fragmentation leading to false localization [258].

Peptide identification software, such as MASCOT or Sequest, calculates the probability for all the different potential phosphorylation sites and the highest score is the most likely candidate, although not necessarily the correct one. Using Sequest for peptide identification, the A score, which is based on the presence of site-determining ions in the MS/MS spectra, can be used to measure the likelihood that a phosphorylation site localization is correct and when this was tested in a large-scale phosphoproteomics study the false positive rate was found to be 1.3% [259]. Similarly, the MASCOT Delta Score, which is based on the difference between scores for different phosphosite assignments, can be used to identify which phosphosite is the most likely [260]. This approach was reported to be as sensitive and specific as using A score but has the additional advantage that it does not require additional complex computational processing following peptide identification analysis [260]. Musite is a computational tool that was designed to perform large-scale predictions of phosphorylation site localization [261]. Prediction models are trained using phosphoproteomics data from multiple organisms and the programme then uses local

sequence similarities, protein disorder scores and amino acid frequencies to determine phosphorylation sites [261]. An additional consideration for bioinformatic analysis is that several features of phosphorylated peptides can impair the efficiency of trypsin digestion, therefore appropriate consideration should be given to peptides with missed cleavage sites during identification and, if appropriate, quantification [262].

There are also specific considerations to be made with regards to phosphopeptide quantification as there are practical difficulties in obtaining highly reproducible data due to the complexity of many phosphoproteomics workflows [177]. Although much work has been performed in the evaluation of phosphopeptide enrichment methods, an assessment of their practicality for quantitative analysis is often overlooked. Our group has attempted to address this issue and has validated that our optimized TiO_2 affinity chromatography phosphopeptide enrichment method is reproducible and suitable for label-free quantitative phosphoproteomics [179, 232].

1.5. Project aims

As discussed above, the PI3K/Akt pathway has a key role in the regulation of essential cellular functions including cell growth, survival and metabolism. As such, the deregulation of this pathway is implicated in the aetiology of a number of diseases, including cancer. Although investigation into the PI3K/Akt pathway has been extensive there are still a number of questions that remain to be addressed.

Mass spectrometry based proteomics is emerging as an important novel tool for biological research. Mass spectrometry analysis is inherently sensitive, specific, quantitative and, crucially, untargeted. Thus, it enables global scale analysis and discovery investigation that was not previously possible with other methods.

This project aims to apply mass spectrometry to investigate PI3K/Akt signalling from a proteomics standpoint and to answer questions that have not been addressed using traditional molecular biology techniques.

One key area in the field of PI3K/Akt signalling that remains underexplored is the likely role of interacting proteins in the regulation of PI3K activity. Our understanding of protein-protein interactions continues to reveal the importance of this mechanism in the regulation of enzymatic activity [263, 264]. Of particular relevance are the findings that protein-protein

interactions regulate the signalling activity of other kinases, including Erk [265], Akt [266] and mTOR [267, 268]. All p110 isoforms have a Ras-binding domain and activation of class I PI3K by Ras has been demonstrated in a variety of *in vitro* studies [2]; however to date, no further interaction partners with a clear role in the modification of the activity of Class IA PI3Ks have been identified, most likely due to limitations in available technology. In the absence of AP-MS, targeted investigation for interaction partners, requiring prior knowledge, is the only approach to investigate this area. This project aimed to utilise emerging AP-MS techniques to perform an untargeted, unbiased screen to identify dynamic interaction partners of class IA PI3K and to characterise their role in the regulation of this kinase.

Another area in the field of PI3K/Akt signalling that has not been comprehensively investigated is the dynamics of signalling activity downstream of Akt. Although many downstream substrates have been identified it is not clear how the different biological roles dependent on this kinase are mediated. Mass spectrometry based phosphoproteomics enables the global investigation of signalling activity, in contrast to traditional proteomic methods for phosphorylation investigation which are targeted towards pathways for which good phosphospecific antibodies are available. This project aimed to apply global, quantitative phosphoproteomics to investigate signalling events downstream of Akt. For this purpose, we also developed a novel *in vitro* assay for the identification of kinase substrates and broad, untargeted quantification of kinase activity.

2. Materials and Methods

2.1. Antibodies

Table 2.1. Antibody reagents and concentration of experimental use.

Target	Specification	Manufacturer	Product Number	Western Blot (WB) Conc.	Immuno precipitation (IP) Conc.
α-tubulin	Mouse mAb	Sigma-Aldrich	T6074	1:10000	
Akt	Rabbit pAb	Cell Signalling	9272	1:5000	
P-Akt Ser473	Rabbit pAb	Cell Signalling	9271	1:1000	
P-Akt Thr308	Rabbit pAb	Cell Signalling	9275	1:1000	
Akt P-Sub	Rabbit mAb	Cell Signalling	9614	1:1000	1:75
Calpain	Rabbit pAb	Santa Cruz	sc-30064	1:1000	1:100*
Calpain 2	Rabbit pAb	Cell Signalling	2539	1:1000	1:100*
LC3	Rabbit pAb	MBL	PM036	1:1000	
p110α	Rabbit mAb	Cell Signalling	4249	1:1000	
p110α	Rabbit pAb	In-House	SK214+215		1:200
p110β	Rabbit pAb	Santa Cruz	sc-602	1:1000	
p110β	Rabbit pAb	In-House	p110b2.1+2.2		1:100
p110δ	Rabbit pAb	Santa Cruz	sc-7176	1:1000	
p110δ	Rabbit pAb	Abcam	ab1678		1:333
p85	Rabbit pAb	Millipore	06-195	1:10000	1:1000*
p85	Rabbit pAb	Millipore	06-497	1:10000	1:1000*
P-PRAS40 Ser246	Rabbit pAb	Cell Signalling	2640	1:1000	
P-S6 Ser 240/244	Rabbit pAb	Cell Signalling	2215	1:1000	
P-S6K Thr389	Rabbit pAb	Cell Signalling	9202	1:1000	
Total IgG	Rabbit pAb	Sigma-Aldrich	I5006		1:2000
Vinculin	Mouse mAb	Sigma-Aldrich	V9131	1:5000	

*Best IP results obtained when used in conjunction with other antibodies for same target.

2.2. Other materials and reagents

Table 2.2. Other materials and reagents.

Reagent	Manufacturer	Product Number	Use
Nano ACQUITY UPLC BEH C18 Column	Waters	186003546	UPLC
Akt1 (recombinant, active, human)	Millipore	14-276	*In vitro* protein kinase assay.
Aktide (synthetic peptide)	Millipore	123900	Substrate for *in vitro* Akt assay
ALLN (Calpain Inhibitor 1)	Sigma-Aldrich	A6185	Calpain inhibitor
ATP	Sigma-Aldrich	A0770	Substrate for *in vitro* protein kinase assays
[γ-33P] ATP	Perkin Elmer	BLU002001MC	Substrate for *in vitro* PI3K lipid kinase assay
Bradford Reagent	BioRad	500-0205	Protein quantification
Calpain 1 (purified, porcine)	EMD	208712	*In vitro* calpain assay
Calpain 2 (recombinant, rat)	EMD	208718	*In vitro* calpain assay
Calpain Activity Assay Kit, Flurogenic	EMD	QIA120	*In vitro* assay for the measurement of calpain activity
CAPNS1 ON_TARGET plus SMARTpool	Thermo Scientific	L-048840-01-0005	siRNA transfection
CellTiter 96® AQueousNon-Radioactive Cell Proliferation Assay	Promega	G5421	Cell viability assay
Cholera toxin	Sigma-Aldrich	C-8052	Cell culture medium supplement
D030/IC87114	Intellikin	Gift	PI3K p110δ inhibitor
DharmaFECT 1 siRNA Transfection Reagent	Thermo Scientific	T-2001-01	siRNA transfection
DMEM/F12 (1:1)	Invitrogen	11965-118	Cell culture medium

Dulbecco's modified eagle's medium (DMEM)	PAA	E15-843	Cell culture medium
Dynabeads SCX	Invitrogen	105-13D	Aktide assay sample purification
EGF (recombinant, human)	Peprotech	AF-100-15	Cell culture medium supplement and growth factor pathway stimulation
Eppendorf LoBind Microcentrifuge Tubes	Sigma-Aldrich	Z666505	Sample preparation for LC-MS/MS analysis
Foetal bovine serum (FBS)	PAA	A15-104	Cell culture medium supplement
FITC Annexin V Apoptosis Detection Kit II	BD Pharmingen	556570	FACS apoptosis assay
G418 (Geneticin)	Invitrogen	10131019	Cell culture medium supplement - selection
Horse serum	Invitrogen	16050-122	Cell culture medium supplement
Hydrocortisone	Sigma-Aldrich	H-0888	Cell culture medium supplement
Immobilium^{TM}-P	Millipore	IPVH00010	Polyvinylidene fluoride (PVDF) membrane for WB
Insulin	Sigma	I-1882	Cell culture medium supplement and growth factor pathway stimulation
L-α-phosphatidylinositol	Sigma-Aldrich	P2517	PI3K lipid kinase assay substrate
Lambda protein phosphatase	NEB	P0753	*In vitro* protein dephosphorylation
LY294002	Merck	681676	PI3K inhibitor
Microcon YM-10 Filters	Millipore	42421	Filter-aided sample preparation (FASP)
OASIS HLB 1cc Extraction cartridges	Waters	WAT094225	Reverse-phase protein extraction
ON-TARGET plus Non-targeting siRNA #2	Thermo Scientific	D-001810-02-20	siRNA transfection
PD Minitrap Column	GEHealthcare	28-9180-07	Size exclusion protein chromatography
Penicillin/Streptomycin	PAA	P11-010	Cell culture medium supplement

PepClean C18 Spin columns	Thermo Scientific	89870	Reverse phase protein extraction and TiO_2 affinity chromatography
Phosphate buffered saline (PBS)	PAA	H15-002	Cell culture
PI-103	Cayman	10009209	PI3K p110α inhibitor
Propidium Iodide	Sigma-Aldrich	P4864	FACS cell cycle analysis
Puromycin	Sigma-Aldrich	P-8833	Cell culture medium supplement - selection
Ribonuclease A	Sigma-Aldrich	R5125	FACS cell cycle analysis
Roswell Park Memorial Institute medium (RPMI-1640)	PAA	E15-842	Cell culture medium
TGX221	Astra-Zeneca	Gift	PI3K p110β inhibitor
Titansphere TiO_2 beads (10 micron)	Capital HPLC ltd	5020-75010	TiO_2 affinity chromatography
TPCK-Trypsin (immobilized)	Thermo Scientific	20230	In-solution protein digestion
Trypsin (sequence grade)	Promega	V511A	In-gel protein digestion
Trypsin-EDTA	PAA	L11-004	Cell culture
U016	Tocris	1144	MEK inhibitor
Vydac C18 HPLC Column	LC Packing	MBO-15-05-C18P3	HPLC

2.3. Cell culture

All cell handling procedures were performed under a laminar flow hood using aseptic techniques and sterile materials.

2.3.1. Cell Lines

Table 2.3. Immortalized cell lines and corresponding medium.

Cell Line	Cell Type	Species	Growth Medium	Starvation Medium	Comments
IC-21	Peritoneal macrophages	Mouse	RPMI-1640 supplemented with 10% FBS, 100 units/ml Pen/Strep, 1% NaPyruvate, 1% Non-Essential Amino Acids and 50 µM β-mercaptoethanol	N/A	
Kasumi-1	Acute Myeloid Leukaemia (AML)	Human	RPMI-1640 supplemented with 10% FBS, 100 units/ml Pen/Strep and 50 µM β-mercaptoethanol	N/A	
MCF10A	Breast epithelium	Human	DMEM:F12 supplemented with 5% horse serum, 100 units/mL of Pen/Strep, 20 ng/ml EGF, 0.5 µg/ml hydrocortisone, 100 ng/ml cholera toxin and 10 µg/ml insulin.	DMEM:F12 supplemented with 100 units/mL of Pen/Strep	Parental cells and cells stably transfected with the myrAktER construct or control empty vector were used.
NIH-3T3	Embryonic fibroblasts	Mouse	DMEM supplemented with 10% FBS and 100 units/ml Pen/Strep	DMEM supplemented with 100 units/ml Pen/Strep	
P31/Fuj	Acute Myeloid Leukaemia (AML)	Human	RPMI-1640 supplemented with 10% FBS, 100 units/ml Pen/Strep and 50 µM β-mercaptoethanol	N/A	

RAW 264.7	Leukaemic monocytic macrophages	Mouse	DMEM supplemented with 10% FBS and 100 units/ml Pen/Strep	N/A	

2.3.2. Cryopreservation

Cells ($2 \times 10^6 – 8 \times 10^6$) were collected by centrifugation at 1300 rpm for 3 min and re-suspended in 1 ml of 10% Dimethyl sulfoxide (DMSO) in FBS. The cells were then transferred into cryovials, which were placed in isopropanol tanks, and cooled slowly (1^{o}C/min) for 18 h in a -80^{o}C freezer. Cell vials were then transferred to liquid nitrogen tanks (-196^{o}C) for long-term storage. Cells were recovered from liquid nitrogen storage by rapid thawing in a water bath at 37^{o}C. Cells were then transferred to a tissue culture flask and diluted in appropriate growth medium.

2.3.3. Growth maintenance

All cells were grown in humidified incubators kept at 37^{o}C with 5% CO_2. Growth media used for each cell type is described in Table 2.3..

Adherent cells (IC-21, MCF10A, NIH-3T3 and RAW 264.7) were passaged when they reached 80 – 90% confluency. Cells were washed with PBS and detached using 0.05% EDTA-trypsin, before inactivation of the trypsin by addition of growth medium (in a minimum of 5 fold excess to trypsin). Cells were then diluted in growth medium in a fresh tissue culture flask. Suspension cells (Kasumi-1 and P31/Fuj) were maintained between 0.5 and 2×10^6 cells/mL and diluted in growth medium in a fresh tissue culture flask as required.

2.3.4. Seeding for experiments

For adherent cells, cells were washed with PBS and detached using 0.05% EDTA-trypsin, before inactivation of the trypsin by addition of growth medium (in a minimum of 5 fold excess to trypsin). Cells were then counted and seeded at the required density, with fresh growth medium added as required, on tissue culture plates. For suspension cells, cells were counted and collected by centrifugation at 1300 rpm for 3 min. 50×10^6 cells were

then re-suspended in fresh growth medium and seeded at a density of 0.5 x 10^6 cells/mL in fresh tissue culture flasks. All cells were counted using the Innovatis CASY Cell Counter.

2.3.5. Serum-starvation

Serum starvation of cells was carried out by first seeding cells in growth medium at the required density. After 18 h, the cells were washed with PBS and the medium was changed to starvation medium (as indicated in Table 2.3.). Starvation was carried out for 18 h (overnight).

2.3.6. Inhibitor treatments

Table 2.4. Inhibitors and treatment conditions used.

Compound	Target	Treatment Concentration	Treatment Time (h)	Cell Lines Treated
ALLN	Calpain	50 µM	1	NIH-3T3
		10 µM	48	NIH-3T3
D030/IC87114	PI3K p110δ	100 nM	1	NIH-3T3
LY294002	PI3K (pan)	5 µM	1	MCF10A and NIH-3T3
		5 µM	48	NIH-3T3
PI-103	PI3K p110α	10 nM	1	NIH-3T3
TGX221	PI3K p110β	100 nM	1	NIH-3T3
U0126	MEK 1/2	10 µM	1	MCF10A and NIH-3T3

2.3.7. Signalling pathway stimulation

All growth factor mediated signalling pathway stimulations were carried out after 18 h starvation and indicated inhibitor treatments. NIH-3T3 cells were stimulated with 10% FBS and MCF10A cells were stimulated with 100 ng/ml EGF. The Akt signalling pathway was activated in MCF10A myrAktER cells by treatment with 4-hydroxytamoxinfen (4-OHT) as indicated.

2.4. Cell viability assay

CellTiter 96® AQueous Non-Radioactive Cell Proliferation Assay (Promega), or MTS assay, for cell viability was carried out following the manufacturer's instructions. Cells were seeded in 96 well plates at densities of 5 x 10^3 – 2 x 10^4 per well, depending on cell type and assay conditions. After the required period of growth and treatment, 20 µl of MTS-PMS solution was added to each well and the plates were incubated in humidified incubators at 37^{o}C with 5% CO_2 for 1 - 3 h. The reduced reaction product, produced by viable cells, is then quantified by spectrophotometric absorbance at 492 nm using a TECAN plate reader. Where indicated, 96-well plate wells were pre-coated with poly-HEMA by adding 200 µl of sterile poly-HEMA solution (10 mg/ml in ethanol) to each well and leaving on the plates to dry overnight.

2.5. FACS analysis

Fluorescence-activated cell sorting (FACS) analysis was used to investigate cell cycle progression and apoptosis. Cell cycle progression was investigated by using FACS to detect propidium iodide (PI) staining of DNA. 1 x 10^6 cells were collected and washed twice with PBS. The cells were then re-suspended in 70% ethanol and fixed at -20^{o}C for 1 h – 1 week. The cells were then washed again twice with PBS and treated with RNase, prior to DNA staining with PI. PI staining was quantified using blue laser excitation and an emission filter of 695 nm on a BD Fortessa FACS analyzer.

Apoptosis was investigated by using FITC Annexin V Apoptosis Detection Kit II and FACS analysis. Annexin V staining of external phosphatidylserine indicates loss of plasma membrane integrity, an early marker of apoptosis, and PI staining of DNA indicates dead and damaged cells. 1 x 10^6 cells were collected and re-suspended in assay binding buffer. The intact cells were then stained with Annexin V and PI. The dyes were measured using FL3 and FL1 channels on a Dako CyAn ADP FACS analyzer.

2.6. Cell lysate preparation

2.6.1. Cell Lysis

Table 2.5. Lysis buffers and indicated use.

Lysis Buffer Composition	Indicated Use
50 mM Tris HCl (pH 7.4), 150 mM NaCl, 1 mM EDTA and 1% Triton X-100. Supplemented with protease inhibitors (0.05 TIU/mg aprotinin, 10 µM leupeptin, 0.7 mM pepstatin A, 27 µM TLCK, 1 mM DTT and 1 mM PMSF) and phosphatase inhibitors if required (50 mM NaF, 1 mM Na_3VO_4 and 1 µM okadaic acid).	Aktide assay, IP and WB
50 mM Tris HCl (pH 7.4), 150 mM NaCl, 1 mM EDTA and 0.3% CHAPS. Supplemented with protease inhibitors (0.05 TIU/mg aprotinin, 10 µM leupeptin, 0.7 mM pepstatin A, 27 µM TLCK, 1 mM DTT and 1 mM PMSF).	Co-IP
40 mM Tris-HCl (pH 7.4), 1% Triton X-100 and 2.5 mM EDTA. Supplemented with protease inhibitors (0.05 TIU/mg aprotinin, 10 µM leupeptin, 0.7 mM pepstatin A, 27 µM TLCK, 1 mM DTT and 1 mM PMSF) and phosphatase inhibitors (50 mM NaF, 1 mM Na_3VO_4 and 1 µM okadaic acid).	*In vitro* protein kinase assay
8 M urea, 20 mM HEPES (pH 8.0) Supplemented with phosphatase inhibitors (1 mM Na_3VO_4, 1 mM NaF, 2.5 mM $Na_4P_2O_7$, 1mM ß-glycerol-phosphate).	Phosphoproteomics

Adherent cells were lysed directly on tissue culture plates and suspension cells were collected by centrifugation at 1300 rpm for 3 min prior to lysis. Plates or tubes were kept on ice throughout the procedure. Cells were washed twice with ice-cold PBS, supplemented with phosphatase inhibitors (1 mM $NaVO_4$ and 1 mM NaF) for phosphoproteomic experiments. Lysis buffer, as required for subsequent investigation (Table 2.5.), was then added to the cells. Adherent lysed cells were then scraped and collected into tubes. Cell lysates were vortexed, or for phosphoproteomic experiments sonicated, and incubated on ice for 30 minutes. Soluble proteins were then clarified by centrifugation at 13,000 rpm for 10 min at 4^{o}C.

2.6.2. Determination of protein concentration

Protein concentration was determined using the Bradford assay. Lysis buffer was used as a blank sample and BSA solutions of 0.5, 1.25, 2.5 and 5 µg/µl were used to construct a calibration curve. All blank, calibration standard and analytical samples were dispensed into

wells on a 96-well plate and 200 µl of Bradford reagent was added. The colour change produced by the binding of Coomassie Brilliant Blue G-250 to protein in the sample was then measured by spectrophotometric absorbance at 595 nm on a TECAN plate reader. A calibration curve was constructed using the known standards and linear regression was used to calculate the protein concentration of samples.

2.7. Immunoprecipitation (IP)

Cell lysates were pre-cleared by incubation with 10-50 µl of Protein G Sepharose, which had previously been washed 3 times in lysis buffer, for 2 h at 4^{o}C with mixing. Samples were then centrifuged at 2000 rpm for 1 min and the cleared sample retained. The required antibodies were added (see Table 2.1. for details of concentrations used) and the samples incubated for 2 - 18 h at 4^{o}C with mixing. 15 – 50 µl of washed Protein G Sepharose were then added and samples incubated for a further 2 h at 4^{o}C with mixing. Samples were then centrifuged for 1 min and the beads retained and washed 5 times with lysis buffer. The beads were then re-suspended in the appropriate buffer for subsequent analysis.

2.8. SDS-PAGE

5 x Sample Buffer (156.25 mM Tris HCl pH 6.8, 5% SDS, 25% glycerol, 0.0025% bromophenol blue and 250 mM DTT) was added to total cell lysate and IP protein samples (minimum 1:5 dilution). Proteins were then denatured by incubation at 100^{o}C for 5 min and separated by size using sodium dodecyl sulphate-polyacrylamide gel electrophoresis (SDS-PAGE).

8 – 15% acrylamide SDS-PAGE gels (acrylamide as indicated, 375 mM Tris pH 8.8, 0.1% SDS, 0.1% ammonium persulphate) were cast between 10 x 8 cm glass plates, with a gel thickness of 1.5 mm, or between 20 x 22 cm plates, with a gel thickness of 3 mm. Once the gel had polymerized, a layer of stacking gel (5% acrylamide, 375 mM Tris pH 8.8, 0.1% SDS, 0.1% ammonium persulphate) was also cast using a comb to produce sample wells. The gels were transferred to tanks containing running buffer (0.025 M Tris, 0.192 M glycine, 0.1% SDS (pH 8.3.)) and samples loaded into the wells. Electrophoresis was then performed at 60 V or 15 min and 100 – 120 V for 2 h for mini-gels or 50 V overnight for large gels.

2.8.1. Western blotting

For WB analysis, separated proteins were transferred onto Immobilium^{TM}-P polyvinylidine fluoride (PVDF) membranes using electroblotting. The PVDF membrane was activated by incubation in ethanol for 1 min. The membrane and gel were then equilibrated in transfer buffer (48 mM Tris-HCl (pH 8.5.), 0.39 M glycine, 0.1% SDS, 20% ethanol). For "wet" transfer the membrane and gel were sandwiched between two sponges and two pieces of Whatman 3 mm paper (also pre-equilibrated in transfer buffer). The case was then placed in a blotting tank filled with transfer buffer (anode>protection>membrane>gel>protection>cathode) and electroblotting was performed at 75 V for 1.5 h or 100 V for 1 h at 4^{o}C. For "semi-dry" transfer using the BioRad Trans-Blot Turbo Blot System, the membrane and gel were sandwiched between four pieces of Whatman 3 mm paper (also pre-equilibrated in transfer buffer) directly upon the anode (anode>filter>membrane>gel>filter>cathode). Excess buffer was absorbed and transfer was performed at 25 V for 30 min.

Following electroblotting, the membranes were then blocked by incubation with 5% milk in TBS-T (Tris-buffered saline (TBS; 0.15 M NaCl, 0.05 M Tris-HCl (pH 7.6.)) supplemented with 0.1% Tween-20) for 30 min. The membranes were then incubated overnight at 4^{o}C with primary antibody (primary antibodies prepared in 5% BSA, 0.05% NaN_3, TBS-T; see Table 2.1. for details of concentrations used). After primary antibody incubation, the membranes were washed with TBS-T for 3 x 5 min prior to incubation with secondary antibody (anti-rabbit or anti-mouse Ig conjugated to horseradish peroxidase; prepared in 5% milk, TBS-T) for 1 h at room temperature. Membranes were then washed again with TBS-T for 3 x 5 min. Antibody binding was visualized using X-ray film after membrane incubation with homemade electro-chemiluminescence (ECL) reagent (20 mM Tris-HCl (pH 8.5.), 0.0096% H_2O_2, 0.1 mM coumaric acid, 0.75 mM 3-aminophtalhydrazide) for 2 – 3 min.

2.8.2. Colloidal Coomassie blue staining

To visualize separated proteins, SDS-PAGE gels were stained using Colloidal Coomassie blue G-250. Gels were first fixed by incubation with 50% ethanol with 2% phosphoric acid for 3 – 18 h at room temperature. The gels were then washed for 3 x 30 min in H_2O and

equilibrated in 34% methanol, 17% ammonium sulphate and 3% phosphoric acid for 30 min. 0.5% (w/v) Colloidal Coomassie Blue G-250 was then added and gels were stained for 18 h. Following staining, the gels were washed in H_2O and de-stained using 35% methanol, 7.5% acetic acid if required.

2.9. *In vitro* calpain activity assay

Calpain activity was measured using a Flurogenic Calpain Activity Assay Kit following the manufacturer's instructions. Total cell lysate (50 µl) or IP (from 1 mg starting protein) protein samples were incubated with a synthetic peptide substrate in the presence of a Ca^{2+}-containing reaction buffer for 15 min at room temperature. Cleavage of the peptide by calpain present in the sample results in the release of an AMC fluorophore, the abundance of which was detected fluorometrically using a FLUOstar OPTIMA plate reader, with an excitation filter of 350 nm and an emission filter of 450 nm.

2.10. *In vitro* PI3K lipid kinase assay

PI3K activity in IP protein samples was measured using an *in vitro* lipid kinase assay [269]. Samples were incubated with 10 µl L-α-phosphatidylinositol (PI) lipid substrate in the presence of 10 µl [γ-^{33}] ATP and 20 µl kinase assay buffer (20 mM Tris-HCl (pH 7.4.), 200 mM NaCl, 1mM EDTA) for 30 – 60 min at room temperature with mixing. The reaction was then stopped by the addition of 100 µl of 1 M HCl.

Phospholipids were then extracted by vigorous vortexing with 200 µl of chloroform:methanol (1:1) followed by retention of the organic (lower) layer. 80 µl of methanol:1M HCl (1:1) was then added to the sample, which was vortexed again, followed by retention of the phospholipid-containing organic (lower). Thin layer chromatography (TLC), developed in 65% propanol-1, 2% acetic acid, was then performed and PIP_3, the lipid product of PI3K, was detected using autoradiography of the TLC plate using a STORM Imaging System.

2.11. *In vitro* "Aktide" assay

Akt protein kinase activity in total cell lysate protein samples was measured using the "Aktide" assay [270, 271], in which Akt active in the sample phosphorylates a synthetic

substrate peptide, which is subsequently quantified by LC-MS. A volume of 2.5 µl of total cell lysate were mixed with 5 µl of reaction mix (150 µM Aktide (peptide sequence: RPRAATF), 4 mM Tris (pH 7.4.), 0.2 mM $NaVO_4$, 5 mM β-glycerol-phosphate, 15 mM $MgCl_2$, 0.15 mM ATP) and incubated at 37^{o}C for 10 min with shaking. The reaction was stopped by the addition of 100 µl of 0.05 µM internal standard (IS) peptide (RP*RAApTF, where P* designates isotopically labelled heavy L-proline ($^{13}C_5$, ^{15}N)) in 20% acetonitrile (ACN), 0.1 % trifluoroacetic acid (TFA).

Substrate and IS peptides were then extracted by strong cation exchange as follows. Samples were incubated with 10 µl of Dynabeads SCX in loading solution (25% ACN, 0.1% TFA, 0.01% Tween-20) for 45 min at room temperature. The beads were then washed twice with loading solution and once with wash solution (25% ACN, 0.1% TFA) before peptides were eluted by incubation with 20 µl of 150 mM Ammonium Bicarbonate (AmBic), 5% ACN, 0.1% TFA for 10 min at room temperature. The eluents were then dried under vacuum at room temperature using a CHRIST Rotational Vacuum Concentrator and stored at -20^{o}C until analysis.

Selected Reaction Monitoring (SRM) analysis was performed on a Thermofisher TSQ-Vantage (see 2.14.2. and 2.15.3. for details of instrument operation). The peak areas of the product fragment ion transitions of the Aktide peptide (parent ion mass to charge ratio (m/z) = 449.767, product fragment ion m/z = 400.685) and IS peptide (parent ion m/z = 452.772, product fragment ion m/z = 403.699) were quantified. Sample Akt activity was expressed as the ratio of Aktide peak intensity to IS peak intensity. Aktide quality control samples of low (50 nM) and high (500 nM) concentrations were analyzed with each sample batch to assess instrument performance.

2.12. *In vitro* protein kinase assay

2.12.1. Akt1 protein kinase activity assay

An *in vitro* assay, which uses intact dephosphorylated proteins as the reaction substrate, was designed to evaluate Akt1 protein kinase activity. Total cell lysate was harvested as described in 2.6.1. and subjected to a protein dephosphorylation treatment. To perform size exclusion chromatography, the lysate was loaded onto Sephadex G-25 columns

and proteins were eluted with 40 mM Tris-HCl (pH 7.0), 1 mM DTT, 0.1 mM EGTA, 0.1% Triton X-100, thus depleting the lysate of small molecules (including ATP). The lysate was then incubated at 30^{o}C for 20 minutes to allow endogenous phosphatases to de-phosphorylate proteins [272]. Protease inhibitors (0.05 TIU/mg aprotinin, 10 µM leupeptin, 0.7 mM pepstatin A, 27 µM TLCK, 1 mM DTT and 1 mM PMSF) and phosphatase inhibitors (50 mM NaF, 1 mM Na_3VO_4 and 1 µM okadaic acid) were then added to the dephosphorylated lysate and total protein concentration was re-quantified (see 2.6.2.).

In an alternative approach, the lysate was dephosphorylated using exogenous lambda protein phosphatase. Total cell lysate was harvested omitting EDTA and phosphatase inhibitors from the lysis buffer. Lambda protein phosphatase, in activating buffer containing 1 mM $MnCl_2$, was then added to the lysate, at a concentration of 10,000 units per mg of protein in lysate, and the mixture was incubated at 37^{o}C for 1 h. Size exclusion chromatography was performed, protease and phosphatase inhibitors were added to the dephosphorylated lysate and total protein concentration was re-quantified, as described above.

Following dephosphorylation treatment, lysate containing 500 µg of protein was diluted 1:1 in 2 x reaction buffer to reach a final concentration of 50 mM Tris-HCl (pH 7.5), 1 mM EGTA, 1 mM DTT, 10 mM $MgCl_2$ and ATP as indicated (0 - 500 µM) [273]. Recombinant, active protein kinase Akt1 was then added, as indicated, and the mixture was incubated at 30^{o}C for 5 min. The reaction was stopped by the addition of solid urea to a final concentration of 8 M. The samples were then subjected to in-solution trypsin digestion (see 2.13.1.4) and phosphopeptide enrichment (see 2.13.2) prior to LC-MS/MS analysis for phosphopeptide identification and quantification (see 2.14.1., 2.15.2. and 2.16.1. for details).

2.12.2. Endogenous protein kinase activity assay

An *in vitro* assay, which uses intact native proteins as the reaction substrate, was designed to investigate the endogenous protein kinase activity of cell lines. Total cell lysate was harvested as described in 2.6.1., omitting EDTA from the lysis buffer. Lysate containing various concentrations of protein, 5 – 500 µg, was then diluted 1:1 in 2 x reaction buffer to reach a final concentration of 50 mM Tris-HCl (pH 7.5), 1 mM EGTA, 1 mM DTT, 10 mM

$MgCl_2$ and ATP as indicated (0 - 500 μM). The mixture was then incubated at 30°C for 5 min and the reaction was stopped by the addition of urea to a final concentration of 8 M. The samples were then subjected to in-solution trypsin digestion (see 2.13.1.4) and phosphopeptide enrichment (see 2.13.2) prior to LC-MS/MS analysis for phosphopeptide identification and quantification (see 2.14.1., 2.15.2. and 2.16.1. for details).

2.13. Preparation of samples for LC-MS/MS analysis

2.13.1. Trypsin digestion

Prior to LC-MS/MS analysis all protein samples were subjected to protease digestion using trypsin. The method used was dependent on sample type and is specified for each experiment. Lo-Bind Eppendorf tubes were used throughout sample processing to minimize the loss of peptides due to binding to plastic surfaces.

2.13.1.1. In-gel digestion

In-gel digestion was used to digest proteins following SDS-PAGE (see 2.8.). Once proteins were visualized by Colloidal Coomassie Blue staining (see 2.8.2.), the individual sample lanes were cut out from the gel and split into 5 -10 fractions, which were the same across all the samples. Each gel piece was then cut up into small pieces, of around 1 mm^2, and collected into a tube for trypsin digestion. The gel pieces were washed 3 times with 50% methanol and once with 100% methanol and dried under vacuum at room temperature using a CHRIST Rotational Vacuum Concentrator. Proteins were then reduced, by incubation with 10 mM DTT in 25 mM AmBic (pH 8.0) at 50°C for 45 min, and alkylated, by incubation with 50 mM iodoacetamide (IAM) in 25 mM AmBic (pH 8.0) in the dark for 1 h. The gel pieces were then washed twice with 50% methanol and dried again. 100 – 500 ng of sequence-grade trypsin in 25 mM AmBic (pH 8.0; quantity dependent on protein content of gel piece but in a minimum ratio of 1:50 trypsin:protein) was then added to each sample, which was then incubated at 37°C for 18 h with mixing. Peptides were then extracted from the gel pieces by sequential elution with 50% methanol, 1% formic acid (FA) and 100 mM AmBic (pH 8.0.). The gel extracts were pooled, dried under vacuum at room temperature

using a CHRIST Rotational Vacuum Concentrator and stored at -20^{o}C. Dried peptide samples were re-constituted in 10 – 15 µl 0.1% TFA immediately prior to LC-MS/MS analysis.

2.13.1.2. In-tube gel polymerization and in-gel digestion

Protein samples were denatured as described for SDS-PAGE (see 2.8.). 100 µl of denatured protein sample was then incorporated into a polyacrylamide gel in a tube by the addition of 51 µl of acrylamide (30%), 5 µl ammonium persulphate (10%) and 2 µl of TEMED [274]. In-gel protein digestion was then performed as described previously.

2.13.1.3. Filter-aided sample preparation (FASP)

Filter-aided sample preparation (FASP) was performed as described by Wisniewski *et al* [142]. Protein samples were denatured in 4% SDS, 0.1 M DTT, 100 mM Tris-HCl (pH 7.6) and loaded onto a Microcon YM-10 10 kDa filter unit, which retains proteins greater than 10 kDa in size upon centrifugation at 14,000 x g. Proteins were then washed with 8 M urea, 0.1 M Tris-HCl (pH 8.5) and alkylated by incubation with 0.05 M IAM in 8 M urea, 0.1 M Tris-HCl (pH 8.5) for 20 min at room temperature. The proteins were then sequentially washed with 8 M urea, 0.1 M Tris-HCl (pH 8.5) and 50 mM AmBic (pH 8.0) and incubated with sequence-grade trypsin in 25 mM AmBic (pH 8.0; quantity dependent on protein amount but in a minimum ratio of 1:50 trypsin:protein) for 18 h at 37^{o}C in a wet chamber. Peptides were eluted by the addition of 50 µl of 0.5 M NaCl and centrifugation at 14,000 x g for 20 min.

The resulting peptide solutions were then desalted and concentrated by solid-phase extraction using PepClean C18 spin columns. Sample buffer was added 1:4 to reach a final concentration of 5% ACN, 0.5% TFA and the solutions were loaded onto columns, which were pre-washed with 50% methanol followed by 5% ACN, 0.5% TFA. The columns were centrifuged at 2,000 rpm for 1 min to allow peptide binding. The columns were then washed twice with 5% ACN, 0.5% TFA and peptides were eluted with 20 µl of 50% ACN, 0.1% TFA. Peptide solutions were then dried under vacuum at room temperature using a CHRIST Rotational Vacuum Concentrator and stored at -20^{o}C. Dried peptide samples were re-constituted in 10 – 15 µl 0.1% TFA immediately prior to LC-MS/MS analysis.

2.13.1.4. In-solution digestion

Protein samples were lysed or denatured in 8 M urea in 20 mM HEPES (pH 8.0). Proteins were then reduced, by incubation with 10 mM DTT for 15 min at room temperature in the dark, and alkylated, by incubation with 16.6 mM IAM for 15 min at room temperature in the dark. The samples were then diluted 1 in 4 with 20 mM HEPES, to reduce the urea concentration to < 2M, and incubated with immobilized TLCK-trypsin for 18 h at 37^{o}C with mixing. Trypsin was inactivated by the addition of TFA to 1% of the final digest volume and the beads were discarded.

The resulting peptide solutions were then de-salted and concentrated by solid-phase extraction using OASIS HLB 1cc Extraction cartridges. The cartridges, which were in a vacuum manifold at pressure <20 inHg, were washed with 100% ACN and equilibrated with 2% ACN, 0.1% TFA. The peptide samples were then loaded onto the column and subsequently washed with 2% ACN, 0.1% TFA. Peptides were then eluted in 500 µl of 1M glycolic acid, 80% ACN, 5% TFA. Peptide solutions were then subjected to phosphopeptide enrichment, using TiO_2 affinity chromatography (see 2.13.2.), or dried under vacuum at room temperature using a CHRIST Rotational Vacuum Concentrator and stored at -20^{o}C. Dried peptide samples were re-constituted in 10 – 15 µl 0.1% TFA immediately prior to LC-MS/MS analysis.

2.13.2. Phosphopeptide enrichment: TiO_2 affinity chromatography

TiO_2 affinity chromatography was used to enrich peptide samples for phosphopeptides as described by Montoya *et al* [232]. PepClean C18 spin columns were used as a solid phase support during TiO_2 Affinity Chromatography. Peptides, in solution in 1M glycolic acid, 80% ACN, 5% TFA following solid-phase extraction de-salting, were incubated with Titansphere TiO_2 beads (10 µm) for 5 min at room temperature with mixing. The samples were then loaded onto the columns, which were pre-washed with 1M glycolic acid, 80% ACN, 5% TFA. TiO_2-bound peptides were then washed sequentially with 1M glycolic acid, 80% ACN, 5% TFA; 50% ACN and 50% ACN, 20 mM ammonium acetate (pH 6.8). TiO_2-bound peptides were then eluted three times with 50 µl 50% ACN, 5 % NH_4OH (pH 11.0). The TiO_2 eluents were pooled and acidified by the addition of FA to a final sample volume of 10%. The peptide samples were then dried under vacuum at room temperature using a CHRIST

Rotational Vacuum Concentrator and stored at -20^{o}C. Dried peptide samples were re-constituted in 10 – 15 µl 0.1% TFA immediately prior to LC-MS/MS analysis.

2.14. Liquid chromatography

2.14.1. Ultra performance liquid chromatography (UPLC)

The Waters Micromass Q-TOF Premier and ThermoFisher LTQ-Orbitrap XL mass spectrometers were coupled to Waters NanoAcquity UPLC systems. Peptide separations were performed using a Waters BEH130 (Ethylene Bridged Hybrid) C18 reverse-phase column (inner diameter = 100 µm, length = 100 mm, particle size = 1.7 µm, pore size = 300 Å). 4 µl of sample were loaded at a flow rate of 2 µL/min for 8 min followed by a gradient elution at 400 nL/min, during which the instrument operated with a back pressure of around 3,000 psi. Gradient elution was from 99% A (A = 0.1% FA in LC-MS grade H_2O), 1% B (B = 0.1% FA in LC-MS grade ACN) to 65% A, 35% B in 45 or 100 min, followed by a 10 min wash at 15% A, 85% B and a 10 min equilibration step at 99% A, 1% B.

2.14.2. High performance liquid chromatography (HPLC)

The ThermoFisher TSQ-Vantage was coupled to a ThermoFisher Accela LC system. Peptide separations were performed using a Vydac C18 reverse-phase column (inner diameter = 0.8 mm, length = 150 mm, particle size = 5 µm, pore size = 300 Å). 10 µl of sample were loaded at a flow rate of 480 µL/min followed by a gradient elution at 200 µL/min, during which the instrument operated with a back pressure of around 200 bar. Gradient elution was from 99% A (A = 0.1% FA in LC-MS grade H_2O), 1% B (B = 0.1% FA in LC-MS grade ACN) to 65% A, 35% B in 6.5 min, followed by a 5 min wash at 99% A, 1% B.

2.15. Mass spectrometry analysis

2.15.1. Waters Micromass Q-TOF Premier mass spectrometer

The Waters Micromass Q-TOF Premier is a quadrupole-TOF hybrid instrument (Fig. 2.1.).

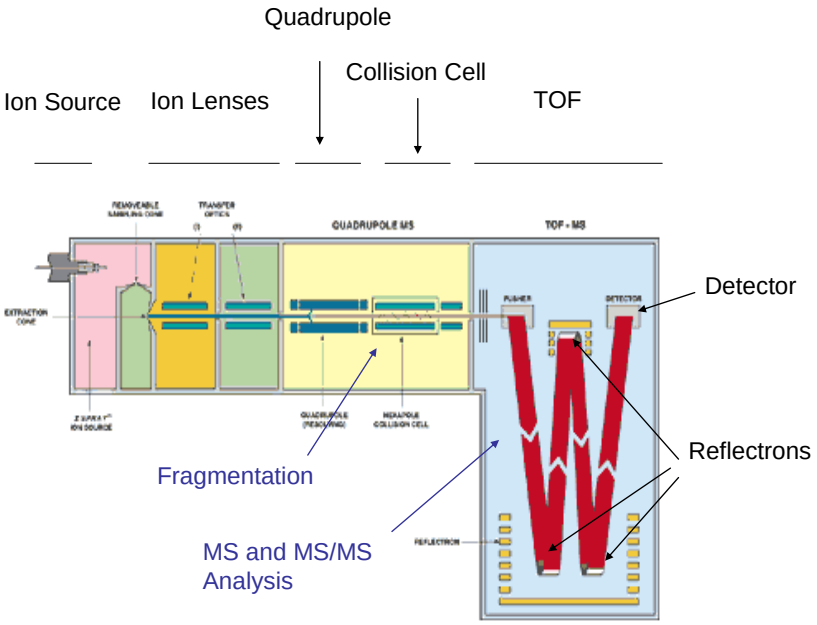

Figure 2.1. Schematics of the ion optics of the Waters Micromass Q-TOF Premier (Image reproduced from Operator User Manual).

This instrument type was specifically designed for the purpose of biomolecule sequencing [275]. As peptides are eluted from the UPLC system they are subjected to electrospray ionization and directed into the mass spectrometer. Ion lenses direct the flow of gas phase ions into the quadrupole analyzer, which consists of 4 parallel metal rods. Each pair of rods is connected electrically and a current is applied between them, creating an electrical field in the centre of the analyzer. This electrical field can be manipulated to direct all ions or only ions with a selected m/z through the analyzer. The quadrupole is followed by a hexapole gas collision cell, which can be used to fragment ions by bombardment with neutral gas molecules in a process known as collision induced disassociation (CID). The TOF analyzer, which follows, uses a high voltage pulse to accelerate the ions down the flight tube towards the detector, whereby they separate as ions with different m/z travel at different speeds. The incorporation of two reflectrons, which are metal plates, allows the beam of ions to traverse the flight tube twice and increases resolution by correcting the kinetic energy distribution of the different ions and by increasing the flight path length. A micro-channel plate at the end of the flight path detects the ion separation.

Quantitative data was obtained using MS mode. In this mode, the quadrupole and collision cell function to focus the stream of ions into the time of flight analyzer (TOF), where the peptide ions are separated according to m/z ratio before detection. Qualitative analysis was obtained using data directed acquisition (DDA) mode, which combines MS and MS/MS analysis. In MS/MS analysis, peptide ions of interest are selected for by the quadrupole and directed to the collision cell, where they are fragmented by CID. The fragment ions are then separated by the TOF analyzer before detection. In DDA, the instrument switches between MS and MS/MS modes depending on the ions detected by the MS scan.

In the DDA method used, a full MS survey scan (m/z 350 – 1800; Fig. 2.2. A) was performed every 0.5 s and if ions of interest, i.e. multiply charged ions likely to be peptides, were detected the 3 most abundant were automatically mass-selected and fragmented in the quadrupole (collision energy 35 V) prior to MS/MS analysis in the TOF analyzer (m/z 50 – 2000; Fig 2.2. B). The length of time the instrument takes to complete an MS survey scan and any required MS/MS scans is known as the duty cycle, which for the DDA cycle used was around 3.5 s. Due to the length of the duty cycle of the Q-TOF, this DDA method is not advisable for the acquisition of quantitative data as the most intense parent ion signal may be missed between MS scans.

A. MS Scan

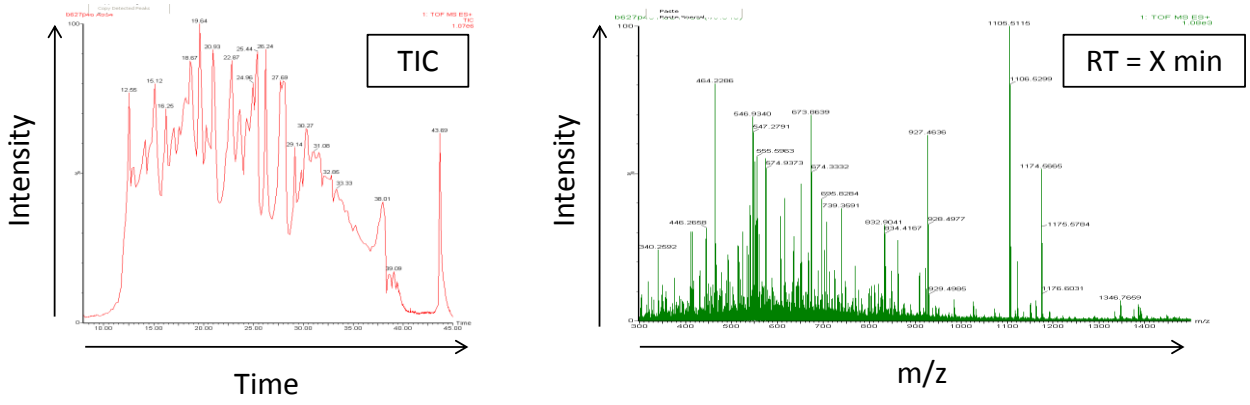

B. MS/MS Spectrum

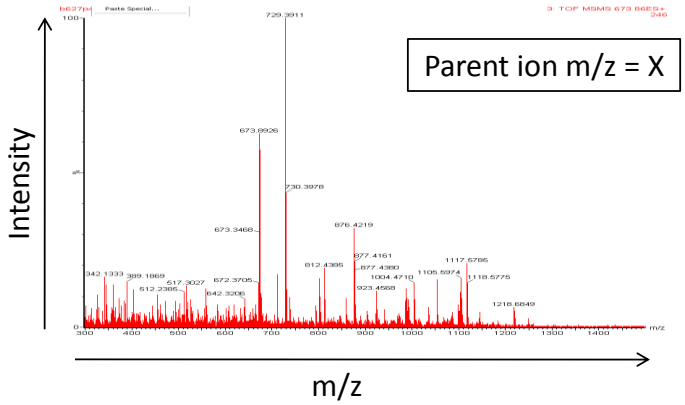

Figure 2.2. Illustration of Waters Micromass Q-TOF Premier data output.
A. Examples of a total ion chromatogram (TIC) and an MS survey scan taking at a given retention time (RT). B. Example of an MS/MS spectrum for a parent ion with a given m/z.

2.15.2. ThermoFisher LTQ-Orbitrap XL mass spectrometer

The ThermoFisher LTQ-Orbitrap XL is a linear (2D) quadrupole ion trap (LTQ) and orbitrap hybrid instrument (Figure 2.3.).

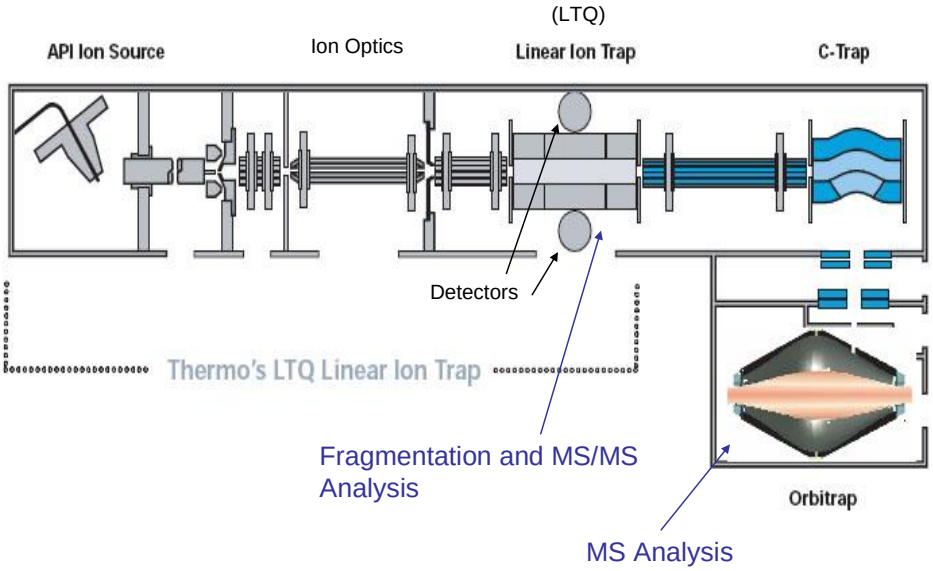

Figure 2.3. Schematic of the ion optics of the ThermoFisher LTQ-Orbitrap XL (Image taken from Operator User Manual)

In this instrument the orbitrap functions as a high accuracy and high resolution mass detection system and the LTQ carries out ion selection and fragmentation. As peptides are eluted from the UPLC, they are subjected to electrospray ionization and directed into the mass spectrometer. The ion optics focus the stream of gas phase ions and direct them into the LTQ, which consists of a triple-sectored hyperbolic rod quadrupole. Voltages are applied to the rods creating an electrical field that can be manipulated to trap ions axially and radially [276], i.e. they cannot exit and orbit within the trap at a frequency determined by their m/z. One function of the LTQ is to collect a required number of ions before sending them to the orbitrap for mass analysis. The c-trap is an important element of this process as it ensures that the ions efficiently transfer to the orbitrap. The LTQ can also select ions of interest by sequentially ejecting all other ions from the trap by manipulation of the electrical field. In addition, the LTQ functions as a collision cell, permitting CID of selected ions. Ions for detection are ejected laterally from the LTQ and detected by a conversion dynode coupled to an electron multiplier.

The orbitrap consists of a central, spindle-shaped, electrode, around which the ions oscillate at a frequency determined by their m/z, and an outer electrode, which creates an electrostatic field with the central electrode. The orbitrap derives the m/z of an ion based on the frequency of its oscillations along the axis of the central electrode [277], which is measured by a Fourier transform.

In MS mode, packets of ions are collected by the LTQ and sent to the orbitrap, via the c-trap, for high accuracy and high resolution mass analysis. In MS/MS mode, ions of interest, i.e. multiply charged ions likely to be peptides, are isolated by the LTQ and fragmented there by CID. The fragment ions are then sequentially ejected from the LTQ and detected. In DDA, the instrument switches between MS and MS/MS modes depending on the ions detected in the MS survey scan.

In the DDA method used, a full MS survey scan (m/z 375 – 1800) was performed at resolution of 30,000 at m/z = 400. If any multiply charged ions of interest were detected, the 5 most abundant were automatically mass-selected, fragmented by CID (normalized collision energy 35%) and analyzed by MS/MS in the LTQ (m/z 50 – 2000; Fig. 2.4. A). Multistage activation, which enhances peptide backbone fragmentation, was used for phosphoproteomic experiments. Dynamic exclusion was enabled, thereby excluding the repeat analysis of the same ion, with the exclusion list restricted to 500 entries, exclusion duration of 40 s and mass window of 10 ppm. Unlike the Q-TOF, the orbitrap performs MS and MS/MS scans in separate analyzers and therefore can move more rapidly between these functions as there is no requirement to wait for the orbitrap to empty before commencing MS/MS scans. As scans are faster and the instrument can move before functions more rapidly, the duty cycle of the DDA method used was around 2 s, therefore quantitative MS and qualitative MS/MS data was obtained from a single analysis. An additional advantage over the Q-TOF analyzer is that the MS and MS/MS data obtained from the LTQ-Orbitrap has a higher degree of mass accuracy and resolution.

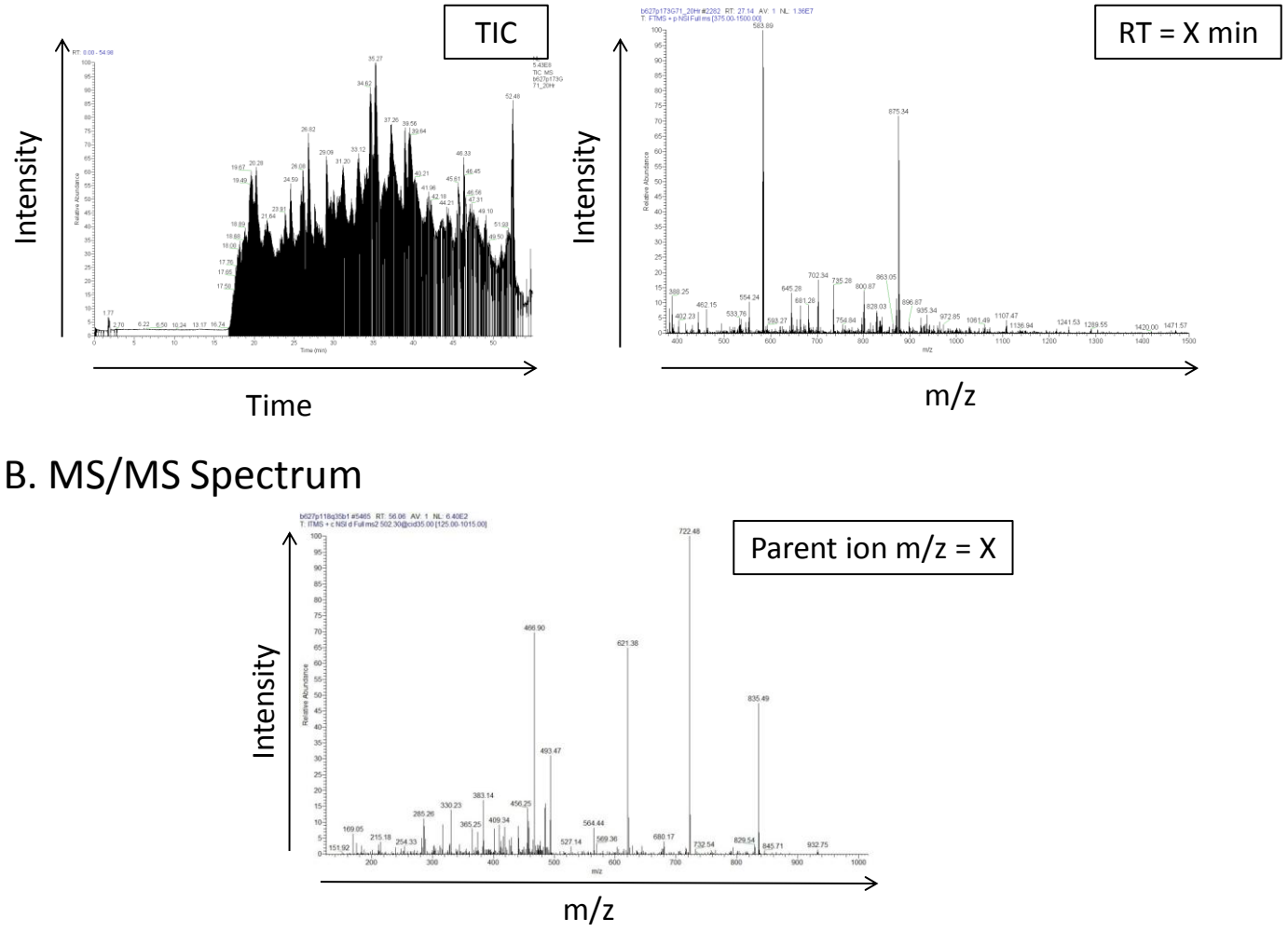

Figure 2.4. Illustration of ThermoFisher LTQ-Orbitrap XL data output.
A. Examples of a total ion chromatogram (TIC) and an MS survey scan taking at a given retention time (RT). B. Example of an MS/MS spectrum for a parent ion with a given m/z.

2.15.3. ThermoFisher TSQ-Vantage mass spectrometer

The ThermoFisher TSQ-Vantage is a triple stage quadrupole mass spectrometer (Fig. 2.5.), an instrument that is optimal for high sensitivity quantitative analysis of peptides and small molecules, e.g. metabolites and drugs.

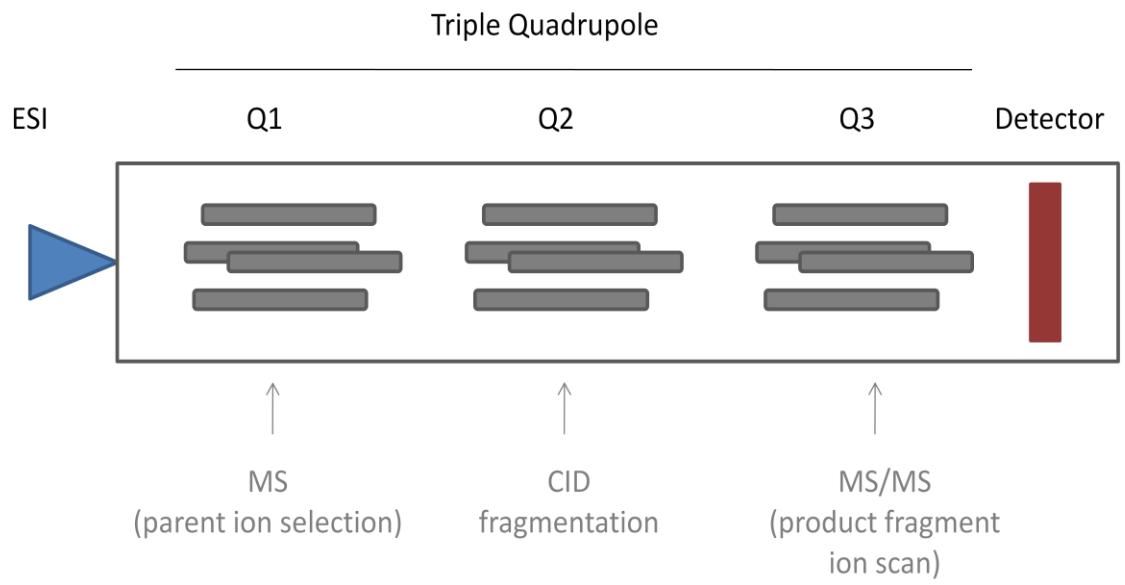

Figure 2.5. Schematic of a typical triple quadrupole instrument.

As peptides are eluted from the HPLC system they are subjected to electrospray ionization and directed into the analyzer. Each quadrupole consists of 4 parallel metal rods that are connected electrically and a current is applied between them, creating an electrical field in the centre of the analyzer. Ion lenses direct the flow of ions into the first quadrupole analyzer (Q1), where the electrical field can be manipulated to direct all ions or only ions with a selected m/z through the analyzer. The flow of ions is then directed into Q2, which functions as a gas collision cell where ions are fragmented by CID. Finally, Q3 acts as a second ion filter directing the required ions towards the electron multiplier detector.

This triple quadrupole instrument was coupled to a HPLC system and used for the SRM analysis of small peptides produced by the Aktide assay (see 2.11.). Parent ions were selected in Q1 and directed to Q2, where they were fragmented by CID (collision energy = 16/17 V). Q3 was then used as a second ion filter to direct selected product fragment ions towards the detector (Fig. 2.6.).

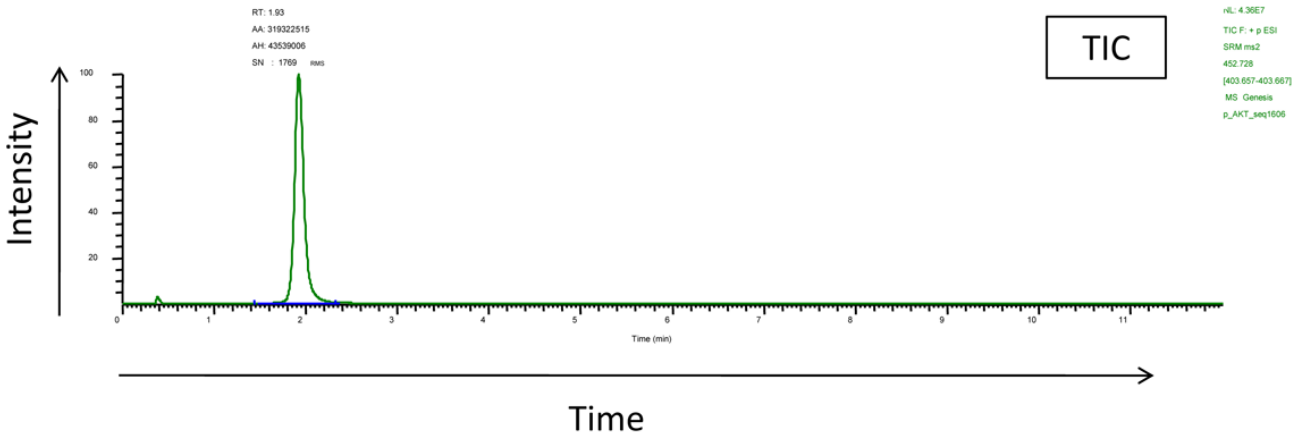

Figure 2.6. Illustration of ThermoFisher TSQ-Vantage SRM data output.
TIC showing the peak of the product fragment ion of a given parent ion, as selected by Q3.

2.16. Data analysis

2.16.1 Mass spectrometry data analysis

MassLynx (Waters) and XCalibur (ThermoFisher) software were used to view mass spectrometry data. ProteinProspector was used in conjunction with XCalibur for the manual verification of MS/MS data. XCalibur was also used for the quantification of ion peaks for Aktide SRM analysis (see 2.11. and 2.15.3.) and to manually verify peptide quantifications derived by other methods.

Mascot Daemon (v2.2.2; Matrix Science, London, UK) was used to automate the analysis of data. This software automates the use of Mascot Distiller (v2.3.2.), to smooth and centroid the MS/MS data, and Mascot search engine (v2.2.02), to search the processed files against all entries in the peptide sequence library of the IPI Mouse database (ipi.MOUSE.v3.56.fasta) or the human Swiss Prot database (downloaded on 03/03/2010 containing 23000 entries) [156]. For LTQ-orbitrap data search parameters included: enzyme, trypsin; number of missed cleavages permitted, 2; fixed modification, Carbamidomethyl (C); variable modifications, Gln->pyro-Glu (N-term Q), Oxidation (M), Phospho (ST), Phospho (Y); mass tolerance for precursor ions, 8 ppm; mass tolerance for fragment ions, 0.8 Da. The data output includes the identification of the peptide (amino acid sequence), parent protein m/z, RT and confidence scores for these identifications based on probability [156]. Peptide

hits were considered significant when they had an Expectation value < 0.05 (as returned by Mascot) and protein scores were considered significant if they had a MASCOT score > 40, with a minimum of three peptides identified. Phosphorylation site assignments were made by MASCOT using the Delta score to determine confidence.

Peptides and proteins were quantitated using Pescal (Peak Statistic Calculator), a software created by Dr Pedro Cutillas [159] that automates the generation of extracted ion chromatograms (XIC) and subsequent quantification of peak height and area. Pescal was used to extract the chromatographic peaks for the first three isotopes of a given peptide from MS data using m/z, retention time (RT) and isotopic charge distribution information derived from the MS scan and MS/MS spectrum (Fig. 2.7.). The restrictions of an m/z window of 7 ppm, RT window of 2 – 5 min (dependent on gradient length) and a coefficient of variation >0.95 between the observed and theoretical isotope distribution were used to ensure the quantification of the correct peak. Peak height and area quantification data was parsed into Excel for normalization and further analysis. Peptide intensities were normalized to the total ion chromatogram intensity for each sample. For protein quantitation, peptide abundance data was averaged to give an estimation of protein abundance. Quantitative data from experimental samples were compared using the Student's t-test function in Excel.

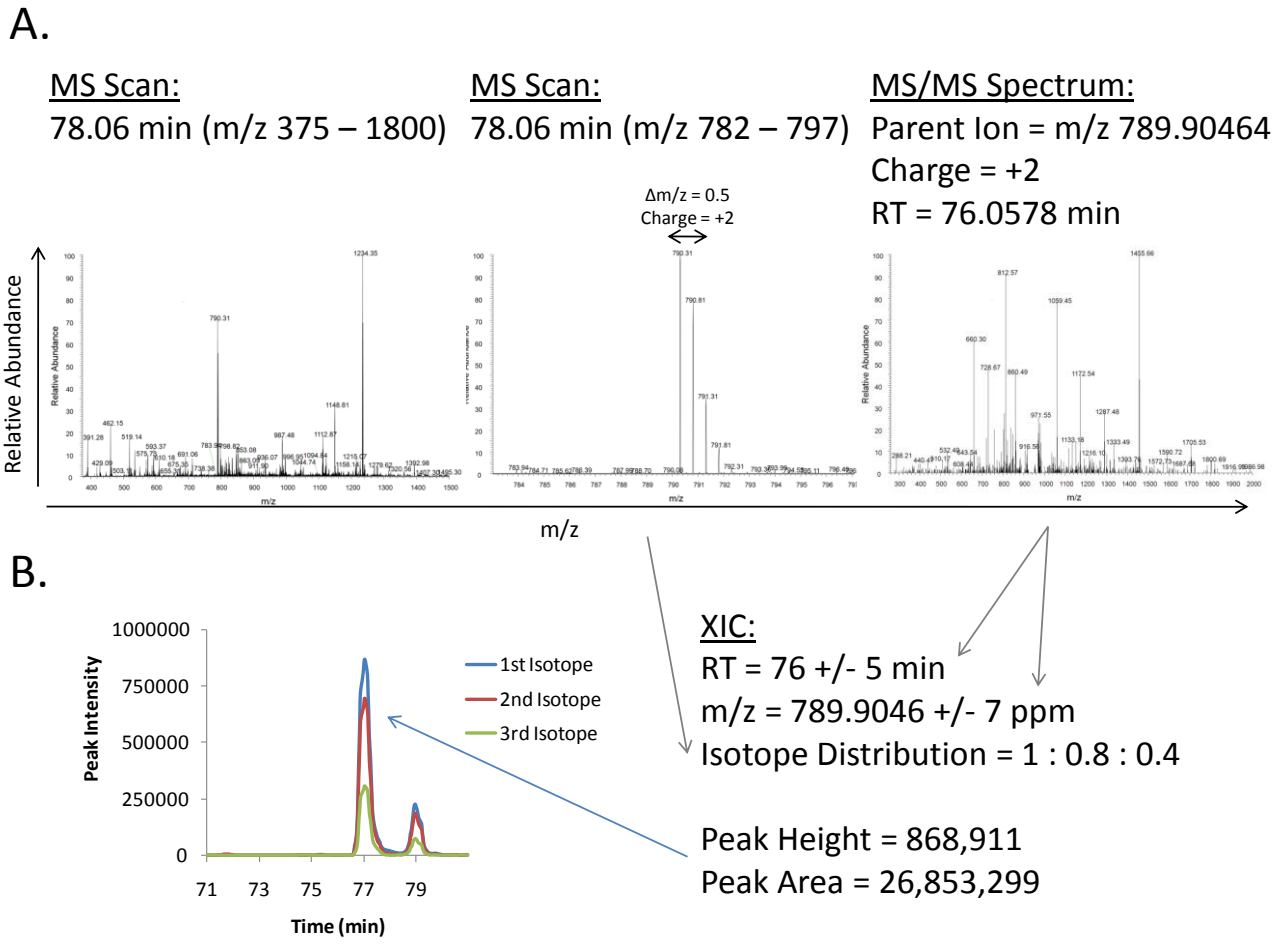

Figure 2.7. Illustration of Pescal.
A. MS and MS/MS data is used to generate identification information for the Enolase 1 peptide AVDDFLISLDGTANK. B. Identifying information is used to generate an XIC and identify the correct ion peak, although it should be noted that for the majority of peptides only one candidate is found within the RT window. The peptide abundance is expressed as peak height and peak area.

2.16.2. Other data analysis

GraphPad Prism was used to illustrate quantitative data and to compare data sets using the Student's t-test (two-tailed). All FACS data was analyzed using FlowJo.

3. Affinity Purification – Mass Spectrometry Screen for Dynamic Interaction Partners of Class IA PI3K

3.1. Introduction and aim of study

Class IA PI3Ks regulate essential cellular functions including growth, survival, metabolism and motility [2, 60], therefore the PI3K/Akt pathway activity is tightly regulated by a number of well-characterized mechanisms. Lipid phosphatases, such as PTEN and SHIP, dephosphorylate PIP_3, the lipid product of class IA PI3Ks, thereby terminating signal transduction [278]. The pathway is also regulated by downstream protein phosphatases, for example PP2A, which dephosphorylates and inactivates the effector protein Akt [85], and by negative feedback loops that terminate the activation signal, for example mTORC1-mediated phosphorylation and subsequent degradation of IRS1 [46].

Signalling activity is often regulated by the formation of multi-protein complexes, which can modulate enzymatic activity [263, 264]. The regulation of signalling processes by protein-protein interactions has been described for several signalling pathways, including Erk [265], Akt [266] and mTOR [267, 268], and many large-scale protein-protein interaction studies are currently underway to expand our knowledge in this area.

Our knowledge of the effects of protein-protein interactions on the activity of PI3K enzymes is currently under-explored. It is known that binding of p85 to p110 leads to an increase in stability and a decrease in lipid kinase activity of p110 *in vitro* [20]. However, whether p85 regulates p110 activity dynamically *in vivo* is not clear as this interaction is very strong and both subunits are constitutively bound in cells [19]. Ras binding to the p110α subunit is known to regulate some PI3K functions [29, 279] however the full implications of this relationship on other isoforms are not clear. A number of other proteins have also been reported to bind p85, including SHIP [280], ezrin [281], Src family members [282] and the PTEN-associated complex [283]. However, the potential roles, if any, of these binding partners in the regulation of PI3K signalling activity have not been investigated extensively.

The aim of the work presented in this Chapter was to identify novel, dynamic interaction partners of class IA PI3K with a functional role in controlling the activity of the pathway. We reasoned that binding partners with an active role in signal modulation would bind PI3K at

different stoichiometries in cells with an active pathway relative to those in which the pathway was inactive. Accordingly, an affinity purification mass spectrometry (AP-MS) strategy, inspired by that described for the identification of EGFR signalosomes [284], was designed to quantify binding partners of class IA PI3K in starved cells relative to cells treated with serum (Fig. 3.1.). This approach was selected as we wished to investigate interaction partners of endogenous PI3K without the need to over-express the protein bait.

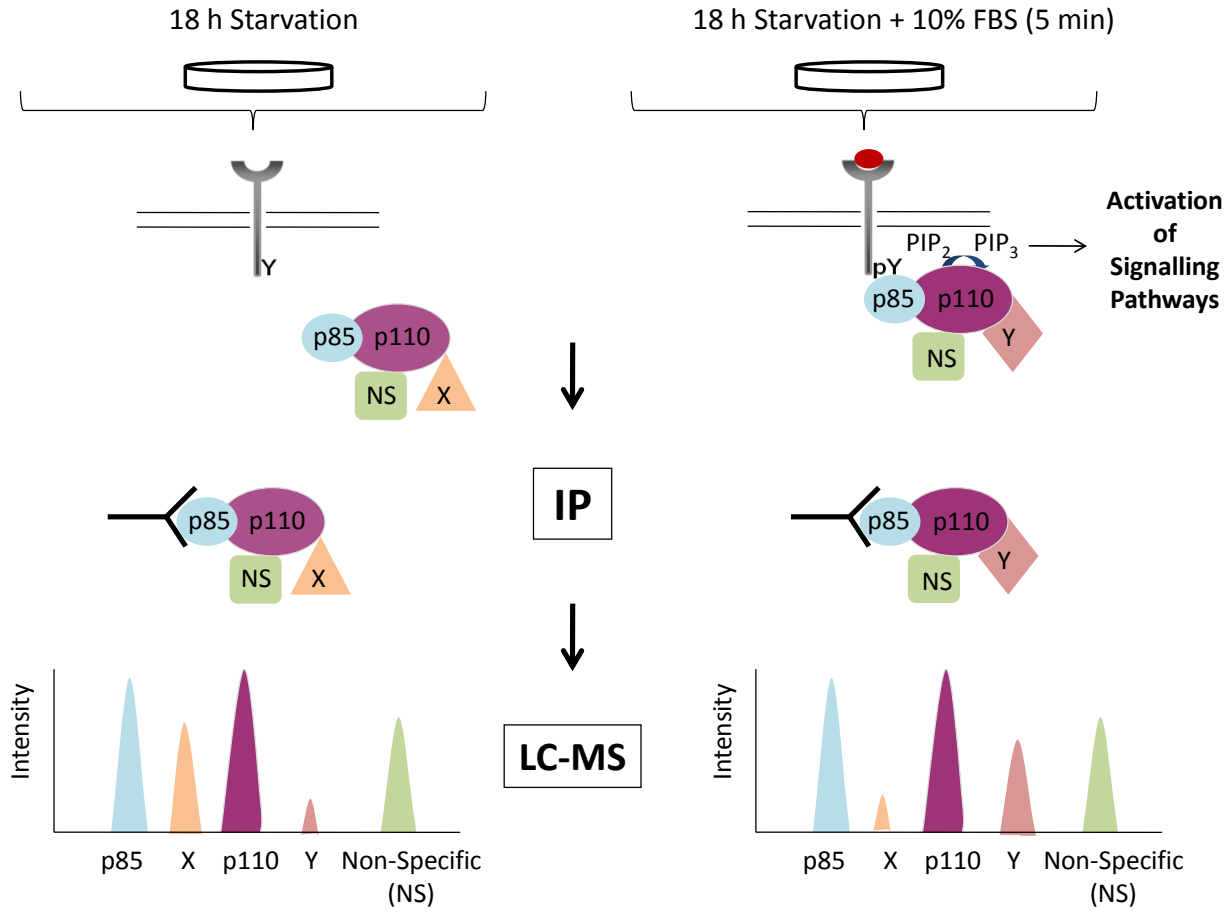

Figure 3.1. Strategy of AP-MS screen for dynamic interaction partners of PI3K. Total cell lysate samples were taken from NIH-3T3 cells that were serum-starved for 18 h (resulting in low levels of pathway activity) or serum-starved for 18 h followed by a 5 min treatment with 10% FBS (resulting in high levels of pathway activity). PI3K protein complexes were purified from both samples using immunoprecipitation directed against the p85 regulatory subunit of PI3K. The purified protein complexes were then separated by SDS-PAGE and subjected to in-gel trypsin digestion followed by LC-MS and LC-MS/MS analysis for quantitative and qualitative proteomic analysis.

3.2. Optimization of AP-MS conditions

An initial series of experiments were conducted to optimize the conditions to be used in the AP-MS screen for dynamic interaction partners of PI3K. Mouse embryonic fibroblast NIH-3T3 cells were selected as the model for the screen as they are well characterized cells and PI3K expression and activity levels have been thoroughly investigated [19]. An additional advantage of using these cells is that follow-up investigation could potentially be transferred to mouse genetic models with relative ease.

3.2.1. Effects of detergent on the stability of protein-protein interactions.

The variable effects of different detergents and their concentrations on affinity purification of protein complexes are well known. For example, Sarbassov *et al* demonstrated that the rictor-mTOR protein complex could only be affinity-purified from total cell lysate using CHAPS-containing buffers [268]. Buffers containing stronger detergents, such as Triton X-100, can disrupt weak protein-protein interactions [193].

An experiment was carried out to compare the effects of CHAPS and Triton X-100 containing buffers on the immunoprecipitation of p85 protein complexes. Total cell lysate, containing 1 mg of total protein, from NIH-3T3 and IC-21 cells was subjected to IP of PI3K p85 protein complexes. Cell lysis and all IP bead washes were carried out using lysis buffer containing 1% Triton X-100 or 0.3% CHAPS and the resulting IP products were fractionated using SDS-PAGE and the gel stained for all proteins using Colloidal Coomassie blue staining (Fig. 3.2.).

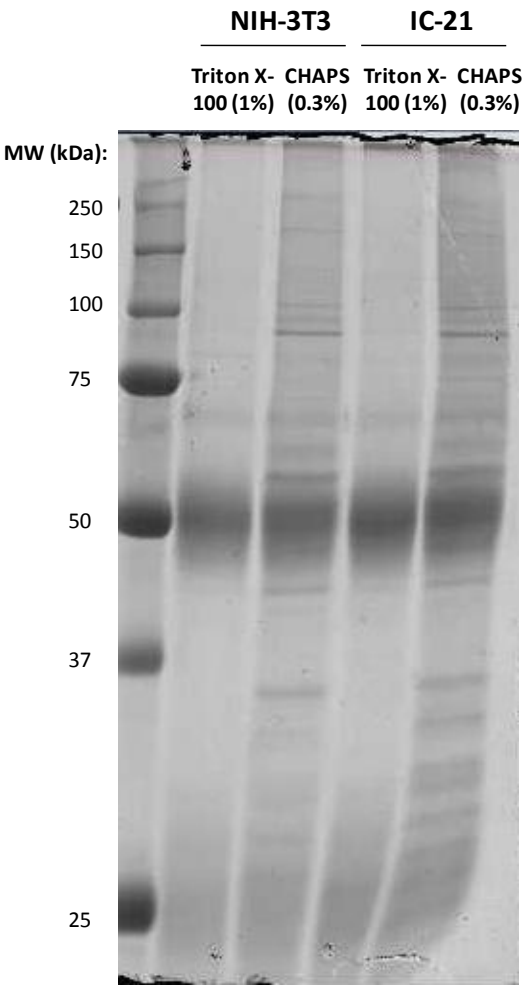

Figure 3.2. The use of 0.3% CHAPS in buffers preserves more protein-protein interactions than the use of 1% Triton X-100. PI3K p85 protein complexes were immunoprecipitated from NIH-3T3 and IC-21 cells using 0.3% CHAPS or 1% Triton X-100 in buffers throughout the purification process. The purified proteins were then separated by SDS-PAGE and visualized using Colloidal Coomassie blue staining.

The results demonstrated that a higher number and abundance of proteins were isolated from total cell lysate when 0.3% CHAPS lysis buffer was used (Fig. 3.2.), thus indicating that this detergent preserves more p85 interactors and/or non-specific interactors than Triton X-100. This is in line with expected findings as a mild detergent, such as CHAPS, should preserve weaker protein-protein interactions than a stronger detergent, such as Triton X-100, thus increasing the number of proteins isolated by affinity purification. However, it should be noted that that weak, non-specific interactions between proteins and with the antibody are also likely to be preserved, thus increasing the number of unspecific proteins present in the AP-MS screen.

3.2.2. Effects of detergent type and concentration on total protein yield.

The effects of the two different detergents on cell lysis were then examined in further detail to establish the implications of their use for the recovery of total protein from cells. 6-well plates were seeded with equal numbers of NIH-3T3 cells (0.7 x 10^6 per well) and the cells were harvested using 200 µl of lysis buffer containing various concentrations of CHAPS or Triton X-100. The experiment was performed in triplicate. The total protein content of the lysates was measured using the Bradford assay (Fig. 3.3).

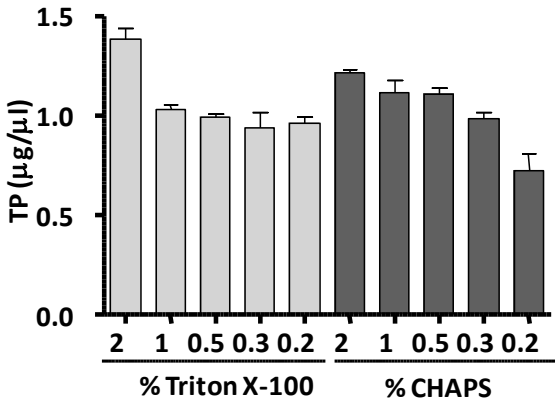

Figure 3.3. Total protein yield is decreased at lower detergent concentrations. Equal numbers of NIH-3T3 cells were lysed in 200 µl of buffer containing various concentrations of CHAPS or Triton X-100 detergent (n = 3). Total protein concentration of each sample was determined using the Bradford assay. Data expressed as mean +/- standard error of the mean (SEM).

These data showed that total protein yield was comparable for both detergents at most concentrations (Fig. 3.3.). The results also showed that total protein yield decreased as the concentration of detergent in the lysis buffer was reduced (Fig. 3.3.). However, this effect was negligible for Triton X-100 lysis buffers containing less than 1% detergent. In contrast, the effect was more pronounced for CHAPS-containing lysis buffer, and protein yield was found to be considerably decreased when this detergent was used at a concentration of 0.2%.

3.2.3. Effects of detergent type and concentration on PI3K p85 yield.

The effects of the two different detergents on cell lysis were then further investigated to determine their effects on the recovery of PI3K from cells. 6-well plates were seeded with

equal numbers of NIH-3T3 cells (0.7 x 10^6 per well) and the cells were harvested using 200 µl of lysis buffer containing various concentrations of CHAPS or Triton X-100. The experiment was performed in triplicate. 30 µl of each lysate was subjected to SDS-PAGE and quantitative WB analysis of p85 (Fig. 3.4.).

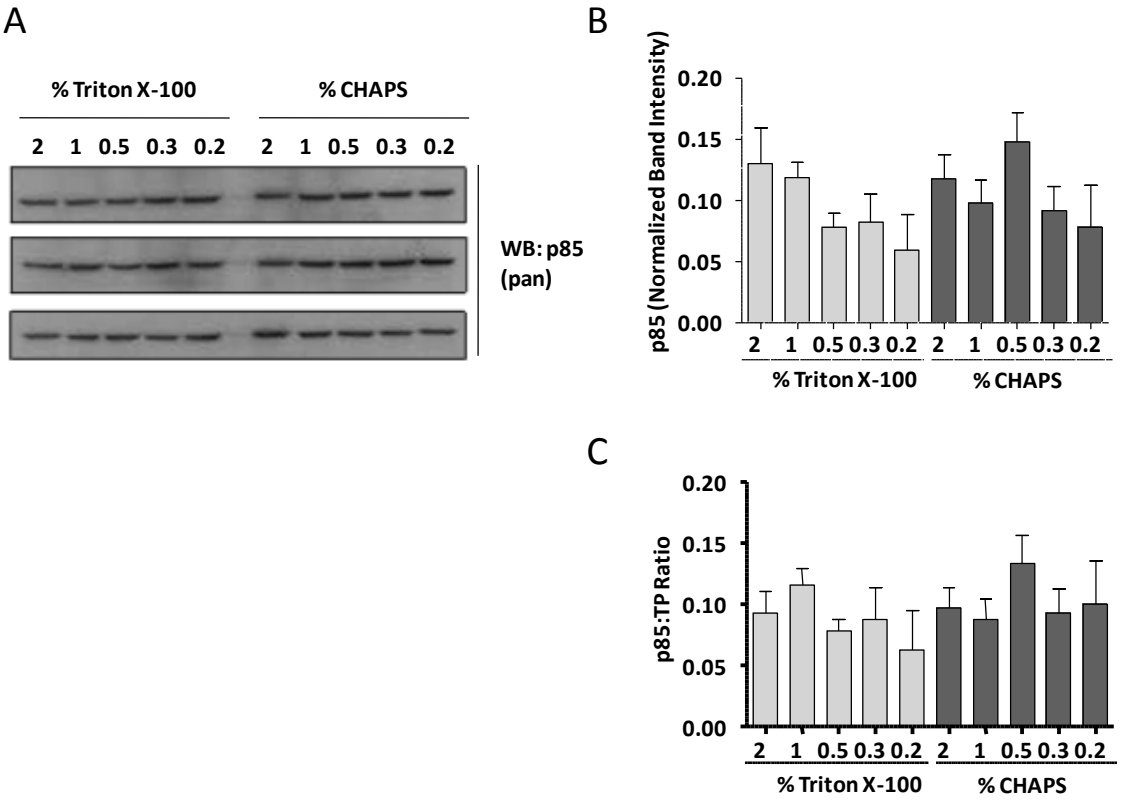

Figure 3.4. PI3K p85 protein yield does not correlate with detergent type or concentration. Equal numbers of NIH-3T3 cells were lysed in 200 µl of buffer containing various concentrations of CHAPS or Triton X-100 detergent (n = 3). A. Representative blot image obtained by analysing 30 µl samples subjected to WB analysis for p85. B. Densitometry analysis of p85 WB results. Band intensity was normalized to the mean band intensity across the experiment. C. p85 quantification was normalized to TP concentration. Data expressed as mean +/- SEM.

The results of this experiment revealed that the quantity of PI3K p85 harvested did not correlate well with the type or concentration of detergent used in the lysis buffer (Fig. 3.4.). In general the discrepancy between replicates was high, which is likely to be a reflection of the limited use of western blots for quantitative analysis. PI3K p85 recovery was lower in the samples with the lowest concentration of detergent (Fig. 3.4. A and B), however when

recovery was normalised to the total protein yield for the corresponding sample, relative p85 recovery was not greatly affected (Fig. 3.4. C).

The combined results of these experiments (3.2.2. and 3.2.3.) led to the selection of 0.3% CHAPS lysis buffer for use in the AP-MS protocol. This lysis buffer was shown to increase the number of proteins purified by IP from total cell lysate (Fig. 3.2.), thus increasing the likelihood that weak protein-protein interactions were preserved. Although the use of 0.3% CHAPS lysis buffer resulted in a reduction in total protein yield (Fig. 3.3.), p85 recovery was not significantly affected (Fig. 3.4.) and thus this was not considered to be a concern.

3.2.4. Optimization of PI3K p85 IP.

A p85 (pan isoform) antibody was selected for affinity purification of PI3K protein complexes as it has been previously observed in this laboratory to have strong affinity for all isoforms of p85 [19]. The use of a pan p85 antibody would also overcome the problem of the presence of multiple PI3K p110 isoforms as all will be immunoprecipitated by targeting this subunit.

Two p85 (pan) antibodies were in routine use in the laboratory: Millipore 06-195 (antisera, raised against intact p85 and N-terminal SH2 domain) and Millipore 06-497 (purified antibody, raised against intact p85). Experiments were carried out to evaluate the affinity for p85 of the two different antibodies and to determine the optimum concentration for IP yield. NIH-3T3 total cell lysate was subjected to IP using antibody 06-497, 06-195 or a 50:50 mix of the two at various ratios of antibody to total protein. The resulting IP products, along with total cell lysate samples and an equivalent volume of supernatant from each IP, were run by SDS-PAGE for WB analysis of p85 (Fig 3.5.).

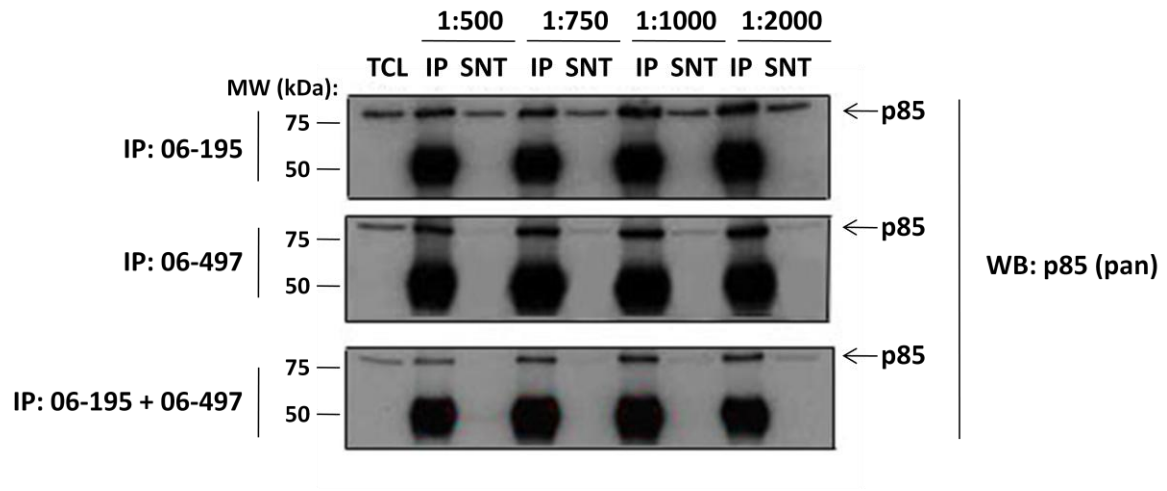

Figure 3.5. A combination of antibodies results in most efficient purification of PI3K p85. NIH-3T3 cell lysates, containing 1 mg protein, were subjected to IP of PI3K p85 using the indicated antibodies at ratios of 1:500, 1:750, 1:1000 or 1:2000 (µl antibody:µg TP). Total cell lysate (TCL), immunoprecipitates (IP) and residual supernatant (SNT) were subjected to WB analysis for p85.

The results showed that antibody 06-195 had a greater affinity for p85 than 06-497, as in the latter there was significant amounts of p85 residual in the IP supernatant relative to p85 in the IP (Fig 3.5.). This is in line with results reported in this laboratory that suggest that 06-195 does not have high affinity for p85β, the predominant p85 isoform expressed in this cell line [19]. However, it should be noted that this greater affinity for p85 may also be due to differences in antibody concentration in the stock solution rather than in absolute epitope affinity. The best result, i.e. highest recovery of p85 in IP and lowest residual p85 in IP supernatant, was obtained using a combination of the two antibodies at a ratio of 1:500 (µl antibody: µg TP) (Fig. 3.5.). These are the IP conditions that were selected for subsequent experiments.

3.3. AP-MS screen results

3.3.1. SDS-PAGE comparison of PI3K p85 protein complexes affinity purified from NIH-3T3 cells.

Following the principles of the strategy previously outlined (Fig. 3.1.), we proceeded to compare the composition of PI3K p85 complexes in starved and stimulated NIH-3T3 cells using SDS-PAGE and Colloidal Coomassie blue staining.

PI3K p85 protein complexes were immunoprecipitated from approximately 8 x 10^6 NIH-3T3 cells (yielding around 10 mg of protein) using a mixture of two antibodies (06-195 and 06-497) against the p85 regulatory subunit of PI3K. Samples were taken from cells treated with 18 h serum-starvation (resulting in low pathway activity) or with 18 h serum-starvation followed by 5 min stimulation with 10% FBS (resulting in high pathway activity). A control sample, a pool of the experimental samples, was subjected to IP using total rabbit IgG for assessment of non-specific interactions with rabbit IgG, protein G and the sepharose bead support. Mild cell lysis conditions (0.3% CHAPS) were used to maximize the chances of retaining weak protein-protein interactions. Purified PI3K protein complexes were then fractionated using SDS-PAGE and proteins were visualized by Colloidal Coomassie blue staining (Fig. 3.6.).

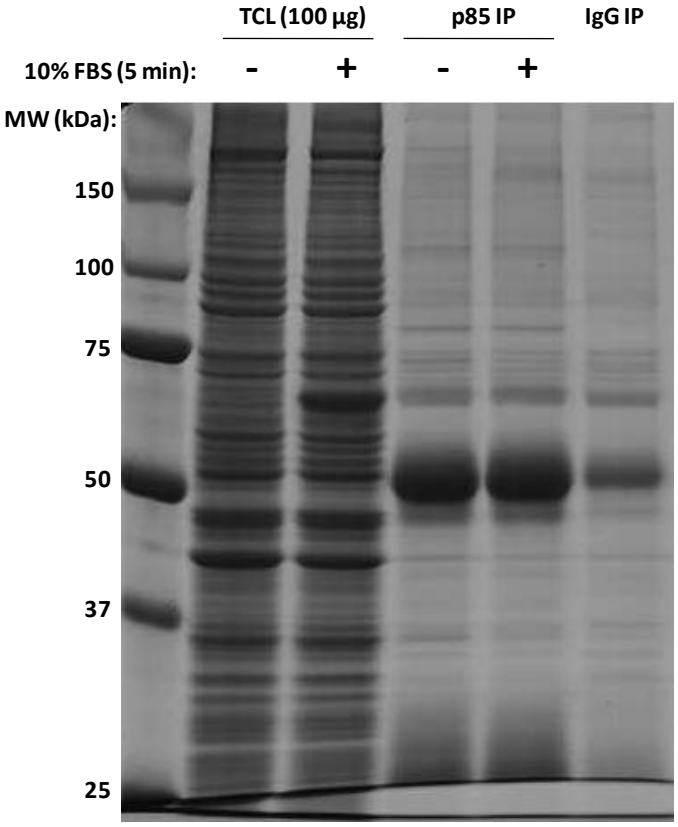

Figure 3.6. SDS-PAGE analysis does not reveal any clear candidate interaction partners dynamically regulated by serum. Total cell lysate samples were taken from NIH-3T3 cells that were serum-starved for 18 h (resulting in low levels of pathway activity) or serum-starved for 18 h followed by a 5 min treatment with 10% FBS (resulting in high levels of pathway activity). PI3K protein complexes were purified from both samples using immunoprecipitation directed against the p85 regulatory subunit of PI3K. The purified protein complexes were then separated by SDS-PAGE and resolved by Colloidal Coomassie blue staining for visual comparison.

Colloidal Coomassie blue staining of isolated PI3K protein complexes failed to identify any obvious differences between the starved and stimulated cell conditions, thus demonstrating that this method is unlikely to be useful in the identification of interaction partners (Fig. 3.6.). The visual comparison of p85 IPs isolated from starved and stimulated samples did however demonstrate the complexity of the IP products, partly due to the likely presence of high numbers of non-specific interactors. The control sample (IgG IP) illustrated the limitations of affinity purification by highlighting the large number of non-specific interactors with the affinity reagents (Fig 3.6.).

3.3.2. AP-MS analysis of PI3K p85 protein complexes from NIH-3T3 cells.

We then proceeded to use a mass-spectrometry based quantitative approach to identify candidate binding partners of PI3K (Fig 3.1.). We reasoned that proteins present in equal abundance in IPs under both conditions were likely to be non-specific or constitutive interactors and therefore were not investigated further. We focused our attention on proteins that interacted dynamically with PI3K upon serum-induced pathway activation as we considered that they may have potential functional roles in the regulation of PI3K signalling.

PI3K p85 protein complexes were isolated from NIH-3T3 cells and fractionated by SDS-PAGE as described in 3.3.1. Following Colloidal Coomassie blue staining, sample lanes were divided into 5 – 10 fractions (dependent on gel size) that were then subjected to in gel-trypsin digestion followed by LC-MS and LC-MS/MS analysis on the ThermoFisher LTQ Orbitrap XL. Three biologically independent experiments were performed and two technical replicates of each were analyzed.

Hundreds of proteins were identified and quantified across the study, with an average of 193 proteins found per experiment. Of these, 81 proteins were identified and quantified in all three replicates (Appendix 1). We used rigorous criteria for both protein identification and quantification to identify potential dynamic binding partners of PI3K. First, proteins had to be identified in IPs with a minimum of 3 peptides per protein and a MASCOT score > 40. Second, proteins had to be identified and quantified across all three of the independent replicates. Third, the average $\log_2$ fold difference of protein abundance in IPs obtained from starved and stimulated cells had to be <-1 or >1 (i.e. two-fold). Finally, the quantitative

difference had to be statistically significant ($p<0.05$ as assessed by the Student's t-test). Three proteins met these criteria (Fig. 3.7. and Table 3.1.).

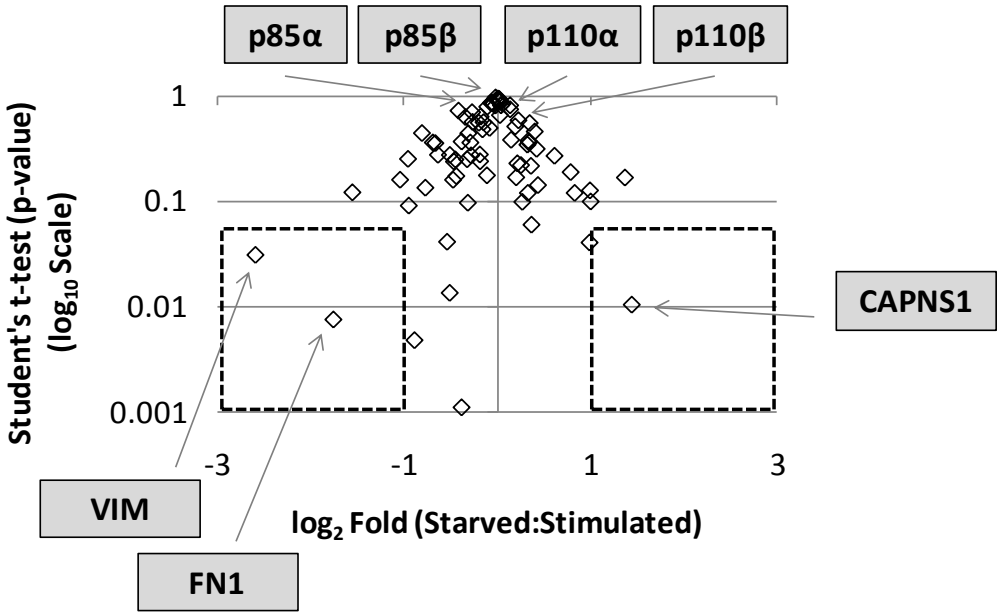

Figure 3.7. AP-MS screen identifies CAPNS1, FN1 and VIM as candidate dynamic interaction partners of Class IA PI3K. Volcano plot illustrating mean relative quantification of proteins identified in all three experiments (n = 81). Total cell lysate samples were taken from NIH-3T3 cells that were serum-starved for 18 h (resulting in low levels of pathway activity) or serum-starved for 18 h followed by a 5 min treatment with 10% FBS (resulting in high levels of pathway activity). PI3K protein complexes were purified from both samples using immunoprecipitation directed against the p85 regulatory subunit of PI3K and subjected to quantitative proteomic analysis (n = 3). Relative protein abundance between starved and stimulated conditions is expressed as $\log_2$ fold and statistical significance was evaluated using the Student's t-test.

Table 3.1. Summary of AP-MS results for proteins of interest (PI3K proteins and candidate dynamic interaction partners).

			Mean (across all 3 experiments)							
Protein	**Protein Accession Number**	**Protein Description**	**Mascot Score**	**No. of Peptides**	**Peak Intensity (Starved)**	**Peak Intensity (Stimulated)**	**Fold (Starved:Stimulated)**	**Log_2 Fold (Starved:Stimulated)**	**SD**	**p - value (Students t-test)**
p85α	IPI00263878	Phosphatidylinositol 3-kinase regulatory subunit alpha	932	29	1.0	1.0	1.0	0.0	0.1	0.663
p85β	IPI00117159	Phosphatidylinositol 3-kinase regulatory subunit beta	934	27	1.0	1.0	1.0	0.0	0.2	0.951
p110α	IPI00309224	Phosphatidylinositol-4,5-bisphosphate 3-kinase catalytic subunit alpha isoform	417	14	0.9	1.1	0.8	-0.3	0.6	0.445
p110β	IPI00136110	Phosphatidylinositol-4,5-bisphosphate 3-kinase catalytic subunit beta isoform	261	10	0.8	1.2	0.7	-0.5	0.5	0.239
CAPNS1	IPI00130992	Calpain small subunit 1	145	7	1.5	0.5	2.7	1.4	0.3	0.010
FN1	IPI00352163	Putative uncharacterized protein (fibronectin 1)	191	14	0.5	1.5	0.3	-1.8	0.3	0.007
VIM	IPI00227299	Vimentin	222	6	0.3	1.7	0.2	-2.6	2.1	0.031

The PI3K subunits p85α, p85β, p110α and p110β were identified and quantified in all three experiments and, as expected, were found to be present in equal abundance under both conditions (Table 3.1. and Fig. 3.8.A). CAPNS1, FN1 and VIM were also identified and quantified in PI3K protein complexes in all three experiments (Table 3.1. and Appendix 1). CAPNS1 was found at lower abundance in serum-stimulated cells relative to starved cells, with a mean $\log_2$ fold difference of 1.45 (SD = 0.3; p = 0.010) (Table 3.1. and Fig. 3.8.B). FN1 and VIM were found at higher abundance in serum-simulated cells relative to starved cells, with mean $\log_2$ fold differences of -1.8 (SD = 0.3; p = 0.007) and -2.6 (SD = 2.1; p = 0.031) respectively (Table 3.1. and Fig. 3.8.B).

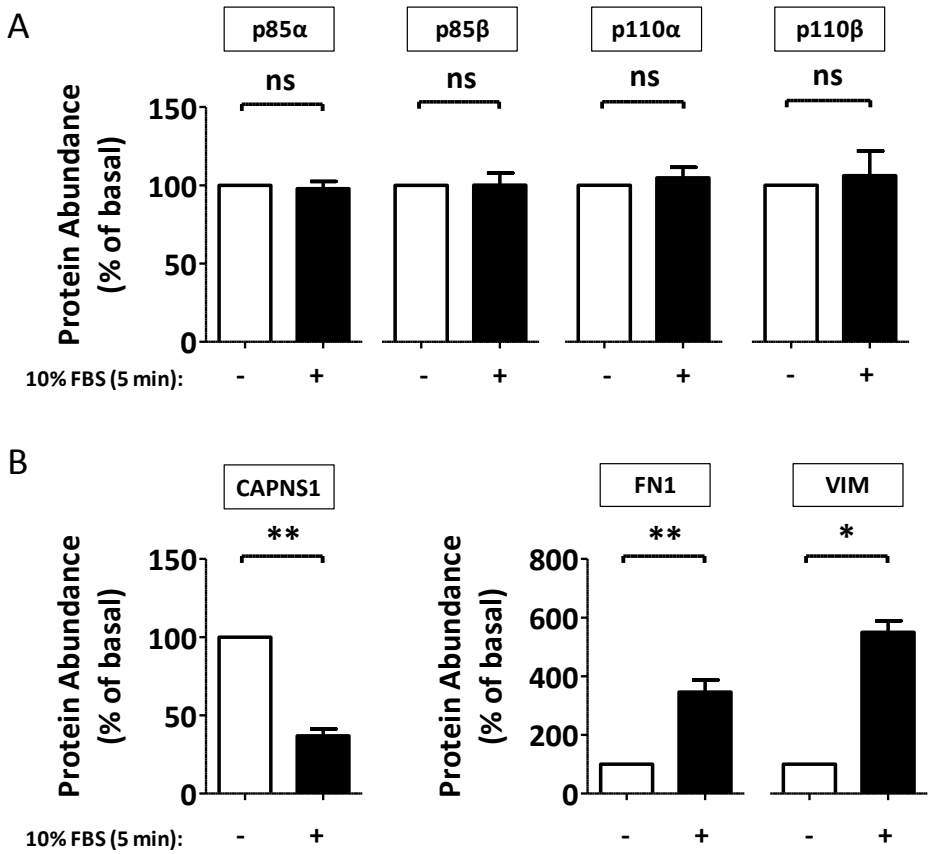

Figure 3.8. AP-MS screen identifies CAPNS1, FN1 and VIM as candidate dynamic interaction partners of Class IA PI3K. Relative protein quantifications of PI3K subunits (A) and candidate interaction partners (B) in serum-starved and stimulated cells. Total cell lysate samples were taken from NIH-3T3 cells that were serum-starved for 18 h (resulting in low levels of pathway activity) or serum-starved for 18 h followed by a 5 min treatment with 10% FBS (resulting in high levels of pathway activity). PI3K protein complexes were purified from both samples using immunoprecipitation directed against the p85 regulatory subunit of PI3K and subjected to quantitative proteomic analysis. Relative protein abundance was expressed as mean ± SEM (n = 3 independent experiments) relative to basal sample.*, p<0.05; **, p < 0.01; ns, non-significant.

3.4. Verification of AP-MS screen results

3.4.1. Manual verification of MASCOT identification of candidate interaction partners.

MASCOT identifications of candidate PI3K interaction partners were partially verified by manual sequencing of an identified peptide for CAPNS1, FN1 and VIM. Predicted ion fragments for each peptide were obtained from ProteinProspector (http://prospector.ucsf.edu/prospector/mshome.htm) and fragment ions were identified in the MS/MS spectra for that peptide (Fig. 3.9.).

A: CAPNS1 - LGFEEFK MASCOT p=0.0009

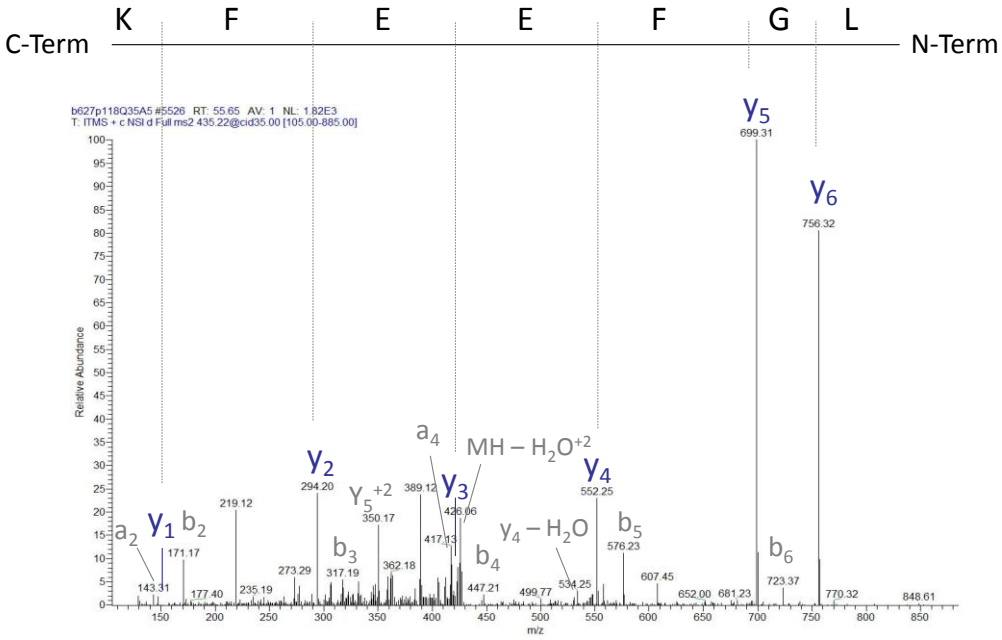

Figure 3.9. A . Manual verification supports MASCOT identification of candidate interaction partners. Manually annotated MS/MS spectra confirming MASCOT sequence results for representative peptide of CAPNS1 (A). Predicted ion fragments for each peptide were obtained from ProteinProspector (http://prospector.ucsf.edu/prospector/mshome.htm) and fragment ions were identified in the MS/MS spectra for that peptide. The MASCOT confidence score for the identification of each peptide is also shown. MASCOT peptide identifications were confirmed thus supporting the AP-MS screen results.

B: FN1 - APITGYIIR MASCOT p=5.9E-5

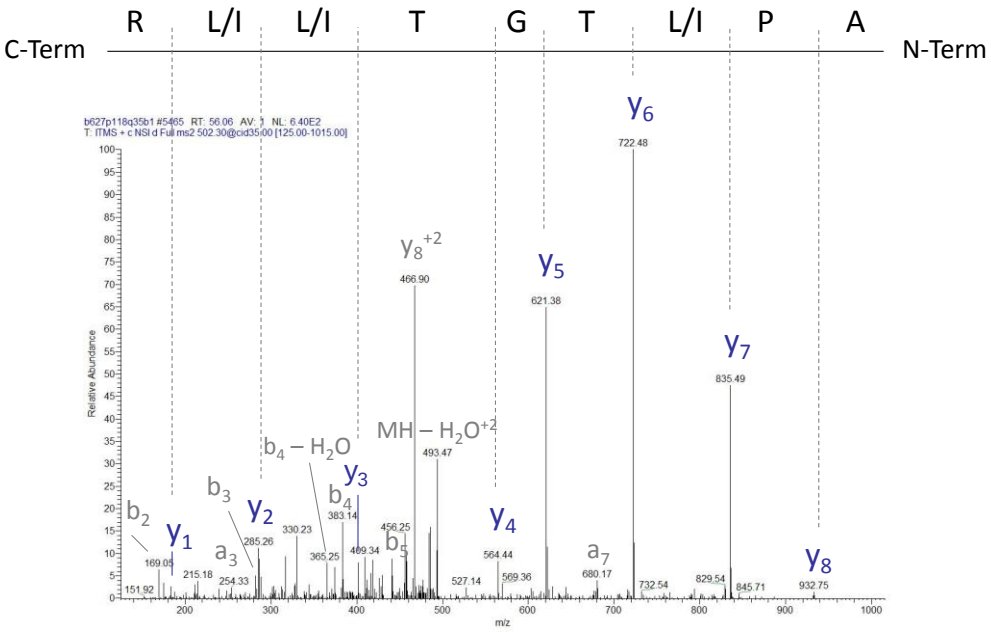

C: VIM - KVESLQEEIAFLKK MASCOT p=0.0022

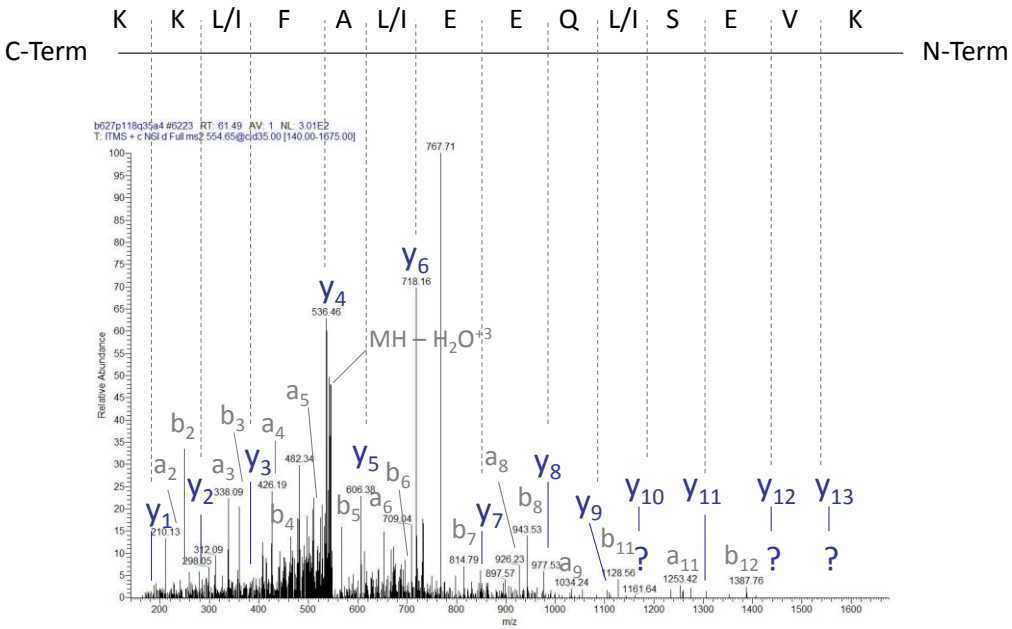

Figure 3.9. B - C. Manual verification supports MASCOT identification of candidate interaction partners. Manually annotated MS/MS spectra confirming MASCOT sequence results for representative peptides of FN1 (B) and VIM (C). Predicted ion fragments for each peptide were obtained from ProteinProspector (http://prospector.ucsf.edu/prospector/mshome.htm) and fragment ions were identified in the MS/MS spectra for that peptide. The MASCOT confidence score for the identification of each peptide is also shown. MASCOT peptide identifications were confirmed thus supporting the AP-MS screen results.

3.4.2. Manual verification of Pescal quantification of candidate interaction partners.

Pescal quantitation results for p85β and for candidate PI3K binding partners CAPNS1, FN1 and VIM were validated by visual inspection of the extracted ion chromatograms of a selection of peptides (Fig. 3.10. A – D).

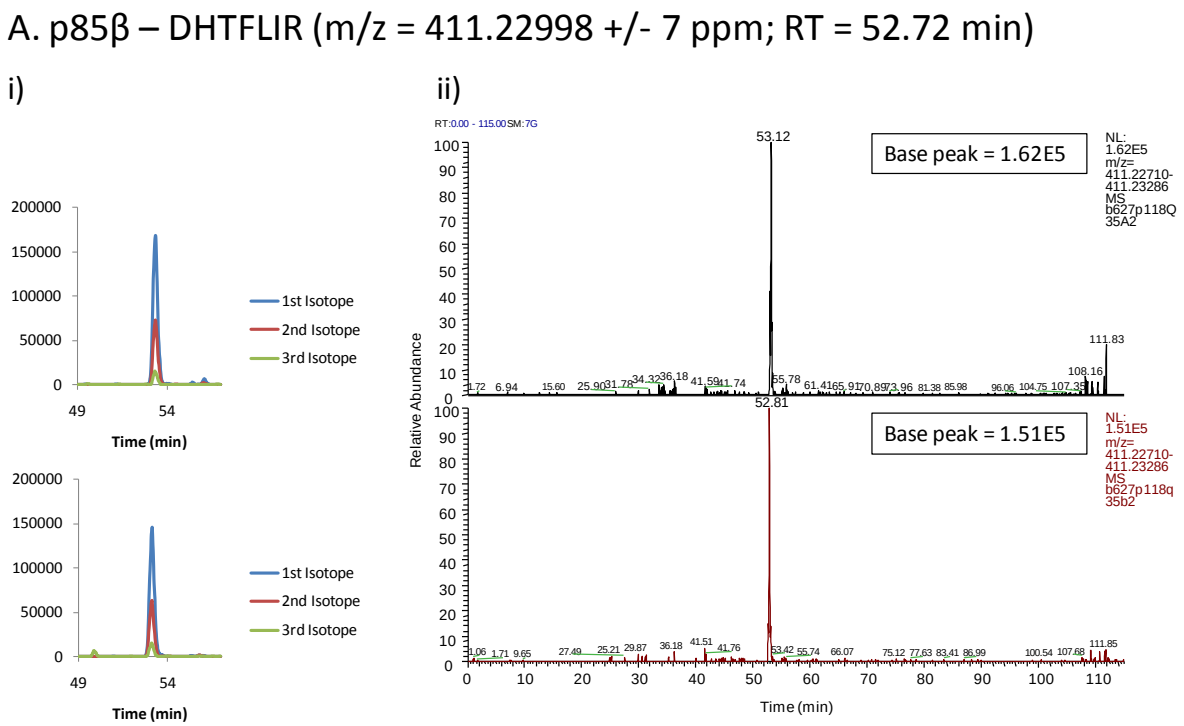

Figure 3.10. A. Manual validation supports Pescal quantification of p85β and candidate interaction partners. Extracted ion chromatograms (XICs) generated by Pescal were manually validated in the MS scan for representative peptides of p85β (A) in starved and stimulated samples. Panel (i) shows the XIC s generated by Pescal (peaks shown on normalized scale). Panel (ii) shows the XIC generated in XCalibur (peaks shown relative to most abundance peak in scan). The peak corresponding to the peptide of interest (indicated by arrow) was identified by retention time and verified in XCalibur using the isotopic distribution.

B. CAPNS1 – LGFEEFK (m/z = 435.22438 +/- 7 ppm; RT = 55.65)

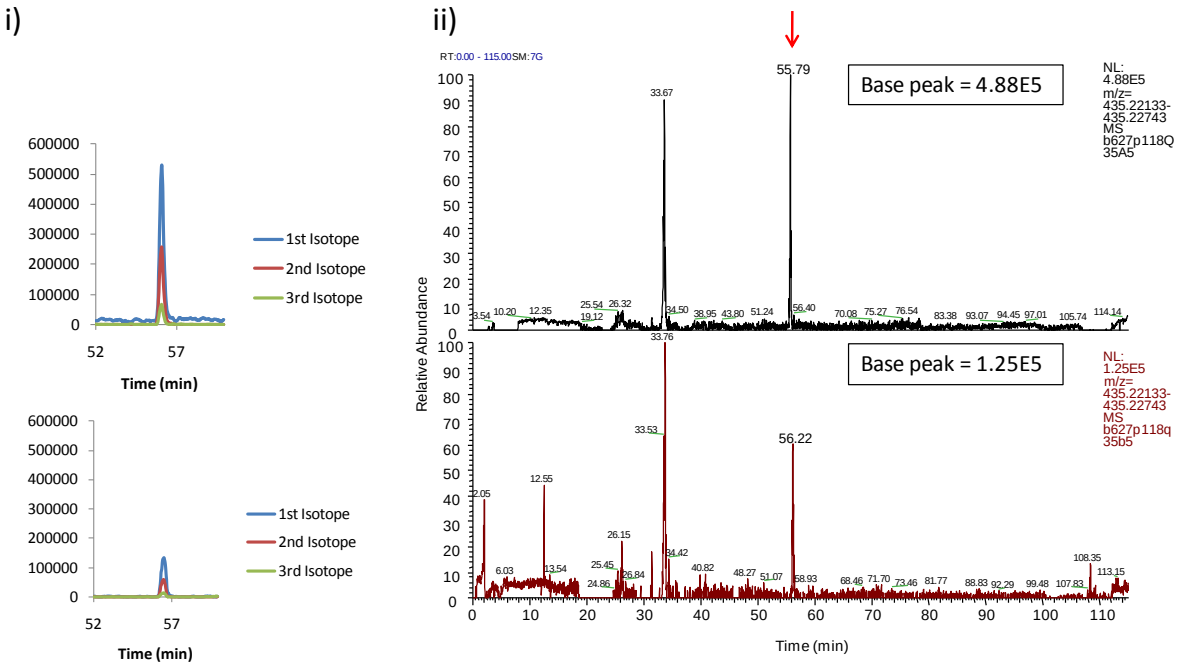

C. FN1 – APITGYIIR (m/z = 502.30093 +/- 7 ppm; RT = 54.66)

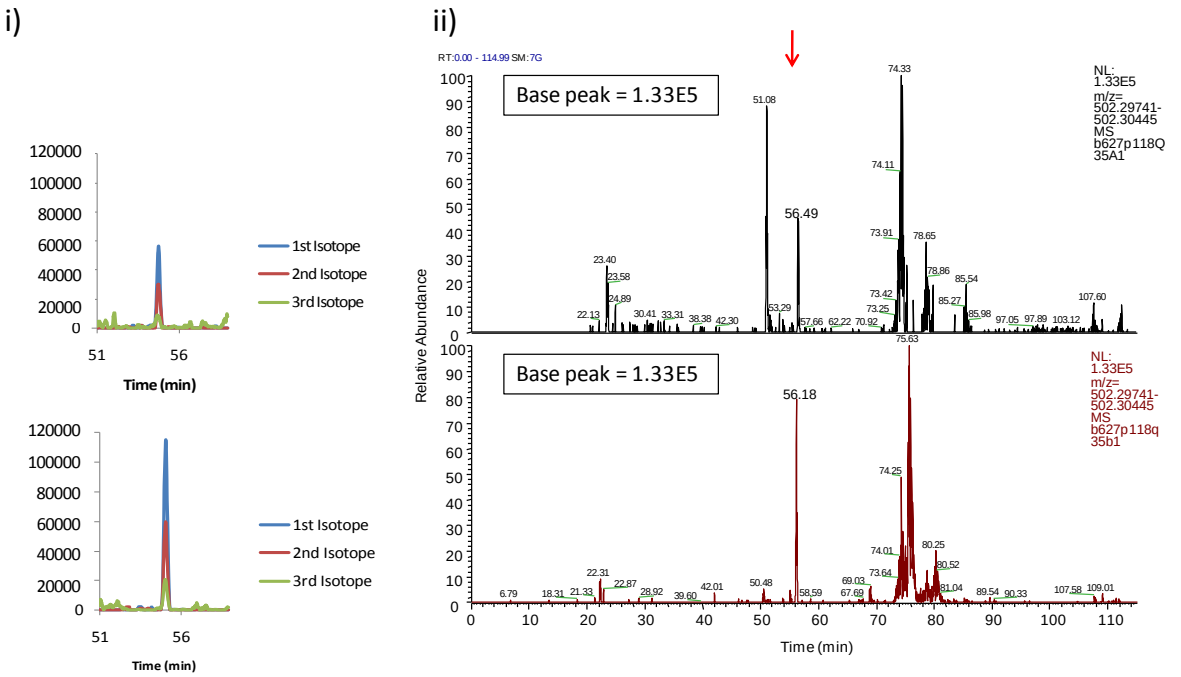

Figure 3.10. B – C. Manual validation supports Pescal quantification of p85β and candidate interaction partners. Extracted ion chromatograms (XICs) generated by Pescal were manually validated in the MS scan for representative peptides of CAPNS1 (B) and FN1 (C) in starved and stimulated samples. Panel (i) shows the XIC s generated by Pescal (peaks shown on normalized scale). Panel (ii) shows the XIC generated in XCalibur (peaks shown relative to most abundance peak in scan). The peak corresponding to the peptide of interest (indicated by arrow) was identified by retention time and verified in XCalibur using the isotopic distribution.

D. VIM – KVESLQEEIAFLKK (m/z = 608.81823 +/- 7 ppm; RT = 54.89)

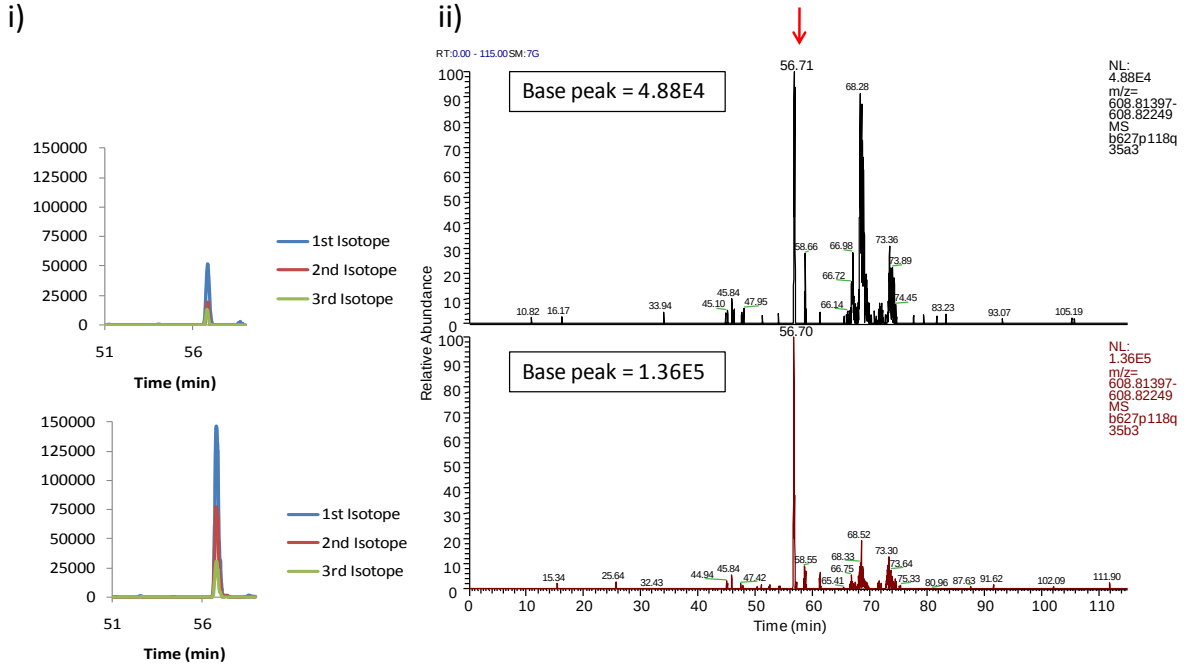

Figure 3.10. D. Manual validation supports Pescal quantification of p85β and candidate interaction partners. Extracted ion chromatograms (XICs) generated by Pescal were manually validated in the MS scan for representative peptides of VIM (D) in starved and stimulated samples. Panel (i) shows the XIC s generated by Pescal (peaks shown on normalized scale). Panel (ii) shows the XIC generated in XCalibur (peaks shown relative to most abundance peak in scan). The peak corresponding to the peptide of interest (indicated by arrow) was identified by retention time and verified in XCalibur using the isotopic distribution.

Several peptides were validated for each protein quantitation from each experiment. The results of visual examination correlated with Pescal quantitation results, thus supporting the AP-MS screen results. These data verify that, whilst p85β was present in equal abundance in p85 IP samples from starved and stimulated cells, CAPNS1 was more strongly associated with the PI3K complex under starved conditions and FN1 and VIM were more strongly associated with PI3K under stimulated conditions.

3.5. Conclusions

We designed an AP-MS strategy to identify candidate dynamic interaction partners of Class IA PI3K. Our strategy (Fig. 3.1.) was designed to compare the composition of the PI3K protein complex in cells that were serum-starved, resulting in low pathway activity, or serum-stimulated, resulting in high pathway activity. We hypothesized that proteins present in equal abundance under both conditions were likely to be non-specific interactors or

constitutive binders, whereas proteins present in different abundance under the two conditions were likely to have an active role in signalling.

We initially conducted a series of experiments to optimize our affinity purification approach. We found that the use of a mild detergent, 0.3% CHAPS, during the sample processing resulted in the purification of a higher number of proteins compared to a stronger detergent, 1% Triton X-100 (Fig. 3.2.). These results demonstrate, in accordance with the findings of others [268], that the use of weak detergent for affinity purification is beneficial as it increases the retention of weak protein-protein interactions. This was of particular importance in our study as our targets of interest were likely to be transient, dynamic interactors forming relatively weak interactions with PI3K.

Further investigations were performed to investigate the effects of the detergents CHAPS and Triton X-100 on cell lysis in more detail. Our results showed that, whilst total protein yield was inversely proportional to the concentration of either detergent (Fig. 3.3.), p85 recovery did not correlate well with detergent type or concentration (Fig. 3.4.). These results suggested that the use of low concentration of 0.3% CHAPS in the affinity purification process would not negatively impact the recovery of PI3K. Therefore, 0.3% CHAPS was the detergent and concentration selected for all further experiments.

A series of experiments were also performed to optimize the purification of PI3K complexes by IP. We chose to use antibodies with affinity for all isoforms of the p85 regulatory subunit of PI3K (p85 pan) as these reagents have previously been demonstrated by our laboratory to be efficient affinity reagents [19]. An additional advantage to this approach is that the different isoforms of the p110 catalytic subunits expressed in cells will all be isolated by this antibody. Our investigation revealed that, whilst both antibodies tested had a high affinity for p85, a combination of the two used at a ratio of 1:500 (µl antibody:µg protein) effectively depleted PI3K p85 from the sample (Fig. 3.5.). These were the IP conditions selected for the AP-MS screen.

PI3K p85 protein complexes were isolated from approximately 8 x 10^6 cells (yielding around 10 mg total protein) that were serum-starved for 18 h (“starved”) or serum-starved for 18 h followed by stimulation with 10% FBS for 5 min (“stimulated”). SDS-PAGE separation and Colloidal Coomassie blue staining revealed the complexity of the immunoprecipitation products isolated and failed to identify any clear differences between

the samples (Fig. 3.6.). These results supported the requirement for a quantitative mass spectrometry approach to identify candidate interaction partners.

To complete the AP-MS screen for dynamic interaction partners of Class IA PI3K, three independent biological experiments were performed. Hundreds of proteins were identified and quantified across the study, however we focused our attention on the 81 proteins that were found in all three replicates (Appendix 1). We then employed strict criteria for protein identification and quantification to identify proteins that were interacting dynamically with PI3K. Critically, candidates were required to be identified to a high degree of confidence in all three experiments and the criteria to be considered quantitatively different between the two conditions was for a minimum of a two-fold change in relative abundance, which was statistically significant as assessed by the Student's t-test.

PI3K proteins were found to be present in equal abundance under both conditions in all three experiments. In contrast, CAPNS1 was found to be more strongly associated with PI3K in starved cells whereas FN1 and VIM were found to be more strongly associated with PI3K in stimulated cells (Fig. 3.7. - 3.8. and Table 3.1.). Qualitative and quantitative analysis of mass spectrometry data was manually assessed leading to the conclusive validation of the results (Fig. 3.9. – 3.10.).

4. Regulation of Class IA PI3K stability and signalling activity by calpain

4.1. Introduction and aim of study

The AP-MS study reported in Chapter 3 revealed that calpain small subunit 1 (CAPNS1) interacts dynamically with Class IA PI3K. CAPNS1 was consistently found to be more abundant (by around 3-fold) in PI3K complexes isolated from serum-starved cells (low pathway activity) compared to serum-stimulated cells (high pathway activity). Although other candidate dynamic interaction partners revealed by the AP-MS screen (FN1 and VIM) showed higher fold changes between the two conditions evaluated, CAPNS1 was of immediate interest due to its known role in the cleavage of other signalling proteins [285] and its implication in Akt signalling [286-288]. Calpains have also been implicated in the regulation of multiple biological processes, including apoptosis, autophagy, proliferation and migration [285, 289-291].

Calpains are a family of highly-conserved calcium-dependent cysteine proteases [292-294]. There are many calpain isoforms ubiquitously expressed, however calpain 1 and calpain 2 (also known as μ-calpain and m-calpain respectively) are the most extensively studied members of the family [291, 293]. Both calpain 1 and calpain 2 are heterodimers comprised of a common 28 kDa regulatory subunit (CAPNS1), thought to act as a chaperone [295], and an 80 kDa catalytically active subunit [291, 293]. The activation and regulation of calpain activity *in vivo* is not well understood [296], although it is an abundant protein with limited proteolytic activity and therefore it is thought to be tightly regulated [289]. Calcium binding is known to induce conformational changes to the molecule by disrupting the electrostatic interactions between the sub domains of the catalytic unit [292]. However, such conformational changes are thought to be insufficient alone to induce activity [285, 296]. In addition, the calcium levels shown to be required for calpain 2 activation *in vitro* are supraphysiological, indicating the requirement for additional regulatory mechanisms [285, 296, 297]. For example, binding of calpain 2 to PIP_2 has been shown to be required for activation of the protease [297, 298]. The sub-cellular localization of calpain is complex and variable, suggesting that this too may be a mechanism for regulation [285, 297]. A major

regulator of calpain activity is the endogenous inhibitor calpastatin, which is also calcium-dependent, although the mechanisms that control the dynamics are very complex [291, 293, 299].

Calpains are thought to cleave proteins at highly-specific recognition sites, however no consensus cleavage sequence has been identified and secondary structural features are thought to be more important recognition factors for the protease [285, 291, 293]. Calpain activity most frequently results in the production of large polypeptide fragments, suggesting that it is more likely to have a role in substrate activity regulation than in substrate digestion [285, 292]. More than a hundred *in vitro* substrates for calpain have been described; including cytoskeletal proteins, transmembrane receptors, transcription factors and signalling enzymes [285, 291]. Reflecting the diversity of their substrates, calpains have been implicated in the regulation of multiple biological processes including apoptosis, autophagy, proliferation and migration [289, 290]. Calpain 1 and 2 are known to have different calcium requirements for activation *in vitro,* however it is not clear if the isoforms have distinct roles *in vivo*. Knockout mice for calpain 1 show no obvious phenotype [300], however knockout of calpain 2 and calpain small subunit 1 are embryonic lethal [301, 302], indicating non-redundant roles of the two isoforms during pre-implantation embryonic development [303]. However, no differences in substrate specificity have been reported for calpain isoforms 1 and 2 [291].

The aims of the work presented in this Chapter were: (i) to validate the interaction between CAPNS1 and Class IA PI3K; (ii) to investigate the nature of the relationship between the two proteins and (iii) to establish if calpain had an active role in the regulation of PI3K signalling activity.

Pharmacological and genetic tools were used to investigate the interaction between PI3K and calpain. Notably, the pan calpain inhibitor N-Acetyl-L-leucyl-L-leucyl-L-norleucinal (ALLN; also known as calpain inhibitor 1), a cell-permeable peptide inhibitor that blocks the active site of the protease was used to inhibit calpain activity *in vivo* [304]. Similarly, LY294002, a small molecule kinase inhibitor that targets PI3K and mTOR was used to investigate the contribution of PI3K *in vivo* in undertaken studies [64, 65]. Genetic tools were also used to inhibit calpain activity. Specifically, small interfering RNA (siRNA) for

CAPNS1 was used to down-regulate CAPNS1 expression, which led to a reduction in the expression of active calpain catalytic subunits and overall calpain activity (Fig. 4.1.)

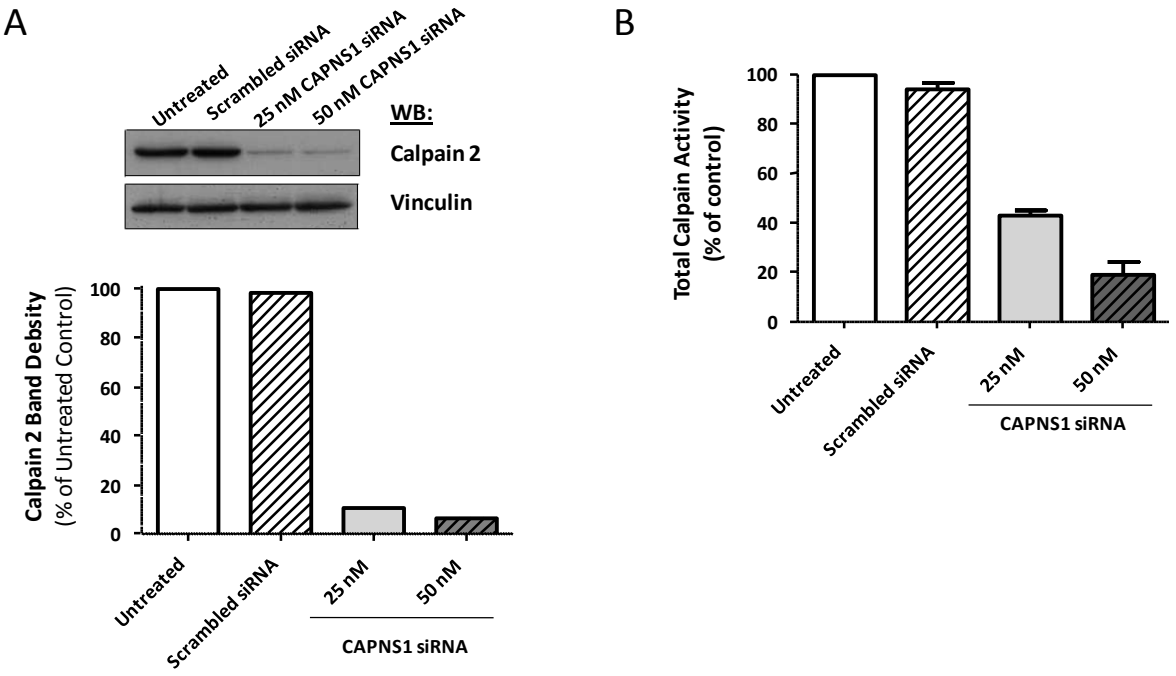

Figure 4.1. siRNA against CAPNS1 reduces the expression of calpain 2 and total calpain activity. NIH-3T3 cells were treated with scrambled siRNA (50 nM) or CAPNS1 siRNA (as indicated) for 48 h. A. Calpain 2 expression was measured by WB analysis. B. Total calpain activity was measured using an *in vitro* calpain activity assay (n = 2). Data expressed as mean+/- SEM.

Data showed that siRNA knockdown of CAPNS1 significantly reduced the expression of the catalytic subunit calpain 2, which is consistent with the down-regulation in expression of the regulatory subunit CAPNS1 [305] (Fig. 4.1. A). Furthermore, this treatment also resulted in approximately a 5-fold reduction of total calpain activity (Fig. 4.1. B).

4.2. Validation of the interaction between calpain and Class IA PI3K

4.2.1. Investigation of calpain activity in PI3K IPs.

We initially sought to confirm the presence of CAPNS1 in PI3K p85 IPs by a mass spectrometry independent method and, furthermore, to investigate if active calpain catalytic subunits were also present in the PI3K protein complex. Due to the limited sensitivity of the available antibodies against calpains for immunoblotting, published studies

have used activity assays to investigate calpain expression in cells [305, 306]. We thus pursued this strategy to test the PI3K – calpain interaction further.

PI3K was immunoprecipitated from 1 mg of protein harvested from starved and serum-stimulated NIH-3T3 cells using antibodies against the p85 regulatory subunit of PI3K (as previously described). Total cell lysate (TCL; 25 µg) and PI3K immunoprecipitates (IPs) were then subjected to an *in vitro* assay for calpain protease activity (Fig. 4.2.).

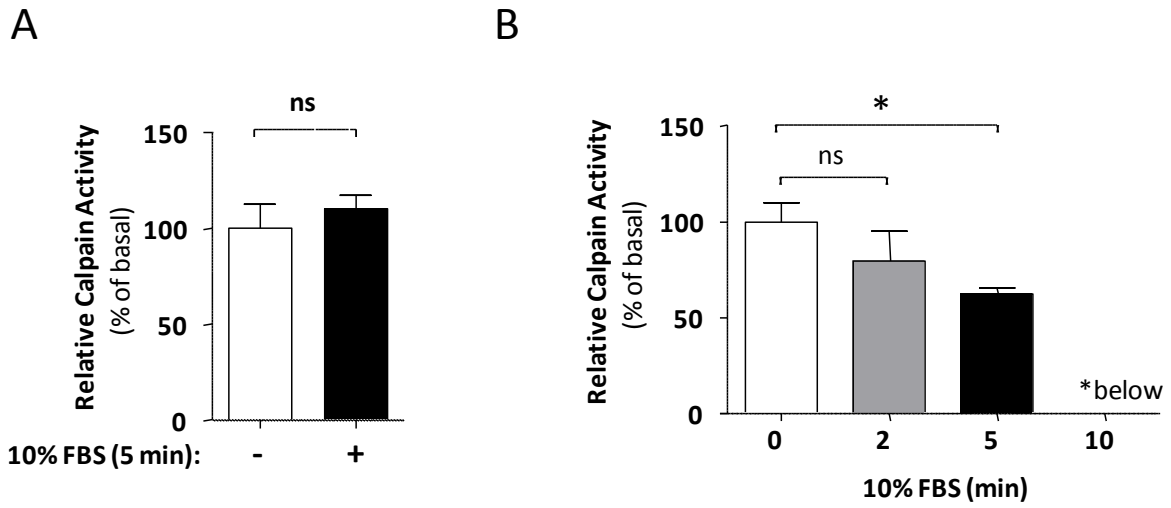

Figure 4.2. Active calpain heterodimers associate dynamically with Class IA PI3K. Total cell lysates (A; n = 3) and purified PI3K p85 protein complexes (B; n = 4) were subjected to an *in vitro* protease assay for calpain activity after serum-starvation for 18 h followed by stimulation with 10% FBS for the indicated times. Data expressed as mean+/- SEM. *below, below limit of assay detection; ns, not significant; *, $p < 0.05$.

Calpain activity was detectable in both total cell lysates and p85 IPs. Calpain activity levels were not found to be significantly different in starved or stimulated NIH-3T3 total cell lysate samples (Fig. 4.2. A). In contrast, calpain activity in p85 IPs was found to be decreased upon serum stimulation (Fig. 4.2. B). These results confirm the findings of the AP-MS study (Fig. 3.8. B) and, in addition, demonstrate that the calpain heterodimers associated with Class IA PI3K in the isolated complex are catalytically active.

4.2.2. Investigation of PI3K activity in calpain IPs.

To further validate the interaction between calpain and PI3K we proceeded to evaluate the PI3K lipid kinase activity of protein complexes purified by immunoprecipitation against calpain proteins. Calpain was immunoprecipitated from 1 mg of total cell lysate harvested

from serum-starved and serum-stimulated NIH-3T3 cells using antibodies against calpain catalytic subunit proteins, including calpain 1 and calpain 2. Purified proteins were then subjected to an *in vitro* lipid kinase assay for PI3K activity [269] (Fig. 4.3.).

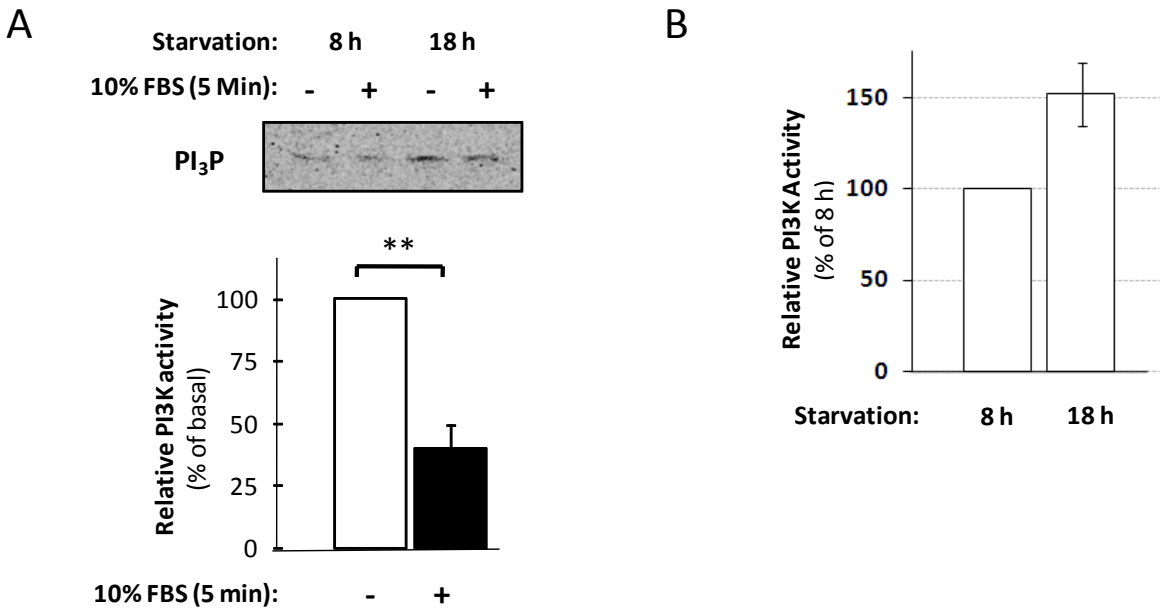

Figure 4.3. Class IA PI3K associates dynamically with calpain. A. An *in vitro* lipid kinase assay was used to detect PI3K activity in calpain immunoprecipitates from cells that were serum-starved for 18 h followed by serum-stimulation as indicated. One representative autoradiograph is shown alongside the quantification data for all experiments performed (n = 3). B. The same assay was used to detect PI3K activity in calpain immunoprecipitates from cells that were serum-starved for 8 or 18 h (n = 2). Data expressed as mean+/- SEM. **, $p < 0.01$.

PI3K activity was detectable in calpain IPs from cells serum-starved for 18 h and was found to be reduced by over 2-fold upon serum stimulation (Fig. 4.3. A). Furthermore, PI3K activity in calpain protein complexes was found to be higher after 18 h serum-starvation compared to 8 h serum-starvation (Fig. 4.3. B). Thus, in line with observations from the AP-MS study (Fig. 3.8. B), these results indicate that the interaction between calpain and PI3K is enhanced in response to serum-starvation and decreased upon cell stimulation that leads to the activation of PI3K signalling.

4.2.3. Investigation into calpain activity of serum-starved cells.

We proceeded to investigate the effects of serum-starvation on total calpain activity in cells. Total cell lysate was taken from NIH-3T3 cells growing in complete cell medium (in the

presence of FBS) or medium free from serum for 18 h. Samples containing around 25 µg of total protein were then subjected to an *in vitro* assay for calpain activity (Fig. 4.4.).

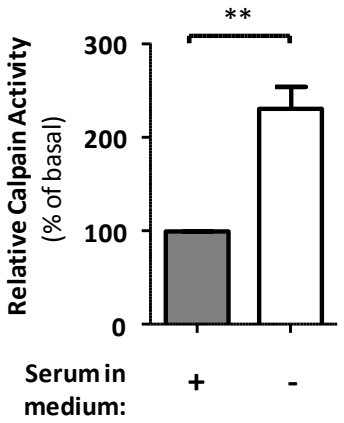

Figure 4.4. Serum-starvation increases calpain activity in NIH-3T3 cells. Total cell lysates (n = 3) taken from NIH-3T3 cells growing exponentially (+ serum in medium) or serum-starved for 18 h (- serum in medium) were subjected to an *in vitro* protease assay for calpain activity. Data expressed as mean+/- SEM. **, $p < 0.01$.

The results of this experiment showed that serum-starvation for 18 h dramatically increased calpain activity, by over 2-fold, in these cells (Fig. 4.4.). These results suggest that serum-starvation triggers a response in cells that results in increased calpain activity, which appears to correlate with an increase in calpain and PI3K association.

4.3. Investigations into the effects of calpain activity on PI3K stability and enzymatic activity.

Since calpain is a protease, we next proceeded to investigate if PI3K proteins were substrates of calpain and to evaluate the effects of the association on PI3K stability and lipid kinase activity.

4.3.1. Effects of calpain activity on PI3K stability *in vitro*.

PI3K proteins were immunoprecipitated from 1 mg of total protein obtained from NIH-3T3 and IC-21 cells using antibodies against the p85 regulatory subunit. The isolated proteins were then used as substrates for an *in vitro* calpain activity assay and purified calpain 1 and calpain 2 proteins were used as the protease source. Western blot (WB)

analysis was then used to evaluate the stability of the different PI3K subunits as a function of incubation with calpains (Fig. 4.5.)

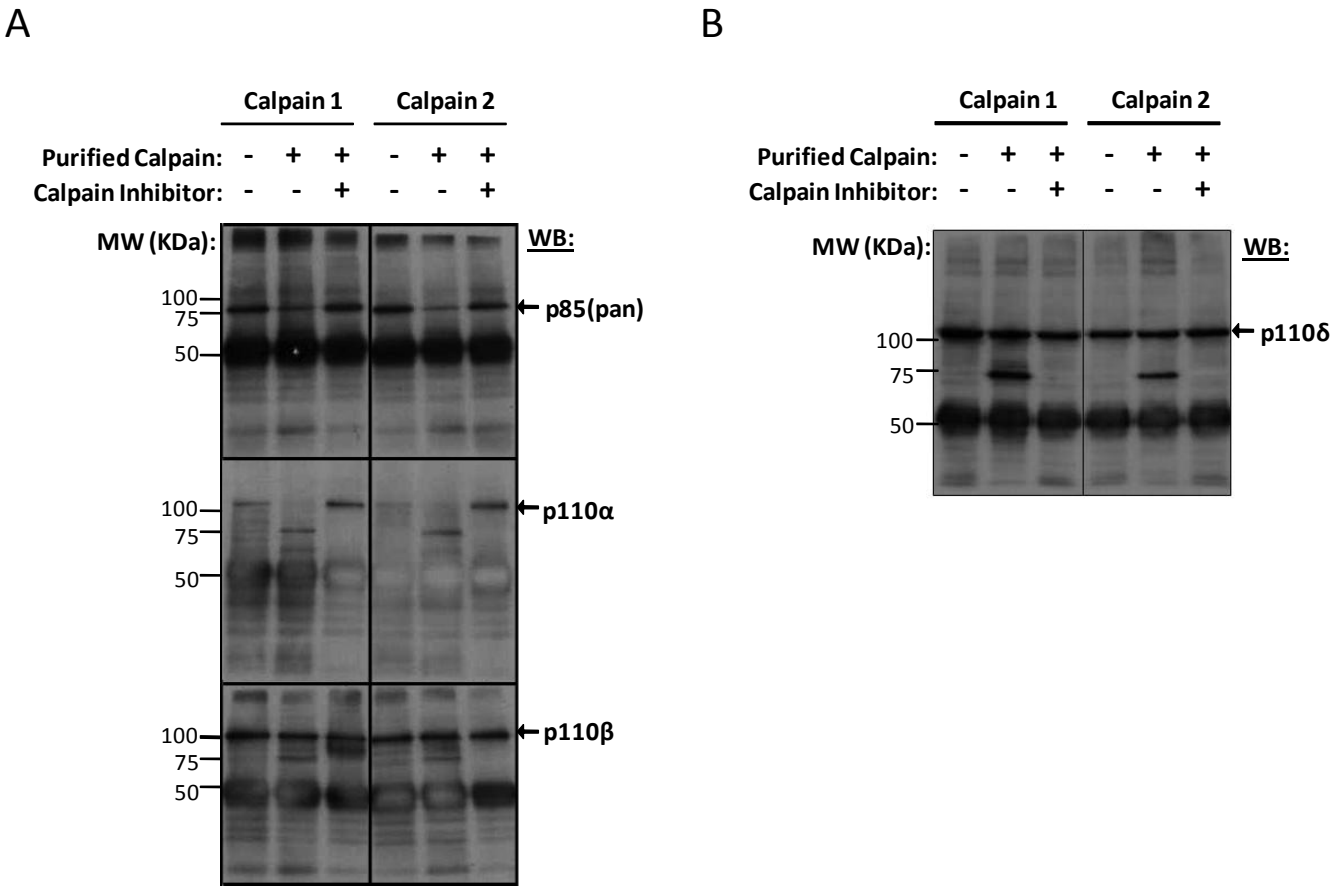

Figure 4.5. Calpain 1 and 2 cleave p110α completely and p110β, p110δ and p85 partially *in vitro*. PI3K subunits were immunoprecipitated from NIH-3T3 (A) and RAW 264.7 (B) cells and used as substrates for an *in vitro* protease digestion using 2 µg of purified calpain isoforms 1 or 2. WB analysis was used to investigate the stability of the different PI3K isoforms (one representative experiment of three shown).

The results revealed that calpain 1 and calpain 2 cleaved p110α extensively, whereas p110δ and p85 were only partially cleaved by both calpain 1 and calpain 2 (Fig. 4.5.). Conversely, the effect of calpain activity on the stability of p110β was negligible (Fig. 4.5. A). These results demonstrate that calpain can cleave PI3K proteins *in vitro* and suggest that calpain may have a role in p110α stability *in vivo*.

4.3.2. Effects of calpain activity on PI3K lipid kinase activity in vitro.

We next investigated the activity of calpain-cleaved PI3K proteins. PI3K proteins were immunoprecipitated from 1 mg of total protein obtained from NIH-3T3 cells, using antibodies against the p85 regulatory subunit, and subjected to an *in vitro* protease digestion using purified calpain followed by a lipid kinase assay for PI3K activity (Fig. 4.6.).

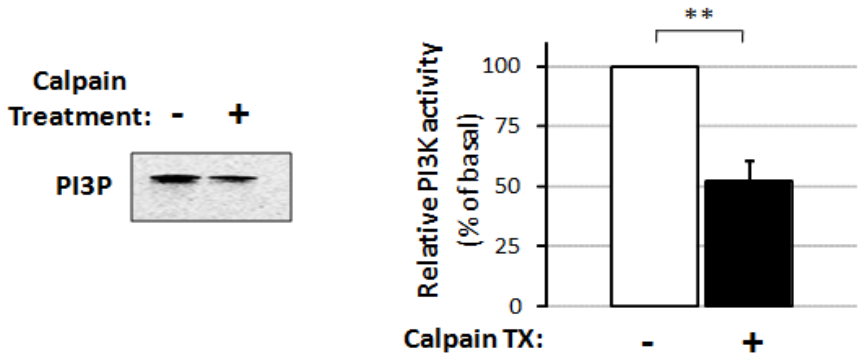

Figure 4.6. Calpain-cleavage of PI3K proteins reduces their lipid kinase activity. PI3K subunits were immunoprecipitated from NIH-3T3 cells and used as substrates for an *in vitro* protease digestion using 2 µg of purified calpain 1. An *in vitro* lipid kinase assay was then performed to measure the activity of digested PI3K subunits. One representative autoradiograph is shown alongside the quantification data for all experiments performed (n = 4) expressed as mean+/- SEM. **, p <0.01.

Results of this experiment demonstrated that cleavage of PI3K proteins resulted in a decrease in lipid kinase activity of approximately 2-fold (Fig. 4.6.). These results therefore indicate that cleavage of p110α by calpains results in a decrease of its lipid kinase activity.

4.3.3. Effects of calpain activity on PI3K stability *in vivo*.

We next set out to evaluate the effects of endogenous calpain activity on the stability of PI3K proteins *in vivo*. Calpain activity in serum-starved NIH-3T3 cells was inhibited for 48 h with the calpain inhibitor ALLN or with siRNA for CAPNS1. WB analysis was then performed to evaluate the stability of PI3K proteins (Fig. 4.7.).

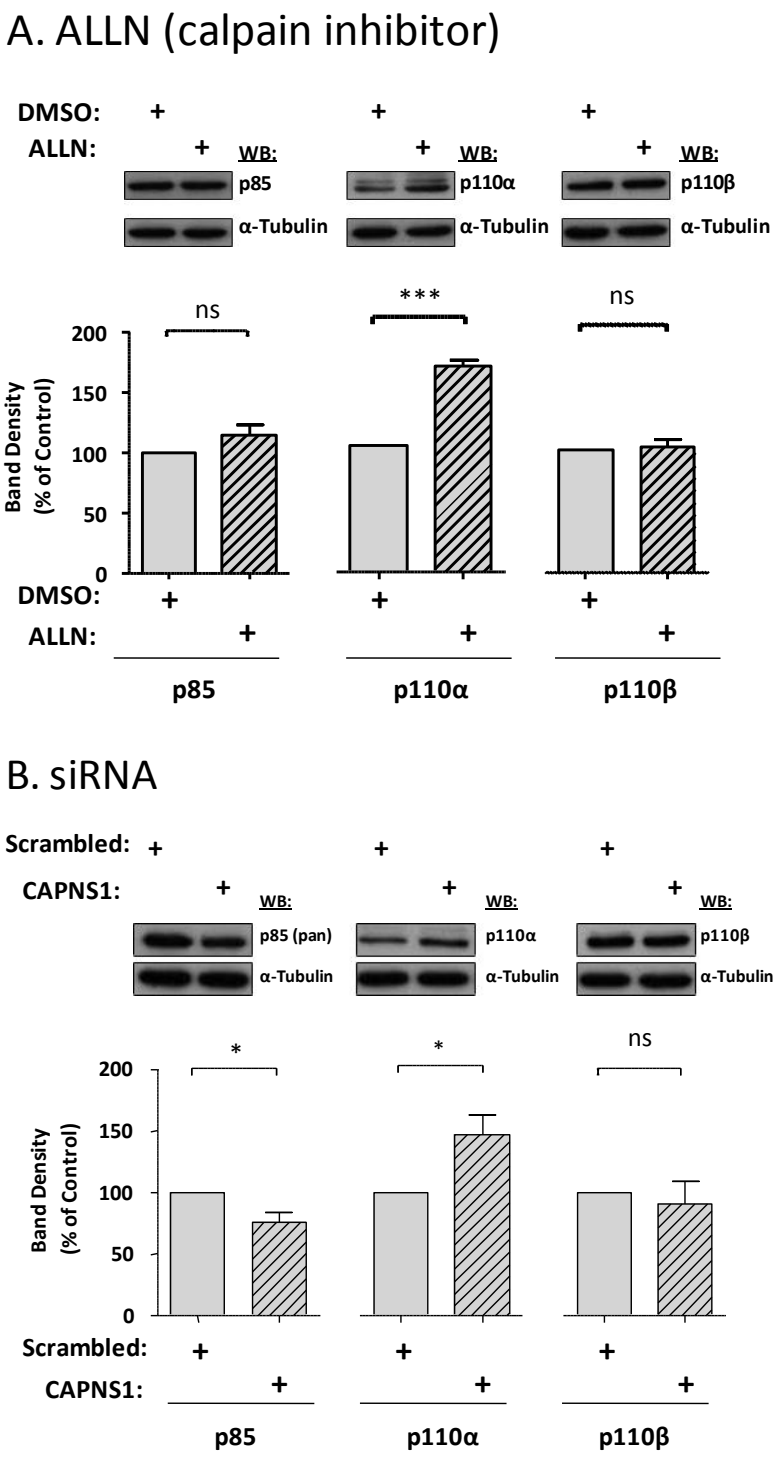

Figure 4.7. Calpain regulates the stability of p110α *in vivo.* Calpain activity in NIH-3T3 cells was inhibited for 48 h using A. the calpain inhibitor ALLN (10 μM; n = 3)) or B. siRNA for CAPNS1 (50 nM; n = 3). p85, p110α and p110β levels were measured by WB. One representative blot is shown alongside quantitative data for all experiments performed (n = 3), shown as mean ± SEM (normalized to α-tubulin). *, p <0.05; ***, p<0.0001; ns, not significant.

WB analysis revealed that the reduction in calpain activity produced by both treatments resulted in a significant increase in p110α levels of approximately 1.5-fold compared to control cells (Fig. 4.7.). In contrast, p110β levels were unaffected by either treatment (Fig. 4.7.). p85 levels were found to be slightly decreased following siRNA treatment (Fig. 4.7. B, however upon ALLN treatment p85 levels remained unchanged (Fig. 4.7. A). These results are consistent with the notion that calpains have a role in regulating p110α levels *in vivo.*

4.4. Investigations into the effects of calpain activity on PI3K signalling activity.

Following on from the discovery that PI3K proteins are calpain substrates, we next proceeded to evaluate the effects of calpain activity on PI3K/Akt signalling.

4.4.1. Effects of calpain on the phosphorylation of Akt.

In order to evaluate the effects of calpain activity on the modulation of PI3K/Akt signalling, NIH-3T3 cells were serum-starved for 18 h and then treated with the calpain inhibitor ALLN for 1 h prior to stimulation with 10% FBS for different lengths of time. WB analysis was then used to evaluate Akt phosphorylation levels (Fig. 4.8.).

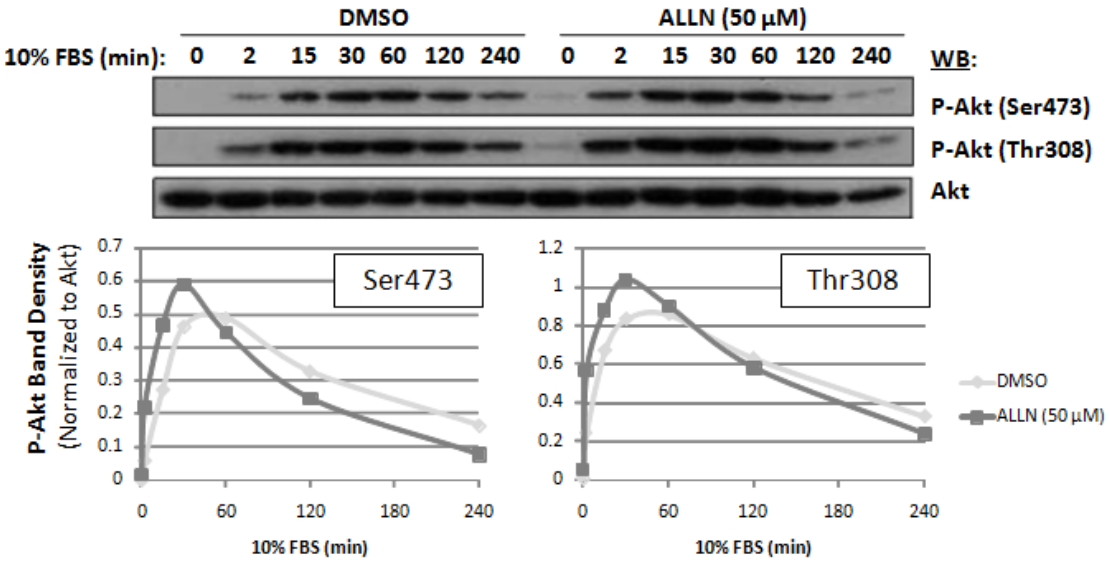

Figure 4.8. Calpain negatively regulates Akt phosphorylation downstream of serum stimulation. NIH-3T3 cells were serum-starved for 18 h followed by a 1 h treatment with DMSO (control) or ALLN (50 µM). The cells were then stimulated with 10% FBS for the indicated time and phosphorylation of Akt was determined by WB analysis. One representative blot and quantification of three is shown.

The results of this experiment revealed that the kinetics of serum-induced Akt phosphorylation, on both sites investigated, were faster in cells treated with ALLN relative to DMSO-treated control cells (Fig. 4.8.). In addition, cells treated with ALLN showed a larger magnitude of both basal and serum-induced Akt phosphorylation relative to cells treated with vehicle (Fig. 4.8.). These results indicate that calpain negatively regulated Akt phosphorylation.

4.4.2. PI3K-dependent effects of calpain on Akt phosphorylation.

Further experiments were performed to investigate the interplay between calpain activity and PI3K/Akt signalling in more detail. NIH-3T3 cells were serum-starved for 18 h and treated for 1 h with DMSO control, the calpain inhibitor ALLN, the PI3K/mTOR inhibitor LY294002 or a combination of the two inhibitors. One set of cells was then stimulated with 10% FBS for 5 min as indicated. WB analysis was then used to evaluate Akt phosphorylation (Fig. 4.9.).

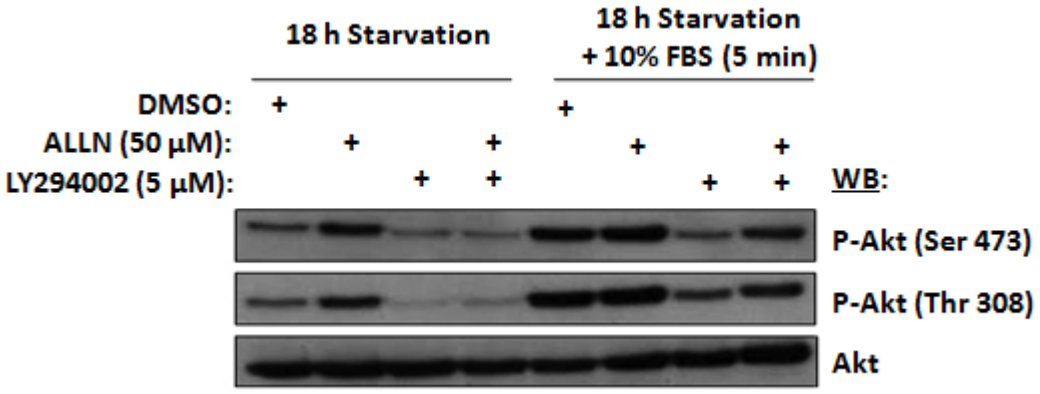

Figure 4.9. Calpain inhibition-induced Akt phosphorylation is dependent upon PI3K/mTOR. NIH-3T3 cells were serum-starved for 18 h followed by a 1 h treatment with DMSO (control), ALLN (50 µM), LY294002 (5 µM) or a combination of the two inhibitors. The cells were then stimulated with 10% FBS for 5 min (where indicated) and phosphorylation of Akt was determined by WB analysis. One representative blot of three is shown.

Consistent with previous data, treatment of cells with ALLN resulted in an increase of Akt phosphorylation at both Ser473 and Thr308 relative to vehicle-treated cells in both un-stimulated and stimulated cells (Fig. 4.9.). As expected, LY294002 treatment decreased Akt phosphorylation on both Akt sites (Fig. 4.9.). Interestingly, the observed increases in Akt phosphorylation upon calpain inhibition were not detected when cells were also treated

with LY294002 (Fig. 4.9.). These results show that increased phosphorylation of Akt as a result of decreased calpain activity (Fig. 4.8. and 4.9.) is dependent on the LY294002 targets PI3K and/or mTOR.

4.4.3. Effects of calpain on Akt activity.

In order to further investigate the effects of calpain on PI3K/Akt signalling, an Aktide assay was performed to quantify Akt activity [270, 271]. NIH-3T3 cells were serum-starved for 18 h and treated with DMSO control, calpain inhibitor ALLN, PI3K/mTOR inhibitor LY294002 or a combination of the two inhibitors for 1 h. One set of cells were then stimulated with 10% FBS for 5 min as indicated. Akt activity was then measured using the Aktide assay (Fig. 4.10.).

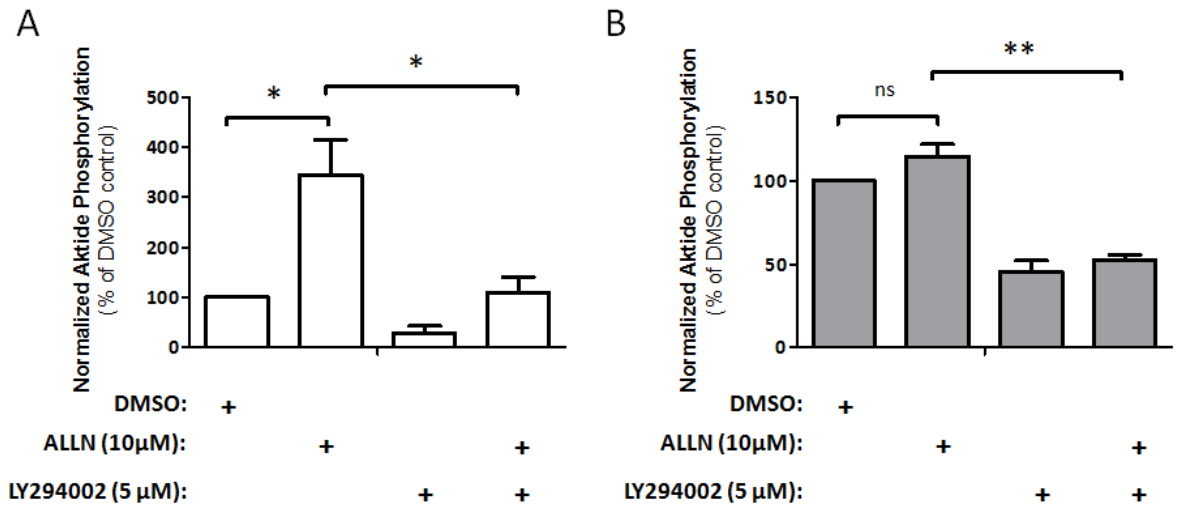

Figure 4.10. Calpain negatively regulates Akt activity. NIH-3T3 cells were serum-starved for 18 h followed by a 1 h treatment with DMSO (control), ALLN (50 µM), LY294002 (5 µM) or a combination of the two inhibitors. Cells were then left with no further treatment (A) or stimulated with 10% FBS for 5 min (B) and Akt activity was quantified using the Aktide assay (n = 3). Data expressed as mean +/- SEM. ns, not significant; *, $p<0.05$; **, $p < 0.01$.

Consistent with WB data (Fig. 4.9.), treatment of cells with ALLN resulted in a significant increase of Akt activity relative to vehicle-treated cells in un-stimulated cells (Fig. 4.10.). A slight increase, which was not found to be significant, was also observed for ALLN treated stimulated cells. As expected, LY294002 treatment decreased Akt activity under both stimulated and un-stimulated conditions (Fig. 4.10.). As previously detected by Akt phosphorylation, the observed increases in Akt activity upon calpain inhibition were not

detected when the cells were also treated with LY294002 (Fig. 4.10.), further supporting the conclusion that this phenomenon is dependent upon PI3K/mTOR.

4.4.4. Effects of calpain on signalling downstream of Akt.

In order to further verify the finding that calpain negatively regulates PI3K/Akt signalling, an experiment was performed to investigate the phosphorylation of the downstream target p70 ribosomal S6K (S6K). NIH-3T3 cells were serum-starved for 18 h and then treated with the calpain inhibitor ALLN for 1 h prior to stimulation with 10% FBS for different lengths of time. WB analysis was then used to evaluate S6K phosphorylation levels (Fig. 4.11.).

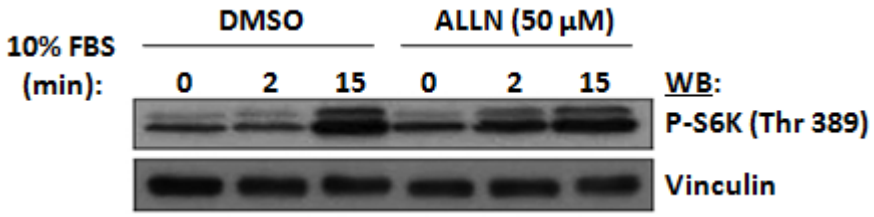

Figure 4.11. Calpain negatively regulates S6K phosphorylation downstream of Akt activity. NIH-3T3 cells were serum-starved for 18 h followed by a 1 h treatment with DMSO (control) or ALLN (50 µM). The cells were then stimulated with 10% FBS for the indicated time and phosphorylation of S6K was determined by WB analysis. One representative blot of three is shown.

WB analysis results showed that S6K phosphorylation was increased upon calpain inhibition (Fig. 4.11.). These results demonstrate that the increased PI3K/Akt signalling as a result of inhibiting calpain activity previously observed (Fig 4.8., 4.9. and 4.10.) was effectively propagated to downstream effectors of the pathway.

4.4.5. Effects of calpain on PI3K/Akt signalling confirmed by siRNA treatment.

In order to verify the findings obtained with the inhibitor ALLN we also tested the impact of siRNA knockdown of CAPNS1 on PI3K/Akt pathway activity. NIH-3T3 cells were transfected with scrambled or CAPNS1 siRNA and 48 h later subjected to 18 h of serum-starvation. Cells were then stimulated with 10% FBS, as indicated, followed by WB analysis (Fig. 4.12.).

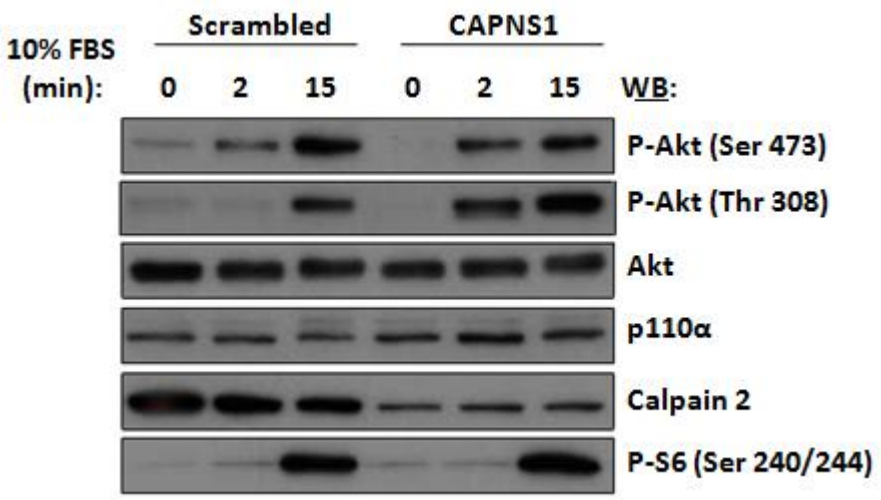

Figure 4.12. siRNA study supports the notion that calpain negatively regulates PI3K/Akt signalling. NIH-3T3 cells were transfected with scrambled or CAPNS1 siRNA (50 nM) followed by 18 h of serum-starvation and stimulation with 10% FBS, as indicated, 48 h post-transfection. Akt phosphorylation, S6 phosphorylation, p110α expression and calpain 2 expression were then assessed by WB analysis. One representative blot of three is shown.

In line with the pharmacological data (Fig. 4.8., 4.9. and 4.11.), Akt phosphorylation on Ser473 and Thr308 and S6 on Ser240/244 were enhanced in cells with reduced calpain expression (Fig. 4.12.). Furthermore, in agreement with the data in Fig. 4.7. B, p110α levels were found to be increased upon calpain inhibition with CAPNS1 siRNA. Calpain 2 expression levels confirmed the efficacy of the siRNA treatment, as previously observed (Fig. 4.1. A). Taken together, these results reinforce the notion that calpain negatively modulates PI3K/Akt signalling activity *in vivo*.

4.5. Investigations into the effects of calpain activity on cell growth and survival.

Having established that calpain has a role in the regulation of PI3K/Akt signalling, we next proceeded to evaluate the functional impact of this phenomenon in terms of cell growth and survival.

4.5.1. Effects of calpain on the viability of serum-starved cells.

We initially investigated the effects of calpain activity in serum-starved cells, as this was the condition where calpain inhibition was found to have the most pronounced effect on

PI3K/Akt signalling (Fig. 4.9. and 4.10.). NIH-3T3 cells were serum-starved for 48 h, during which calpain and PI3K/mTOR activities were inhibited using pharmacological inhibitors (ALLN and LY294002) or siRNA knockdown. Cell viability was assessed using an MTS assay (Fig. 4.13.).

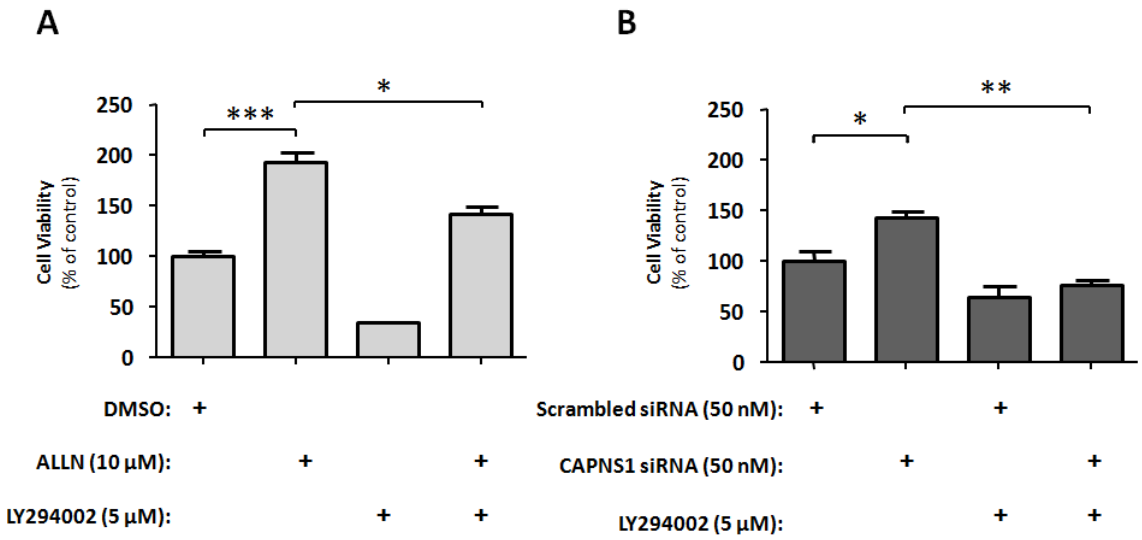

Figure 4.13. Inhibition of calpain increases cell viability during serum-starvation. NIH-3T3 cells were starved of serum for 48 h. The impact of calpain activity was investigated by concurrent treatment with A. DMSO control, ALLN (10 µM), LY294002 (5 µM) or a combination of the two inhibitors for 48 h or B. scrambled siRNA, CAPNS1 siRNA (50 nM), LY294002 (5 µM) or a combination of siRNA and PI3K inhibitor. Cell viability was then assessed using an MTS assay. Data expressed as mean ± SEM (n = 3).*, $p < 0.05$; **, $p < 0.01$; ***, $p < 0.001$.

Inhibition of calpain by ALLN resulted in an approximately 2-fold increase in the number of viable cells (Fig. 4.13.A), whilst siRNA treatment increased cell numbers by approximately 1.5-fold (Fig. 4.13.B). As expected, treatment with LY294002 reduced cell viability (Fig. 4.13.). Interestingly, inhibition of calpain activity, with either ALLN or with CAPNS1 siRNA, in conjunction with LY294002 treatment opposed the effects of calpain inhibition in increasing viability (Fig. 4.13.).These data thus suggest that the effects of calpain in modulating proliferative signals are at least partly dependent on PI3K/mTOR. These results also indicate that calpain has a role in the negative regulation of PI3K/mTOR-dependent growth and survival during serum-starvation.

4.5.2. Effects of calpain on the viability of growing cells.

We also investigated the role of calpain activity in the regulation of growth and survival in exponentially growing cells. NIH-3T3 cells, in complete growth medium, were treated with the calpain inhibitor ALLN or siRNA against CAPNS1 in the presence or absence of the PI3K/mTOR inhibitor LY294002. Cell viability was assessed using an MTS assay (Fig. 4.14.).

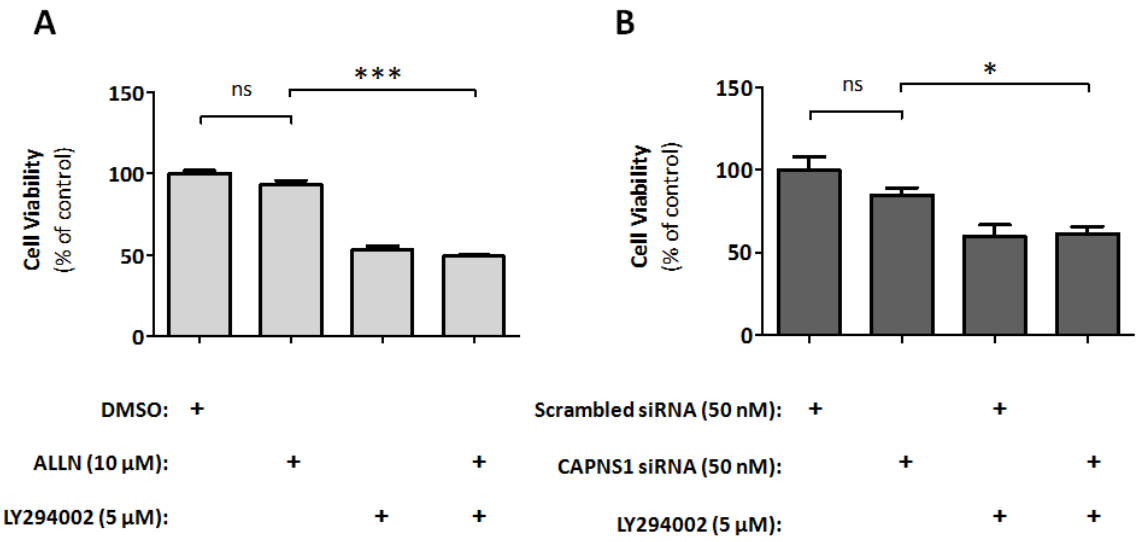

Figure 4.14. Inhibition of calpain does not significantly affect the viability of exponentially growing cells. NIH-3T3 cells were treated with A. DMSO control, ALLN (10 µM), LY294002 (5 µM) or a combination of the two inhibitors or B. scrambled siRNA, CAPNS1 siRNA (50 nM), LY294002 (5 µM) or a combination of siRNA and inhibitor for 48 h. Cell viability was then assessed using an MTS assay. Data expressed as mean ± SEM (n = 3). ns, not significant; *, $p < 0.05$; ***, $p < 0.001$.

Inhibition of calpain, by either approach, did not significantly affect cell viability, although a slight decrease was observed (Fig. 4.14.). As expected, treatment with LY294002 reduced cell viability and concurrent treatment with ALLN was not found to affect this inhibitory effect (Fig. 4.14.). These results suggest that calpain has no significant impact on the regulation of cell growth and survival under standard cell culture growth conditions.

4.5.3. Effects of calpain on the cell cycle progression of serum-starved cells.

Having established that calpain has a significant impact on cell viability during serum-starvation, we next proceeded to investigate the underlying mechanisms for this phenomenon. We first investigated the effects of calpain activity on cell cycle progression. NIH-3T3 cells were serum-starved and treated with the calpain inhibitor ALLN and/or the

PI3K/mTOR inhibitor LY294002 for 48 h. Cell cycle progression was then evaluated using FACS analysis of PI stained cells (Fig. 4.15.).

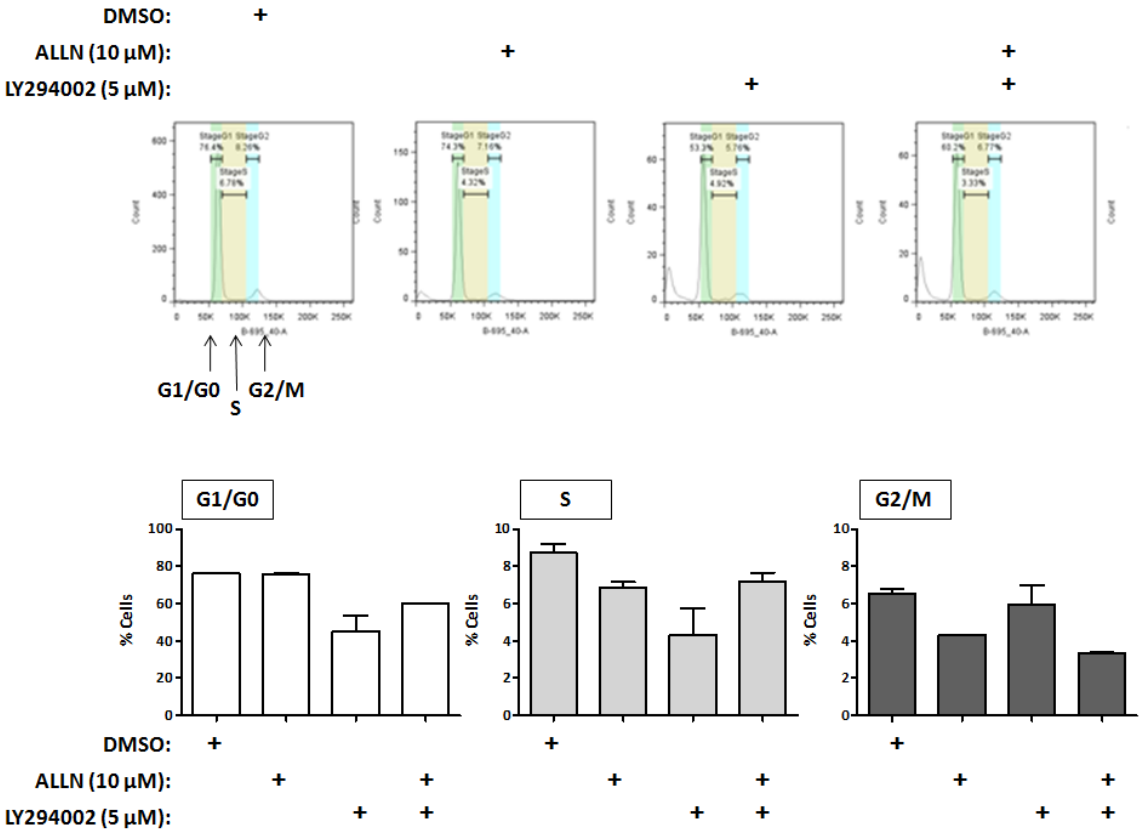

Figure 4.15. Calpain inhibition promotes cell cycle arrest in a PI3K-independent manner. NIH-3T3 cells were serum-starved and treated with DMSO control, ALLN (10 µM), LY294002 (5 µM) or a combination of the two inhibitors for 48 h. Cells were then fixed using ethanol and stained with PI prior to FACS cell cycle analysis. FACS output for one representative experiment and quantitative data for all experiments performed (n = 2) is shown. Data expressed as mean ± SEM.

FACS analysis revealed that PI3K/mTOR inhibition resulted in a considerable decrease in the percentage of cells in G1/G0 and S phases (by around 2-fold), whereas the fraction of cells in G2/M was only slightly decreased (Fig. 4.15.). In contrast, calpain inhibition resulted in no change in the percentage of cells in G1/G0 phase, whereas the fraction of cells in S and G2/M phases was reduced (Fig. 4.15.), indicating that the cells were more arrested compared to control cells. However, when PI3K/mTOR was also inhibited the effects of calpain inhibition were not opposed, indicating that these effects were unlikely to be

PI3K/mTOR dependent. These results therefore suggest that the calpain-PI3K interaction does not significantly affect cell cycle progression.

4.5.4. Effects of calpain on apoptosis in serum-starved cells.

We next investigated the effects of calpain on apoptosis in serum-starved cells. NIH-3T3 cells were serum-starved and treated with the calpain inhibitor ALLN and/or the PI3K/mTOR inhibitor LY294002 for 48 h. Apoptosis was then evaluated using FACS analysis of Annexin V and PI stained cells (Fig. 4.16.).

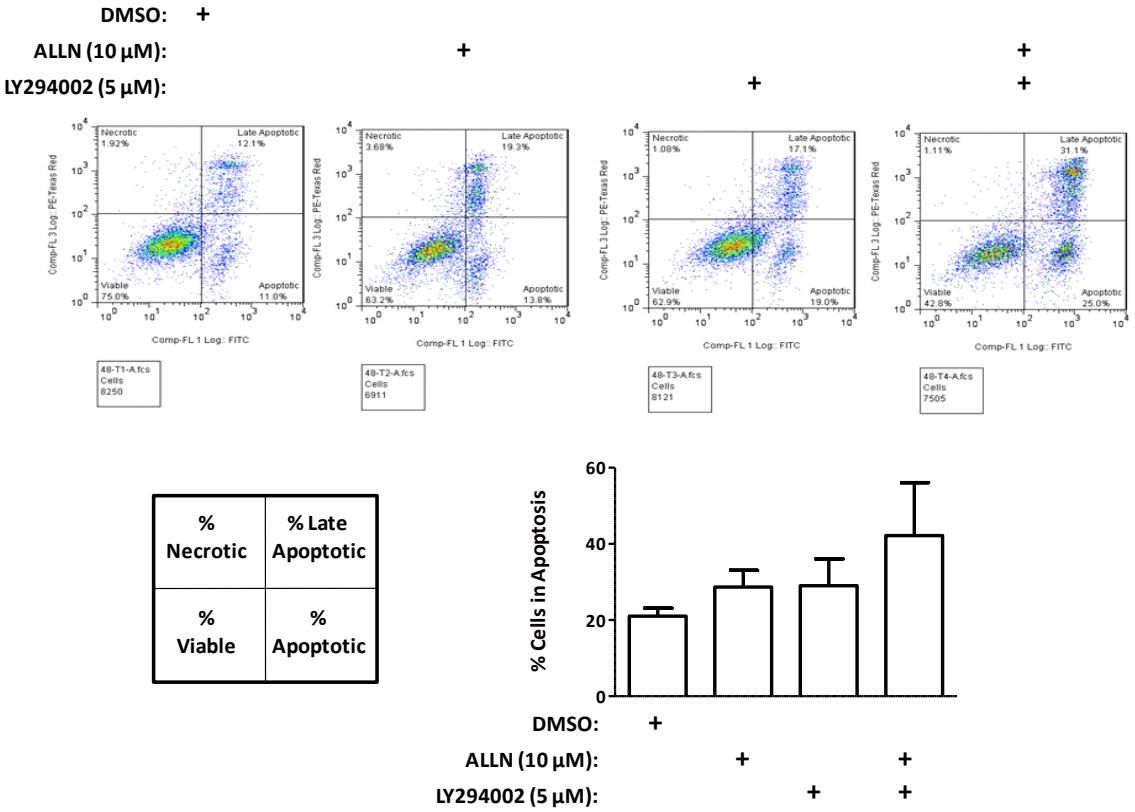

Figure 4.16. Calpain and PI3K inhibition promote apoptosis via complementary mechanisms. NIH-3T3 cells were serum-starved and treated with DMSO control, ALLN (10 µM), LY294002 (5 µM) or a combination of the two inhibitors for 48 h. Cells were then stained with Annexin V and PI prior to FACS analysis for apoptotic and necrotic markers. FACS output for one representative experiment and quantitative data for all experiments performed (n = 2) is shown. Data expressed as mean ± SEM.

FACS analysis revealed that both calpain and PI3K/mTOR inhibition increased the percentage of cells undergoing apoptosis (Fig. 4.16.). The combined effects of the two inhibitors were cumulative (Fig. 4.16.), indicating that the mechanisms were complimentary.

These data thus suggest that the calpain-PI3K interaction does not affect apoptosis outcome upon serum-starvation.

4.5.5. Effects of calpain on autophagy in serum-starved cells.

Finally, we investigated the effects of calpain on autophagy, as this process is strongly implicated in cell growth and survival. NIH-3T3 cells were serum-starved and treated with the calpain inhibitor ALLN and/or the PI3K/mTOR inhibitor LY294002 for 48 h. The cells were then subjected to WB analysis of the autophagic marker LC3 [307](Fig. 4.17.).

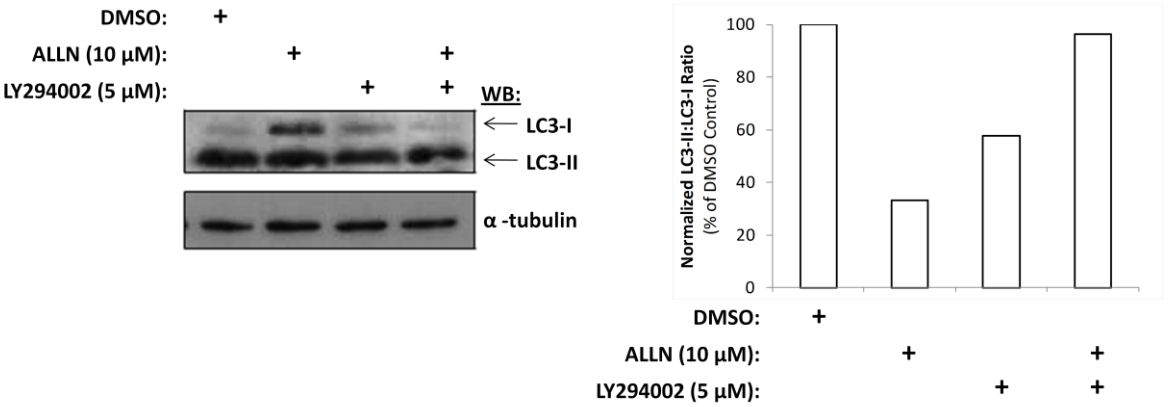

Figure 4.17. Calpain inhibition reduces autophagy in a PI3K-dependent manner. NIH-3T3 cells were serum-starved and treated with DMSO control, ALLN (10 μM), LY294002 (5 μM) or a combination of the two inhibitors for 48 h. Cells were then subjected to WB analysis for the autophagic marker LC3. One representative blot and quantification of LC3-II:LC3-I ratio of three is shown.

The LC3-II to LC3-I ratio, a quantitative marker of autophagy [290], indicated that calpain inhibition reduced autophagic activity by over 2 fold (Fig. 4.17.). PI3K inhibition also resulted in a reduction of autophagy, however the use of the two inhibitors in combination reversed the effects of calpain inhibition (Fig. 4.17.). These data suggest that calpain has a role in the regulation of autophagy that is mediated through PI3K/mTOR. These results may provide some insight into the mechanism for increased cell viability upon calpain inhibition in serum-starved cells.

4.6. Conclusions

We initially sought to confirm the finding described in Chapter 3 from the AP-MS screen indicating that CAPNS1 interacts with Class IA PI3K. Furthermore, we sought to investigate if

the active calpain heterodimer was part of the PI3K complex and what the implications of this association were for the regulation of PI3K activity.

We isolated PI3K protein complexes from starved and stimulated NIH-3T3 cells and used an *in vitro* calpain activity assay to confirm the presence of active calpain heterodimers in the complex (Fig. 4.2.). Furthermore, we demonstrated that, in line with the AP-MS findings, the association between PI3K and calpain was higher in serum-starved cells compared to serum-stimulated cells (Fig. 4.2.). To further validate the findings from the AP-MS study, we also isolated calpain protein complexes and used an *in vitro* lipid kinase assay to confirm the presence of PI3K in the protein complex (Fig. 4.3.) and showed, again, that the association was higher in serum-starved cells compared to serum-stimulated cells. Further investigation also revealed that the association between PI3K and calpain increased as serum-starvation time progressed (Fig. 4.3.) and that total calpain activity of the cells was also increased upon serum-starvation (Fig. 4.4.).

Having confirmed the association between calpain and class IA PI3K, we next proceeded to investigate if PI3K was a substrate for this protease. We isolated PI3K proteins from NIH-3T3 and RAW 264.7 cells and subjected them to *in vitro* protease digestion using purified calpain 1 and calpain 2. WB analysis of the different PI3K proteins revealed that p110α was completely cleaved by both calpain proteins, whereas p110δ and p85 proteins were only partially cleaved and p110β was virtually unaffected (Fig. 4.5.). Further investigation revealed that calpain-mediated cleavage of p110α resulted in a decrease in lipid kinase activity (Fig. 4.6.). We inhibited calpain activity in cells, pharmacologically and genetically, and used WB analysis of PI3K proteins to demonstrate that calpain also regulated the stability of p110α *in vivo* (Fig. 4.7.).

We next investigated the effects of calpain on PI3K/Akt signalling pathway activity. WB analysis revealed that pharmacological calpain inhibition affected the kinetics of Akt phosphorylation, producing a faster response and reaching a higher peak (Fig. 4.8.). Further investigation, using inhibitors, also demonstrated that this increase in Akt phosphorylation was dependent on PI3K/mTOR activity (Fig. 4.9.). Subsequent investigations also demonstrated that this increase in Akt phosphorylation results in a true increase in Akt activity (Fig. 4.10.) and that the signal was effectively propagated downstream to the

effector p70 S6K (Fig. 4.11.). These effects of calpain on PI3K/Akt signalling were also confirmed using genetic inactivation of calpain by siRNA treatment (Fig. 4.12.).

We then evaluated if the negative regulation of PI3K/Akt signalling by calpain had any functional impact on cell growth and survival. We used an MTS assay to investigate the effects of calpain and PI3K inhibition, using inhibitors and siRNA, on the viability of serum-starved cells. The results of these experiments revealed that calpain inhibition promotes survival of cells under serum-starvation in a PI3K/mTOR-dependent manner (Fig. 4.13.). In contrast, calpain was not found to have any significant effect on the viability of cells under cell culture growth conditions (Fig. 4.14.).

We next investigated the potential mechanisms for increased cell viability upon calpain inhibition in serum-starved cells. FACS cell cycle analysis revealed that, whilst calpain inhibition did contribute to cell cycle arrest, this effect was independent of PI3K/mTOR (Fig. 4.15.). Similarly, FACS analysis of apoptosis failed to identify a role for the PI3K-calpain interaction in the regulation of apoptosis (Fig. 4.16.). However, quantification of the autophagy marker LC3-II:LC3-I ratio suggested that the interaction of calpain with PI3K may have a role in the promotion of autophagy, which is also dependent on PI3K activity (Fig. 4.17.).

In summary, we have verified that active calpain heterodimers associate with class IA PI3K. Furthermore, this work indicates that calpain has a role in the regulation of PI3K protein stability and signalling activity. One of the identified biological outcomes of this relationship is that calpain inhibition increases cell viability under serum-starvation, possibly through the regulation of autophagy.

5. Identification of Phosphorylation Events Downstream of Akt

5.1. Introduction and aim of study

Having explored the regulation of PI3K by interaction partners we next focused our attention on the investigation of the dynamics of signalling downstream of PI3K. Akt, a protein kinase activated downstream of class I PI3K activity, forms part of the critically important signalling node: the PI3K/Akt pathway [2, 60]. This pathway plays an essential role in the regulation of a wide range of cellular functions including cell survival, growth, proliferation, migration and metabolism [2, 60].

Akt is recruited to the cell membrane through the binding of its PH domain with PIP_3, the product of PI3K lipid kinase activity. This translocation permits the phosphorylation of Akt at the residue Thr308, by PDK1 [78], and at the residue Ser473, by the mTORC2 complex [149], thus activating Akt. The most important regulators of Akt activity are the balance of PIP_2 and PIP_3 at the cell membrane [83] and the activity of protein phosphatases, such as PP2A and PHLLP [85, 308]. Phosphorylation of Akt substrates can result in positive or negative regulation of protein activity and affects many important cellular processes. Many downstream substrates have been well characterized, including but not limited to BAD, FOXO, PRAS40, GSK-3 and TSC2 [90, 148, 309-312]. However, there are many more reported potential substrates, some of which have not been fully validated *in vivo* [60].

Phosphoproteomics is the area of proteomics that is dedicated to the characterisation of protein phosphorylation and the most notable application of this method is in the study of signalling pathways, as phosphorylation is a key mechanism in their regulation [200-202]. Mass spectrometry based global phosphoproteomics has revolutionized this area of research, permitting the large-scale quantitative evaluation of dynamic pathway activity, which is not possible using any other method [203, 205]. Understanding the intricacies of signalling activity can lead to the identification of novel therapeutic targets and biomarkers.

Global phosphoproteomics enables the qualitative and quantitative evaluation of hundreds, or even thousands, of phosphorylation events in a single analysis. In addition, no prior knowledge of a phosphorylation site is necessary and novel sites can be concomitantly identified and quantified. However, there remains a key limitation for this technique when

used for the investigation of kinase signalling activity: we do not always know the identity of the kinase that is phosphorylating a particular site [205]. Thus, our interpretations of the signalling dynamics under investigation are hampered. Annotation of the phosphoproteome with this important information would enable the advancement of progress in this field. In addition, the identification of phosphorylation events that are characteristic of activity of a particular pathway may have useful applications as biomarkers [205, 313].

The aim of the work presented in this Chapter was to apply our optimised quantitative phosphoproteomic approach [232] (Fig. 5.1.) to identify phosphorylation events downstream of Akt, thus annotating this fraction of the phosphoproteome. We used two complementary strategies, an *in vivo* cell line model and an *in vitro* assay, to carry out this work and cross-referenced the data to maximise confidence.

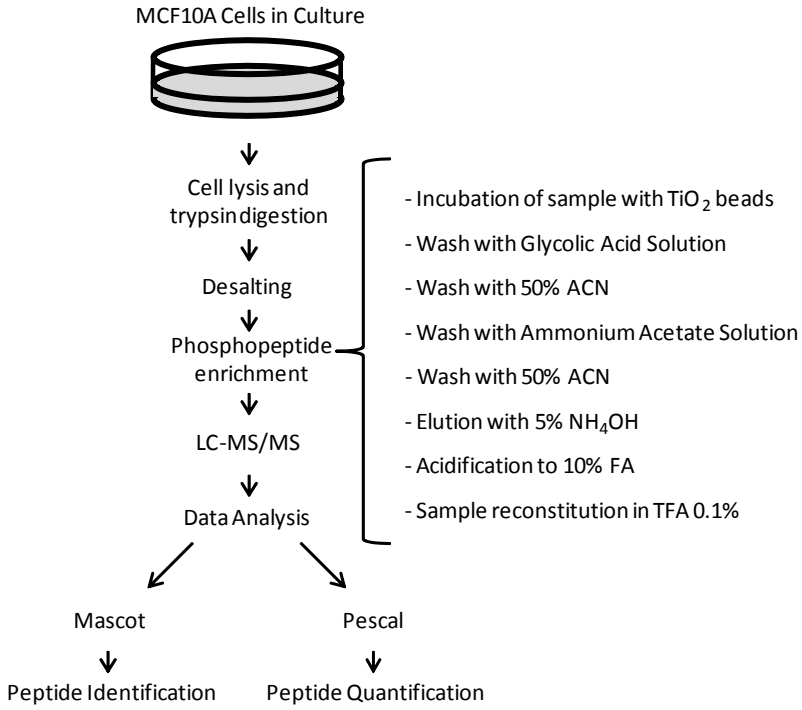

Figure 5.1. Summary of phosphoproteomic approach. Samples were lysed, reduced, alkylated and digested with trypsin prior to de-salting by RP chromatography. The solution was then incubated with TiO_2 beads to enable peptide binding followed by the removal of un-phosphorylated peptides by sequential washing with glycolic acid solution, 50% ACN, ammonium acetate solution and 50% ACN. Phosphopeptides were then eluted using NH_4OH prior to acidification followed by drying and reconstitution for LC-MS/MS analysis. Figure reproduced (with modifications) from[232].

The *in vivo* cell model approach we used applied global phosphoproteomics to the MCF10A myrAktER cell line, an immortalised mammary epithelial cell line stably transfected with the myrAktER (myristoylated Akt and mutant oestrogen receptor hormone binding domain fusion protein) construct (Fig. 5.2. A). This construct contains a constitutively active form of Akt which is inducible by treatment with 4-hydroxytamoxifen (4-OHT) [314] (Fig. 5.2. B), thus providing a refined system for the investigation of the biochemistry of Akt activity and its contribution to the regulation of cell biology. The MCF10A myrAktER cell line was generated by Dr Subham Basu and was a kind gift for this project.

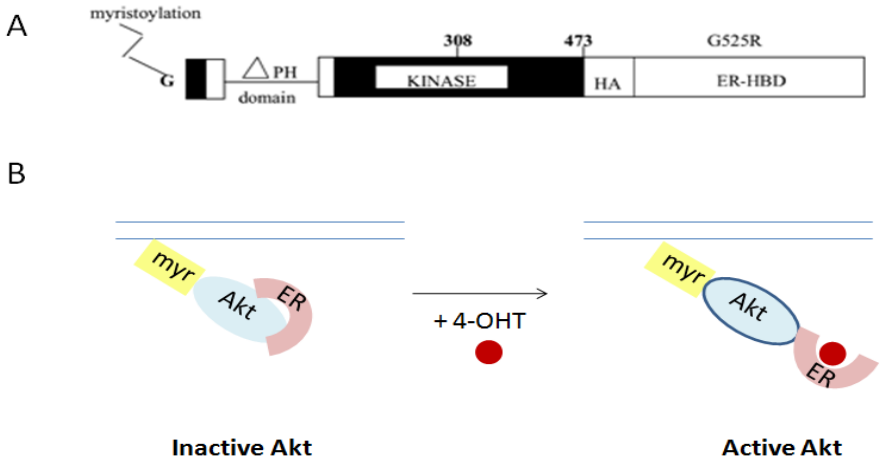

Figure 5.2. MCF10A myrAktER cell model. A. Representation of the myrAktER construct designed by Kohn *et al* (figure reproduced from [314]. B. Illustration of the induction of Akt activity using the myrAktER construct. The myr tag constitutively targets the myrAktER construct to the cell membrane, however the mutant oestrogen receptor hormone binding domain inhibits Akt activity by steric hindrance. Upon 4-OHT treatment, the mutant oestrogen receptor hormone binding domain binds the drug thereby releasing its inhibitory effect and rendering Akt constitutively active.

In the *in vitro* assay approach, we applied global phosphoproteomics in combination with an *in vitro* kinase assay, originally developed by the Cohen group [272, 273], which uses intact dephosphorylated proteins as the assay substrate (Fig. 5.3.). In addition to the identification of phosphorylation events downstream of Akt, we also developed this strategy further to enable the quantification of kinase activity in a global fashion.

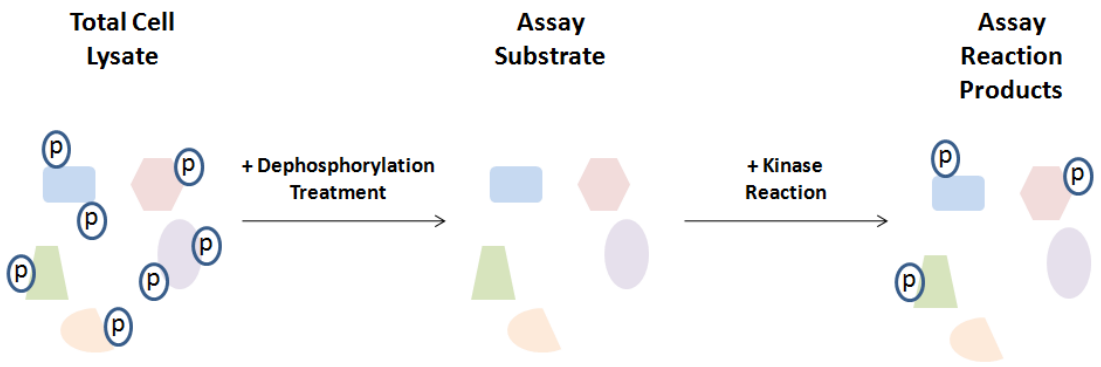

Figure 5.3. Illustration of the principles of the *in vitro* kinase assay. Total cell lysate was harvested from cells and dephosphorylated using endogenous or exogenous phosphatase activity. The dephosphorylated proteins were then used as the substrate for an *in vitro* kinase assay. Reaction products reflect the phosphorylation activity of the kinase under investigation.

5.2. Characterisation of the MCF10A myrAktER model

We initially sought to characterise the activity of the myrAktER construct to confirm the suitability of this cell line model for the investigation of phosphorylation events downstream of Akt.

5.2.1. Phosphorylation of the myrAktER construct in response to 4-OHT dose and treatment time.

We performed a set of experiments to investigate the phosphorylation of the myrAktER construct in response to 4-OHT treatment. Exponentially growing myrAktER cells, in full growth medium, were treated with 4-OHT or ethanol control at the indicated dose for the given time length. WB analysis was then performed to evaluate the effects of the treatment on Akt phosphorylation (Fig. 5.4.).

A

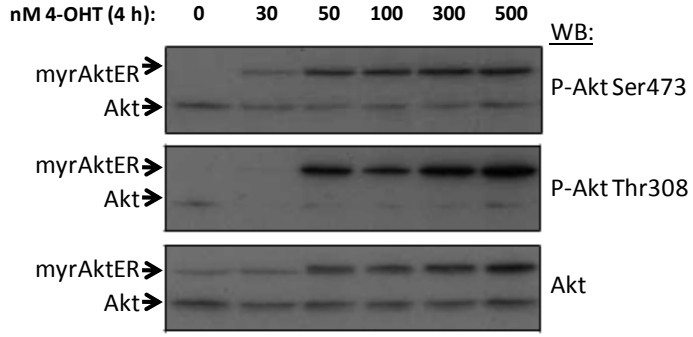

B

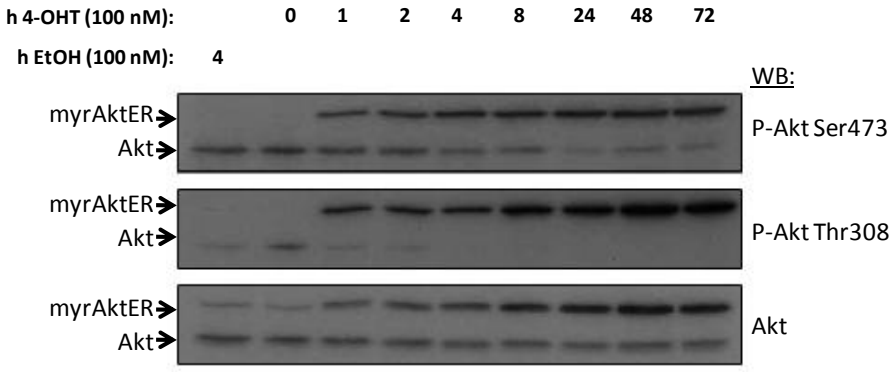

Figure 5.4. 4-OHT treatment enables controlled phosphorylation of the myrAktER construct. MCF10A myrAktER cells were treated with A. 0, 30, 50, 100, 300 or 500 nM 4-OHT for 4 h or B. 100 nM 4-OHT for 0, 1, 2, 4, 8, 24, 48 or 72 h or ethanol (EtOH) control for 4 h. Samples were then subjected to WB analysis of Akt phosphorylation. One representative blot of two is shown.

Results of these experiments showed that myrAktER phosphorylation was not completely induced at the lowest doses of 4-OHT treatment (30 nM) (Fig. 5.4. A). However, phosphorylation of myrAktER, at Ser473 and Thr308, was observed at all the other doses tested (Fig. 5.4.A). myrAktER phosphorylation levels were observed to increase slightly as the dose increased and total myrAktER levels were found to be higher for cells where the construct was active (Fig. 5.4. A).

Results also showed that, at a dose of 100 nM, 4-OHT induced the phosphorylation of myrAktER, at both at Ser473 and Thr308, within 1 hour (Fig. 5.4. B). This phosphorylation was shown to increase considerably over the time-course, up to 72 hours, most likely due to the resistance of this Akt construct to normal negative feedback regulatory mechanisms (Fig. 5.4. B). Interestingly, total myrAktER was also shown to increase over the time-course

(Fig. 5.4. B). The observed increases in total myrAktER upon activation of the construct may be due to resistance of myrAktER to normal regulatory feedback mechanisms, such as proteolytic degradation, or may indicate that the myrAktER construct is not detected well by the total Akt antibody when in its inactivated conformation. Endogenous Akt phosphorylation in treated cells was shown to decrease as myrAktER phosphorylation increased (Fig. 5.4. B). These results suggest that negative regulatory mechanisms against Akt activity within the cells are active. The data also show that the ethanol vehicle has no effect upon the phosphorylation of the myrAktER construct (Fig. 5.4. B).

These data show that myrAktER phosphorylation can be rapidly induced upon 4-OHT treatment. Furthermore, the results of the time course experiment show that the extent of Akt phosphorylation can be controlled by treatment time, thus enabling fine-tuned control of the model.

5.2.2. Akt activity in response to 4-OHT dose and treatment time.

To further investigate the activation of the myrAktER construct by 4-OHT treatment we next proceeded to quantify Akt activity in response to different doses and treatment times of 4-OHT. Exponentially growing myrAktER cells, in full growth medium, were treated with 4-OHT or ethanol control at the indicated dose for the given time length. The Aktide assay [270, 271] was then performed to quantify Akt pathway activation (Fig. 5.5.).

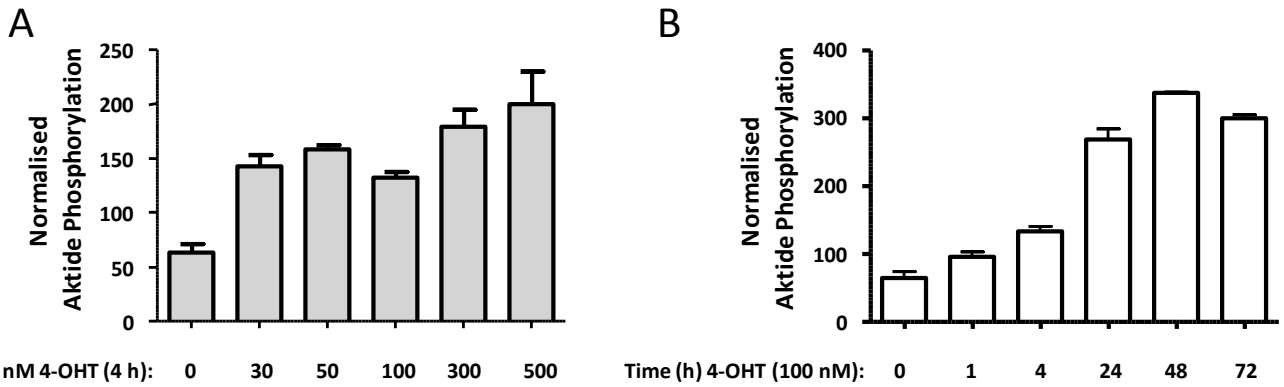

Figure 5.5. 4-OHT treatment enables controlled activation of Akt. MCF10A myrAktER cells were treated with A. 0, 30, 50, 100, 300 or 500 nM 4-OHT for 4 h or B. 100 nM 4-OHT for 0, 1, 4, 24, 48 or 72 h. Samples were then subjected to an Aktide assay for Akt activity (n = 3). Data expressed as mean +/- SEM.

These data show that Akt pathway activation was induced by the treatment with all concentrations of 4-OHT (Fig. 5.5. A). In line with the myrAktER phosphorylation data (Fig. 5.4. A), Akt activity increased slightly as the dose was escalated (Fig. 5.5. A). Akt pathway activation was also shown to increase significantly as treatment time was extended, reaching a peak of activity after 48 h treatment (Fig. 5.5. B).

These results support the WB data previously obtained and show that treatment time is the most important parameter for controlling Akt activity using the myrAktER model. Furthermore, these data also show that the highest levels of Akt activity can be obtained with prolonged treatment rather than with higher doses of 4-OHT.

5.2.3. Phosphorylation of substrates downstream of Akt in response to 4-OHT dose and treatment time.

We also investigated the effects of 4-OHT treatment of the myrAktER MCF10A cells on the phosphorylation of downsteam targets of Akt. Exponentially growing myrAktER cells, in full growth medium, were treated with 4-OHT or ethanol control at the indicated dose for the given time length. WB analysis was then used to evaluate the phosphorylation of PRAS40, a direct target of Akt, and S6, a target downstream of mTORC1 which is further down in the pathway (Fig. 5.6.).

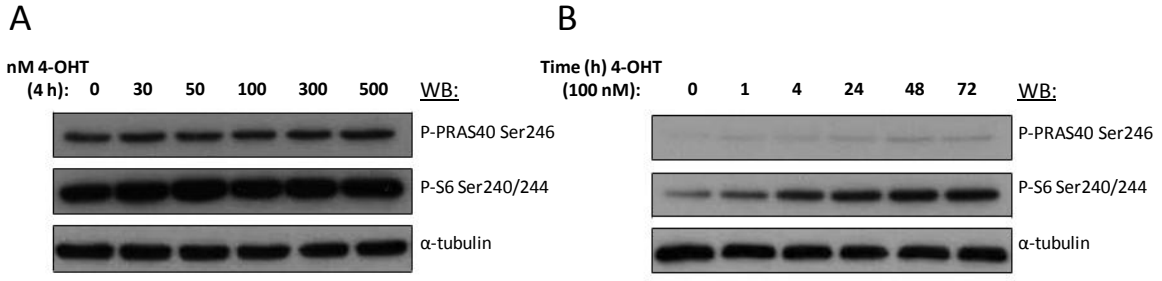

Figure 5.6. 4-OHT treatment enables the phosphorylation of downstream targets of Akt. MCF10A myrAktER cells were treated with A. 0, 30, 50, 100, 300 or 500 nM 4-OHT for 4 h or B. 100 nM 4-OHT for 0, 1, 2, 4, 8, 24, 48 or 72 h. Samples were then subjected to WB analysis for phosphorylation of the downstream targets PRAS40 and S6. One representative blot of two is shown.

These data showed that phosphorylation of targets downstream of Akt was induced by the treatment with all concentrations of 4-OHT (Fig. 5.6. A). Indeed, 4-OHT dose was shown to have little effect on the degree of phosphorylation of downstream targets (Fig. 5.6. A)

despite previous evidence showing that Akt phosphorylation and activity was variable to some degree (Fig. 5.4. A and 5.5. A). In contrast, phosphorylation of targets downstream of Akt increased as treatment time was extended (Fig. 5.6. B), reaching a peak of phosphorylation at around 48 h of treatment.

These results further support the myrAktER data previously obtained and show that treatment time is the most important parameter for controlling activity of pathway activity downstream of Akt.

5.2.4. Proliferation and survival of cells in response to 4-OHT treatment.

We finally sought to verify whether activity of the myrAktER construct had an impact on the biology of our cell model. MCF10A cells are anchorage-dependent and thus typically exhibit anoikis (detachment-induced apoptosis) upon detachment from the extracellular matrix (or artificial substitute i.e. tissue culture plastic) [315, 316]. However, increased Akt activity has been shown to inhibit apoptosis and thus reduce the incidence of anoikis in these cells [315, 316]. We attempted to verify the biological activity of the myrAktER construct by assessing the incidence of anoikis in the MCF10A myrAktER cells.

MCF10A control cells, transfected with the empty vector, (MCF10A ctrl) and MCF10A myrAktER cells were plated on 96 well-plates at a density of 2×10^4 cells per well. The wells on the plates were either uncoated or coated with poly-HEMA, a cross-linked polymer hydrogel which prevents cell attachment. The cells were treated with 100 nM 4-OHT or ethanol overnight prior to seeding and during the assay cells were cultured in growth medium containing 1% serum and were treated with 100 nM 4-OHT or ethanol as indicated. The incidence of anoikis was then assessed in terms of cell viability using an MTS assay (Fig. 5.7.).

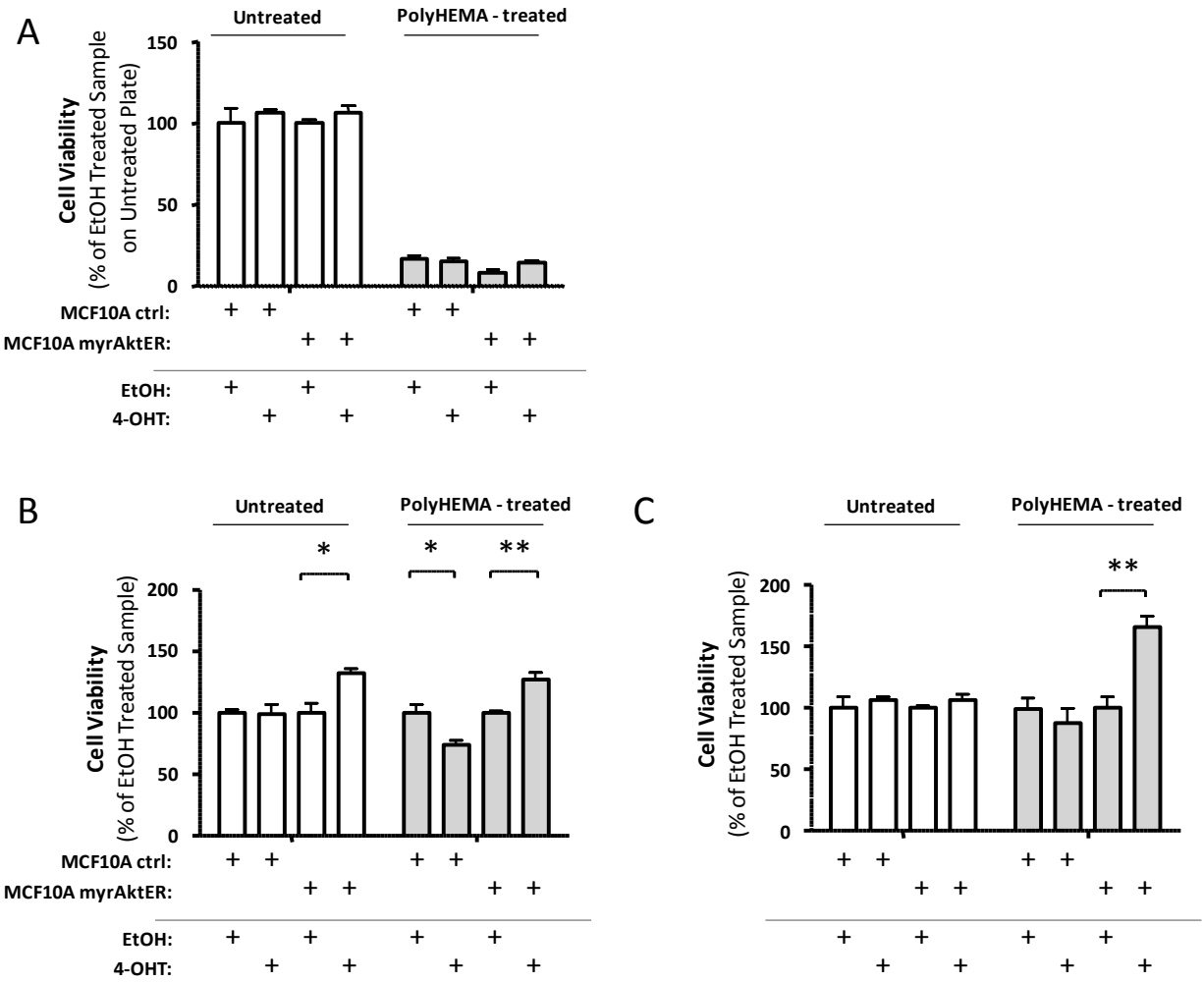

Figure 5.7. 4-OHT treatment of MCF10A myrAktER cells protects them from anoikis. MCF10A ctrl and MCF10A myrAktER cells were seeded onto 96-well plates where the wells were untreated or coated with poly-HEMA. Cells were treated as indicated O/N prior to seeding and were cultured in growth medium containing 1% medium and treatment conditions as described. Cell viability was then assessed using the MTS assay. A. Cell viability after 72 h treatment expressed as a percentage of the ethanol control on untreated wells (n = 3). B. Cell viability after 48 h expressed as a percentage of their own ethanol control according to well treatment (n = 3). C. Cell viability after 72 h as in (A) but expressed as a percentage of their own ethanol control according to well treatment (n = 3). Data expressed as mean +/- SEM. *, $p<0.05$; **, $p<0.01$.

The measurement of cell viability after 72 h revealed that cells seeded on poly-HEMA treated wells were much less abundant than those seeded on uncoated wells (Fig. 5.7. A). These data indicate that MCF10A control and myrAktER cells seeded on poly-HEMA coated wells undergo anoikis.

Measurement of cell viability after 48 h suggested that myrAktER activation by 4-OHT treatment induced increased cell proliferation on untreated wells as compared to the control samples (Fig. 5.7. B). In addition, the results for the cells plated on poly-HEMA

treated wells suggested that 4-OHT treatment was slightly toxic to MCF10A ctrl cells, as viability was significantly reduced compared to the control sample (Fig. 5.7. B). In contrast, proliferation of MCF10A myrAktER cells treated with 4-OHT was increased compared to the ethanol treated sample (Fig. 5.7. B). Measurement of cell viability after 72 h treatment showed no significant effect on cell proliferation when cells were plated on untreated wells (Fig. 5.7. C). However, when cells were plated on poly-HEMA treated wells, myrAktER activation by 4-OHT treatment resulted in significantly increased cell survival compared to the control samples (Fig. 5.7. C).

These results therefore confirmed that phosphorylation of myrAktER has a functional consequence for cell viability and therefore that the MCF10A myrAktER cell line is likely to be a useful model for the investigation of Akt activity.

5.3. Phosphoproteomic investigation of the MCF10A myrAktER model

Having established the suitability of the MCF10A myrAktER model for the investigation of Akt activity, we next proceeded to design a phosphoproteomic experiment, using our optimised quantitative phosphoproteomic strategy [232] (Fig. 5.1.), to investigate Akt-dependent phosphorylation events.

MCF10A myrAktER cells were treated with ethanol for 18 h (minimal Akt activity), treated with 100 nM 4-OHT for 1 h (low Akt activity) or treated with 100 nM 4-OHT for 48 h (high Akt activity) in full growth medium. Three biological replicates were performed per condition, each of which was analyzed in three technical replicates. Cell lysates were then harvested and 500 µg of protein were subjected to a phosphoproteomic strategy using techniques optimised in our laboratory [232]. In brief, proteins were lysed in a denaturing buffer containing 8 M urea and, following reduction and alkylation of proteins, these were subjected to in-solution trypsin digestion. The resulting peptide solution was then enriched for phosphopeptides using TiO_2 affinity chromatography. Samples were subsequently analysed by LC-MS/MS on the ThermoFisher LTQ-Orbitrap XL mass spectrometer prior to qualitative and quantitative data analysis.

Our criteria for a confident phosphopeptide identification was a MASCOT Expectation value of <0.05. A database was compiled containing 1961 unique phosphopeptide identifications across all of the experimental samples. This database was then used by

Pescal to quantify every phosphopeptide identified in each of the experimental samples (n = 27) (Fig. 5.8.).

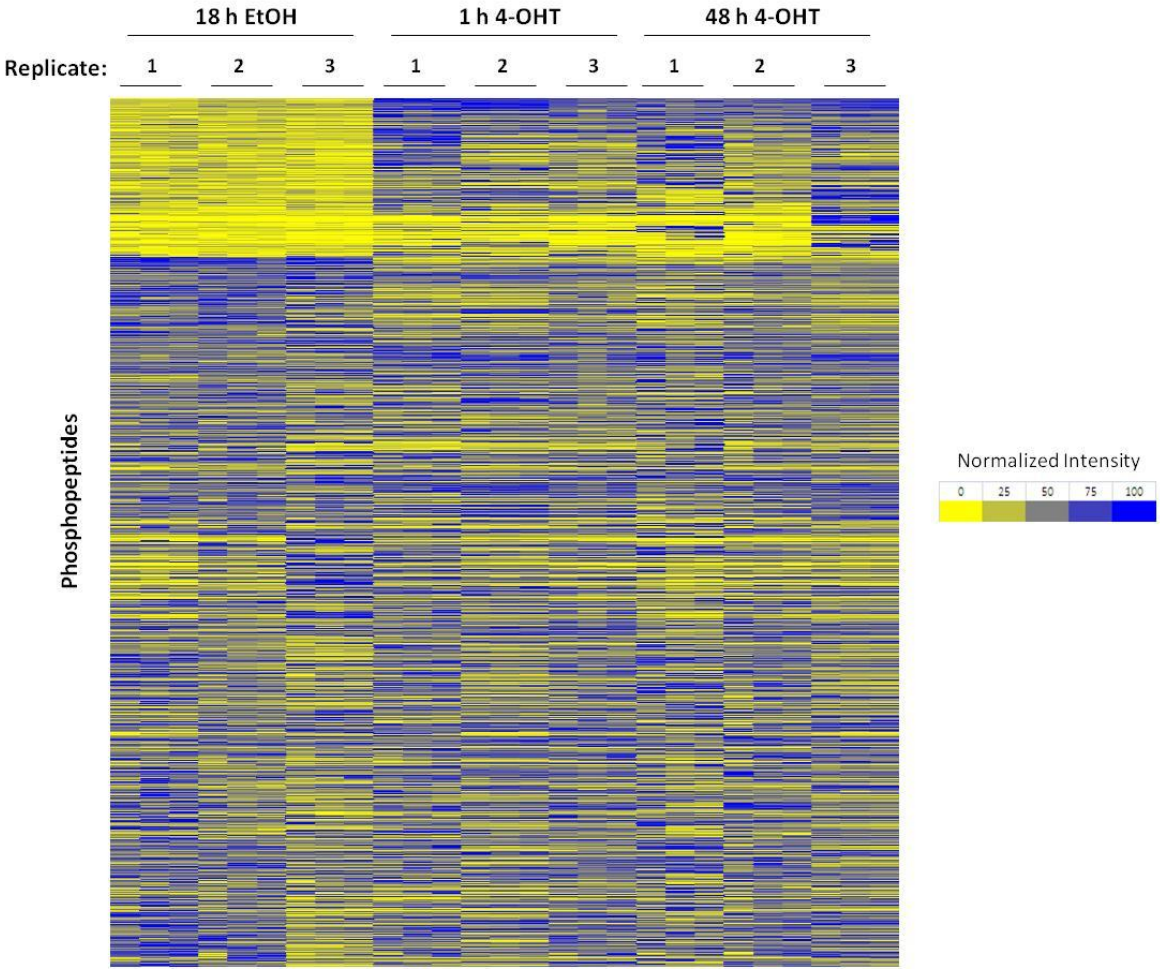

Figure 5.8. Quantitative analysis reveals phosphoproteomic response of 4-OHT treated MCF10A myrAktER cells. MCF10A cells were treated with EtOH for 18 h (minimal Akt activity), treated with 100 nM 4-OHT for 1 h (low Akt activity) or treated with 100 nM 4-OHT for 48 (high Akt activity) in full growth medium and subjected to phosphoproteomic analysis. Three biological replicates were performed per condition, each of which was analyzed in triplicate (n = 9). Quantification of all 1961 phosphopeptides identified was represented as a heat map, where phosphopeptide intensity was expressed as a percentage of the maximum intensity for that phosphopeptide.

The 1961 phosphopeptides identified in the experiment were quantified in all 27 experimental samples (3 biological replicates x 3 technical replicates x 3 conditions). The heat map representation of the quantitative data generated revealed the presence of a small cluster of phosphopeptides where phosphorylation was increased upon 4-OHT treatment of the MCF10A myrAktER cells (Fig. 5.8.).

ANOVA statistical analysis was performed to identify phosphopeptides that were quantitatively altered in one or more conditions and principal component analysis (PCA) was performed for the 564 phosphopeptides found to be significantly different ($p < 0.05$) (Fig. 5.9.).

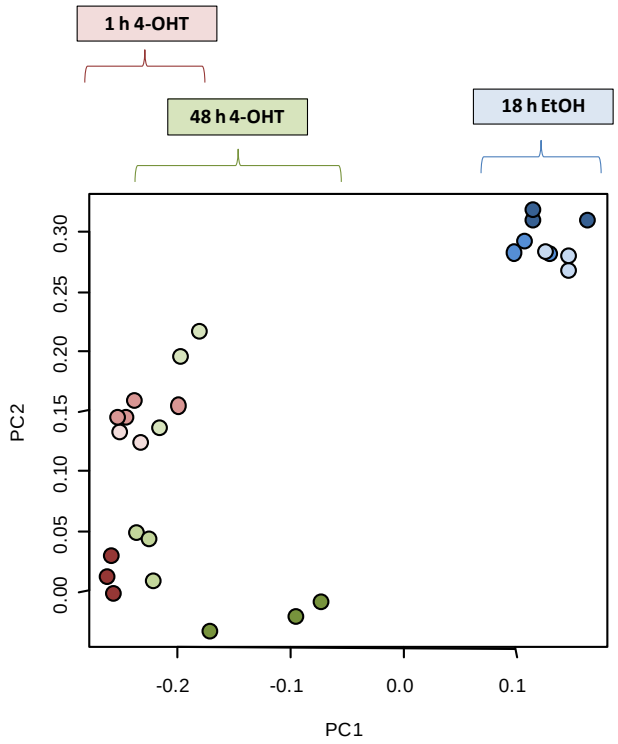

Figure 5.9. PCA separates 4-OHT treatment of MCF10A myrAktER cells according to their phosphoproteomic profile. MCF10A cells were treated with EtOH for 18 h (minimal Akt activity), treated with 100 nM 4-OHT for 1 h (low Akt activity) or treated with 100 nM 4-OHT for 48 h (high Akt activity) in full growth medium and subjected to phosphoproteomic analysis. Three biological replicates were performed per condition, each of which was analyzed in triplicate. PCA was performed for quantitative results of the 564 phosphopeptides found by ANOVA analysis to be quantitatively different under one or more conditions (n = 9).

PCA revealed that 4-OHT treatment of MCF10A myrAktER cells clustered together and distinctly from the control treated cells on the first principal component, indicating that myrAktER activation was the major factor determining variance between sample conditions (Fig. 5.9.). The separation of cells treated for 1 h or 48 h with 4-OHT was not complete on the second principal component, indicating that treatment time was not a major factor in determining variance (Fig. 5.9.).

We proceeded to define arbitrary criteria for a phosphorylation event to be considered dependent on Akt activity and therefore a downstream target. Phosphorylation events were

considered to be Akt-dependent if the fold change between either of the 4-OHT treated samples and the control sample was a minimum of 2-fold. Furthermore, the fold difference was required to be statistically significant ($p < 0.05$) as assessed by the Student's t-test ($n = 9$). A total of 238 phosphopeptides met these criteria, including some known substrates of Akt (Fig. 5.10. – 5.11. and Appendix 2).

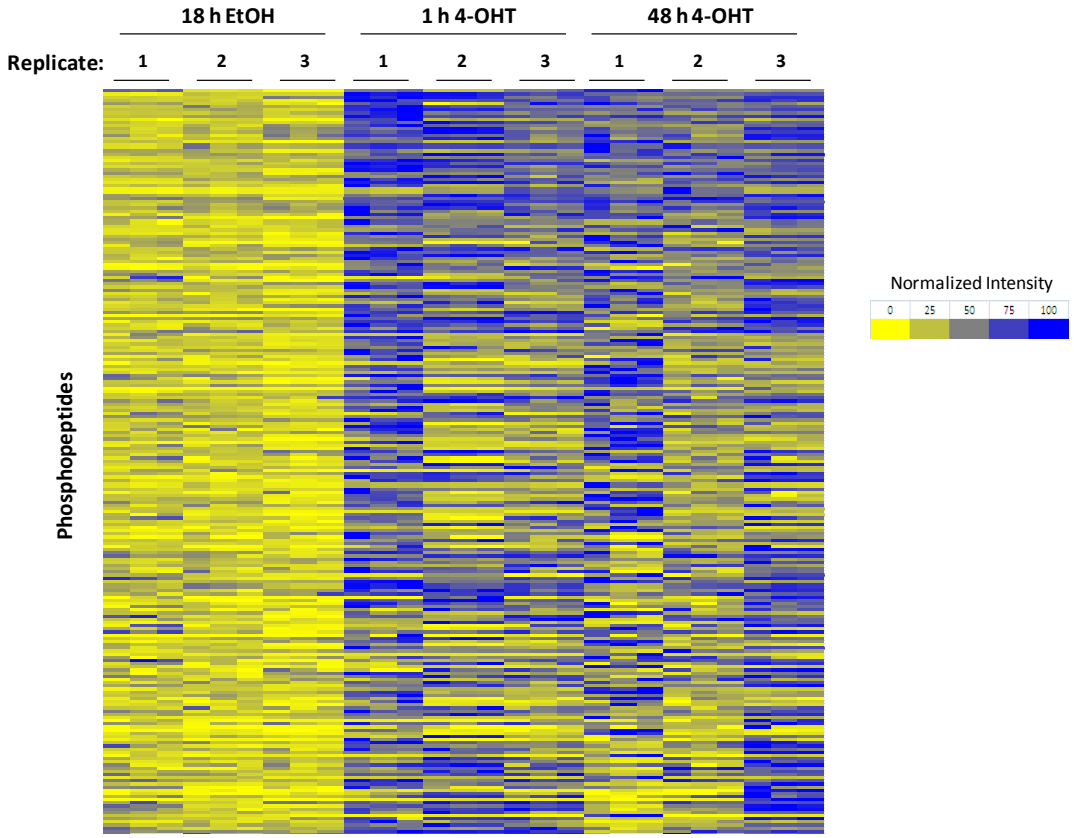

Figure 5.10. Quantitative analysis identifies phosphorylation events downstream of Akt in MCF10A myrAktER cells. MCF10A cells were treated with EtOH for 18 h (minimal Akt activity), treated with 100 nM 4-OHT for 1 h (low Akt activity) or treated with 100 nM 4-OHT for 48 h (high Akt activity) in full growth medium and subjected to phosphoproteomic analysis. Three biological replicates were performed per condition, each of which was analyzed in triplicate ($n = 9$). Phosphorylation events were considered to be downstream of Akt if the fold change between either of the 4-OHT treated samples and the starved sample was a minimum of 2-fold and statistically significant ($p < 0.05$) as assessed by the student's t-test. Quantification of the 238 phosphopeptides that met these criteria was represented as a heat map, where phosphopeptide intensity was expressed as a percentage of the maximum intensity for that phosphopeptide.

The heat map representation of quantitative data illustrates the increase in phosphorylation upon 4-OHT treatment in MCF10A myrAktER cells for candidate phosphorylation sites downstream of Akt (Fig. 5.10. and Appendix 2). It is interesting to note that for the majority of sites downstream of Akt there is little difference between the

phosphorylation response obtained after 1 h treatment compared to 48 h treatment (Fig. 5.10.) even though differences in Akt activity levels at these time points were clearly observed (5.2.1. – 5.2.2.). These results suggest that only low levels of Akt activity are required to produce full pathway activation.

Some specific examples of phosphorylation sites downstream of Akt in MCF10A myrAktER cells are also illustrated (Fig. 5.11.).

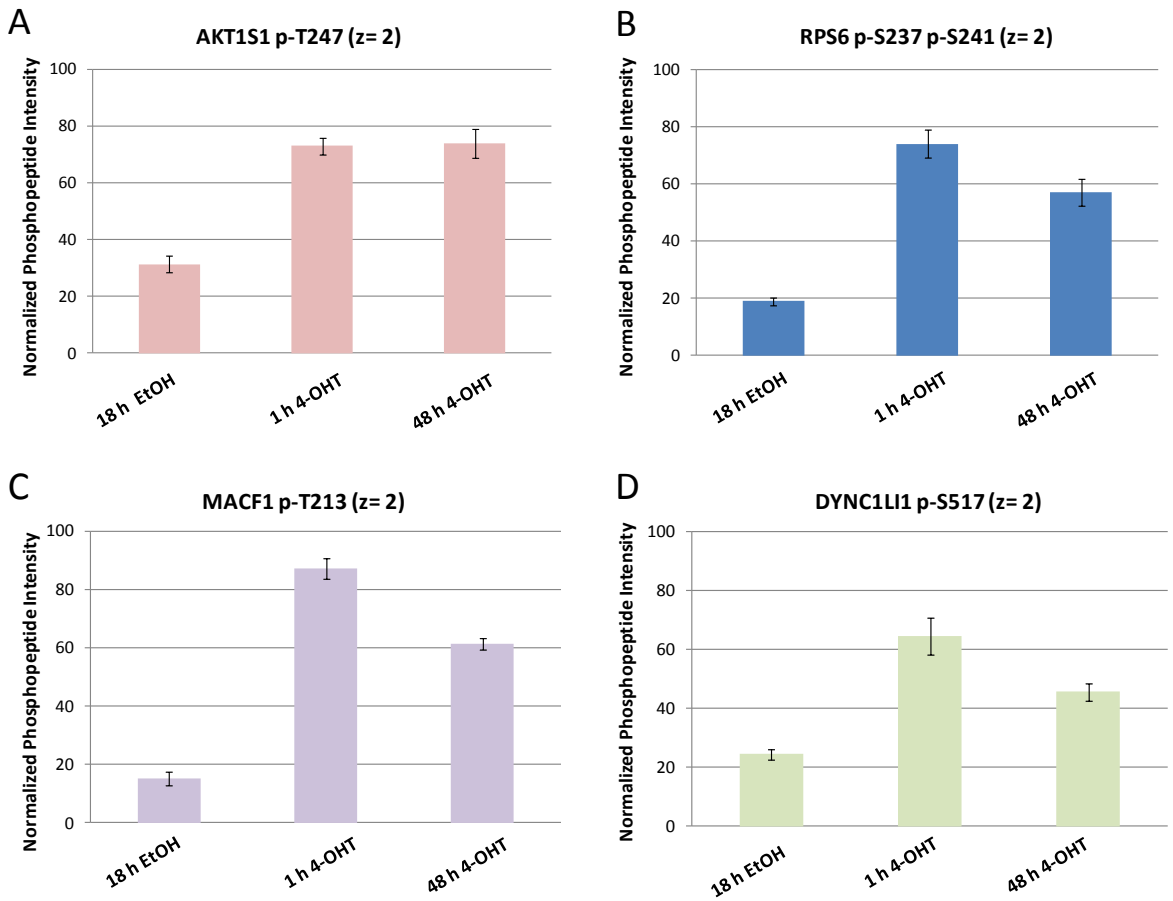

Figure 5.11. Examples of phosphorylation events downstream of Akt in MCF10A myrAktER cells. MCF10A cells were treated with EtOH for 18 h (minimal Akt activity), treated with 100 nM 4-OHT for 1 h (low Akt activity) or treated with 100 nM 4-OHT for 48 h (high Akt activity) in full growth medium and subjected to phosphoproteomic analysis. Three biological replicates were performed per condition, each of which was analyzed in triplicate (n = 9). Phosphorylation events were considered to be downstream of Akt if the fold change between either of the 4-OHT treated samples and the starved sample was a minimum of 2-fold and statistically significant ($p < 0.05$) as assessed by the student's t-test. Mean phosphopeptide intensity values are illustrated for the named examples from proteins A. Proline-rich AKT1 substrate (known substrate of Akt) B. 40S ribosomal protein S6 (known to be phosphorylated downstream of Akt). C. Microtubule-actin cross-linking factor 1 isoform 1 (not currently linked to Akt pathway). D. Cytoplasmic dynein 1 light intermediate chain 1 (not currently linked to Akt pathway). Data expressed as mean +/- SEM (n = 9).

5.4. An *in vitro* kinase assay to identify phosphorylation events downstream of Akt1

In addition to the use of the MCF10A myrAktER cells, an *in vitro* assay was developed to identify phosphorylation events downstream of Akt. In this approach we applied an *in vitro* kinase assay, originally developed by the Cohen group [272, 273], in conjunction with shotgun phosphoproteomics to identify *in vitro* protein substrates of recombinant Akt1. In brief, proteins in total cell lysate were dephosphorylated and used as the substrate for an *in vitro* assay using recombinant, active Akt1 as the kinase (Fig. 5.3.). Phosphorylated products were then identified and quantified using the phosphoproteomic method previously outlined (Fig. 5.1.). Reaction conditions were manipulated and quantitative comparison between samples enabled the identification of Akt1-dependent phosphorylation events and, furthermore, the quantification of the affinity of Akt1 for each of these sites.

5.4.1. Identification of phosphorylation events downstream of Akt1 using different concentrations of kinase

In our initial approach we performed the *in vitro* assay with different concentrations of Akt1. Thus, phosphorylation events that were only found to occur in the presence of Akt1 could be considered to be *in vitro* downstream substrates.

Total cell lysate from MCF10A cells was de-phosphorylated by exploitation of the endogenous phosphatase activity of the sample. 500 µg of dephosphorylated protein substrates were then incubated with 0, 2 or 10 µg of Akt1 and 100 µM of ATP (and relevant co-factors) for 5 min at 30^{o}C. The reaction was stopped by denaturation of the proteins using 8 M urea and the proteins were subsequently subjected to in-solution digestion. The peptide samples were then enriched for phosphopeptides using TiO_2 affinity chromatography prior to analysis (2 x technical replicates) on a ThermoFisher LTQ-Orbitrap. Qualitative and quantitative analysis of the data were then performed.

561 phosphopeptides were identified, with a minimum MASCOT expectancy < 0.05, across all samples in this experiment and were compiled into a database. These 561 phosphopeptides were quantified in all experimental samples using Pescal (Fig. 5.12.).

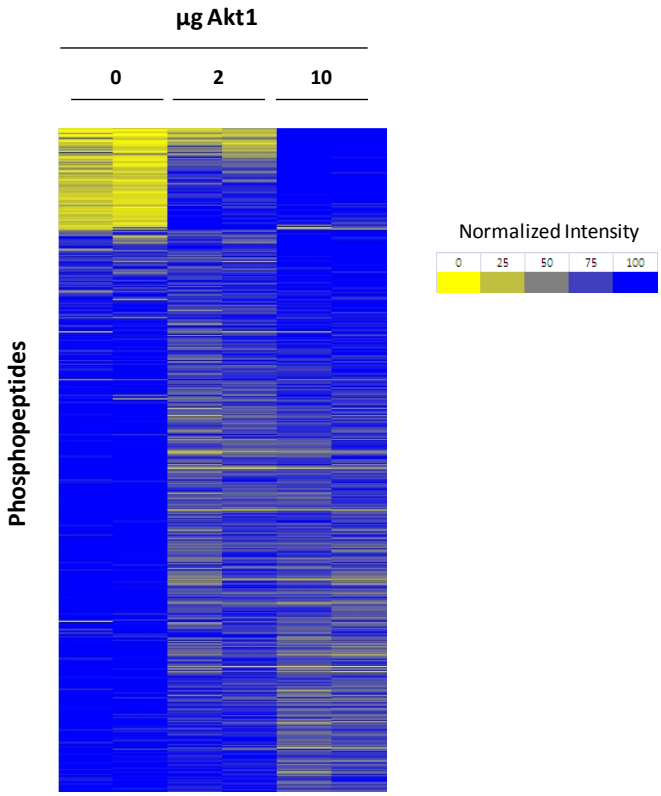

Figure 5.12. Quantitative analysis reveals phosphoproteomic response in response to Akt1 in an *in vitro* kinase assay. MCF10A cell lysate was de-phosphorylated and incubated *in vitro* with 0, 2 or 10 µg of Akt1 and 100 µM ATP for 5 min at 30°C. The resulting phosphorylated proteins were then subjected to phosphoproteomic analysis. The quantification of all 561 phosphopeptides was represented as a heat map, where phosphopeptide intensity was expressed as a percentage of the maximum intensity for that phosphopeptide.

Quantification of the 561 phosphopeptides identified in this experiment revealed a subset of phosphorylation events that were produced in response to the presence of Akt1, whilst the majority were found to be unchanged or slightly decreased (Fig. 5.12.).

PCA was performed for the entire dataset (Fig. 5.13.).

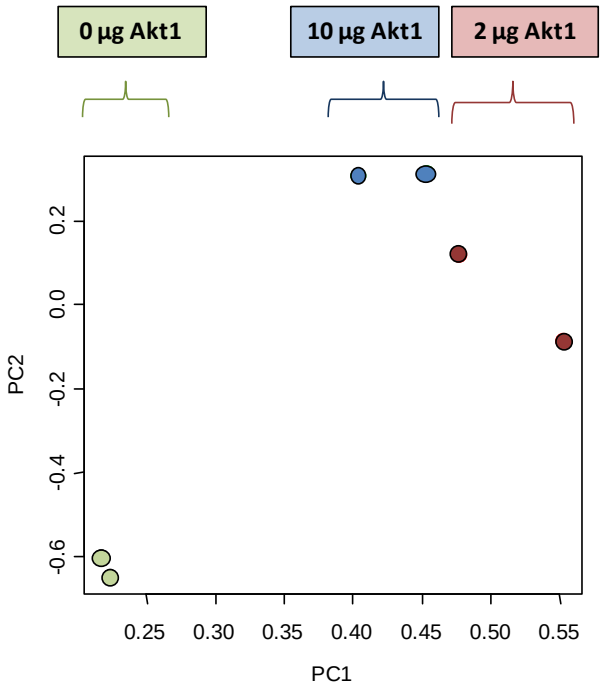

Figure 5.13. PCA reveals that Akt1 activity results in a distinct phosphoproteomic profile to that for control treatment. MCF10A cell lysate was de-phosphorylated and incubated *in vitro* with 0, 2 or 10 µg of Akt1 and 100 µM ATP for 5 min at 30°C. The resulting phosphorylated proteins were then subjected to phosphoproteomic analysis. PCA analysis was performed for all 561 phosphopeptides identified and quantified in this experiment.

PCA revealed that samples which included active Akt1 in the reaction clustered together and distinctly from the control treated cells on the first principle component, indicating that Akt1 activity was the major factor determining variance between sample conditions (Fig. 5.13.). The separation of cells treated with 2 or 10 µg Akt1 on the second principal component indicated that Akt1 concentration was also a factor differentiating the samples (Fig. 5.13.).

We proceeded to define arbitrary criteria for a phosphorylation event to be considered dependent on Akt1 activity and therefore a downstream target. Phosphorylation events were considered to be Akt1-dependent if the fold change between the sample that was incubated with 10 µg Akt1 and the control sample was a minimum of 2-fold. 86 phosphopeptides met these criteria, including some known substrates of Akt (Fig. 5.14. – 5.15. and Appendix 3).

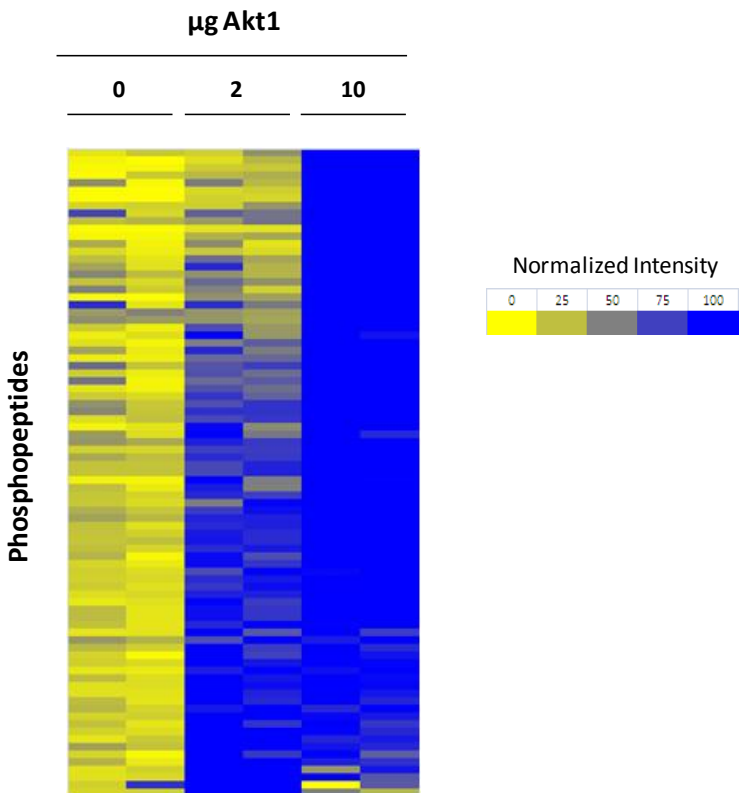

Figure 5.14. An *in vitro* kinase assay identifies phosphorylation events downstream of Akt1. MCF10A cell lysate was de-phosphorylated and incubated *in vitro* with 0, 2 or 10 µg of Akt1 and 100 µM ATP for 5 min at 30°C. The resulting phosphorylated proteins were then subjected to phosphoproteomic analysis. The quantification of the 86 phosphopeptides that were found to increase in response to Akt1 was represented as a heat map, where phosphopeptide intensity was expressed as a percentage of the maximum intensity for that phosphopeptide.

The heat map representation of quantitative data illustrated the increase in phosphorylation of candidate phosphorylation sites downstream of Akt that occurred in the presence of Akt1 in the *in vitro* reaction (Fig. 5.14.). Candidate sites can be broadly classified into two groups: those for which phosphorylation increases proportionally to the concentration of Akt1 and those for which phosphorylation increases at the lower dose of Akt1 and remains unchanged with the higher dose (Fig. 5.14.). Some specific examples of phosphorylation events found to be dependent on Akt1 by this method are illustrated (Fig. 5.15.).

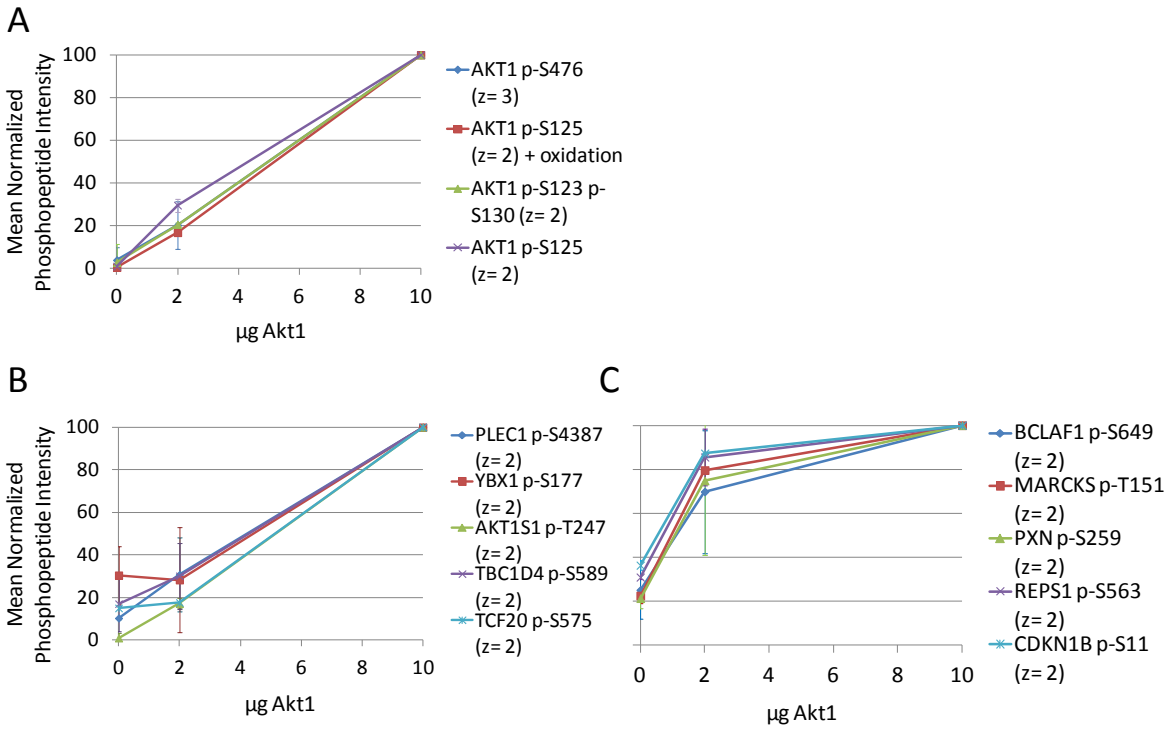

Figure 5.15. Examples of phosphorylation events downstream of Akt1 identified using an *in vitro* kinase assay. MCF10A cell lysate was de-phosphorylated and incubated *in vitro* with 0, 2 or 10 µg of Akt1 and 100 µM ATP for 5 min at 30°C. The resulting phosphorylated proteins were then subjected to phosphoproteomic analysis. The mean normalized peptide intensities (n = 2) are shown for representative phosphopeptides that A. Belong to Akt1 (internal control). B. Increase in a linear fashion in response to Akt1 concentration. C. Increase rapidly in response to Akt1. Data expressed as mean +/- SD (n = 2).

Quantitation of the phosphorylation sites on Akt1 itself serve as an internal control for the experiment (Fig. 5.15. A). Furthermore, results show that a number of phosphorylation sites increase in abundance in the presence of Akt1. Such increases may follow a linear pattern in relation to Akt1 (Fig. 5.15. B) or may plateau at when higher concentrations of the kinase were included in the reaction (Fig. 5.15. C).

5.4.2. Identification of phosphorylation events downstream of Akt1 using different concentrations of ATP

We next proceeded to further develop our method to increase the amount of information that could be obtained. We reasoned that an improvement over the previous strategy (5.4.1.) would be to perform the *in vitro* kinase reaction with different

concentrations of ATP in the presence or absence of Akt1. Thus, we would be able to identify Akt1-dependent phosphorylation events as those that occurred only in the presence of Akt1. Furthermore, the use of various concentrations of ATP would enable the investigation of the dynamics of phosphorylation of each site, thus enabling the identification of the most efficient reactions that are more likely to occur *in vivo.*

Total cell lysate from MCF10A cells was de-phosphorylated using exogenous lambda protein phosphatase. A total of 500 µg of dephosphorylated protein substrates were then incubated with 0, 10, 50, 100 or 500 µM ATP in the absence or presence of 2 µg Akt1 (and relevant co-factors) for 5 min at 30^{o}C. The reaction was stopped by denaturation of the proteins using 8 M urea and the proteins were subsequently subjected to in-solution digestion. The peptide samples were then enriched for phosphopeptides using TiO_2 affinity chromatography prior to analysis (2 x technical replicates) by LC-MS/MS on a ThermoFisher LTQ-Orbitrap XL. Qualitative and quantitative analysis of the data were then performed.

At total of 856 phosphopeptides were identified, with a minimum MASCOT expectancy < 0.05, across all samples in this experiment and were compiled into a database. These 856 phosphopeptides were then quantified in all experimental samples using Pescal (Fig. 5.16.).

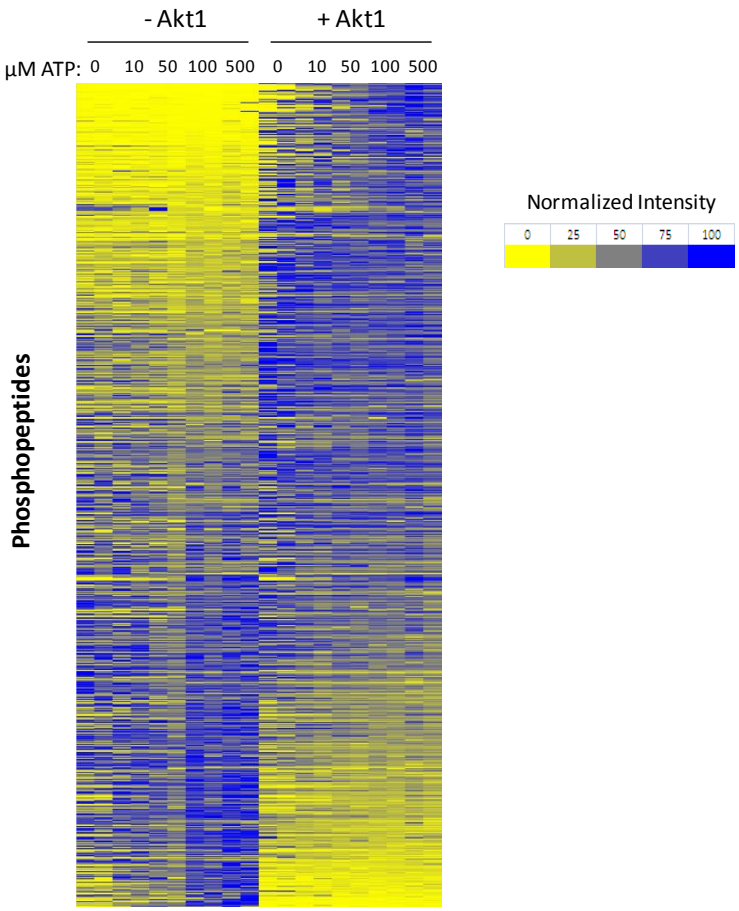

Figure 5.16. Quantitative analysis reveals phosphoproteomic response to an increasing concentration of ATP in the presence or absence of Akt1 in an *in vitro* kinase assay. MCF10A cell lysate was de-phosphorylated and incubated *in vitro* with 0, 10, 50, 100 or 500 µM ATP in the absence or presence of 2 µg Akt1 for 5 min at 30°C. The resulting phosphorylated proteins were then subjected to phosphoproteomic analysis. The quantification of all 856 phosphopeptides was represented as a heat map, where phosphopeptide intensity was expressed as a percentage of the maximum intensity for that phosphopeptide.

Quantification of the 856 phosphopeptides identified in this experiment revealed a subset of phosphorylation events that were observed to increase in response to ATP concentration only in the presence of Akt1 (Fig. 5.16.). Many other phosphorylation sites were found to be unchanged or to decrease only in the presence of Akt1 (Fig. 5.16.).

PCA was performed for the entire dataset (Fig. 5.17.).

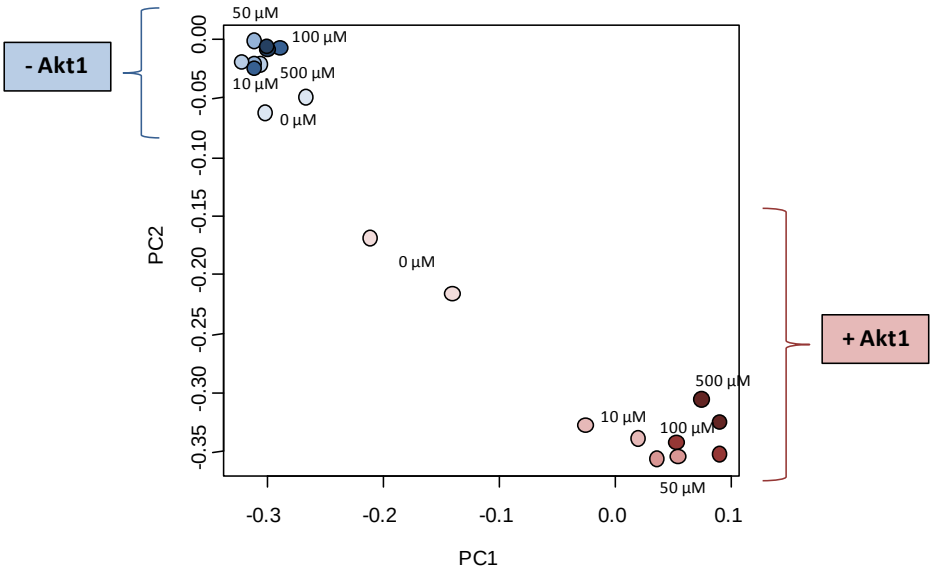

Figure 5.17. PCA reveals that the presence of Akt1 in an *in vitro* reaction confers a distinct phosphoproteomic profile. MCF10A cell lysate was de-phosphorylated and incubated in vitro with 0, 10, 50, 100 or 500 µM ATP in the absence or presence of 2 µg Akt1 for 5 min at 30oC. The resulting phosphorylated proteins were then subjected to phosphoproteomic analysis. PCA analysis was performed for all 856 phosphopeptides identified and quantified in this experiment.

PCA revealed that samples which included active Akt1 in the reaction clustered together and distinctly on the first principle component from those in which no Akt1 was included, indicating that the presence of Akt1 in the reaction was the major factor determining sample variance between conditions (Fig. 5.17.). In the absence of Akt1, the samples at different concentrations of ATP clustered together on the second principal component suggesting that ATP concentration did not greatly affect the phosphoproteomic profile under these conditions (Fig. 5.17.). In contrast, the samples including Akt1 separated more across the second principal component, indicated that ATP concentration was also a factor differentiating samples under these conditions (Fig. 5.17.).

We proceeded to define arbitrary criteria for a phosphorylation event to be considered dependent on Akt1 activity and therefore a downstream target. Phosphorylation events were considered to be Akt1-dependent if the fold change between the samples incubated with 100 µM ATP in the absence or presence of 2 µg Akt1 was a minimum of 2-fold. A total of 253 phosphopeptides met these criteria, including some known substrates of Akt (Fig. 5.18. – 5.19. and Appendix 4).

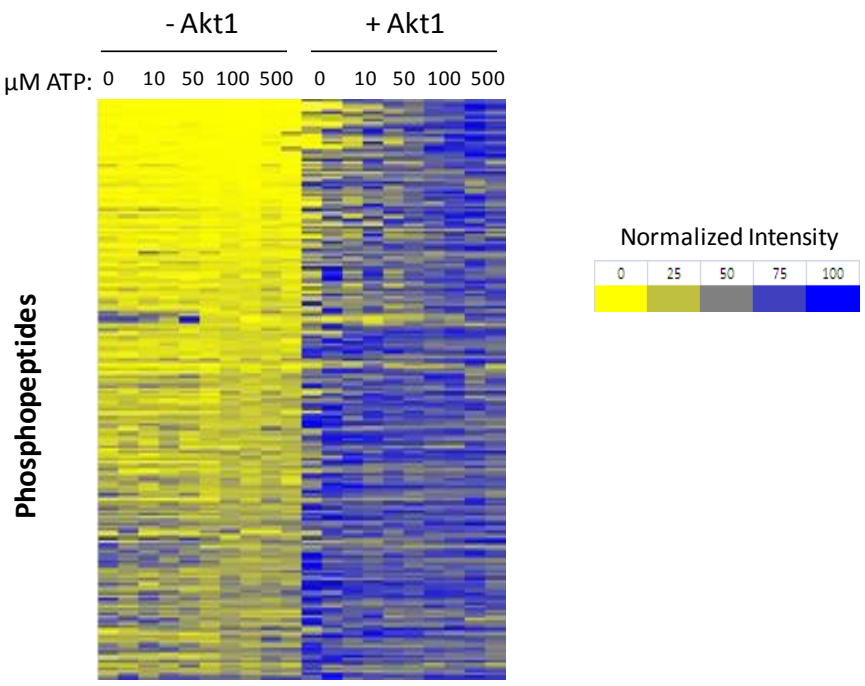

Figure 5.18. An *in vitro* kinase assay identifies phosphorylation events downstream of Akt1 in the presence of different concentrations of ATP. MCF10A cell lysate was de-phosphorylated and incubated *in vitro* with 0, 10, 50, 100 or 500 µM ATP in the absence or presence of 2 µg Akt1 for 5 min at 30^{o}C. The resulting phosphorylated proteins were then subjected to phosphoproteomic analysis. The quantification of the 253 phosphopeptides that were found to increase in response to ATP in the presence of Akt1 was represented as a heat map, where phosphopeptide intensity was expressed as a percentage of the maximum intensity for that phosphopeptide.

The heat map representation of quantitative data illustrates the increase in phosphorylation of candidate phosphorylation sites downstream of Akt that occurred in response to increasing concentrations of ATP in the presence of Akt1 in the *in vitro* reaction (Fig. 5.18.).

Some specific examples of phosphorylation events found to be dependent on Akt1 by this method are illustrated (Fig. 5.19.).

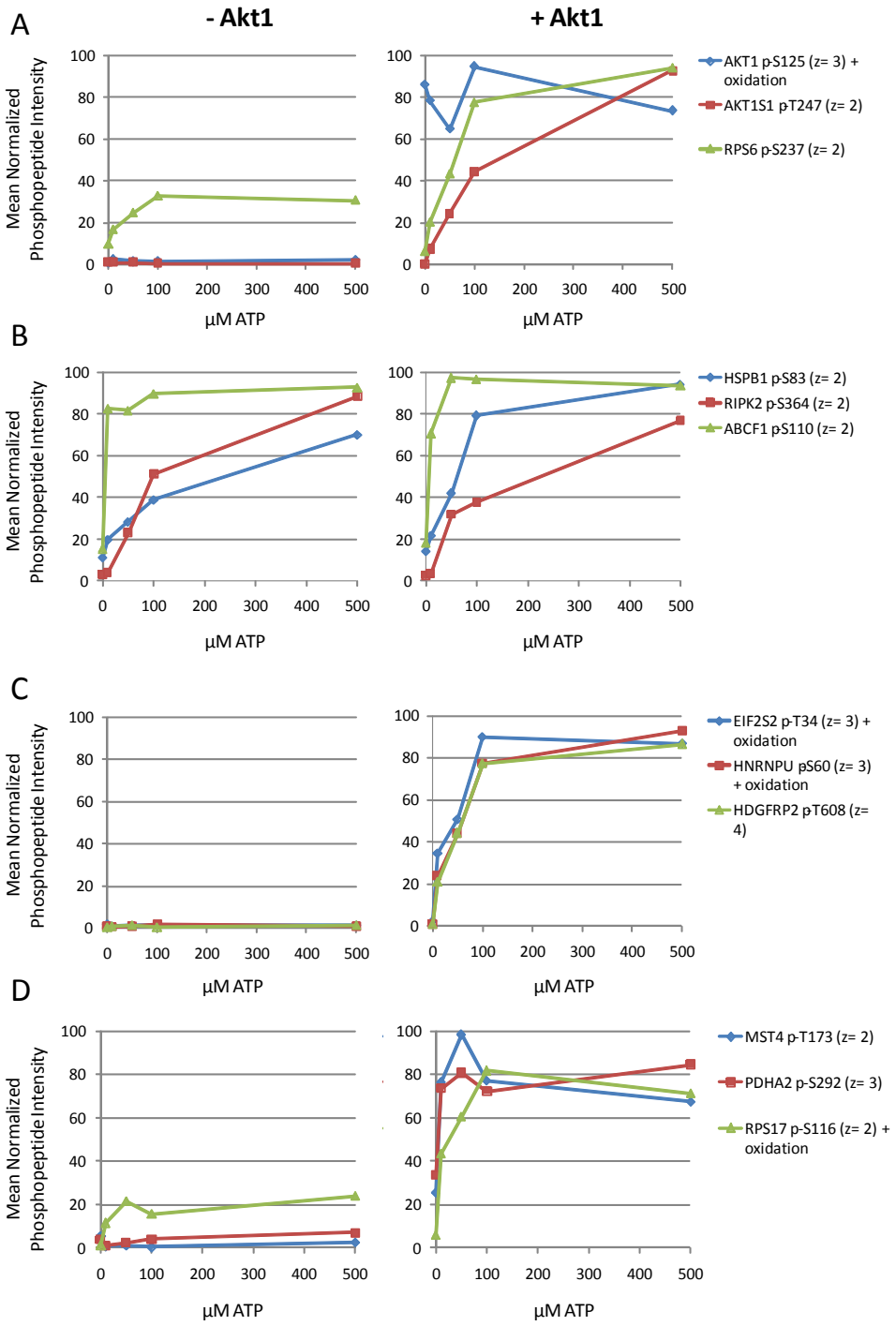

Figure 5.19. Examples of phosphorylation events downstream of Akt1 identified using an *in vitro* kinase assay in the presence of different concentrations of ATP. MCF10A cell lysate was de-phosphorylated and incubated *in vitro* with 0, 10, 50, 100 or 500 µM ATP in the absence or presence of 2 µg Akt1 for 5 min at 30°C. The resulting phosphorylated proteins were then subjected to phosphoproteomic analysis. The mean normalized peptide intensities (n = 2) are shown for representative phosphopeptides: known to be downstream of Akt1 (**A**), Akt1-independent (**B**), Akt1-dependent with relatively low affinity for ATP (**C**) and Akt1-dependent with relatively high affinity for ATP (**D**).

Quantitation of the phosphorylation site S125 on Akt1 itself serves as an internal control for the experiment, as levels are undetectable when Akt1 is not added to the reaction mix and remain steady and high when Akt1 is present (Fig. 5.19. A). Furthermore, results show that the phosphorylation of known Akt1 targets PRAS40 (AKTS1) and S6 (RPS6) increases significantly in response to increasing concentrations of ATP in the presence of Akt1 (Fig. 5.19. A); these positive controls further demonstrate the suitability of this approach to identify Akt1 substrates.

5.4.3. Quantification of Akt1-ATP affinity – a method to evaluate reaction efficiency

The *in vitro* Akt1 kinase assay was performed using different concentrations of ATP (5.4.2.) as we reasoned that we could use this information to quantify the affinity of Akt1 for ATP for each phosphorylation site and thus estimate reaction efficiency and Akt1 affinity for that site. The rational for this strategy was that phosphorylation reactions should follow the same dynamics as any other enzyme-substrate reaction. Thus, one could apply the principles of Michaelis-Menten kinetics to define Akt1-ATP affinity as the ATP concentration required to reach 50% of the maximum reaction rate (K_{ATP}) and rank novel candidate Akt1 substrates by reaction efficiency (Fig. 5.20.).

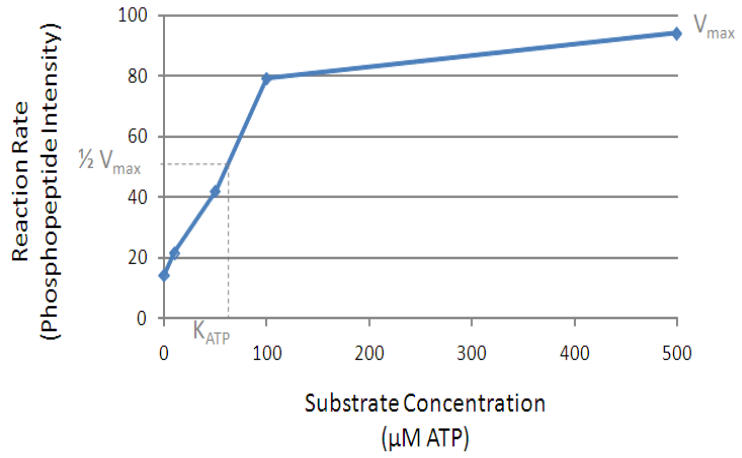

Figure 5.20. Quantification of Akt1-ATP affinity (K_{ATP}). The kinetics of phosphorylation efficiency can be expressed for each site by plotting substrate concentration (ATP concentration) against the reaction rate (phosphopeptide intensity). Using the principles of Michaelis-Menten kinetics, Akt1-ATP affinity, which is defined as the ATP concentration required to reach 50% of the maximum reaction rate, (K_{ATP}) can then be calculated using non-linear regression.

It should be noted that these *in vitro* phosphorylation reactions do not adhere to all the principles of Michaelis-Menten kinetics, for example substrate source may not be present in excess, thus K_{ATP} is not equivalent to K_m but is a useful estimate of the affinity of Akt1 for ATP and thus an approximation of the reaction efficiency for that site that enables ranking identified substrates by this value.

K_{ATP} was calculated (as illustrated in Fig. 5.20.) for all phosphorylation events found to be Akt-1 dependent using our *in vitro* strategy (5.4.2. Fig. 5.19.). Reaction kinetics and corresponding K_{ATP} values are illustrated for some named examples (Fig. 5.21.).

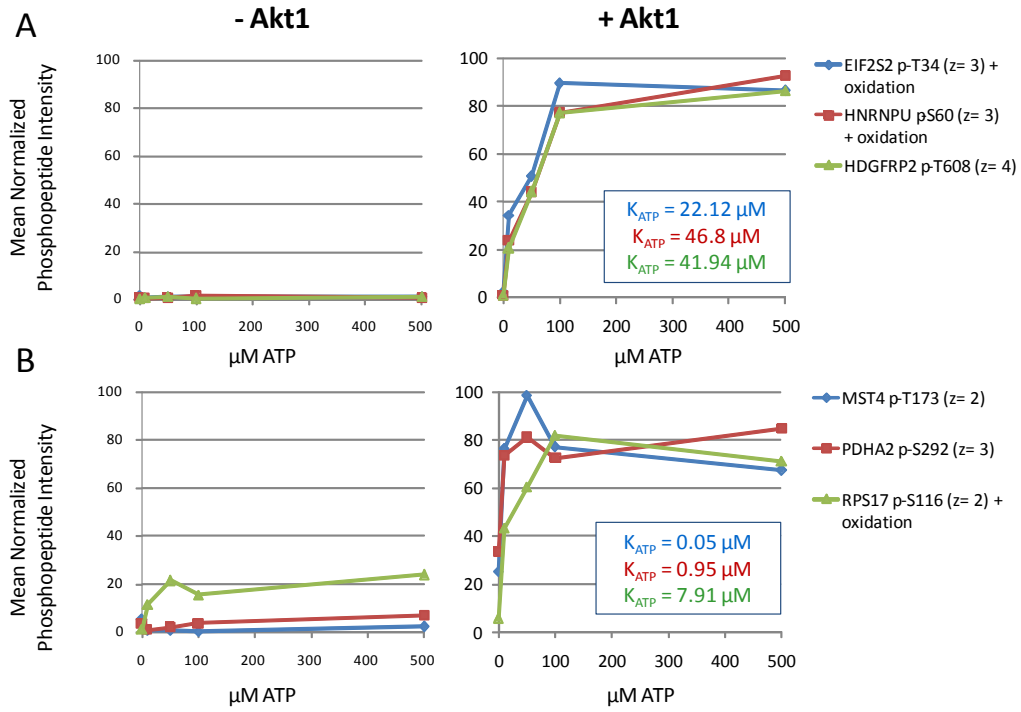

Figure 5.21. K_{ATP} correlates with reaction efficiency. K_{ATP} was calculated (Fig. 5.19.) for phosphopeptides found to be dependent on Akt1 activity (Fig. 5.18.). Examples of phosphopeptides that showed A. relatively low affinity for ATP and B. relatively high affinity for ATP are shown.

As expected, K_{ATP} was found to negatively correlate with reaction efficiency i.e. phosphorylation sites that showed relatively low affinity for ATP had higher K_{ATP} values than sites that showed higher affinity for ATP (Fig. 5.21.). Thus, K_{ATP} values can be used quantify reaction efficiency, which may be useful to rank reactions by the likelihood that they truly occur *in vivo.*

We used motif analysis to validate the hypothesis that reaction efficiency, as quantified by K_{ATP}, may be a useful parameter to investigate the likelihood of an Akt1-dependent phosphorylation event found using an *in vitro* reaction to occur *in vivo*. We grouped phosphorylation sites according to their K_{ATP} value and quantified the abundance of the phosphorylation motifs RXRXXS/XXRXXS, recognised by Akt and its downstream target p70S6K [87], and XXDXXS, a control motif (Fig. 5.22.).

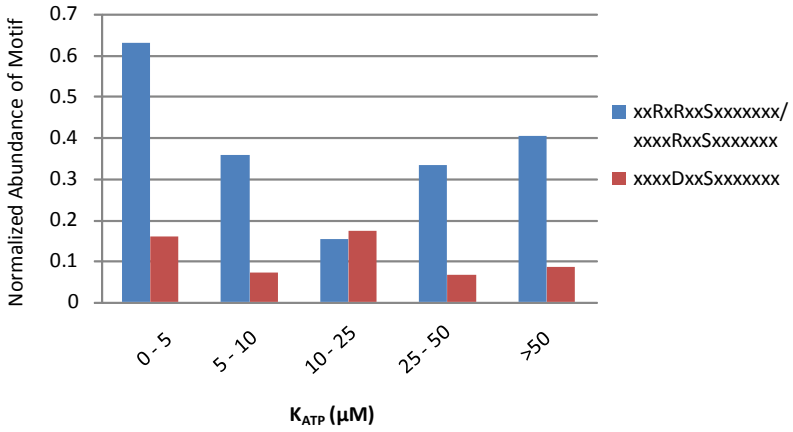

Figure 5.22. Low K_{ATP} indicates enrichment for Akt1 pathway motifs. Phosphorylation sites were grouped according to their K_{ATP} value and the abundance of the phosphorylation motifs RXRXXS/XXRXXS, recognised by Akt and its downstream target p70S6K, and XXDXXS, a control motif were evaluated. Motif events were normalized to the total number of peptides per group.

The data showed that the group of phosphorylation sites with the lowest K_{ATP} values (K_{ATP} 0 – 5 µM) were enriched (by approximately 2-fold) for the phosphorylation motifs RXRXXS/XXRXXS, which are recognised by Akt and its downstream target p70S6K (Fig. 5.22.). In contrast, there was no clear correlation between K_{ATP} and the abundance of the control motif XXDXXS (Fig. 5.22.). Thus, these data suggest that K_{ATP} may be a useful parameter to validate *in vitro* phosphorylation targets as *bona fide in vivo* substrates.

5.4.4. Cross-reference of data generated using MCF10A myrAktER model and *in vitro* kinase assay.

In order to obtain a list of high-confidence phosphorylation events dependent on Akt activity we compared the dataset obtained from the *in vivo* MCF10A myrAktER model (5.3.)

with that from the *in vitro* Akt1 assay (5.4.2.). The overlapping phosphorylation sites are listed (Table 5.1.).

Table 5.1. Akt-dependent phosphorylation events identified using both *in vivo* and *in vitro* models.

Accession Number	Phosphopeptide Identification	Motif (*denotates phosphorylation site and bold indicates conformance with Akt/S6 recognition motif)	Known Akt Substrate
ABCF1_HUMAN	ABCF1 p-S110 (z= 3)	LSVPTS*DEEDEV	
AKTS1_HUMAN	AKT1S1 p-T247 (z= 2)	**LNT*SDFQK**	*
CALX_HUMAN	CANX p-S584 (z= 3)	DEILNRS*PR	
CALX_HUMAN	CANX p-S565 (z= 4)	EDGGTVS*QEEEDR	
CALX_HUMAN	CANX p-S555 (z= 3)	**QKS*DAEEDG**	
DAP1_HUMAN	DAP p-S52 (z= 3)	QEWESPS*PPKPTV	
DC1L2_HUMAN	DYNC1LI2 p-S206 (z= 3)	GPLTSGS*DEENVA	
DPOD3_HUMAN	POLD3 p-S308 (z= 3)	VALS*DDETKE	
EF1B_HUMAN	EEF1B2 p-S107 (z= 4)	DIDLFGS*DDEEES	
HDGF_HUMAN	HDGF p-S166 (z= 2)	GDLLEDS*PK	
HDGF_HUMAN	HDGF p-S134 (z= 3)	GNAEGSS*DEEGKL	
HS90A_HUMAN	HSP90AA1 p-S264 (z= 3)	EIEDVGS*DEEEEK	
HS90A_HUMAN	HSP90AA1 p-S253 (z= 3)	**ES*EDKPEI**	
HS90B_HUMAN	HSP90AB1 p-S256 (z= 2)	IEDVGS*DEEDDS	
HSPB1_HUMAN	HSPB1 p-S83 (z= 2)	**QLS*SGVSEI**	
HTSF1_HUMAN	HTATSF1 p-S580 (z= 3)	DLDEEGS*EKELHE	
KPCD_HUMAN	PRKCD p-S665 (z= 2)	SAFAGFS*FVNPK	
MK01_HUMAN	MAPK1 p-T186 (z= 3)	HTGFLT*EYVATR	
NDRG1_HUMAN	NDRG1 p-S331 (z= 2)	**TAS*GSSVTS**	
NP1L4_HUMAN	NAP1L4 p-S126 (z= 3)	AESEWHS*ENEEEEK	
PGRC1_HUMAN	PGRMC1 p-S182 (z= 3)	EEPTVYS*DEEEPK	
RS6_HUMAN	RPS6 p-S237 p-S241 (z= 2)	**LSS*LRAS*TSK**	*
TPIS_HUMAN	TPI1 p-S22 (z= 3)	**KQS*LGELIG**	

The list of high-confidence Akt-dependent phosphorylation events using both strategies described in this chapter (Table 5.1.) represents around just 10% of phosphosites identified in each independent experiment. The majority of the phosphorylation sites have not previously been linked directly to Akt activity. It is interesting to note that phosphorylation sites for the known Akt substrates and some other candidates conform to the Akt/S6K

recognition motif. It should be noted however that downstream candidates may not be directly phosphorylated by Akt or S6K and therefore may not adhere to this motif.

5.5. Conclusions

The work described in this chapter aimed to identify phosphorylation events downstream of Akt, thus potentially enabling further annotation of the phosphoproteome and/or identification of possible biomarkers of pathway activity. We used two distinct approaches to carry out this work.

In the first approach, we used a cell line model stably transfected with an inducible, constitutively active Akt construct [314] to investigate Akt activity in the human breast epithelial cell MCF10A (Fig. 5.2.). Initial work was performed to characterise the cell line and evaluate the activity of the MCF10A myrAktER construct. WB and Aktide assay results demonstrated that the myrAktER construct was activated in response to 4-OHT treatment and, furthermore, that the greater control of activity levels could be obtained by modulating treatment time compared to using different doses (Fig. 5.4. – 5.5.). Investigation of the phosphorylation of substrates downstream of Akt further supported these results (Fig. 5.6.). An assay for anoikis (detachment-induced apoptosis) also demonstrated the biological output of the activation of the construct (Fig. 5.7.).

We then proceeded to perform a phosphoproteomic experiment to evaluate the effects of myrAktER activity on the phosphoproteome. MCF10A myrAktER cells treated with EtOH overnight (minimal Akt activity), treated for 1 h 4-OHT (low Akt activity) or 48 h 4-OHT (high Akt activity) were lysed and subjected to phosphopeptide enrichment prior to shotgun phosphoproteomics for peptide identification and quantification. 1961 phosphorylation events were identified and heat-map representation of phosphopeptide quantification and PCA revealed that activation of the myrAktER construct affected the phosphoproteomic profile of cells (Fig 5.8. – 5.9.). Criteria for a phosphorylation event to be considered Akt dependent were defined (based upon a statistically-significant increase in phosphorylation upon myrAktER activation) and 238 phosphopeptides were classified within this group, including some known Akt targets (Fig. 5.10. – 5.11. and Appendix 2).

Our second strategy for the identification of Akt-dependent phosphorylation events coupled a previously described *in vitro* method for the identification of kinase substrates,

which uses de-phosphorylated full-length endogenous proteins as the reaction substrate (Fig. 5.3.) [272, 273], with global shotgun phosphoproteomics. Initially we sought to investigate if *in vitro* reaction products were proportional to enzyme activity. De-phosphorylated proteins were incubated *in vitro* with different concentrations of recombinant, active Akt1 (0, 2 and 10 μg) and a reaction buffer that included ATP and the products subjected to shotgun phosphoproteomics. A total of 561 phosphopeptides were identified and heat-map representation of peptide quantification and PCA revealed that Akt1 activity in the *in vitro* assay conferred a distinct phosphoproteomic profile (Fig. 5.12. – 5.13.). Criterium was defined for a phosphorylation event to be considered Akt1-dependent (based on an increase in phosphorylation in response to Akt1 presence in the reaction) and 86 phosphopeptides were classified within this group, including known Akt targets (Fig. 5.14. – 5.15. and Appendix 3).

We next further developed the strategy as, in addition to the identification of Akt1-dependent phosphorylation events, we wished to evaluate phosphorylation efficiency as we hypothesized that this may indicate the likelihood of the *in vitro* reaction occurring *in vivo*. De-phosphorylated proteins were incubated with different concentrations of ATP (0, 10, 50, 100 or 500 μM) in the presence or absence of 2 μg of recombinant, active Akt1 prior to performance of shotgun phosphoproteomics. A total of 856 phosphopeptides were identified and heat-map representation of peptide quantification and PCA revealed that the presence of Akt1 in the reaction conferred a distinct phosphoproteomic response (Fig. 5.16. – 5.17.). Criteria was defined for a phosphorylation site to be considered Akt1-dependent (based on phosphorylation increasing in response to increasing ATP concentration only in the presence of Akt1) and 253 phosphopeptides were classified within this group, including some known Akt substrates (Fig. 5.18. – 5.19. and Appendix 4).

We next proceeded to use the same data to quantify the affinity of Akt1 for ATP for each phosphorylation site, thus providing an estimation of phosphorylation efficiency. Akt1-ATP affinity (K_{ATP}) was calculated using non-linear regression based on the principles of Michaelis-Menten reaction kinetics (Fig. 5.20.). Evaluation of Akt1-dependent phosphorylation events revealed that K_{ATP} inversely correlated with phosphorylation efficiency i.e. low K_{ATP} indicates efficient phosphorylation (Fig. 5.21.). These data suggest that K_{ATP} may be a useful parameter to identify efficient Akt phosphorylation reactions,

which may be more likely to occur *in vivo*. Motif analysis supported this notion as phosphopeptides with low K_{ATP} were found to be enriched for motifs known to be phosphorylated by Akt and its downstream substrate p70S6K (Fig. 5.22.), although this correlation was not strong.

Finally, datasets of phosphopeptides found to be Akt-dependent using the MCF10A myrAktER model and the *in vitro* kinase assay were cross-referenced to produce a short-list of high-confidence Akt-dependent phosphorylation events (Table 5.1.). These proteins represent potential novel Akt pathway targets of interest for future investigation.

6. Global Kinase Activity Profiling (GKAP)

6.1. Introduction and aim of study

In the previous chapter we demonstrated the utility of an *in vitro* assay coupled to shotgun phosphoproteomics to investigate the molecular biology of PI3K/Akt signalling. We next proceeded to investigate if this strategy could have wider applications for the investigation of signalling pathway activities.

Protein phosphorylation by kinases is a key regulatory mechanism of signalling pathway activity [200-202]. Mass-spectrometry based global phosphoproteomics has enabled great advances in this field as it provides the unprecedented opportunity to perform large-scale, unbiased identification and quantification of phosphorylation events [203, 205]. However, although protein phosphorylation levels provide an indication of overall pathway activity, they do not necessarily correlate directly with kinase activity as there are multiple mechanisms regulating this post-translational modification (Fig. 6.1.) [204].

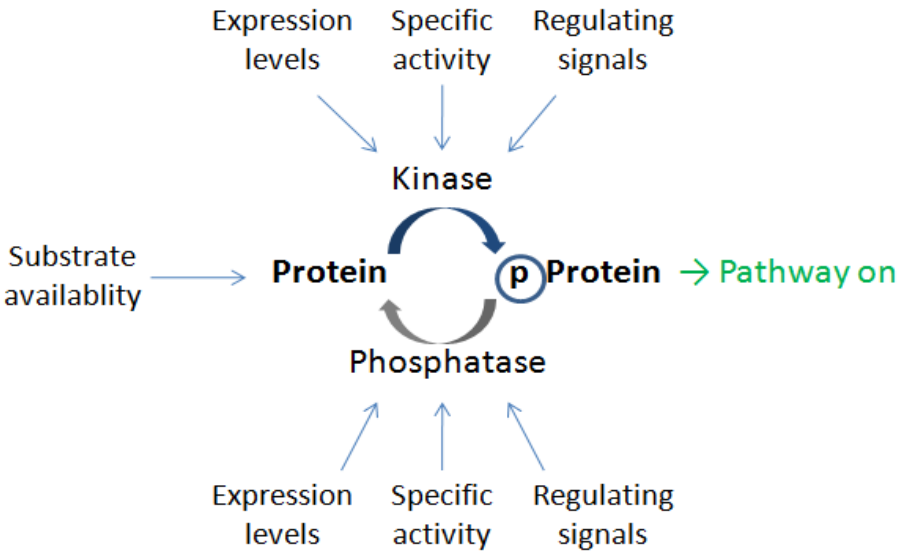

Figure 6.1. Regulation of protein phosphorylation. Protein phosphorylation is primarily regulated by the balance between kinase and phosphatase activity, and multiple factors affect the outcome of this relationship. Figure adapted from [204].

There are circumstances where understanding of absolute kinase activity is advantageous over measurement of overall pathway activity. For example, small molecule

inhibitors exist for many kinases, however they are only likely to be effective as treatment if inappropriate pathway activity is attributable to kinase activity itself rather than to other factors, for example underactive phosphatases [317]. Evaluation of the contribution of kinases to signalling activity can also help in the de-convolution of complex pathways and improve our understanding of how they are de-regulated.

In vitro kinase reaction assays have been available for decades but such methods were previously dependent on radioactivity labelling or other indirect detection strategies, such as antibodies [318, 319]. More recently, mass-spectrometry has been successfully applied to provide a detection method for such reactions. The nature of mass spectrometry is highly desirable as a read-out for kinase activity as it enables simultaneous detection and quantification of reaction products. In addition, mass-spectrometry can provide information that cannot be obtained by other methods, for example the specific localization of a phosphorylation site.

Mass-spectrometry based kinase assays were initially developed using short peptides as substrates, the first application of which was in the quantification of PI3K/Akt signalling [270, 271]. This approach was then further developed for application to multiple kinases [320] and multiplexed, enabling the simultaneous quantification of the activities of several kinases using up to 90 peptide substrates [321]. Although these approaches have been successful, their application is limited by the use of synthetic purified peptide substrates that require specific knowledge of the kinase target site. Such information is not always available and thus restricts the application of these methods to well-characterized kinases. Another significant limitation in the use of peptide substrates is that substrate recognition by some kinases is known to be dependent on conformational interaction between proteins in addition to recognition of the short linear phosphorylation motif [322, 323].

The aim of the work presented in this chapter was to develop a mass-spectrometry based *in vitro* assay for global endogenous kinase activity that used full-length proteins as the reaction substrate. We followed on from the kinase assay developed in Chapter 5 to develop this novel methodology, which we termed global kinase activity profiling (GKAP). In this method, full-length proteins are isolated from cells and incubated *in vitro* with different concentrations of ATP (and co-factors), enabling their phosphorylation by endogenous

active kinases. Reaction products are then analyzed using shotgun phosphoproteomics and quantitative data is then used to identify and quantify kinase activity (Fig. 6.2.).

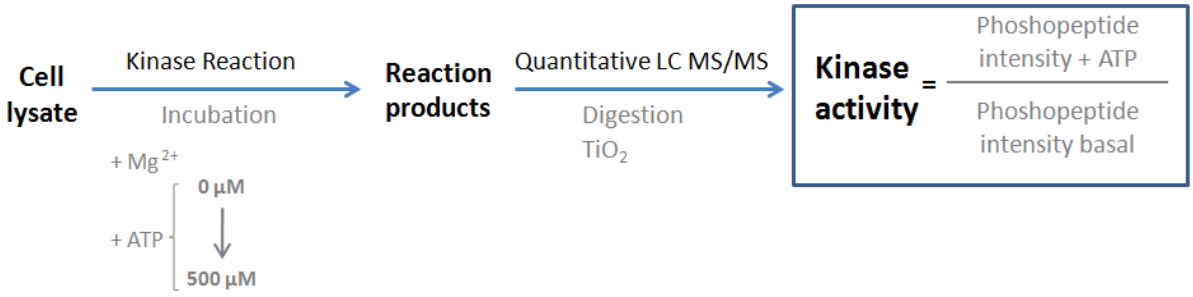

Figure 6.2. Summary of GKAP Strategy. Protein substrates are isolated from total cell lysates and incubated *in vitro* with various concentrations of ATP and necessary co-factors. Kinase activity results in protein phosphorylation, which is then detected by phosphoproteomics. Quantitative analysis of phosphopeptide intensity before and after incubation with ATP (i.e. kinase activity) is used to identify and quantify kinase activity.

6.2. Detection of phosphopeptide signals using GKAP

We initially proceeded to investigate if phosphorylation of full-length proteins as a result of *in vitro* endogenous kinase activity could be detected by mass spectrometry.

To perform the *in vitro* reaction, total cell lysate samples from the P31/Fuj cell line containing 5, 50 or 100 µg of protein were incubated for 5 min at 30^{o}C with reaction buffer containing 10 or 100 µM ATP or not incubated with the reaction mix (baseline). The reaction was then stopped by the addition of urea and the reaction protein products were subjected to in-solution trypsin digestion. The samples were enriched for phosphopeptides, using TiO_2 affinity chromatography, prior to LC-MS analysis on the LTQ-Orbitrap XL (two technical replicates were performed) for qualitative and quantitative phosphoproteomic analysis (Fig. 6.3. – 6.4.).

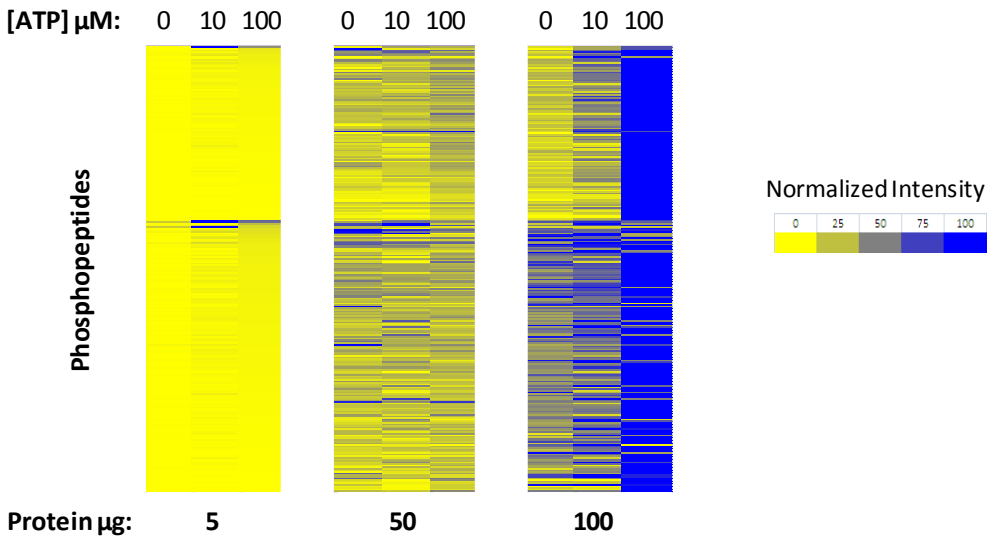

Figure 6.3. Quantitative analysis reveals the response of phosphopeptide intensity to ATP concentration in an *in vitro* reaction. Total cell lysate samples from P31/Fuj cells containing 5, 50 or 100 µg of protein were incubated for 5 min at 30°C with reaction buffer containing 10 or 100 µM ATP or were not incubated (0 µM). Reaction products were then subjected to quantitative phosphoproteomic analysis. Mean phosphopeptide intensities were normalized as a percentage of the maximum value for all conditions and represented on a heat map (n = 2).

281 phosphopeptides were identified and quantified in this experiment (Fig. 6.3.). The data showed that, as expected, phosphopeptide intensities were higher for samples where higher amounts of protein were used in the reaction (Fig. 6.3.). Furthermore, the results also showed that phosphopeptide intensity increased in response to reaction incubation and was proportional to ATP concentration for many phosphopeptides (Fig. 6.3.). These data therefore indicate that *in vitro* phosphorylation of proteins by endogenous kinases is detectable by mass spectrometry and that amplification of signal occurs, due to the potential for each active kinase molecule to act upon multiple substrate molecules.

In this experiment, kinase activity was defined as a minimum of a 2-fold increase of phosphopeptide signal after incubation with ATP relative to the baseline value. Using 100 µg of protein in the reaction mix, 76 kinase activities were detected after incubation with 10 µM ATP and 195 after incubation with 100 µM ATP.

The relationship between phosphopeptide intensity and ATP concentration, using different amounts of protein in the reaction, was illustrated in greater detail (Fig. 6.4.).

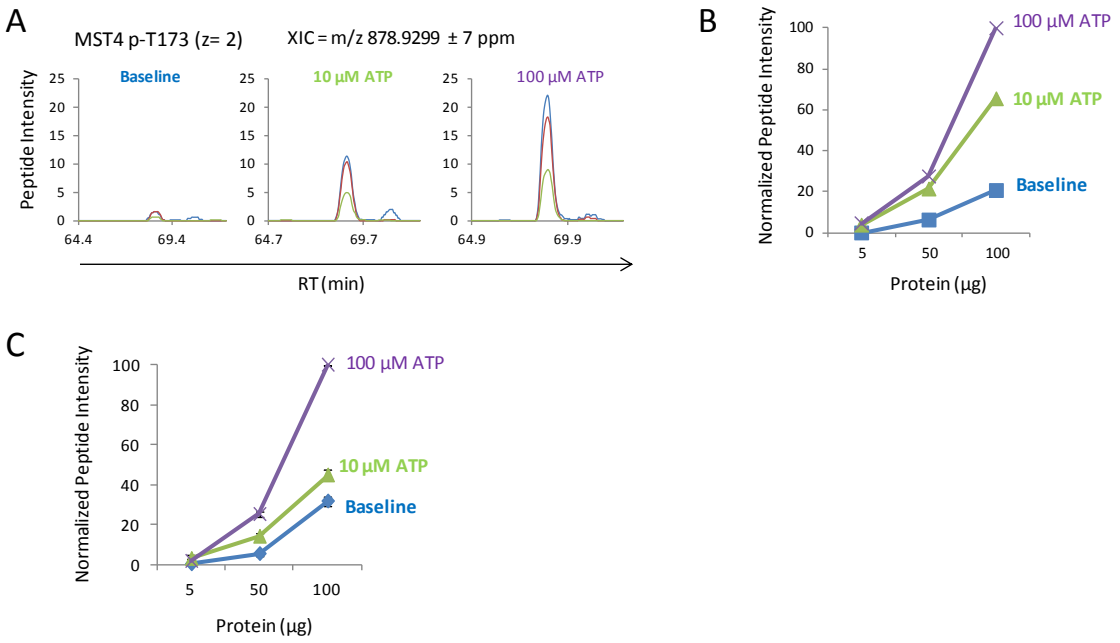

Figure 6.4. Phosphopeptide intensities increase upon incubation with ATP in a GKAP reaction. Total cell lysate samples from P31/Fuj cells containing 5, 50 or 100 µg of protein were incubated for 5 min at 30°C with reaction buffer containing 10 or 100 µM ATP or were not incubated (baseline). Reaction products were then subjected to quantitative phosphoproteomic analysis. A. Extracted ion chromatograms for the example phosphopeptide MST4 p-T173 (z= 2) after no incubation (baseline) or incubation with 10 or 100 µM ATP using 5 µg starting material. B. Normalized intensities for the same phosphopeptide after no incubation (baseline) or incubation with 10 or 100 µM ATP using 5, 50 or 100 µg starting material. C. Mean normalized intensities for all phosphopeptides for which kinase activity was detected after no incubation (baseline) or incubation with 10 or 100 µM ATP using 5, 50 or 100 µg starting material (n = 195). Data is expressed as mean +/- SEM.

The data for the illustrated example demonstrated that phosphopeptide intensity increased in proportion to ATP concentration included in the reaction mix, using just 5 µg of protein in the reaction (6.4. A). This phenomenon was also found to be true for this phosphopeptide when 50 or 100 µg of protein were used in the reaction mix (6.4. B). The mean normalized data for all kinase activities detected also illustrated how phosphopeptide intensity increased in proportion to ATP present in the reaction mix (Fig. 6.4. C).

These data show that endogenous kinase activity results in an increase in phosphopeptide intensity proportional to ATP concentration, thus following the principles of Michaelis-Menten enzyme kinetics, and that these reaction kinetics are detectable by mass spectrometry analysis. Furthermore, these data illustrate that the *in vitro* reaction enables signal amplification that does not appear to be limited by substrate availability.

These results suggest that GKAP may be a suitable method for the quantification of endogenous kinase activity.

6.3. Use of GKAP to investigate basal kinase activity in two AML cell lines

We next proceeded to use GKAP to compare basal kinase activity levels in two acute myeloid leukaemia (AML) cell lines with characterised differences in signalling pathway activities. P31/Fuj cells are resistant to the effects of MEK, JAK and PI3K inhibitors on cell proliferation whereas Kasumi-1 cells are sensitive to these compounds [179].

Total cell lysate samples from P31/Fuj and Kasumi-1 cells, under basal growth conditions, containing 50 μg of protein were incubated for 5 min at 30^{o}C with reaction buffer containing 10, 50 or 500 μM ATP or not incubated with the reaction mix (0 μM). The reaction was then stopped by the addition of urea and the reaction protein products were subjected to in-solution trypsin digestion. The samples were enriched for phosphopeptides, using TiO_2 affinity chromatography, prior to LC-MS analysis on the LTQ-Orbitrap XL (two technical replicates performed) for qualitative and quantitative phosphoproteomic analysis (Fig. 6.5. – 6.7.).

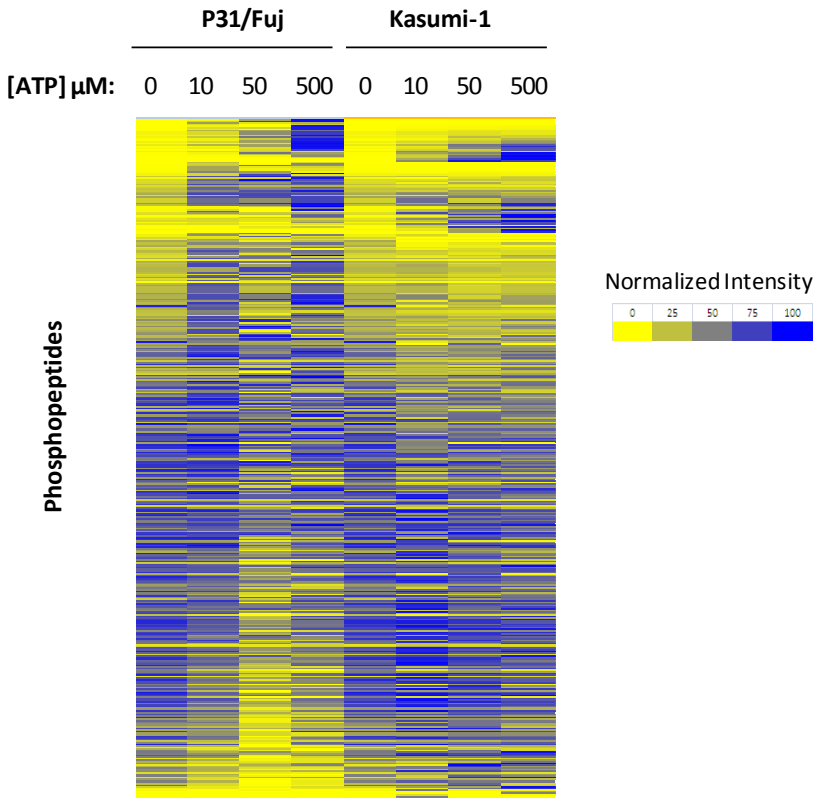

Figure 6.5. Quantitative analysis reveals distinct phosphoproteomic responses of P31/Fuj and Kasumi-1 cell lines in a GKAP assay. Total cell lysate samples from P31/Fuj and Kasumi-1 cells containing 50 µg of protein were incubated for 5 min at 30°C with reaction buffer containing 10, 50 or 500 µM ATP or were not incubated (0 µM). Reaction products were then subjected to quantitative phosphoproteomic analysis. Mean phosphopeptide intensities were normalized as a percentage of the maximum value for all conditions and represented on a heat map (n = 2).

A total of 430 phosphopeptides were identified and quantified in this experiment (Fig. 6.5.). The heat-map analysis of quantitative data revealed the different phosphoproteomic responses of the P31/Fuj and Kasumi-1 cell lines to GKAP, indicating differential pathway activation (Fig. 6.5.). Kinase activity was again defined as a minimum of a 2-fold increase of phosphopeptide signal after incubation with ATP relative to the baseline value. The phosphoproteomic dynamics of peptides found to be products of a kinase reaction in either cell line were examined in more detail (Fig. 6.6.).

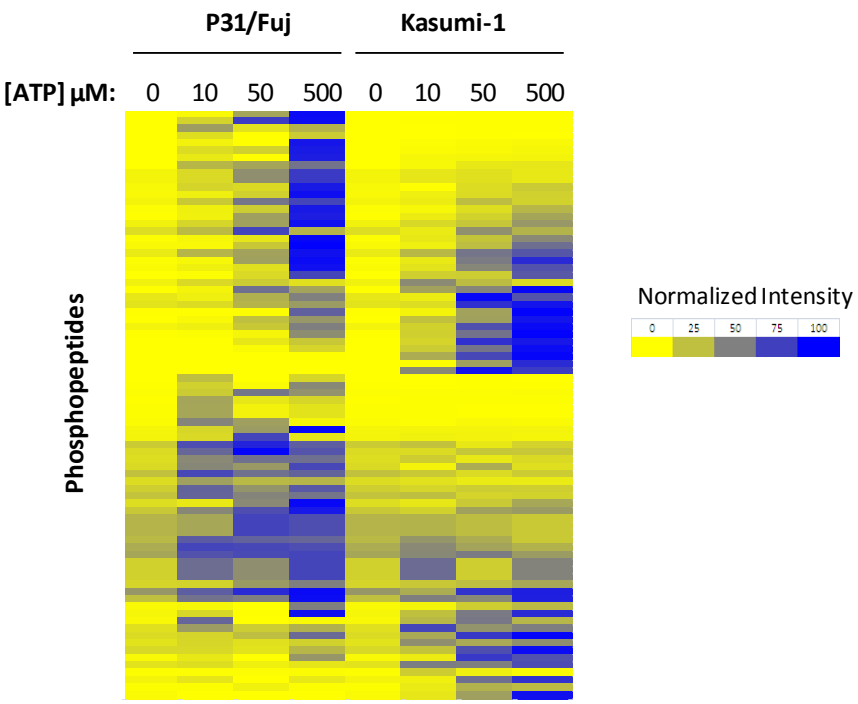

Figure 6.6. GKAP analysis reveals differential kinase pathway activation of P31/Fuj and Kasumi-1 cell lines. Total cell lysate samples from P31/Fuj and Kasumi-1 cells containing 50 µg of protein were incubated for 5 min at 30°C with reaction buffer containing 10, 50 or 500 µM ATP or were not incubated (0). Reaction products were then subjected to quantitative phosphoproteomic analysis. Mean phosphopeptide intensities (n = 2) for phosphopeptides found to be a result of *in vitro* kinase activity were normalized as a percentage of the maximum value for all conditions and represented on a heat map.

Heat-map analysis of phosphopeptide quantification clearly demonstrated that kinase activities were distinct and showed little overlap between the P31/Fuj and Kasumi-1 cell lines (Fig. 6.6.). A total of 67 and 49 activities were detected in basal P31/Fuj and Kasumi-1 cells respectively and quantified as area under the kinetic curve (Appendix 5). Some specific examples of identified kinase activities are illustrated (Fig. 6.7.).

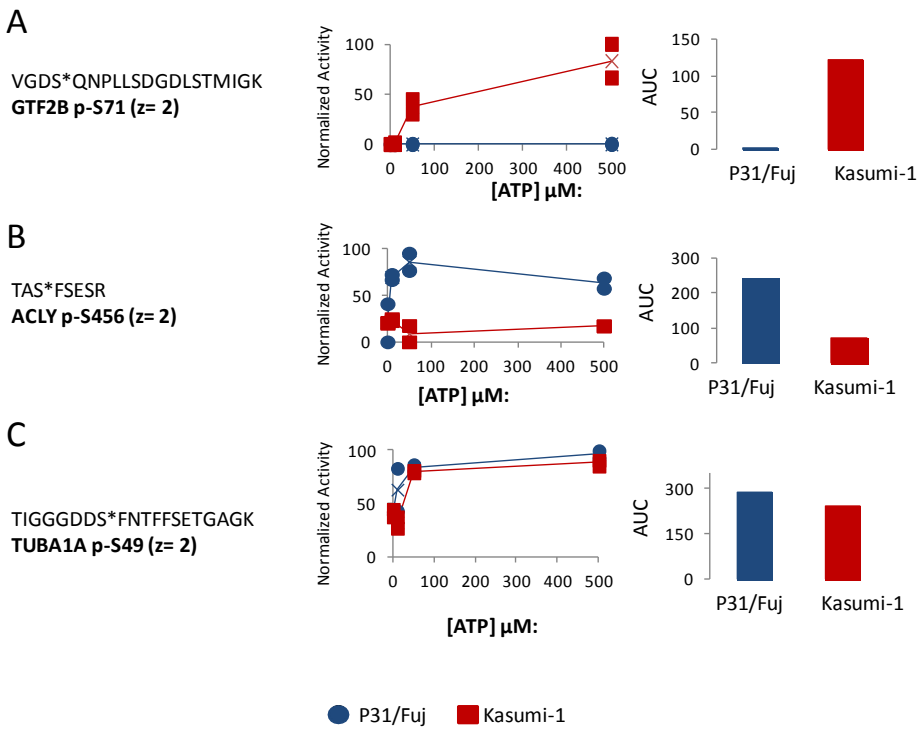

Figure 6.7. GKAP reveals distinct activation of kinases in P31/Fuj and Kasumi-1 cells. Total cell lysate samples from P31/Fuj and Kasumi-1 cells containing 50 µg of protein were incubated for 5 min at 30°C with reaction buffer containing 10, 50 or 500 µM ATP or were not incubated (0 µM). Reaction products were then subjected to quantitative phosphoproteomic analysis. Mean phosphopeptide intensities (n = 2) were normalized as a percentage of the maximum value for all conditions and expressed as a kinetic curve (left panel) or as AUC, a measure of kinase activity (right panel). Examples are shown for A. A kinase active only in Kasumi-1 cells. B. A kinase active only in P31/Fuj cells. C. A kinase active in both cell types.

These results show that GKAP can be effectively used to identify differences in basal signalling pathway activation in two different cancer cell lines that are known to be dependent on distinct kinases for proliferation. Further analysis was performed to verify that the kinase activities identified using GKAP were representative of the pathways previously found to be active in these cells using traditional global phosphoproteomics. In addition to the GKAP experiment already performed, a conventional phosphoproteomic experiment was carried out using P31/Fuj and Kasumi-1 cells. Total cell lysate, containing 500 µg of protein, was harvested and subjected to in-solution trypsin digestion followed by phosphopeptide enrichment, using TiO_2 affinity chromatography, and LC-MS/MS analysis. A list of 44 known phosphorylation motifs was compiled [324] and the incidence of each was established for the GKAP and conventional phosphoproteomic datasets (Fig. 6.8.).

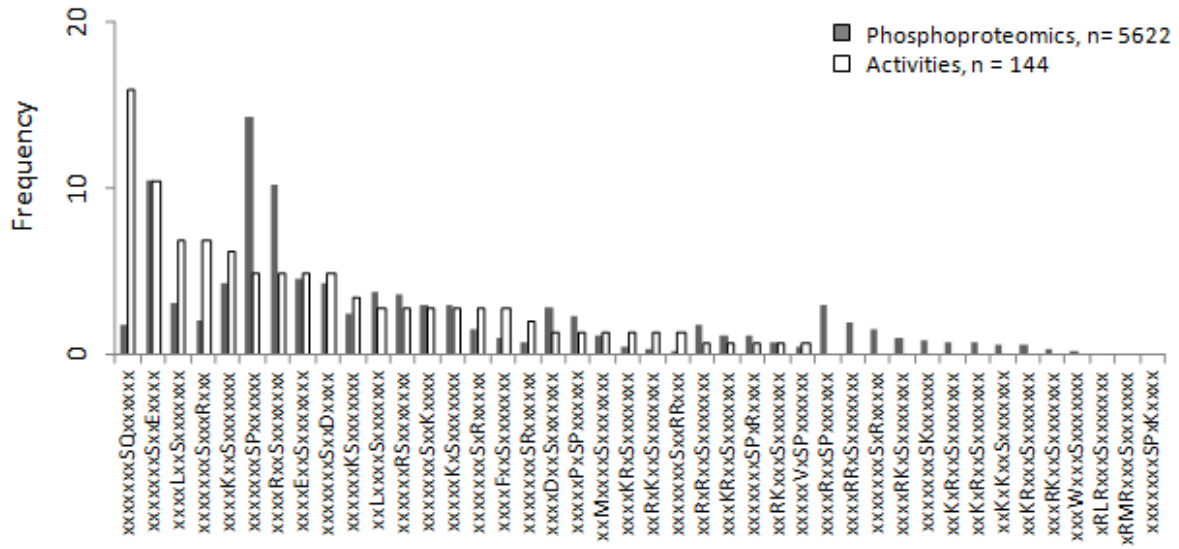

Figure 6.8. GKAP detects the activity of a broad range of kinases active in P31/Fuj and Kasumi-1 cells. GKAP and conventional phosphoproteomic experiments were performed using P31/Fuj and Kasumi-1 cells. The respective datasets were subjected to motif analysis using in-house software.

The results demonstrated that a broad range of kinase activities were identified using GKAP (Fig. 6.8.). Furthermore, the range of represented kinases correlated relatively well with those obtained using conventional phosphoproteomic experiments (Fig. 6.8.). These results suggest that GKAP is suitable for the detection of global kinase activity in these cells as a wide range of kinases were represented in the dataset, including those found by other methods to be active.

6.4. Use of GKAP to investigate signalling pathway activation and inhibition

We next proceeded to apply GKAP to investigate the activation of signalling pathways by growth factor stimulation and the effects of small molecule kinase inhibitors on such a response. MCF10A cells were starved of serum and growth factors for 18 h prior to stimulation with 100 ng/ml epidermal growth factor (EGF) for 10 min. Where indicated, cells were treated with the PI3K inhibitor LY294002 (5 µM) or the MEK inhibitor UO126 (10 µM) for 1 h prior to EGF stimulation. Total cell lysate samples from treated cells, containing 50 µg of protein, were then incubated for 5 min at 30^{o}C with reaction buffer containing 10, 50, 100 or 500 µM ATP or not incubated with the reaction mix (0 µM). The reaction was then

stopped by the addition of urea and the reaction protein products were subjected to in-solution trypsin digestion. The samples were enriched for phosphopeptides, using TiO_2 affinity chromatography, prior to LC-MS analysis on the LTQ-Orbitrap XL (two technical replicates performed) for qualitative and quantitative phosphoproteomic analysis (Fig. 6.9. – 6.10.).

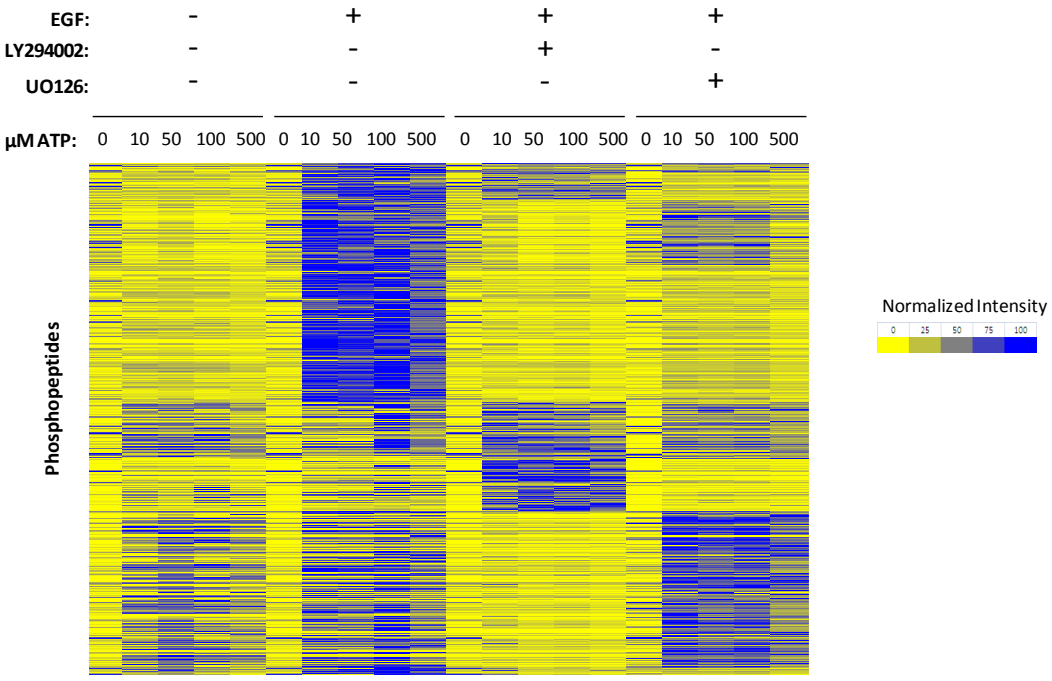

Figure 6.9. GKAP reveals distinct pathway activation in MCF10A cells stimulated with EGF and treated with LY294002 or UO126. MCF10A cells were starved of serum and growth factors for 18 h prior to treatment with 100 ng/ml EGF for 10 min. Where indicated, cells were pre-treated with 5 µM LY294002 or 10 µM UO126 for 1 h prior to stimulation. Total cell lysate samples containing 50 µg of protein were incubated for 5 min at 30°C with reaction buffer containing 10, 50, 100 or 500 µM ATP or were not incubated (0 µM). Reaction products were then subjected to quantitative phosphoproteomic analysis. Mean phosphopeptide intensities were normalized as a percentage of the maximum value for all conditions and represented on a heat map (n = 2).

A total of 622 phosphopeptides were identified and quantified in this experiment (Fig. 6.9.). The heat-map analysis of quantitative data revealed the different phosphoproteomic responses of MCF10A cells under the tested treatment conditions, indicating differential pathway activation (Fig. 6.9.).

In this experiment we applied more stringent criteria to define kinase activity to enable greater discrimination between the multiple conditions; a minimum of a 2-fold increase of

phosphopeptide signal after incubation with 10 µM ATP and a minimum of 3-fold increase after incubation with 50, 100 and 500 µM ATP were required relative to the baseline value. Following these conditions, 241 kinase activities were detected in untreated cells (Appendix 6). This number increased to 372 upon EGF stimulation and was decreased by around 30% to 246 and 293 by LY294002 or UO126 treatment respectively, thus restoring the number of kinase activities detected back to similar levels to that of untreated cells (Appendix 6). Some specific examples of identified kinase activities, quantified as AUC, are illustrated (Fig. 6.10.).

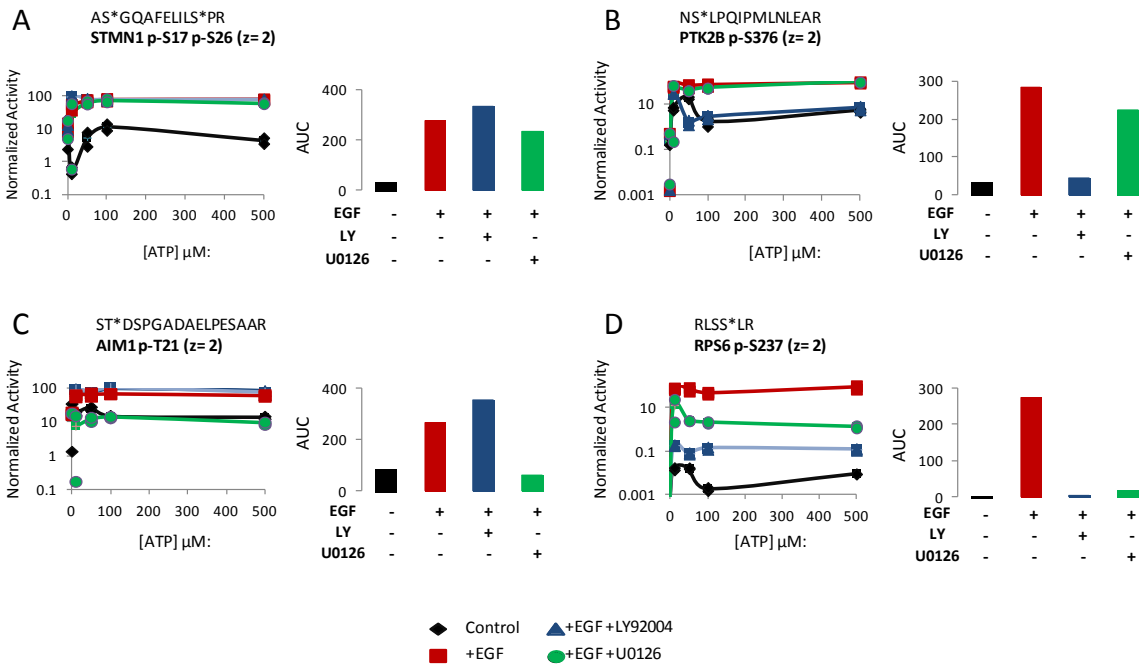

Figure 6.10. GKAP reveals distinct activation of kinases in MCF10A cells stimulated with EGF and treated with LY294002 and UO126. MCF10A cells were starved of serum and growth factors for 18 h prior to treatment with 100 ng/ml EGF for 10 min. Where indicated, cells were pre-treated with 5 µM LY294002 or 10 µM UO126 for 1 h prior to stimulation. Total cell lysate samples containing 50 µg of protein were incubated for 5 min at 30°C with reaction buffer containing 10, 50, 100 or 500 µM ATP or were not incubated (0 µM). Reaction products were then subjected to quantitative phosphoproteomic analysis. Mean phosphopeptide intensities (n = 2) were normalized as a percentage of the maximum value for all conditions and expressed as a kinetic curve (left panel) or as AUC, a measure of kinase activity (right panel). Examples are shown for A. A kinase reaction active upon EGF stimulation and unaffected by the two inhibitors. B. A kinase reaction active upon EGF stimulation and inhibited by LY294002. C. A kinase reaction active upon EGF stimulation and inhibited by UO126. D. A kinase reaction active upon EGF stimulation and inhibited by both LY294002 and UO126.

These results showed that GKAP can be effectively used to identify kinase activity following pathway activation by growth factor stimulation and, furthermore, that this method can also detect changes to such activities that occur upon inhibitor treatment (Fig. 6.10). It is also noteworthy that kinase activities inhibited by small molecule treatment closely resembled that of the un-stimulated sample, indicating that phosphorylation induced by EGF treatment is highly specific and not the result of off-target activity by other kinases.

As before, further analysis was performed to verify that the kinase activities identified using GKAP were representative of the pathways previously found to be active in MF10A cells using conventional phosphoproteomics. In addition to the GKAP experiment already performed, a conventional phosphoproteomic experiment was carried out using MCF10A cells that were serum and growth factor starved for 18 h followed by no further treatment or stimulation with 100 ng/ml EGF for 10 min. Total cell lysate, containing 500 µg of protein, was harvested and subjected to in-solution trypsin digestion followed by phosphopeptide enrichment, using TiO_2 affinity chromatography, and LC-MS/MS analysis. The incidence of common phosphorylation motifs was established for the GKAP and conventional phosphoproteomic datasets (Fig. 6.11.).

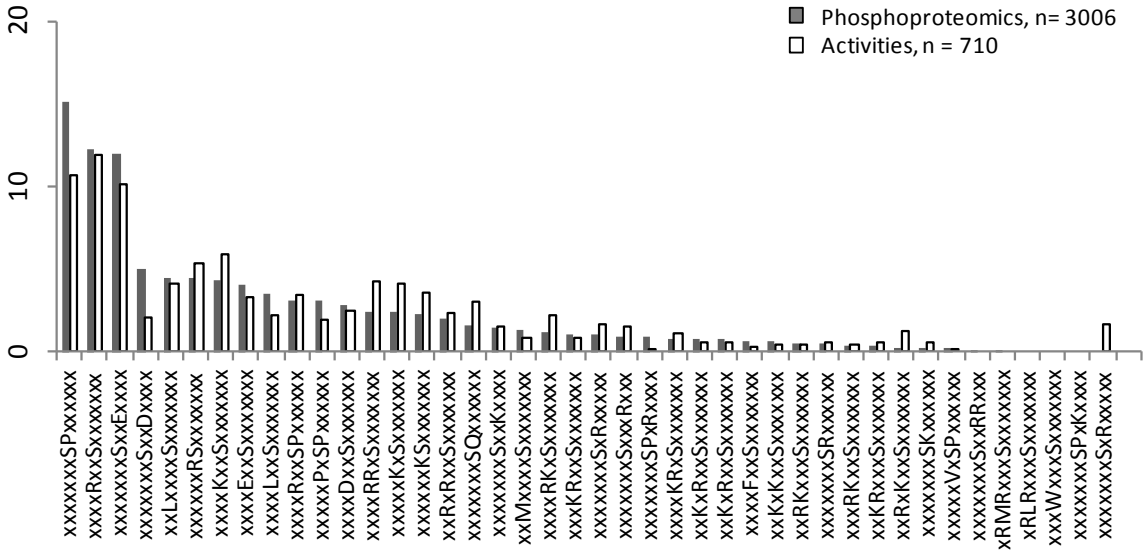

Figure 6.11. GKAP detects the activity of a broad range of kinases active in EGF-stimulated MCF10A cells. GKAP and conventional phosphoproteomic experiments were performed using starved and EGF-stimulated MCF10A cells. The respective datasets were subjected to motif analysis.

As before, the results demonstrated that a broad range of kinase activities that correlated well with those obtained using conventional phosphoproteomics were identified using GKAP (Fig. 6.11.). These results further support the notion that GKAP is suitable for the detection of global kinase activity in cells as a wide range of kinases were represented in the dataset, including those confirmed by other methods to be active.

6.5. Conclusions

The aim of the work presented in this chapter was to develop an assay for the investigation of endogenous kinase activities on a global scale. We followed on from our work in Chapter 5 to develop an assay that coupled an *in vitro* kinase reaction with shotgun phosphoproteomics for the detection of reaction products (Fig. 6.2.). In brief, total cell lysates were incubated with reaction buffer containing different concentration of ATP and necessary co-factors to allow phosphorylation of full-length protein substrates by endogenous kinases. Phosphorylation events were then identified and quantified using mass-spectrometry based phosphoproteomic techniques. We termed the technique global kinase activity profiling (GKAP).

We initially sought to investigate if endogenous kinases were active in an *in vitro* reaction and whether such activity could be detected by mass spectrometry. Total cell lysates of different total protein composition (5 – 100 µg) were taken from P31/Fuj cells and incubated with different concentrations of ATP (0, 10 or 100 µM). Quantitative phosphoproteomic analysis revealed that phosphopeptide signal increased as total protein in the reaction was increased and, furthermore, that many phosphopeptide signals increased as the concentration of ATP in the reaction mix increased, suggesting that kinases were phosphorylating targets *in vitro* (Fig. 6.3.). Closer investigation of kinase activities revealed that phosphopeptide intensity appeared to be proportional to ATP concentration in the reaction mix, suggesting Michaelis-Menten like reaction dynamics (Fig. 6.4.).

Having established that the *in vitro* activities of endogenous kinases could be detected by mass spectrometry, we next proceeded to investigate if the GKAP method could be used to identify the different levels of kinase activities in two AML cell lines shown to have differential activation of signalling pathways under basal conditions [179]. P31/Fuj cells (MEK, JAK and PI3K inhibitor resistant) and Kasumi-1 cells (MEK, JAK and PI3K inhibitor

sensitive) were lysed and samples containing 50 µg of protein were incubated with reaction mix containing 0, 10, 50 or 500 µM ATP. Phosphoproteomic analysis revealed that the two cell lines showed distinct responses to GKAP (Fig. 6.5.). More detailed investigation revealed distinct, non-overlapping clusters of kinase activity in the two cell lines suggesting differential pathway activation (Fig. 6.6. and 6.7.). Motif analysis was performed and compared to that of conventional phosphoproteomic experiments to demonstrate that a wide range of kinase activities were represented in the GKAP database (Fig. 6.8.).

We then applied GKAP to MCF10A cells to investigate if the method was suitable for the detection of growth factor stimulated pathway activation and small molecule kinase inhibition. MCF10A cells were starved of serum and growth factors for 18 h and then stimulated with EGF after treatment with the kinase inhibitors LY294002 and UO126 as indicated. Cells were lysed and 50 µg of total protein were incubated with reaction buffer containing 0, 10, 50, 100 or 500 µM ATP. Phosphoproteomic analysis revealed that the treatments resulted in distinct responses to GKAP (Fig. 6.9.). Detailed investigation showed that kinase activity induced by EGF treatment (Fig. 6.10.) and inhibition of EGF-induced kinase activity by inhibitor treatment were detected (Fig 6.10. B – D). Motif analysis was performed and, as before, showed that a wide-range of kinases including those known to be active in these cells was represented in the GKAP dataset (Fig. 6.11.).

These results suggest that GKAP is a useful method for the detection of endogenous kinase activities. The use of full-length protein substrates in this assay presents a major advantage over existing kinase assays and the GKAP method may therefore prove to be a useful tool for future investigation.

7. Discussion

The PI3K/Akt pathway has an essential role in the regulation of key cellular functions in health and disease. With this project we used innovative mass spectrometry techniques to address some remaining questions about the regulation and activity of this critical cell signalling pathway from a proteomics standpoint.

Mass spectrometry based proteomics is increasingly being applied to advance our knowledge in many fields of biochemical research. In addition to being a sensitive, specific and quantitative method, its untargeted nature also enables an investigative approach that is not possible with more conventional molecular biology techniques. Thus, it enables global scale analysis and discovery investigation that was not previously possible with other methods. This project applied the discovery potential and global scale analysis qualities of mass spectrometry to investigate PI3K/Akt signalling.

One key area in the field of PI3K/Akt signalling that remained underexplored is the role of interacting proteins in the regulation of PI3K activity. Using a rigorous and un-targeted AP-MS screen we identified three candidate interaction partners for class IA PI3Ks (Chapter 3). Furthermore, we were able to validate the interaction between PI3K and calpain, one of the identified candidates, and establish a clear role in the regulation of PI3K signalling and biological activity (Chapter 4).

Another aspect of PI3K/Akt signalling that has not been comprehensively investigated is the dynamics of signalling activity downstream of Akt. We applied global, quantitative mass-spectrometry based phosphoproteomics to investigate signalling events downstream of this kinase (Chapter 5). We first developed two different strategies for this approach; utilising both an *in vivo* model and an *in vitro* assay that we developed to identify phosphorylation events downstream of Akt (Chapter 5). In addition, as an extension of the utility of the approach, we applied our *in vitro* assay as a novel approach for the quantification of global kinase activity (Chapter 6).

7.1. AP-MS screen for dynamic interaction partners of class IA PI3K

PI3K activity is tightly regulated *in vivo* to enable controlled cell growth and tissue homeostasis [60, 111, 325]. As such, a number of mechanisms to regulate PI3K activity have been identified and well-characterized (discussed in Chapter 1) [19, 27, 29, 85, 266, 278].

The regulation of enzymatic activity by protein-protein interactions has been repeatedly established [263, 264] and multiple kinases involved in cell signalling are known to be regulated by the formation of protein complexes [265-268]. However, the regulation of class IA PI3K by interaction partners remains under-explored, most likely due to the lack (until recently) of suitable molecular biology techniques for a discovery investigation of transient and low affinity protein-protein interactions on a global-scale.

Another area of interest is the possible role of interaction partners in regulating isoform-specific activity of class IA PI3Ks. Binding partners have the potential to form isoform-specific interactions and therefore to regulate PI3K activity, e.g. through cytoplasmic localization or by direct interaction with the catalytic subunit, in an isoform-selective way.

PI3K has previously been shown to interact with a number of proteins [58, 283, 326], however a clear mechanism for the regulation of total or isoform-selective PI3K activity has not yet been established. Our AP-MS screen for PI3K binding partners aimed to identify novel binding partners of PI3K that may have a role in regulating its activity.

7.1.1. AP-MS strategy for identification of class IA PI3K interaction partners

7.1.1.1. Principles behind AP-MS strategy

Affinity purification of protein complexes followed by proteomic analysis by mass spectrometry has established itself as the method of choice for the identification of protein-protein interactions in protein complexes. AP-MS can be used for a global approach and can identify multimeric complexes, in contrast to techniques such as Y2H, which only yield binary results.

Crucially for this project, the technique also enables the assessment of endogenous binding relationships (without over-expression of the bait) under different growth conditions, thus providing valuable information about the dynamic interactions that occur during cell signalling events. This aspect was crucial for the success of this project as it can

be hypothesized that regulation of PI3K by functional binding partners is most likely to involve dynamic interactions as a function of PI3K activation status.

We designed an AP-MS strategy based on quantitative LC-MS to identify functional binding partners of endogenous class IA PI3K (Fig. 3.1.). In this approach, AP-MS is performed on cells expressing endogenous levels of proteins under different growth conditions. Quantitative analysis of the resulting conditions can be used to identify dynamic interactors, which are more likely to be functionally significant, and to identify proteins that are unchanged under different states, which are more likely to be non-specific interactors.

Although alternative AP-MS strategies based on the over-expression or tagging of the protein bait are widely used to identify constitutive protein-protein interactions [196, 197] we reasoned that this strategy was not suitable for our investigation as subcellular localization, physiological responses and functional interactions may be disrupted by changes in protein abundance ratios [194, 195]. In addition, dynamic interactions may occur through modifications or conformations not identified *a priori* and therefore not necessarily present in over-expressed proteins. Furthermore, false positive results are more likely when bait proteins are tagged and expressed at high levels [187].

Our quantitative AP-MS approach has previously been successfully applied to a number of protein interaction studies in mammalian cells [193, 284, 327]. However, to date it has not been successfully applied to identify binding partners of PI3K. Factors that may have influenced this outcome include the relatively low abundance of PI3K in cells, the likelihood that interactions are dynamic, that partners may be present in sub-stochiometric levels and the general under-use of mass spectrometry in the field of PI3K investigation.

7.1.1.2. Technical considerations of AP-MS strategy

We designed an AP-MS strategy to identify candidate dynamic interaction partners of Class IA PI3K (Fig. 3.1.). Our strategy was designed to compare the composition of the PI3K protein complex in cells that were serum-starved, resulting in low pathway activity, or serum-stimulated, resulting in high pathway activity. We hypothesized that proteins present in equal abundance under both conditions were likely to be non-specific interactors or constitutive binders, whereas proteins present in different abundance under the two conditions were likely to have an active role in signalling. We selected NIH-3T3 mouse

embryonic fibroblasts (MEFs) as our model cell line as it is a well characterized cell line that is widely used as a model experimental system and is easy to work with on the scale required for AP-MS investigations.

The major technical drawbacks of AP-MS relate to the affinity purification stage. When using immunoprecipitation to isolate protein complexes, the technique is limited by the specificity of the antibody as non-specific interactions will complicate the identification of true interaction partners. This problem is particularly significant when “bait” proteins are in low abundance, as occurs with signalling enzymes. Another consideration is that interacting partners may not be present in equimolar ratios, therefore high amounts of “bait” protein may be required to ensure sufficient recovery of binding partners to enable confident identification. In addition, dynamic interaction partners, such as those we were hoping to identify, are likely to have relatively low binding affinity for their interaction partners.

In order to overcome these limitations the affinity purification strategy was optimized by conducting a series of initial experiments. We showed that the use of 0.3% CHAPS, a mild detergent, during IP resulted in the co-purification of a higher number of proteins compared to 1% Triton X-100, a stronger detergent (Fig. 3.2.). These results demonstrated, in line with the findings of others [268], that, the use of weak detergent for affinity purification maximises the retention of weak protein-protein interactions, thus increasing the number of potential binding partners. This was of particular importance in our study as our targets of interest were likely to be transient, dynamic interactors forming relatively weak interactions with PI3K. However, the use of weak detergents also increases the likelihood of non-specific interactions between proteins thus potentially generating a more complex dataset with an increased incidence of non specific identification. Our quantitative strategy was designed to overcome the limitations of low specificity associated with AP-MS and thus the increase in non-specific interactions was not considered to be an issue. In addition, in each experiment we analyzed a control sample, produced by carrying out a parallel IP with total IgG instead of an anti-PI3K antibody as the affinity reagent, and used the data to verify that any candidates were not interacting in a non-specific way.

Further investigations were performed to investigate the effects of the detergents CHAPS and Triton X-100 on cell lysis in more detail. Our results showed that, whilst total protein yield was inversely proportional to the concentration of either detergent (Fig. 3.3.),

the amounts of p85 recovered did not correlate well with detergent type or concentration (Fig. 3.4.). These results suggested that the use of low concentration of 0.3% CHAPS in the affinity purification process would not negatively impact the recovery of PI3K. These data further supported our strategy to use a weak detergent for IP.

A series of experiments were also performed to identify the optimal antibodies and associated conditions for the purification of PI3K complexes by IP. We chose to use antibodies with affinity for all isoforms of the p85 regulatory subunit of PI3K (p85 pan) as these reagents have previously been demonstrated to be efficient affinity reagents [19]. An additional advantage to this approach is that the different isoforms of the p110 catalytic subunits expressed in cells will all be isolated by this antibody. Our investigation revealed that, whilst both antibodies tested had a high affinity for p85, a combination of the two used at a ratio of 1:500 (µl antibody:µg protein) effectively depleted PI3K p85 from the sample (Fig. 3.5.). Therefore, these were the antibody IP conditions selected for the AP-MS screen.

It should be noted that it is extremely challenging to comprehensively prevent non-specific interactions thus appropriate consideration to this matter was given during experimental design and data analysis. It should also be taken into consideration that AP-MS was used as an initial screening tool to identify potential protein-protein interactions. Validation with an alternative method is advocated to confirm AP-MS screen findings.

7.1.2. AP-MS screen for class IA PI3K protein complexes

Three independent biological experiments were performed to conduct the AP-MS screen. In each, PI3K p85 protein complexes were isolated from NIH-3T3 cells that were serum-starved for 18 h (“starved”) or serum-starved for 18 h followed by stimulation with 10% FBS for 5 min (“stimulated”). SDS-PAGE separation and Colloidal Coomassie blue staining revealed the complexity of the IP products isolated and failed to identify any clear differences between the samples (Fig. 3.6.). Furthermore, qualitative mass-spectrometry analysis did not identify any proteins that were associated with the complex exclusively under one condition. However, we anticipated this finding as functional binding partners are likely to have a dynamic rather than constitutive association with PI3K. Our initial results

supported the requirement for a quantitative mass spectrometry approach to identify candidate interaction partners.

7.1.2.1. Quantitative analysis of class IA PI3K AP-MS screen results

Mass spectrometry analysis was used to identify and quantify hundreds of proteins across the study, however we focused our attention on the 81 proteins that were identified in all three replicate experiments (Appendix 1). We employed stringent data quality criteria for protein identification and quantification to identify proteins that were interacting dynamically with PI3K. Critically, candidates were required to be identified to a high degree of confidence in all three experiments and the criteria to be considered quantitatively different between the two conditions was for a minimum of a two-fold change in relative abundance, which was statistically significant as assessed by the Student's t-test. The selection criteria included proteins with a relatively modest fold change, which we hypothesized to be the likely scenario for a dynamic interaction relationship.

PI3K proteins were found to be present in equal abundance under both conditions in all three experiments. Identification of p85α, p85β, p110α and p110β in all the experiments confirmed that the affinity purification technique was successful.

The high number of other proteins also identified illustrated well the challenges involved in the identification of PI3K interaction partners. It is technically challenging to identify low abundance proteins of potential interest against a high background of non-specific interactors. A contributing factor is the low abundance of PI3K in cells, thus rendering the isolation of significant amounts of the PI3K protein complex technically challenging. Another likely complication to this investigation is that interaction partners may not be associated with PI3K in an equimolar ratio. Thus, when a modest amount of PI3K is isolated the abundance of binding partner in relation to non-specific interactors may be very low.

We considered our approach to mass spectrometry analysis in order to maximize the number of protein identifications and, more importantly, to enhance the quality of identification data for low abundance proteins. Each independent biological sample set was analyzed once and the MS/MS dataset analyzed by MASCOT. These data were then used to generate an exclusion list that, when applied to the mass spectrometry method during a

second technical replicate analysis, prevented the repeat MS/MS analysis of the same peptides thus producing a richer data set. The data from both analyses were then pooled to carry out the qualitative analysis. It should be noted that a high number of MS/MS spectra were generated during analysis however only a relatively low number (around 10%) were assigned by MASCOT to a known peptide. This suggests that the quality of the MS/MS spectra generated by these samples was relatively low, which may be due to the presence of many proteins in low abundance.

Despite the technical challenges discussed, three proteins that exhibited a dynamic relationship, as assessed using rigorous criteria, with PI3K in response to changes in growth conditions were identified. CAPNS1 was found to be more strongly associated with PI3K in starved cells whereas FN1 and VIM were found to be more strongly associated with PI3K in stimulated cells (Fig. 3.7. - 3.8. and Table 3.1.).

Our approach was biased towards specificity rather than sensitivity i.e. by using such rigorous criteria for accepting protein identification and quantification the risk of false positive identification of interaction partners was low but it is likely that other *bona fide* binding partners were excluded for further consideration. For example, we only accepted for consideration as potential interaction partners proteins that were identified in all three biological replicate experiments. Due to the phenomenon of "under-sampling", qualitative agreement between just two technical replicates is typically around only 60% [193]. Indeed, our dataset of 81 proteins identified in all three experiments represented just 27% of the total number of proteins identified across all three experiments. Thus, it cannot be excluded that more candidate interaction partners could be found within our dataset.

7.1.2.2. Limitations of class IA PI3K AP-MS screen

The major factor hampering our quantitative AP-MS investigation was the use of gel electrophoresis for the separation of proteins during sample preparation for mass spectrometry analysis. Due to inherent physical variabilities during the performance of SDS-PAGE, the resulting fractions from each of the three experiments were not directly comparable; i.e. the same proteins could not be located within the same fraction in every experiment. The major problem that this presented was that a distinct database for PESCAL quantitation, based on the qualitative data, had to be applied to each fraction for each

experiment. The qualitative and quantitative data for all the fractions was then pooled to allow comparison between samples. However, only proteins that were identified in all three experiments could be quantitatively compared between all biological replicates as the qualitative data from one experiment could not be used for quantitation of proteins in another. Thus, the quantitative analysis was limited by the qualitative analysis.

A considerable improvement to this investigation would have been to use a method for sample preparation for mass spectrometry that did not involve sample fractionation. A number of such methods, including in-gel digestion of un-fractionated samples, filter-aided sample preparation and in-solution digestion, were evaluated (data not shown); however results were disappointing in our hands as a very low number of peptide identifications were obtained and data quality was low. It is likely that the limited success of these methods is due to the low abundance of a high number of proteins in our AP-MS samples. Thus, mass-spectrometry analysis of the un-fractionated, complex sample resulted in the identification of a low number of high abundance peptides. The use of more modern mass spectrometers with greater sensitivity and faster (shorter) duty cycles (e.g., new generation of orbitrap or Q-TOF mass analysers) could in the future be used to identify additional PI3K functional binders.

7.1.3. Verification of AP-MS screen results

These results of qualitative and quantitative analysis of mass spectrometry data were validated by manual sequencing of representative peptides from candidate interaction proteins identified by MASCOT. This analysis confirmed their identification and thus supported the proposal that these peptides, and thus the proteins they derived from, interact with p85 (Fig. 3.9. – 3.10.*J*. Due to the time-consuming nature of this exercise, it is not practical to manually validate the identification of large numbers of peptides; however it is a useful tool for the validation of MASCOT data where peptide identification confidence values are low and/or numbers of peptide identifications per protein are also low. This was not the case for the candidate p85 binding partners in question as a minimum of 4 peptides (mean = 9.2) were identified for each protein in each experiment and MASCOT protein scores were high (mean = 185) (Appendix 1).

The manual quantification (using the vendor software Xcalibur) of a series of peptide peaks correlated well with automated quantitation with the in-house program PESCAL (Fig. 3.11. – 3.13.). Thus we validated the quantitative findings of the AP-MS screen and the accuracy of PESCAL.

7.1.4. Implications of study: candidate class IA PI3K interaction partners

Our AP-MS strategy was successfully applied to identify the proteins CAPNS1 (calpain small subunit 1), FN1 (fibronectin) and VIM (vimentin) as candidate PI3K interaction partners. All three of these proteins exhibited a dynamic relationship with p85 PI3K in response to changes in growth conditions (which correlates with signalling activity), with CAPNS1 found to be more strongly associated with PI3K in starved cells and FN1 and VIM found to be more strongly associated with PI3K in stimulated cells (Figs. 3.7. and 3.8. and Table 3.1.). To date, there have been no reported observations of interaction between PI3K and these three proteins. It should be noted that although the stringency of data quality for our AP-MS study was high, we employed this strategy as a screening tool. Thus, we undertook further investigation and validation work to confirm one of these candidates as a true interaction partner of class IA PI3K and to elucidate the functional significance of such associations.

Calpains are a family of calcium-dependent cysteine proteases that have been shown to have key roles in the regulation of important cellular functions including apoptosis, autophagy, proliferation and migration [289, 290, 293]. Intriguingly, at the time of concluding our AP-MS screen recent studies had reported that calpain negatively regulates signalling pathways, including PI3K, in monocytes although the mechanism for this phenomenon was not described [288].

Fibronectin is an extracellular matrix glycoprotein secreted by fibroblasts, such as NIH-3T3 cells. The protein has been implicated in the stimulation of intracellular signalling pathways, including PI3K, and has been linked to the development of lung carcinogenesis [328]. Vimentin is an intermediate filament protein, important for cytoskeletal structure and has been implicated in cell attachment, migration and signalling through its role in regulating cytoplasmic localization of other proteins [329].

Our follow-up investigative work from the AP-MS screen (Chapter 4) focused on the potential interaction between PI3K p85 and CAPNS1. Although CAPNS1 was not the candidate binding partner with the highest fold change, this path was undertaken because existing work implicated calpain in the cleavage of other signalling proteins [285] and in the regulation of Akt signalling [286-288]. Furthermore, calpain had been extensively implicated in a number of key cellular functions that are also regulated by PI3K but the mechanisms by which it exhibited control remained poorly understood. Thus, we concluded that a functional relationship between class IA PI3K may be a potential explanation for some of these reported activities (for which mechanistic insights were lacking) and that the relationship between the two proteins may potentially be of great physiological significance. However, this does not preclude the possibility that class IA PI3K also interacts with fibronectin and/or vimentin and that such functional relationships might be of equal biological significance.

One notable observation of our AP-MS screen results is that we did not identify other reported interaction partners of PI3K as candidate dynamic binding partners. For example, p85α was reported to bind directly with PTEN, enhancing its lipid phosphatase activity, upon EGF stimulation of HeLa cells [52]. One possible explanation for the discrepancy between our studies is the difference in ligand stimulation, as Chagpar *et al* exclusively stimulated EGF receptors whereas our use of FBS resulted in a wider response of growth factor receptors. An alternative explanation may be found in the observation that the authors were unable to co-purify endogenous PTEN-p85-p110 complexes, leading them to suggest that it is only free p85 that binds to PTEN [52]. Since the existence of significant amounts of free p85 in NIH-3T3 cells has been disputed [19] this may account for the lack of PTEN among our candidate binding partners. In addition, this work was performed using human HeLa cells whereas we used a mouse fibroblast cell line (NIH-3T3) as the model system; it is thus feasible that PI3K interactions may be species, or indeed tissue, specific.

p85 has also been reported to bind X-box binding protein-1 during periods of ER stress and to increase its nuclear translocation thus regulating the unfolded protein response [50, 51]. Again, these studies were conducted under different growth conditions and in a different cell model system and were unable to purify endogenous complexes of X-box

binding protein-1 with the PI3K heterodimer; these studies were therefore reliant on the "free p85 hypothesis", which has been disputed [19].

$G\alpha_{16}$ has also been reported to bind class IA PI3K complexes and to consequentially inhibit EGF-induced Akt phosphorylation in haematopoietic cells (i.e. expressing high levels of p110δ) [53]. However, the association between these proteins at endogenous levels was only investigated under basal conditions and therefore this may not be a dynamic association and may be specific to the p110δ PI3K isoform. Furthermore, the investigation into effects of the association on signalling was investigated using over-expression of $G\alpha_{16}$ so may be unrepresentative of *in vivo* signalling dynamics.

All p110 isoforms have a Ras-binding domain and Ras binding to the p110α subunit is known to regulate some PI3K functions [29, 279]. However, the interaction does not survive biochemical purification, indicating that it is a weak and transient interaction, and a high degree of variability has been demonstrated in the response of PI3K to Ras binding depending on the Ras GTPase and p110 isoform investigated [28]. Thus, the contribution of Ras in PI3K regulation remains unclear.

The considerations outlined above (in terms of different approaches in experimental design and techniques and the use of different biological models used to identify PI3K interactors) provide a rational explanation of why proteins previously shown to associate with PI3K were not present in our dataset of potential PI3K protein binders. It should be noted that most of the protein binders of PI3K descried previously were identified in a single study and for most cases there are not corroborative data from independent laboratories.

7.2. Regulation of class IA PI3K stability and signalling activity by calpain

As discussed above, CAPNS1 was consistently found to be more abundant in p85 protein complexes isolated from starved cells in all three experiments (Fig. 3.8. B). We next sought to validate the interaction between calpain and class IA PI3K and to investigate any potential functional significance of such an association.

7.2.1. Validation of the interaction between calpain and class IA PI3K

Our initial experiments aimed to confirm the finding from our AP-MS screen that CAPNS1 interacts with Class IA PI3K. Furthermore, we sought to investigate if the active

calpain heterodimer was part of the PI3K complex as this was likely to be of more functional significance.

We isolated PI3K protein complexes from starved and stimulated NIH-3T3 cells and used an *in vitro* calpain activity assay to confirm the presence of active calpain heterodimers in the complex (Fig. 4.2.). Furthermore, we confirmed that the association between PI3K and calpain was higher in serum-starved cells compared to serum-stimulated cells (Fig. 4.2.), thus validating our AP-MS screen results.

To further verify the AP-MS study findings, we also isolated calpain protein complexes by IP and used an *in vitro* lipid kinase assay to confirm the presence of PI3K in the protein complex (Fig. 4.3.). This approach also verified our AP-MS screen findings and confirmed that the association between the proteins was higher in serum-starved cells compared to serum-stimulated cells.

Enzymatic assays were used to investigate the association between calpain and PI3K because of the lack of high affinity antibodies available against calpains. Enzymatic assays can provide greater sensitivity of detection than WB, which is dependent on antibody affinity. The use of enzymatic methods is a well established approach in the field of calpain investigation and other groups have used them extensively, for example to verify the genetic knockdown of CAPNS1 [301, 305, 306]. Casein zymography [330] was used in the examples cited but we chose to use a less-cumbersome commercially available *in vitro* assay to detect calpain activity. An additional benefit of the use of enzymatic assays to validate the CAPNS1-p85 interaction is that the data also provided further functional information, confirming that both proteins are present in the complex as part of enzymatically active heterodimers.

Further investigation also revealed that the association between PI3K and calpain increased as serum-starvation time progressed (Fig. 4.3.). These data suggest that the association between PI3K and calpain is an adaptive response to cellular stress caused by growth factor starvation. Total calpain activity of NIH-3T3 cells was also shown to be increased in serum-starved cells compared to exponentially growing cells (Fig. 4.4.). Investigations into the role of calpain in cell survival have revealed discordant results and both calpain 1 and 2 have been implicated in pro and anti-apoptotic signals [290, 305, 331]. Our discovery that calpain activity and association with PI3K is increased in NIH-3T3 cells

during serum starvation would support a role for this protein in the adaptive regulation of cell survival during cellular stress.

Further follow-up work performed by our group has also confirmed that calpain interacts with class IA PI3K in human colorectal DLD-1 cancer cells (Appendix 7). The association between the two proteins in these cells was found to be higher in starved cells compared to insulin stimulated cells, in line with our findings for NIH-3T3 cells (Appendix 7).

7.2.2. Effects of calpain on PI3K stability and enzymatic activity

Having confirmed the association between calpain and class IA PI3K, we next proceeded to investigate if PI3K was a substrate for this protease as this would be a logical functional relationship. We isolated PI3K proteins from NIH-3T3 cells (which highly express p110α and p110β PI3K isoforms [19]) and RAW 264.7 cells (which highly express p110δ in addition to p110α and p110β PI3K isoforms [75]) and subjected them to *in vitro* protease digestion using purified calpain 1 and calpain 2. WB analysis of the different PI3K isoforms revealed that the p110α PI3K isoform was completely cleaved by both calpain proteins, whereas p110δ and p85 PI3K subunits were only partially cleaved and p110β was virtually unaffected (Fig. 4.5.). These results show that, as hypothesized, PI3K proteins are *in vitro* substrates of calpain. However, we noted that p110β was cleaved to a much lower extent than p110α, demonstrating that calpain preferentially cleaves p110α over p110β and p110δ in this assay. These results suggest an isoform-specific role for calpain in the regulation of PI3K activity.

We then proceeded to investigate if cleavage of PI3K proteins by calpain resulted in a functional outcome. Results revealed that calpain-mediated cleavage of p110α resulted in a decrease in lipid kinase activity *in vitro* (Fig. 4.6.). These data reveal a key role for calpain in the direct regulation of PI3K activity that has not previously been reported.

To investigate if these exciting *in vitro* results had any implications for *in vivo* functionality we next proceeded to investigate the effects of calpain activity on PI3K stability *in vivo*. We inhibited calpain activity in cells, pharmacologically and genetically, and used WB analysis of PI3K proteins to demonstrate that calpain also regulated the stability of p110α in a live context (Fig. 4.7.). From this data we could also infer that calpain inhibits p110α activity *in vivo.* In contrast, p85 and p110β levels were found to be minimally affected by calpain activity.

We also attempted to investigate the converse response by investigating the effects of increased calpain activity on PI3K protein stability. However, calcium ionophore (calpain activator) is highly toxic to cells and unsuitable for the longer term treatments (i.e. longer than 15 m) required to investigate *in vivo* protein stability.

We attempted to identify the cleavage site on p110α targeted by calpain. Calpains are thought to cleave proteins at highly-specific recognition sites, however no consensus cleavage sequence has been identified and secondary structural features are thought to be more important recognition factors for the protease than specific short motifs [285, 293]. Several bioinformatic tools have been developed that identify candidate calpain cleavage sites based on learned algorithms e.g. GPS-CCD and CaMPDB [332, 333]. We used these tools to analyze the sequence of p110α and a number of candidate sites were identified; however there was no agreement between the two different prediction models used. Furthermore, the p110β sequence was also analyzed in an attempt to identify differences between the PI3K isoforms that may indicate the correct site. Agreement of prediction sites between p110α and p110β was high for each prediction model suggesting that the correct p110α cleavage site could not be identified using the bioinformatics tools currently available.

7.2.3. Effects of calpain on PI3K signalling activity

Having established that calpain negatively regulates PI3K lipid kinase activity *in vitro* we next proceeded to investigate the effects of calpain activity on PI3K activity *in vivo*. PI3K signalling activity is typically quantified using phosphorylation levels of the downstream target Akt as a surrogate marker of activity. Lipid kinase assays can be used to measure PI3K activity directly [269] however these methods require purification of PI3K proteins and the use of radio-labelling and thus are low throughput and technically cumbersome and are not used routinely to investigate signalling. Similarly, assays to measure the levels of PIP_3 (the product of the PI3K reaction) in cells directly are technically challenging and not routinely used, although a mass-spectrometry based method that overcomes many of these limitations has recently been described [334].

Therefore, we proceeded to use WB analysis of Akt phosphorylation to investigate the effects of calpain activity *in* vivo on PI3K signalling activity. WB analysis revealed that

pharmacological calpain inhibition resulted in increased PI3K signalling activity, as measured by the quantification of Akt phosphorylation (Fig. 4.8.). Thus, we inferred that calpain has a role in the negative regulation of PI3K activity *in vivo.*

Calpain activity has been previously shown to inhibit Akt phosphorylation in human neutrophils and monocytes, although no mechanism was described [287, 288]. Haematopoietic cells express p110δ PI3K isoform, which is partially cleaved by calpain, more highly than other cell types but they are also dependent on the p110α isoform [75], which is completely cleaved by calpain. Calpain activity was also shown to inhibit Akt phosphorylation in p110δ-rich rat diaphragm muscle tissue although, again, no mechanism was determined [335]. However, in contrast to our findings, another study showed that genetic inactivation of calpain in MEFs resulted in a decrease in Akt phosphorylation compared to wild type cells when subjected to acute nutrient deprivation [286]. This effect was determined to be dependent on the effects of calpain on the Akt phosphatase PP2A [286]. Nonetheless, our results indicate that the association between PI3K and calpain increases as serum-starvation progresses and therefore the PI3K-mediated effects of calpain on Akt phosphorylation that we observed are unlikely to occur during the short starvation treatments (up to 20 minutes) used by Bertoli *et al* [286]. Another study also reported that genetic inactivation of calpain in MEFs resulted in decreased Akt phosphorylation in response to cell-death stimuli [305]. However, in contrast to other challenges reported, this effect was not clear in the data illustrating the effects of serum starvation on Akt phosphorylation and the authors do not comment on this phenomenon. These conflicting results suggest that the regulation of PI3K/Akt signalling by calpain is likely to be a complex relationship that involves the regulation of multiple nodules in this pathway. Furthermore, the interacting roles of these two proteins may differ in different organisms and indeed in different tissue cell types.

Further work, using the PI3K inhibitor LY294002, demonstrated that the observed increase in Akt phosphorylation upon calpain inhibition was dependent on PI3K/mTOR activity (Fig. 4.9.). As occurs with most pharmacological inhibitors, LY294002 has off-target effects, including the downstream substrate mTOR [65]; therefore PI3K-dependence of calpain effects on signalling could only be fully confirmed by further investigation using more specific models, e.g. siRNA inactivation, or inhibitors with different off-target effects.

Nonetheless, collectively the data presented in this thesis support the notion that the observed increases in Akt phosphorylation upon calpain inhibition are mediated through a direct effect on PI3K activity.

Subsequent investigations also demonstrated the functional significance of the calpain-PI3K interaction in that the increase in Akt phosphorylation upon calpain inhibition resulted in an increase in Akt activity, as measured using an Akt activity assay, (Fig. 4.10.) and that the signal was effectively propagated downstream to the effector p70 S6K (Fig. 4.11.). The effects of calpain on PI3K/Akt signalling were additionally confirmed using genetic inactivation of calpain by siRNA treatment (Fig. 4.12.).These results clearly demonstrated that calpain activity has a role in the regulation of downstream events in the PI3K/Akt signalling axis, most likely as a result of its interaction with PI3K.

7.2.4. Effects of calpain in class IA PI3K-dependent cell growth and survival

We next evaluated if the negative regulation of PI3K/Akt signalling by calpain had any functional impact on cell growth and survival. We used an MTS assay to investigate the effects of calpain and PI3K inhibition, using inhibitors and siRNA, on the viability of NIH-3T3 cells.

Results revealed that calpain inhibition promotes the survival of cells subjected to serum-starvation in a PI3K/mTOR-dependent manner, indicating that calpain activity may have a role in stress-induced cell death (Fig. 4.13.). In contrast, calpain was not found to have any significant effect on the viability of cells under normal growth conditions (Fig. 4.14.). Our previous data showed that the association between calpain and PI3K increased in response to serum-starvation. Therefore, it is unsurprising that an effect of calpain activity on cell viability was only observed when cells were deprived of serum. These data further support our hypothesis that the association between calpain and PI3K and the resulting effects on signalling are a response to cellular stress.

We attempted to investigate the potential mechanisms for increased cell viability upon calpain inhibition in serum-starved cells. Cell cycle arrest is a potential mechanism to regulate cell survival in response to cell stress. FACS cell cycle analysis revealed that, whilst calpain inhibition did contribute to cell cycle arrest, this effect was independent of

PI3K/mTOR (Fig. 4.15.) and therefore unlikely to be the result of the effects of calpain on PI3K/Akt signalling.

Apoptosis is a major mechanism for controlled cell death and thus an increase in apoptotic activity might contribute to calpain-dependent cell death in response to cell stress. FACS analysis to quantify apoptosis revealed that, contrary to our initial hypothesis, apoptosis increased upon inhibition of both calpain and PI3K and that the effects were cumulative (Fig. 4.16.). Therefore, increased apoptosis was unlikely to be the mechanism through which cell death was mediated by the calpain-PI3K interaction. Previous reports suggest a discordant role for calpain in the regulation of apoptosis as both calpain 1 and 2 have been implicated in pro and anti-apoptotic signals. [290, 305 , 331]. For example, genetic inactivation of calpain in mouse embryonic fibroblast decreased apoptosis induced by serum starvation, puromycin, hydrogen peroxide and UV stress but increased apoptosis in response to tumour necrosis factor and staurosporine [305]. Thus, calpain is likely to have a complex role in the regulation of apoptosis that is unlikely to be regulated primarily through PI3K.

Autophagy is a tightly regulated catabolic process by which cells regulate cell growth and is key for the maintenance of essential cellular processes during nutrient starvation. However, recent studies have also revealed a role for autophagy in controlled cell death [336, 337]. Quantification of the autophagy marker LC3-II:LC3-I ratio suggested that calpain may have a PI3K-dependent role in the promotion of autophagy (Fig. 4.17.). Our findings are supported by the findings of Demarchi *et al,* which showed that genetic inactivation of calpain in MEFs resulted in a decrease in autophagic activity as assessed by electron microscopy of phagosome formation during serum-starvation [338]. This group hypothesized that calpain may be required to break down a cytoskeletal barrier for autophagosome formation or may affect the phosphatidylinositol signalling that regulates autophagy [290]. However, conflicting reports have also suggested that calpain activity results in autophagy impairment through the cleavage of ATG5 and α-subunit of heterodimeric G proteins respectively [339, 340].

Our findings on the role of calpain in autophagy, although preliminary, suggest that calpain may promote cell death in a PI3K-dependent manner during cellular stress by

increasing autophagic activity. However, it is clear from the diverse results reported in the literature that calpain has a complex, multi-factorial role in autophagy.

7.2.5. Implication of study and future work

The discovery that calpain regulates the stability of PI3K proteins has great physiological implications due to the implicit link between protein concentration and potential activity levels. Basal PI3K levels were thought to be mainly regulated through transcriptional control and therefore relatively stable [27]. However, more recently, it has been proposed that cellular PI3K levels are dynamic and regulated through a cycle of proteasomal degradation and re-synthesis [341]. This process was reported to confer protection to the overall MCF10A cell population survival in a culture as the PI3K/Akt pathway is only active in a subset of cells at a given time [341]. Our finding that calpain regulates PI3K stability may have a role in this dynamic maintenance of PI3K levels or may represent an additional mechanism for the regulation of PI3K protein stability under certain circumstances, such as during stress.

The implications of the finding that calpain selectively regulated the stability and activity of PI3K p110α remain unclear. Although isoform specific roles have been clearly established for different PI3K isoforms [34, 67, 70, 71], it has also been shown that cell key cellular roles are not dependent on any single PI3K isoform [72]. Furthermore, this work demonstrated that very low levels of activity of a single PI3K isoform are able to sustain proliferation and survival [72]. Therefore, the regulation of p110α by calpain is unlikely to be a universal mechanism for the control of key cellular functions.

Although the full implications of the interaction between calpain and class IA PI3K remain to be fully explored, we have clearly demonstrated a functional relationship between these proteins. The interaction between calpain and PI3K appears to be enhanced in response to serum-starvation induced cell stress and the resulting effects on the regulation of PI3K/Akt signalling promote cell death. We therefore propose a model that describes the calpain-PI3K interaction as a mechanism to reduce growth activity and promote death when cells are subjected to environmental stress (Fig. 7.1.).

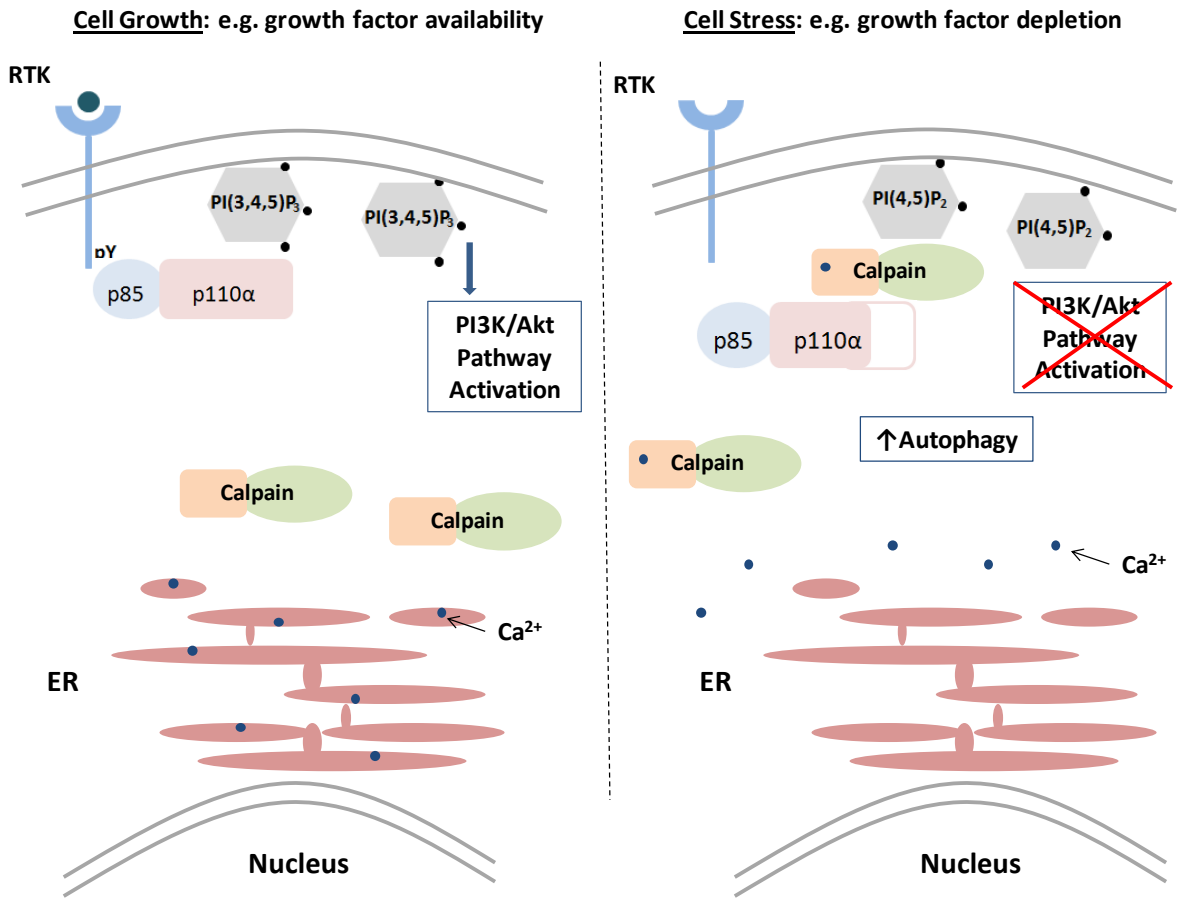

Figure 7.1. Proposed model for a cell death mechanism mediated by the calpain-PI3K interaction. Under cell growth conditions, calcium (Ca^{2+}) homeostasis is carefully regulated and intracellular Ca^{2+} is retained within the endoplasmic reticulum (ER). Calpain activity is low. PI3K is recruited to activated RTKs and generates PIP_3 as a result of its lipid kinase activity resulting in activation of the PI3K/Akt signalling pathway. Under cell stress conditions, intracellular Ca^{2+} is released by the ER [342, 343]**.** PI3K activity is low and PIP_2 accumulates at the cell surface membrane. Calpain protease activity is activated by intracellular calcium availability and interaction with PIP_2 [297, 298]. Active calpain interacts with PI3K, resulting in cleavage of the p110α protein and a reduction in lipid kinase activity. PI3K/Akt pathway activity is reduced but autophagic activity is enhanced, possibly through a reduction in mTOR activity [344]. Disruption of the tight regulation governing autophagy has been implicated in cell death [336, 337].

Loss of this environmental response mechanism may result in inappropriate cell growth and potentially contribute to the development of disease.

Calpain has been implicated in the pathogenesis of many diseases including cancer, neurodegeneration, cataract formation, multiple sclerosis, diabetes type 2, Duchenne's muscular dystrophy, and limb-girdle muscular dystrophy type 2A [331, 345, 346].

Increased expression of calpain or decreased expression of calpastatin, the endogenous inhibitor of calpain, has been observed in a variety of solid tumours and linked to poor prognosis and reduced response to treatment [290, 331]. In this scenario, calpain is thought to promote tumorigenesis through its role in cell migration and apoptosis, mediated by the cleavage of FAK and BCL-2 respectively [331, 347]. However, calpain is likely to have a complex role in the development of cancer as it has been implicated in the degradation of both oncogene gene products, e.g. c-Src (and now PI3K), and tumour suppressors, e.g. p53 [347].

Decreased calpain activity has also been implicated in the development of cancers. Higher protein expression levels of calpastatin have been found in endometrial carcinoma compared to benign endometrial tissue [348]. Calpain 1 protein expression was also shown to be reduced in basal cell carcinomas compared to normal tissue [349]. Furthermore, high levels of calpain 1 activity have been associated with decreased PI3K/Akt signalling in response to insulin in brain tissue of patients suffering from Alzheimer's or Type 2 diabetes [350].

The PI3K-calpain interaction may reveal a previously underexplored mechanism for the regulation of PI3K/Akt signalling and a potential source of pathogenesis. Reduced calpain activity may result in increased PI3K/Akt activity during periods of nutrient depletion, a phenomenon that could contribute to tumorigenesis. In contrast, increased calpain activity may result in increased cell death and tissue damage during stress.

Our data have shown that active calpain heterodimers associate with class IA PI3K. Furthermore, calpain was shown to have a role in the regulation of PI3K protein stability and signalling activity that appeared to be selective for the p110α isoform. One of the identified functional outcomes of this relationship was that calpain activity reduces PI3K/Akt signalling activity, resulting in increased cell death in response to serum-starvation.

However, the relationship between calpain and PI3K remains poorly understood and the implications of this association are unknown. Future work might attempt to further investigate the mechanism of cell death in response to decreased PI3K/Akt signalling upon calpain-mediated cleavage of PI3K. Although autophagy has been implicated by our data this phenomenon requires further investigation. It would also be of interest to investigate the roles of the two major calpain isoforms in the cleavage of PI3K proteins. Both calpain 1

and 2 were shown to cleave p110α *in vitro* however it is unclear whether one or both isoforms are involved *in vivo*. Finally, where calpain activity deregulation has been implicated in pathogenesis, it would be of interest to investigate the corresponding PI3K/Akt pathway activity to investigate if this is a significant mechanism for the development of disease.

7.3. Identification of phosphorylation events downstream of Akt

In addition to our investigations into the regulation of PI3K activity by interaction partners we also wished to use proteomics to investigate the activity of the PI3K/Akt signalling pathway on a global scale. Over 100 proteins have been reported as substrates of Akt, however many of these have not been characterized fully *in vivo* [60]. Substrates that have been investigated thoroughly reveal that substrates downstream of Akt have essential roles in survival, growth, proliferation, motility and metabolism [60]. Furthermore, evidence is increasingly emerging indicating that the three distinct Akt isoforms may regulate specific non-redundant functions [60, 104], as is the case for PI3K.

The identification of phosphorylation events downstream of Akt and quantification of PI3K/Akt pathway activity is of great interest due to their important role in normal and disease biology. Identification of kinase substrates is arguably the rate-limiting step in advancing our knowledge of cell signalling [351] and further characterization of signalling pathway dynamics is likely to improve our understanding of signalling in health and disease. The most reliable measure of Akt activity is likely to be analysis of phosphorylation downstream, a biomarker of PI3K/Akt pathway activation that would be of great interest given its importance in tumourogenesis [352]. The finding that the Akt inhibitor A-443654 inhibits the activity of downstream substrates but hyperphosphorylates Akt [138] further supports the use of downstream phosphorylation events as biomarkers of pathway activity. In addition, identification of biomarkers for PI3K/Akt pathway activity may be useful for the targeted use of pathway inhibitors in the treatment of cancer [139].

This part of the project aimed to investigate the phosphorylation events downstream of Akt using an optimised quantitative global phosphoproteomic approach (Fig. 5.1.). We used two complementary strategies, an *in vivo* cell line model and an *in vitro* assay that also enabled Akt activity quantification, to carry out this work.

7.3.1. Phosphoproteomics of the MCF10A myrAktER model

7.3.1.1. The MCF10A myrAktER model

In the first approach, we used a cell line model stably transfected with an inducible, constitutively active Akt construct [314] to investigate Akt activity in the human breast epithelial cell MCF10A (Fig. 5.2.). This model is useful for the investigation of Akt pathway dynamics as it enables controlled Akt activation. The myrAktER construct has previously been used successfully to investigate Akt activity, for example to identify Akt-regulated genes in NIH-3T3 cells using a cDNA array [353]. This study uncovered the possibility of a negative feedback action of Akt upon RTK expression [353] which was later demonstrated [137].

Initial work was performed to characterise the cell line and evaluate the activity of the MCF10A myrAktER construct. WB analysis of Akt phosphorylation demonstrated that the myrAktER construct was activated in response to 4-OHT treatment (Fig. 5.4.). Aktide assay results, an MS-based method to quantify Akt activity, further demonstrated that the construct was enzymatically active following 4-OHT treatment (Fig. 5.5.). These results showed that greater control of myrAktER activity levels could be obtained by modulating treatment time compared to using different doses (Fig. 5.4. – 5.5.). Total myrAktER was also shown to increase over the time-course (Fig. 5.4. B), which may be due to myrAktER's resistance to normal regulatory mechanisms, such as proteolytic degradation, when active or may indicate that the myrAktER construct is not detected well by the total Akt antibody when in its inactivated conformation. The data also showed that the ethanol vehicle had no effect upon the phosphorylation of the myrAktER construct (Fig. 5.4. B). Investigation of the phosphorylation of substrates downstream of Akt further demonstrated enzymatic activity of the myrAktER construct in response to 4-OHT treatment (Fig. 5.6.).

MCF10A cells are anchorage-dependent and typically exhibit anoikis (detachment-induced apoptosis) upon detachment from the extracellular matrix (or artificial substitute i.e. tissue culture plastic) [315, 316]. However, increased Akt activity has been shown to inhibit apoptosis and thus reduce the incidence of anoikis in these cells [315, 316]. We verified the biological activity of the myrAktER construct by assessing the incidence of anoikis in the MCF10A myrAktER cells. Results showed that myrAktER activation resulted in

protection from anoikis thereby demonstrating the functional output of the myrAktER construct (Fig. 5.7.). Taken together these results demonstrated the suitability of the myrAktER MCF10A cell line as a refined model for the investigation of Akt-specific phosphorylation events.

7.3.1.2. Phosphoproteomic analysis of the MCF10A myrAktER model

Having established the suitability of the model for the investigation of Akt activity we then proceeded to perform a phosphoproteomic experiment to evaluate the effects of myrAktER activity on the phosphoproteome in MCF10A cells.

MCF10A myrAktER cells were treated with ethanol vehicle control or 4-OHT (to induce myrAktER activity) prior to shotgun phosphoproteomics. A high level of analytical replication (three independent biological replicates, each analyzed in technical triplicate) was undertaken to maximise the quality of results by enabling a greater degree of discrimination by statistical tests. The use of an efficient TiO_2-affinity phospho-enrichment strategy that does not require sample fractionation [232] enables multiple rounds of mass-spectrometry analysis as run time per sample is not prohibitively long. In addition, the quantitative method PESCAL is not limited by sample number and can be used to quantify large numbers of samples per experiment.

A total of 1961 phosphorylation events were identified across all the samples to the standard for confident identification (MASCOT Expectation value <0.05). This identification criteria is arbitrary but widely used in phosphoproteomics even though evidence suggests it may lead to a high number of false negatives [158]. Qualitative data results were pooled across all the samples and conditions to generate a common phosphopeptide database to use for quantification. This approach, which is possible due to the nature of PESCAL, maximises data mining as a phosphopeptides can be confidently quantified in a sample even if it was not identified in that same run. Heat-map representation of phosphopeptide quantification and PCA revealed that, as predicted, activation of the myrAktER construct affected the phosphoproteomic profile of MCF10A cells (Fig 5.8. – 5.9.). Akt-dependent phosphorylation events were arbitrarily defined as those which exhibited a statistically significant ($p < 0.05$ as assessed by the Student's t-test) increase of a minimum two-fold in response to 4-OHT treatment compared to the control sample. Statistical significance was

employed in our selection criteria to minimise the number of false positive results. As previously mentioned, the use of PESCAL for quantitation permits the analysis of a high number of replicate samples to enable this additional level of data selection. A relatively low fold change increase was considered significant by our criteria to prevent exclusion of subtle phosphoproteomic changes that may be of importance.

A total of 238 phosphorylation events were defined to be Akt-dependent, including some already known to be directly phosphorylated by Akt (e.g. PRAS40 [310] and others known to be phosphorylated downstream of Akt activity (e.g. S6 [87]) (Fig. 5.10. – 5.11. and Appendix 2). The discovery of phosphorylation events previously shown to be downstream of Akt validated our approach. The discovery of a number of previously un-described events illustrated that our knowledge of the PI3K/Akt pathway is not comprehensive and that, despite extensive research into this field, we have still not fully characterized this signalling pathway. However, the limitations of our model also need to be taken into consideration when interpreting results. Due to the nature of the experimental design we cannot rule out that some of the phosphoproteomic changes may be Akt-independent and induced by the 4-OHT treatment itself. However, the normal mechanism of action of 4-OHT is the partial activation of the endogenous nuclear oestrogen receptor and associated effects on gene expression [354] rather than effects on growth factor pathway signalling. Furthermore, MCF10A cells are oestrogen receptor negative cells [355], therefore endogenous effects of 4-OHT are likely to be minimal. An alternative approach would have been to use 4-OHT MCF10A cells that lacked the myrAktER construct as the control, however false positives would also be possible with this approach as divergent populations of cells might have acquired mutations affecting the phosphoproteomic profile.

Our dataset may have a number of potential applications. The profile of Akt-dependent phosphorylation events, or a subset of those identified, may be a useful phosphoproteomic signature for use as a biomarker of Akt activity. Further investigation using a different method to affect Akt activity and a different cell model system would be useful to evaluate the potential of this application. Phosphorylation events identified as Akt-dependent by our study may also have identified novel Akt signalling pathway components that require further investigation. However, the findings of this investigation should be validated in a different cell system before pursuing extensive follow-up studies. With this consideration in

mind, we also investigated another strategy for the investigation of phosphorylation downstream of Akt (5.4.) and cross-referenced the data sets to identify a list of high-confidence phosphorylation events dependent on Akt (Table 5.1.).

7.3.2. *In vitro* Akt1 assay

In order to provide further insights on the proteomics of PI3K signalling, we also investigated the use of *in vitro* kinase assays to identify phosphorylation events downstream of Akt. *In vitro* assays have been extensively used in the identification of kinase substrates. The classical approach in this strategy is to incubate the kinase of interest with candidate substrates, in the presence of radio-labelled ATP, and use the detection of radiation in proteins to confirm the relationship. However, this approach is time-consuming, hazardous and targeted [356] and therefore unsuitable for a global-scale study.

A modification of this strategy to an untargeted, more global approach was most notably utilised by the Cohen group in a strategy they termed Kinase Substrate Tracking and Elucidation (KESTREL) [272, 356]. In this approach, kinases were incubated with total cell extracts in the presence of radio-labelled ATP prior to purification of substrates by an extensive series of purification steps followed by MS/MS identification [356]. The purification of substrates is time-consuming because several rounds of chromatography are needed to identify just one potential substrate and often difficult and low-abundance proteins are hard to identify by this method. Nevertheless KESTREL was successfully applied to identify substrates of many kinases e.g. SGK1, Akt, MAPK and CDK6 [356].

Other modifications of the classical approach have also been developed over the years. Peptide arrays, in which hundreds or thousands of peptides are spotted onto an array and incubated with the kinase under investigation prior to detection of interaction, have been widely used [351, 357, 358]. Protein arrays, which utilise the same strategy but use thousands of full-length proteins spotted onto chips, have also been developed [359-361]. The use of arrays is a considerable innovation in the identification of kinase substrates as they are large-scale, relatively fast and require low amounts of kinase material [360]. Protein arrays are a preferable option to peptide arrays as the use of full-length protein "bait" is likely to result in greater specificity of interactions and reduce the number of false positives [360]. Furthermore, bioinformatic modelling can be applied to array data to

identify phosphorylation motifs and extrapolate to related datasets [351, 360, 362]. However, protein arrays are not without practical limitations; recombinant protein expression may be challenging and lack required post-translational modifications and protein immobilization may obscure phosphorylation sites, denature the protein and alter reaction kinetics [360, 363].

Other proteomic strategies for the identification of kinase substrates have also been developed and a recent innovation involves the use of analog-sensitive kinases. In this approach, kinases are genetically engineered so that the active site cannot utilise ATP but preferentially uses a labelled ATP analogue [363, 364]. These kinases are incubated with protein mixes and then the labelled, modified substrates are affinity purified and identified, using a variety of techniques [363]. Although this approach has yielded some success, the requirement for the design of an artificial kinase can be costly and time-consuming and can be a limiting step as it is estimated that 30% of kinases lose some catalytic activity, and resulting functionality, upon the introduction of the analog mutation [363, 365].

Another untargeted strategy developed for the identification of kinase substrates is the use of active catalytic kinase domains as an affinity purification reagent [366]. Proteins purified from protein mixes or cell extracts are then identified using mass spectrometry [366]. However, a drawback of this approach is that the site of kinase activity on the protein cannot be identified as other kinases may have been active in the protein mix.

Against this backdrop, we attempted to develop an *in vitro* method which, in combination with shotgun proteomics, would enable the un-targeted, global-scale identification of kinase substrates. Our strategy was inspired by the KESTREL approach [272]. We incubated active recombinant Akt with de-phosphorylated total cell extracts (Fig. 5.3.) under conditions to enable optimum kinase activity and we then used global phosphoproteomics to identify and quantify phosphorylation events. This approach encompasses many desirable characteristics of an *in vitro* kinase assay as it involves a kinase reaction with endogenous, full-length proteins and the identification method enables the determination of phosphorylation sites [363]. In addition, we developed this *in vitro* assay further to enable the quantification of kinase activity for each phosphorylation site.

7.3.2.1. Development of an *in vitro* assay for the identification of phosphorylation events downstream of Akt1

We applied our *in vitro* assay to identify phosphorylation events downstream of Akt. Total cell extracts from MCF10A cells were de-phosphorylated by exploitation of the endogenous phosphatase activity of the sample in the absence of phosphatase inhibitors. We used this de-phosphorylation technique as the simple addition of phosphatise inhibitors was sufficient to terminate the process thus enabling a simple workflow. Our total cell extract substrate was then incubated *in vitro* with different concentrations of recombinant, active Akt1 and a reaction buffer that included ATP. The quantities of recombinant active Akt1 used vastly exceed the *in vivo* levels of Akt however a short reaction time and a relatively low reaction temperature were used as these conditions are likely to minimise non-specific kinase reactions [272, 356], a concern as kinases are able to phosphorylate proteins *in vitro* that are not true *in vivo* substrates [351, 363].

The *in vitro* reaction products were then subjected to our phosphoproteomic protocol. A total of 561 phosphopeptides were identified to the required level of confidence (MASCOT Expectancy < 0.05) and quantified in this experiment and heat-map representation of the peptide quantification and PCA revealed that, as expected, Akt1 activity in the *in vitro* assay conferred a distinct phosphoproteomic profile compared to the control sample (Fig. 5.12. – 5.13.).

An arbitrary criterium was defined for a phosphorylation event to be considered Akt1-dependent: a minimum of a two-fold increase in phosphopeptide intensity in the reaction performed with 10 µg Akt1 compared to the control sample. Our control sample, which contained no exogenous Akt1 but was subjected to the reaction incubation, accounted for any non-Akt endogenous kinase activity in the sample although this should have been low due to the de-phosphorylation treatment. Thus, any increases upon incubation with Akt1 should be specific for the *in vitro* activity of Akt and kinases activated downstream. However, it should be noted that this does not necessarily correlate directly with *in vivo* activity [351, 363]. It was interesting to observe that many phosphopeptide intensities decreased as a result of the reaction (Fig. 5.12.), which may indicate the activation of phosphatases downstream of Akt activity. The activation of phosphatases downstream of

kinase activity remains underexplored in global phosphoproteomics experiments and may be an interesting area to explore further for Akt.

A total of 86 phosphopeptides were identified to be Akt1-dependent (according to our criteria) in this reaction, including some known Akt targets thus validating our strategy (Fig. 5.14. – 5.15. and Appendix 3). However, we wished to further develop our *in vitro* assay strategy to improve the data yield of the approach by investigating the efficiency of the measured activities of Akt on their substrates and thus rank the identified substrates according to the likelihood that they are physiological

7.3.2.2. Use of an *in vitro* assay to identify phosphorylation events downstream of Akt1 and quantify reaction efficiency

We reasoned that an improvement to our strategy would be to perform the *in vitro* kinase reaction with different concentrations of ATP in the presence or absence of Akt1. Thus, we would be able to identify Akt1-dependent phosphorylation events, as those that occurred only in the presence of Akt1, and to investigate the dynamics of the Akt phosphorylation reaction, through the use of various concentrations of ATP. Thus, our assay would enable the identification of the most efficient reactions that are more likely to occur *in vivo.* An additional improvement to our strategy was the use of exogenous lambda protein phosphatase for the de-phosphorylation reaction to improve efficiency as we remained vigilant against background kinase activity.

De-phosphorylated proteins were incubated in an *in vitro* reaction with different concentrations of ATP in the presence or absence of recombinant, active Akt1. It should be noted that endogenous ATP was removed from the sample during the size exclusion chromatography that forms part of the de-phosphorylation protocol. The concentrations of ATP used in the reaction are well within those estimated to be present in the cytoplasm *in vivo*. Intracellular ATP concentrations are dynamically regulated by the cellular adenylate pool, which is in turn determined by the balance between energy expenditure and energy production [367, 368]. Therefore, intracellular ATP concentration varies widely between tissues and even between cells of the same tissue at different stages in differentiation [367]. Furthermore, ATP concentrations are also distinct in different intracellular compartments

[369]. However, various studies estimate intracellular ATP concentration to be between 1 – 5 mM, depending on cell type and conditions [368, 370] and the intracellular ATP concentration of MCF10A cells has been reported to be 1.2 – 2.7 nmol per 10 million cells, which approximates a concentration of 1.2 – 2.7 mM [371]. As previously, a short reaction time and a relatively low reaction temperature were used to minimise non-specific kinase reactions [272, 356].

The reaction products were then subjected to trypsin digestion, phosphopeptide enrichment and shotgun phosphoproteomics for peptide identification and quantification. As for the previous strategy, samples were analyzed in technical replicate to maximise the identification of phosphopeptides and thus the size of the database used by PESCAL for quantification.

A total of 856 phosphopeptides were identified to the required level of confidence (MASCOT Expectancy < 0.05) and quantified in the experiment. The heat-map representation of peptide quantification and PCA revealed that, as previously observed, the presence of active Akt1 in the reaction conferred a distinct phosphoproteomic response (Fig. 5.16. – 5.17.). Again, it was interesting to note that the intensity of many phosphorylation events decreased in the presence of Akt1. We defined a criterium for phosphorylation events to be considered Akt1-dependent: a minimum of a two-fold increase in intensity upon incubation with 100 µM ATP in the presence of Akt1 compared to in the absence of Akt1. 253 phosphopeptides were classified within this group, including some known Akt substrates, which validated this strategy (Fig. 5.18. – 5.19. and Appendix 4).

We next proceeded to use the same data to quantify the affinity of Akt1 for ATP for each phosphorylation site, thus providing an estimation of phosphorylation efficiency. We hypothesized that this data would be useful to discriminate between *bona fide in vivo* substrates, which would be likely to have a high affinity for Akt1, and non-specific reactions, which would be likely to have a lower affinity for Akt1. Akt1-ATP affinity (K_{ATP}) was calculated from the relationship between ATP concentration and phosphopeptide intensity using non-linear regression based on the principles of Michaelis-Menten reaction kinetics (Fig. 5.20.). It should be noted that phosphorylation reactions do not meet all the principles of Michaelis-Menten kinetics, for instance substrate availability was not unlimited, and that

a low number of data points were used per reaction so K_{ATP} is not equivalent to K_m but is a useful indicator to rank sites phosphorylated by Akt according to reaction efficiency.

The evaluation of Akt1-dependent phosphorylation events revealed that K_{ATP} inversely correlated with phosphorylation efficiency i.e. low K_{ATP} indicates efficient phosphorylation (Fig. 5.21.). These data support our hypothesis suggesting that K_{ATP} may be a useful parameter to identify efficient phosphorylation reactions, which may be more likely to occur *in vivo*. Motif analysis further supported this notion as phosphopeptides with low K_{ATP} were found to be enriched for the motifs known to be phosphorylated by Akt and its downstream substrate p70S6K (Fig. 5.22.). Therefore, we can conclude that K_{ATP} can be used to predict the likelihood of an *in vitro* substrate being a true *in vivo* substrate thus providing additional information regarding the confidence of results when conducting large-scale studies for the identification of kinase substrates.

As concluded for the myrAktER MCF10A study, our dataset of candidate Akt substrates may have a number of potential applications. The profile of Akt-dependent phosphorylation events, or a subset of those identified, may be a useful phosphoproteomic signature for use as a biomarker of Akt activity. Phosphorylation events identified as Akt-dependent by our study may also have identified novel Akt signalling pathway components that require further investigation. More exhaustive data analysis and validation would be required to establish more clearly the relationship between *in vitro* K_{ATP} and *in vivo* substrate activity, however our strategy and this relationship may enable significant advances in large-scale investigations of kinase substrates.

Finally, the datasets of phosphopeptides found to be Akt-dependent using the MCF10A myrAktER model and the *in vitro* kinase assay were cross-referenced to produce a short-list of high-confidence Akt-dependent phosphorylation events (Table 5.1.). Several of the phosphorylation sites were known to be targets of Akt activity but the majority have not previously been described. These phosphorylation sites are of great potential interest for follow-up investigation as they are likely to reveal novel PI3K/Akt pathway components and may unveil previously unknown functions of this pathway.

7.3.3. Implications of study and future work

As previously mentioned, following further validation studies the phosphorylation sites identified by our investigations may have useful applications as a biomarker phosphopeptide signature of Akt activity or may provide leads for future investigation into the activity of this pathway. Furthermore, we have established a method to quantify kinase activity *in vivo* that, as demonstrated by Chapter 6, has great potential to advance the investigation of signalling pathway activities. Specifically relating to Akt, it would be interesting to use this approach to compare the activities of fully phosphorylated Akt compared to partially phosphorylated Akt and it would also be interesting to compare the different isoforms of Akt to establish their distinct effects upon the phosphoproteome.

Other large-scale proteomic studies have been used to identify hundreds of downstream substrates driven by the Akt pathway [372, 373]. We hope that the addition of our dataset may contribute to the detailed mapping of the PI3K/Akt signalling pathway.

7.4. Global kinase activity profiling

Quantification of kinase activity is of great interest as it provides information that may be useful for the investigation of signalling pathway aberrations, the identification of therapeutic targets and as a biomarker for diagnosis and therapeutic monitoring.

In vitro kinase reaction assays have been available for decades, however such methods were previously dependent on cumbersome and hazardous detection methods [318, 319]. More recently, mass-spectrometry has been successfully applied to provide a detection method for such reactions.

Mass-spectrometry based kinase assays, which may be multiplexed to measure multiple kinase activities, have been developed using short peptides as substrates [270, 271, 320, 321]. Although these approaches have been successful, their application is limited as the use of synthetic purified peptide substrates requires specific knowledge of the kinase target site and substrate recognition by some kinases is known to be dependent on conformational interaction between proteins in addition to recognition of the short linear phosphorylation motif [322, 323, 351].

We followed on from the *in vitro* kinase assay designed in Chapter 5 to develop a novel methodology, which we termed global kinase activity profiling (GKAP), to enable the global-scale quantification of endogenous kinase activity (Fig. 6.2.).

7.4.1. Development of an assay for the global profiling of endogenous kinase activity (GKAP)

Our GKAP approach exploits the fact that all protein kinases in a cell extract will be active upon incubation with ATP and co-factors [356]. We initially investigated whether endogenous protein kinase activities responded to an *in vitro* kinase assay in the same way as recombinant Akt1 (5.4.) and whether this activity was detectable using mass spectrometry.

Total cell lysates of different total protein composition were taken from P31/Fuj cells and incubated with different concentrations of ATP in a kinase reaction prior to shotgun phosphoproteomics. I*n vitro* reaction conditions (5 min incubation at 30^{o}C) were previously established and were not modified for GKAP, however it is possible that there is scope for optimisation for this modified approach. Results demonstrated that, indeed endogenous kinases were active in an *in vitro* reaction mix and that the level of activity appeared to be proportional to ATP concentrations (Fig. 6.3. – 6.4.). The results also illustrated the signal-amplification inherent to the method as kinase activity was detectable in very small sample volumes (5 µg). These preliminary results supported the notion that GKAP is suitable for the quantification of endogenous kinase activities.

7.4.2. Application of GKAP to identify differential pathway activation in two cancer cell lines

Having established that the *in vitro* activities of endogenous kinases could be detected by mass spectrometry, we next proceeded to investigate if the GKAP method could be used to detect the different levels of kinase activities in two AML cell lines shown to have differential activation of signalling pathways under basal conditions [179]. Analysis revealed that the two cell lines showed distinct responses to GKAP (Fig. 6.5.), suggesting differential pathway activation (Fig. 6.6.). Kinase activities were quantified as area under the kinetic curve (AUC) and data showed differential activation of some kinases between the two cell

lines (Fig. 6.7.). These results demonstrated that GKAP is a suitable method to discriminate between signalling pathways with different levels of basal activation, thus validating our hypothesis. Furthermore, motif analysis demonstrated that a wide range of kinase activities were represented in the GKAP data (Fig. 6.8.), demonstrating that, in contrast to other *in vitro* kinase assays, it is a truly global method.

7.4.3. Application of GKAP to detect growth factor induced pathway activation and drug mediated kinase inhibition

We then applied GKAP to MCF10A cells to investigate if the method was suitable for the detection of growth factor stimulated pathway activation and small molecule kinase inhibition, which would demonstrate the suitability of its use for biomarker monitoring. Analysis revealed that, as expected, the various cell treatments resulted in distinct responses to GKAP (Fig. 6.9.). Detailed investigation showed that kinase activity induced by EGF treatment was detected by GKAP (Fig. 6.10.). Furthermore, inhibition of EGF-induced kinase activity by inhibitor treatment was also detected (Fig 6.10. B – D). Therefore, these data demonstrate that GKAP is suitable for the detection of signalling pathway activation and corresponding inhibition by pharmacological treatment, highlighting an important potential application in a biomedical context. Motif analysis was performed and, as before, showed that a wide-range of kinases including those known to be active in these cells was represented in the GKAP dataset (Fig. 6.11.) as it is a global, unbiased method.

7.4.4. Implications of study and future work

These results demonstrate that GKAP is a useful method for the detection of endogenous kinase activities. In contrast to alternative kinase assay approaches, GKAP uses endogenous, full-length proteins, thereby reducing false positives, and detects global kinase activities in an untargeted way. A further advantage of GKAP is that the reaction not only takes into account kinase activity but is also affected by substrate availability therefore it is a remarkably faithful representation of the *in vivo* scenario.

The characteristics of GKAP suggest a wide range of applicability. It is a suitable approach for discovery investigations into understanding signal pathway transduction. In addition, the technique may have extremely useful applications in the pin-pointing of

signalling aberrations in disease. Furthermore, due to the low sample volume requirements the method may have an important role in the diagnosis and monitoring of disease in patients.

7.5. Concluding remarks

The PI3K/Akt pathway is a fundamental signal transduction pathway and as such is highly complex; despite extensive research in this field there remains a great deal to discover and understand. Mass-spectrometry based proteomics is an exciting field that is rapidly developing and is enabling research strategies that were previous not possible. As such, the use of proteomics to further our understanding of cell signalling is a necessary and exciting prospect.

We applied emerging proteomic techniques to address two major under-explored areas of PI3K/Akt biochemistry: the role of interaction partners in the regulation of PI3K activity and characterization of global phosphorylation downstream of its key target Akt.

Our results have revealed exciting new findings that contribute to our understanding of the mechanisms by which the PI3K/Akt pathway operates. Furthermore, they have provided leads for further innovative discoveries and have demonstrated the power of mass-spectrometry based proteomics for the dissection of signalling pathways.

Bibliography

1. Zvelebil, M.J., et al., *Structural and Functional Diversity of Phosphoinositide 3-Kinases [and Discussion].* Philosophical Transactions of the Royal Society of London. Series B: Biological Sciences, 1996. **351**(1336): p. 217-223.
2. Vanhaesebroeck, B., et al., *The emerging mechanisms of isoform-specific PI3K signalling.* Nat Rev Mol Cell Biol, 2010. **11**(5): p. 329-341.
3. Cantley, L.C., *The Phosphoinositide 3-Kinase Pathway.* Science, 2002. **296**(5573): p. 1655-1657.
4. Vanhaesebroeck, B., et al., *Synthesis and function of 3-phosphorylated inositol lipids.* Annual Review of Biochemistry, 2001. **70**(1): p. 535-602.
5. Arcaro, A., et al., *Class II Phosphoinositide 3-Kinases Are Downstream Targets of Activated Polypeptide Growth Factor Receptors.* Mol. Cell. Biol., 2000. **20**(11): p. 3817-3830.
6. Falasca, M. and T. Maffucci, *Rethinking phosphatidylinositol 3-monophosphate.* Biochimica et Biophysica Acta (BBA) - Molecular Cell Research, 2009. **1793**(12): p. 1795-1803.
7. Domin, J., et al., *The class II phosphoinositide 3-kinase PI3K-C2β regulates cell migration by a PtdIns(3)P dependent mechanism.* Journal of Cellular Physiology, 2005. **205**(3): p. 452-462.
8. Falasca, M., et al., *The Role of Phosphoinositide 3-Kinase C2a in Insulin Signaling.* Journal of Biological Chemistry, 2007. **282**(38): p. 28226-28236.
9. Domin, J., et al., *Cloning of a human phosphoinositide 3-kinase with a C2 domain that displays reduced sensitivity to the inhibitor wortmannin.* Biochem. J., 1997. **326**(1): p. 139-147.
10. Gillooly, D.J., C. Raiborg, and H. Stenmark, *Phosphatidylinositol 3-phosphate is found in microdomains of early endosomes.* Histochemistry and Cell Biology, 2003. **120**(6): p. 445-453.
11. Birkeland, H. and H. Stenmark, *Protein targeting to endosomes and phagosomes via FYVE and PX domains.* Curr Top Microbiol Immunol, 2004. **282**: p. 89 - 115.
12. Slessareva, J.E., et al., *Activation of the Phosphatidylinositol 3-Kinase Vps34 by a G Protein βγ Subunit at the Endosome.* Cell, 2006. **126**(1): p. 191-203.
13. Backer, J.M., *The regulation and function of Class III PI3Ks: novel roles for Vps34.* Biochem J, 2008. **410**(1): p. 1-17.
14. Nobukuni, T., et al., *Amino acids mediate mTOR/raptor signaling through activation of class 3 phosphatidylinositol 3OH-kinase.* Proceedings of the National Academy of Sciences of the United States of America, 2005. **102**(40): p. 14238-14243.
15. Schu, P., et al., *Phosphatidylinositol 3-kinase encoded by yeast VPS34 gene essential for protein sorting.* Science, 1993. **160**(5104): p. 88 - 91.
16. Vanhaesebroeck, B., P. Vogt, and C. Rommel, *PI3K: from the bench to the clinic and back.* Curr Top Microbiol Immunol, 2010. **347**: p. 1 - 19.
17. Vanhaesebroeck, B., et al., *Signalling by PI3K isoforms: insights from gene-targeted mice.* Trends in Biochemical Sciences, 2005. **30**(4): p. 194-204.
18. Chamberlain, M.D., et al., *Disrupted RabGAP Function of the p85 Subunit of Phosphatidylinositol 3-Kinase Results in Cell Transformation.* Journal of Biological Chemistry, 2008. **283**(23): p. 15861-15868.
19. Geering, B., et al., *Class IA phosphoinositide 3-kinases are obligate p85-p110 heterodimers.* Proceedings of the National Academy of Sciences, 2007. **104**(19): p. 7809-7814.
20. Yu, J., et al., *Regulation of the p85/p110 Phosphatidylinositol 3'-Kinase: Stabilization and Inhibition of the p110alpha Catalytic Subunit by the p85 Regulatory Subunit.* Molecular and Cellular Biology, 1998. **18**(3): p. 1379-1387.

21. Huang, C.-H., et al., *The Structure of a Human p110α/p85α Complex Elucidates the Effects of Oncogenic PI3Kα Mutations.* Science, 2007. **318**(5857): p. 1744-1748.
22. Zhang, X., et al., *Structure of Lipid Kinase p110b/p85b Elucidates an Unusual SH2-Domain-Mediated Inhibitory Mechanism.* Molecular Cell, 2011. **41**(5): p. 567-578.
23. Berndt, A., et al., *The p110d structure: mechanisms for selectivity and potency of new PI(3)K inhibitors.* Nat Chem Biol, 2010. **6**(2): p. 117-124.
24. Walker, E.H., et al., *Structural insights into phosphoinositide 3-kinase catalysis and signalling.* Nature, 1999. **402**(6759): p. 313-320.
25. Brachmann, S.M., et al., *Role of Phosphoinositide 3-Kinase Regulatory Isoforms in Development and Actin Rearrangement.* Mol Cell Biol, 2005. **25**(7): p. 2593-2606.
26. Luo, J. and L.C. Cantley, *Then Negative Regulation of Phosphoinositide 3-Kinase Signaling by p85 and Its Implication in Cancer.* Cell Cycle, 2005. **4**(10): p. 1309-1312.
27. Kok, K., B. Geering, and B. Vanhaesebroeck, *Regulation of phosphoinositide 3-kinase expression in health and disease.* Trends in Biochemical Sciences, 2009. **34**(3): p. 115-127.
28. Rodriguez-Vizciana, P., C. Sabatier, and F. McCormick, *Signaling Specificity by Ras Family GTPases Is Determined by the Full Spectrum of Effectors They Regulate.* Mol Cell Biol, 2004. **24**(11): p. 4943-4954.
29. Gupta, S., et al., *Binding of Ras to Phosphoinositide 3-Kinase p110alpha Is Required for Ras-Driven Tumorigenesis in Mice.* Cell, 2007. **129**(5): p. 957-968.
30. Ramjaun, A.R. and J. Downward, *Ras and Phosphoinositide 3-Kinase: Partners in Development and Tumorigenesis.* Cell Cycle, 2007. **6**(23): p. 2902-2905.
31. Voigt, P., et al., *Assigning Functional Domains within the p101 Regulatory Subunit of Phosphoinositide 3-Kinase γ.* Journal of Biological Chemistry, 2005. **280**(6): p. 5121-5127.
32. Brock, C., et al., *Roles of G-beta-gamma in membrane recruitment and activation of p110gamma/p101 phosphoinositide 3-kinase {gamma}.* J. Cell Biol., 2003. **160**(1): p. 89-99.
33. Guillermet-Guibert, J., et al., *The p110β isoform of phosphoinositide 3-kinase signals downstream of G protein-coupled receptors and is functionally redundant with p110γ*. PNAS, 2008. **105**(24): p. 8292–8297.
34. Graupera, M., et al., *Angiogenesis selectively requires the p110alpha isoform of PI3K to control endothelial cell migration.* Nature, 2008. **453**(7195): p. 662-666.
35. Schafer, B., A. Gschwind, and A. Ullrich, *Multiple G-protein-coupled receptor signals converge on the epidermal growth factor receptor to promote migration and invasion.* Oncogene, 2003. **23**(4): p. 991-999.
36. Jimenez, C., et al., *The p85 Regulatory Subunit Controls Sequential Activation of Phosphoinositide 3-Kinase by Tyr Kinases and Ras.* Journal of Biological Chemistry, 2002. **277**(44): p. 41556-41562.
37. Ueki, K., et al., *Positive and Negative Roles of p85alpha and p85beta Regulatory Subunits of Phosphoinositide 3-Kinase in Insulin Signaling.* Journal of Biological Chemistry, 2003. **278**(48): p. 48453-48466.
38. Ueki, K., et al., *Molecular Balance between the Regulatory and Catalytic Subunits of Phosphoinositide 3-Kinase Regulates Cell Signaling and Survival.* Molecular and Cellular Biology, 2002. **22**(3): p. 965-977.
39. Ueki, K., et al., *Increased insulin sensitivity in mice lacking p85alpha subunit of phosphoinositide 3-kinase.* Proceedings of the National Academy of Sciences of the United States of America, 2002. **99**(1): p. 419-424.
40. Maehama, T. and J.E. Dixon, *The Tumor Suppressor, PTEN/MMAC1, Dephosphorylates the Lipid Second Messenger, Phosphatidylinositol 3,4,5-Trisphosphate.* Journal of Biological Chemistry, 1998. **273**(22): p. 13375-13378.
41. Zhang, S. and D. Yu, *PI(3)King Apart PTEN's Role in Cancer.* Clinical Cancer Research, 2010. **16**(17): p. 4325-4330.

42. Leslie, N.R., et al., *Understanding PTEN regulation: PIP2, polarity and protein stability.* Oncogene, 2008. **27**(41): p. 5464-5476.
43. Papakonstanti, E.A., A.J. Ridley, and B. Vanhaesebroeck, *The p110delta isoform of PI 3-kinase negatively controls RhoA and PTEN.* EMBO J, 2007. **26**(13): p. 3050-3061.
44. Ooms, L.M., et al., *The role of the inositol polyphosphate 5-phosphatases in cellular function and human disease.* Biochem J, 2009. **419**(1): p. 29-49.
45. Harrington, L.S., et al., *The TSC1-2 tumor suppressor controls insulin-PI3K signaling via regulation of IRS proteins.* The Journal of Cell Biology, 2004. **166**(2): p. 213-223.
46. O'Reilly, K.E., et al., *mTOR Inhibition Induces Upstream Receptor Tyrosine Kinase Signaling and Activates Akt.* Cancer Research, 2006. **66**(3): p. 1500-1508.
47. Zhang, H., et al., *PDGFRs are critical for PI3K/Akt activation and negatively regulated by mTOR.* The Journal of Clinical Investigation, 2007. **117**(3): p. 730-738.
48. Vasudevan, K.M., et al., *Suppression of PTEN Expression Is Essential for Antiapoptosis and Cellular Transformation by Oncogenic Ras.* Cancer Research, 2007. **67**(21): p. 10343-10350.
49. Xia, D., et al., *Mitogen-activated Protein Kinase Kinase-4 Promotes Cell Survival by Decreasing PTEN Expression through an NFKB-dependent Pathway.* Journal of Biological Chemistry, 2007. **282**(6): p. 3507-3519.
50. Park, S.W., et al., *The regulatory subunits of PI3K, p85a and p85b, interact with XBP-1 and increase its nuclear translocation.* Nat Med, 2010. **16**(4): p. 429-437.
51. Winnay, J.N., et al., *A regulatory subunit of phosphoinositide 3-kinase increases the nuclear accumulation of X-box-binding protein-1 to modulate the unfolded protein response.* Nat Med, 2010. **16**(4): p. 438-445.
52. Chagpar, R.B., et al., *Direct positive regulation of PTEN by the p85 subunit of phosphatidylinositol 3-kinase.* Proceedings of the National Academy of Sciences, 2010. **107**(12): p. 5471-5476.
53. Yeung, W.W.S. and Y.H. Wong, *Ga16 interacts with Class IA phosphatidylinositol 3-kinases and inhibits Akt signaling.* Cellular Signalling, 2010. **22**(9): p. 1379-1387.
54. Harlan, J.E., et al., *Pleckstrin homology domains bind to phosphatidylinositol-4,5-bisphosphate.* Nature, 1994. **371**(6493): p. 168-170.
55. Isakoff, S.J., et al., *Identification and analysis of PH domain-containing targets of phosphatidylinositol 3-kinase using a novel in vivo assay in yeast.* EMBO J, 1998. **17**(18): p. 5374-5387.
56. Klarlund, J.K., et al., *Signaling by Phosphoinositide-3,4,5-Trisphosphate Through Proteins Containing Pleckstrin and Sec7 Homology Domains.* Science, 1997. **275**(5308): p. 1927-1930.
57. Welch, H.C.E., et al., *P-Rex1, a PtdIns(3,4,5)P3- and Gbetagamma-Regulated Guanine-Nucleotide Exchange Factor for Rac.* Cell, 2002. **108**(6): p. 809-821.
58. Patrucco, E., et al., *PI3Kgamma modulates the cardiac response to chronic pressure overload by distinct kinase-dependent and -independent effects.* Cell, 2004. **118**(3): p. 375-87.
59. Lehmann, K., et al., *PI3Kgamma controls oxidative bursts in neutrophils via interactions with PKCalpha and p47phox.* Biochem J, 2009. **419**(3): p. 603-610.
60. Manning, B.D. and L.C. Cantley, *AKT/PKB Signaling: Navigating Downstream* Cell, 2007. **129**(7): p. 1261-1274.
61. Cain, R.J. and A.J. Ridley, *Phosphoinositide 3-kinases in cell migration.* Biol Cell, 2009. **101**(1): p. 13-29.
62. Arcaro, A. and M. Wymann, *Wortmannin is a potent phosphatidylinositol 3-kinase inhibitor: the role of phosphatidylinositol 3,4,5-trisphosphate in neutrophil responses.* Biochem J. , 1993. **296**(2): p. 297 - 301.
63. Powis, G., et al., *Wortmannin, a Potent and Selective Inhibitor of Phosphatidylinositol-3-kinase.* Cancer Research, 1994. **54**(9): p. 2419-2423.

64. Vlahos, C.J., et al., *A specific inhibitor of phosphatidylinositol 3-kinase, 2-(4-morpholinyl)-8-phenyl-4H-1-benzopyran-4-one (LY294002).* Journal of Biological Chemistry, 1994. **269**(7): p. 5241-5248.
65. Brunn, G.J., et al., *Direct inhibition of the signaling functions of the mammalian target of rapamycin by the phosphoinositide 3-kinase inhibitors, wortmannin and LY294002.* EMBO J, 1996. **15**(19): p. 5256-67.
66. Sadhu, C., et al., *Essential Role of Phosphoinositide 3-Kinase δ in Neutrophil Directional Movement.* The Journal of Immunology, 2003. **170**(5): p. 2647-2654.
67. Jackson, S.P., et al., *PI 3-kinase p110b: a new target for antithrombotic therapy.* Nat Med, 2005. **11**(5): p. 507-514.
68. Williams, O., et al., *Discovery of Dual Inhibitors of the Immune Cell PI3Ks p110α and p110δ: a Prototype for New Anti-inflammatory Drugs.* Chemistry & Biology, 2010. **17**(2): p. 123-134.
69. Hirsch, E., et al., *Central Role for G Protein-Coupled Phosphoinositide 3-Kinase γ in Inflammation.* Science, 2000. **287**(5455): p. 1049-1053.
70. Okkenhaug, K., et al., *Impaired B and T Cell Antigen Receptor Signaling in p110δ PI 3-Kinase Mutant Mice.* Science, 2002. **297**(5583): p. 1031-1034.
71. Foukas, L.C., et al., *Critical role for the p110a phosphoinositide-3-OH kinase in growth and metabolic regulation.* Nature, 2006. **441**(7091): p. 366-370.
72. Foukas, L.C., et al., *Activity of any class IA PI3K isoform can sustain cell proliferation and survival.* Proceedings of the National Academy of Sciences, 2010. **107**(25): p. 11381-11386.
73. Ali, K., et al., *Essential role for the p110d phosphoinositide 3-kinase in the allergic response.* Nature, 2004. **431**(7011): p. 1007-1011.
74. Ali, K., et al., *Isoform-Specific Functions of Phosphoinositide 3-Kinases: p110delta but Not p110gamma Promotes Optimal Allergic Responses In Vivo.* J Immunol, 2008. **180**(4): p. 2538-2544.
75. Papakonstanti, E.A., et al., *Distinct roles of class IA PI3K isoforms in primary and immortalised macrophages.* J Cell Sci, 2008. **121**(24): p. 4124-4133.
76. Andjelkovic, M., et al., *Role of Translocation in the Activation and Function of Protein Kinase B.* Journal of Biological Chemistry, 1997. **272**(50): p. 31515-31524.
77. Stocker, H., et al., *Living with Lethal PIP3 Levels: Viability of Flies Lacking PTEN Restored by a PH Domain Mutation in Akt/PKB.* Science, 2002. **295**(5562): p. 2088-2091.
78. Alessi, D.R., et al., *3-Phosphoinositide-dependent protein kinase-1 (PDK1): structural and functional homology with the Drosophila DSTPK61 kinase.* Current Biology, 1997. **7**(10): p. 776-789.
79. Alessi, D.R., et al., *Characterization of a 3-phosphoinositide-dependent protein kinase which phosphorylates and activates protein kinase B[alpha].* Current Biology, 1997. **7**(4): p. 261-269.
80. Ding, Z., et al., *Physical Association of PDK1 with AKT1 Is Sufficient for Pathway Activation Independent of Membrane Localization and Phosphatidylinositol 3 Kinase.* PLoS One, 2010. **5**(3): p. e9910.
81. Sarbassov, D.D., et al., *Phosphorylation and Regulation of Akt/PKB by the Rictor-mTOR Complex.* Science, 2005. **307**(5712): p. 1098-1101.
82. Hart, J.R. and P.K. Vogt, *Phosphorylation of AKT: a Mutational Analysis*. 2011. Vol. 2. 2011.
83. Ma, K., et al., *PI(3,4,5)P3 and PI(3,4)P2 levels correlate with PKB/akt phosphorylation at Thr308 and Ser473, respectively; PI(3,4)P2 levels determine PKB activity.* Cellular Signalling, 2008. **20**(4): p. 684-694.
84. Sato, S., N. Fujita, and T. Tsuruo, *Modulation of Akt kinase activity by binding to Hsp90.* Proceedings of the National Academy of Sciences, 2000. **97**(20): p. 10832-10837.

85. Resjo, S., et al., *Protein phosphatase 2A is the main phosphatase involved in the regulation of protein kinase B in rat adipocytes.* Cell Signal, 2002. **14**(3): p. 231-8.
86. Wu, Y.-T., et al., *mTOR Complex 2 Targets Akt for Proteasomal Degradation via Phosphorylation at the Hydrophobic Motif.* Journal of Biological Chemistry, 2011. **286**(16): p. 14190-14198.
87. Alessi, D.R., et al., *Molecular basis for the substrate specificity of protein kinase B; comparison with MAPKAP kinase-1 and p70 S6 kinase.* FEBS Letters, 1996. **399**(3): p. 333-338.
88. Obata, T., et al., *Peptide and Protein Library Screening Defines Optimal Substrate Motifs for AKT/PKB.* Journal of Biological Chemistry, 2000. **275**(46): p. 36108-36115.
89. Datta, S.R., et al., *14-3-3 Proteins and Survival Kinases Cooperate to Inactivate BAD by BH3 Domain Phosphorylation.* Molecular Cell, 2000. **6**(1): p. 41-51.
90. Tran, H., et al., *The Many Forks in FOXO's Road.* Sci. STKE, 2003. **2003**(172): p. re5-.
91. Mayo, L.D. and D.B. Donner, *A phosphatidylinositol 3-kinase/Akt pathway promotes translocation of Mdm2 from the cytoplasm to the nucleus.* Proceedings of the National Academy of Sciences, 2001. **98**(20): p. 11598-11603.
92. Maurer, U., et al., *Glycogen Synthase Kinase-3 Regulates Mitochondrial Outer Membrane Permeabilization and Apoptosis by Destabilization of MCL-1.* Molecular Cell, 2006. **21**(6): p. 749-760.
93. Manning, B.D. and L.C. Cantley, *Rheb fills a GAP between TSC and TOR.* Trends in Biochemical Sciences, 2003. **28**(11): p. 573-576.
94. Sancak, Y., et al., *PRAS40 Is an Insulin-Regulated Inhibitor of the mTORC1 Protein Kinase.* Molecular Cell, 2007. **25**(6): p. 903-915.
95. Porstmann, T., et al., *A new player in the orchestra of cell growth: SREBP activity is regulated by mTORC1 and contributes to the regulation of cell and organ size.* Biochem Soc Trans, 2009. **37**(1): p. 278 - 283.
96. Liang, J., et al., *PKB/Akt phosphorylates p27, impairs nuclear import of p27 and opposes p27-mediated G1 arrest.* Nature Medicine, 2002. **8**(10): p. 1153 - 1160.
97. Medema, R.H., et al., *AFX-like Forkhead transcription factors mediate cell-cycle regulation by Ras and PKB through p27kip1.* Nature, 2000. **404**(6779): p. 782-787.
98. Garcia, Z., et al., *Phosphoinositide 3-kinase controls early and late events in mammalian cell division.* EMBO J, 2006. **25**(4): p. 655-661.
99. Kohn, A.D., et al., *Expression of a Constitutively Active Akt Ser/Thr Kinase in 3T3-L1 Adipocytes Stimulates Glucose Uptake and Glucose Transporter 4 Translocation.* Journal of Biological Chemistry, 1996. **271**(49): p. 31372-31378.
100. Sano, H., et al., *Insulin-stimulated Phosphorylation of a Rab GTPase-activating Protein Regulates GLUT4 Translocation.* Journal of Biological Chemistry, 2003. **278**(17): p. 14599-14602.
101. Elstrom, R.L., et al., *Akt Stimulates Aerobic Glycolysis in Cancer Cells.* Cancer Research, 2004. **64**(11): p. 3892-3899.
102. Zelzer, E., et al., *Insulin induces transcription of target genes through the hypoxia-inducible factor HIF-1alpha/ARNT.* EMBO J, 1998. **17**(17): p. 5085-5094.
103. Ericson, K., et al., *Genetic inactivation of AKT1, AKT2, and PDPK1 in human colorectal cancer cells clarifies their roles in tumor growth regulation.* Proceedings of the National Academy of Sciences, 2010. **107**(6): p. 2598-2603.
104. Dummler, B. and B.A. Hemmings, *Physiological roles of PKB/Akt isoforms in development and disease.* Biochemical Society Transactions, 2007. **035**(2): p. 231-235.
105. Katome, T., et al., *Use of RNA Interference-mediated Gene Silencing and Adenoviral Overexpression to Elucidate the Roles of AKT/Protein Kinase B Isoforms in Insulin Actions.* Journal of Biological Chemistry, 2003. **278**(30): p. 28312-28323.

106. Dillon, R.L., et al., *Akt1 and Akt2 Play Distinct Roles in the Initiation and Metastatic Phases of Mammary Tumor Progression.* Cancer Res, 2009. **69**(12): p. 5057-5064.
107. Chin, Y.R. and A. Toker, *The Actin-Bundling Protein Palladin Is an Akt1-Specific Substrate that Regulates Breast Cancer Cell Migration.* Molecular Cell, 2010. **38**(3): p. 333-344.
108. Brognard, J., et al., *PHLPP and a Second Isoform, PHLPP2, Differentially Attenuate the Amplitude of Akt Signaling by Regulating Distinct Akt Isoforms.* Molecular Cell, 2007. **25**(6): p. 917-931.
109. Bandyopadhyay, G.K., et al., *Increased p85/55/50 Expression and Decreased Phosphotidylinositol 3-Kinase Activity in Insulin-Resistant Human Skeletal Muscle.* Diabetes, 2005. **54**(8): p. 2351-2359.
110. Barroso, I.s., et al., *Candidate Gene Association Study in Type 2 Diabetes Indicates a Role for Genes Involved in beta-Cell Function as Well as Insulin Action.* PLoS Biol, 2003. **1**(1): p. e20.
111. Engelman, J.A., J. Luo, and L.C. Cantley, *The evolution of phosphatidylinositol 3-kinases as regulators of growth and metabolism.* Nat Rev Genet, 2006. **7**(8): p. 606-619.
112. Thong, F.S.L., C.B. Dugani, and A. Klip, *Turning Signals On and Off: GLUT4 Traffic in the Insulin-Signaling Highway.* Physiology, 2005. **20**(4): p. 271-284.
113. Yuan, T.L. and L.C. Cantley, *PI3K pathway alterations in cancer: variations on a theme.* Oncogene, 2008. **27**(41): p. 5497-5510.
114. Wee, S., et al., *PTEN-deficient cancers depend on PIK3CB.* Proc Natl Acad Sci U S A, 2008. **105**(35): p. 13057-62.
115. Edgar, K.A., et al., *Isoform-Specific Phosphoinositide 3-Kinase Inhibitors Exert Distinct Effects in Solid Tumors.* Cancer Res, 2010. **70**(3): p. 1164-1172.
116. Jiang, X., et al., *Phosphoinositide 3-Kinase Pathway Activation in Phosphate and Tensin Homolog (PTEN)-deficient Prostate Cancer Cells Is Independent of Receptor Tyrosine Kinases and Mediated by the p110α and p110β Catalytic Subunits.* Journal of Biological Chemistry, 2010. **285**(20): p. 14980-14989.
117. Samuels, Y., et al., *High Frequency of Mutations of the PIK3CA Gene in Human Cancers.* Science, 2004. **304**(5670): p. 554.
118. Campbell, I.G., et al., *Mutation of the PIK3CA Gene in Ovarian and Breast Cancer.* Cancer Research, 2004. **64**(21): p. 7678-7681.
119. Samuels, Y., et al., *Mutant PIK3CA promotes cell growth and invasion of human cancer cells.* Cancer Cell, 2005. **7**(6): p. 561-73.
120. Zhang, H., et al., *Comprehensive analysis of oncogenic effects of PIK3CA mutations in human mammary epithelial cells.* Breast Cancer Research and Treatment, 2008. **112**(2): p. 217-227.
121. Zhao, L. and P.K. Vogt, *Class I PI3K in oncogenic cellular transformation.* Oncogene, 2008. **27**(41): p. 5486-5496.
122. Gabelli, S.B., et al., *Somatic mutations in PI3Kalpha: Structural basis for enzyme activation and drug design.* Biochimica et Biophysica Acta (BBA) - Proteins & Proteomics, 2010. **1804**(3): p. 533-540.
123. Dbouk, H.A., et al., *A biochemical mechanism for the oncogenic potential of the p110b catalytic subunit of phosphoinositide 3-kinase.* Proceedings of the National Academy of Sciences, 2010. **107**(46): p. 19897-19902.
124. Vasudevan, K.M., et al., *AKT-Independent Signaling Downstream of Oncogenic PIK3CA Mutations in Human Cancer.* Cancer Cell, 2009. **16**(1): p. 21-32.
125. Edling, C.E., et al., *Key Role of Phosphoinositide 3-Kinase Class IB in Pancreatic Cancer.* Clinical Cancer Research, 2010. **16**(20): p. 4928-4937.
126. Philp, A.J., et al., *The Phosphatidylinositol 3'-kinase p85alpha Gene Is an Oncogene in Human Ovarian and Colon Tumors.* Cancer Research, 2001. **61**(20): p. 7426-7429.
127. Jaiswal, B.S., et al., *Somatic Mutations in p85alpha Promote Tumorigenesis through Class IA PI3K Activation.* Cancer Cell, 2009. **16**(6): p. 463-474.

128. Bleeker, F.E., et al., *AKT1E17K in human solid tumours.* Oncogene, 2008. **27**(42): p. 5648-5650.
129. She, Q.-B., et al., *4E-BP1 Is a Key Effector of the Oncogenic Activation of the AKT and ERK Signaling Pathways that Integrates Their Function in Tumors.* Cancer Cell, 2010. **18**(1): p. 39-51.
130. Oda, K., et al., *PIK3CA Cooperates with Other Phosphatidylinositol 3'-Kinase Pathway Mutations to Effect Oncogenic Transformation.* Cancer Research, 2008. **68**(19): p. 8127-8136.
131. O'Brien, C., et al., *Predictive Biomarkers of Sensitivity to the Phosphatidylinositol 3 Kinase Inhibitor GDC-0941 in Breast Cancer Preclinical Models.* Clinical Cancer Research, 2010. **16**(14): p. 3670-3683.
132. Morrow, C.J., A. Gray, and C. Dive, *Comparison of phosphatidylinositol-3-kinase signalling within a panel of human colorectal cancer cell lines with mutant or wild-type PIK3CA.* FEBS Letters, 2005. **579**(23): p. 5123-5128.
133. Engelman, J.A., et al., *Effective use of PI3K and MEK inhibitors to treat mutant Kras G12D and PIK3CA H1047R murine lung cancers.* Nat Med, 2008. **14**(12): p. 1351-1356.
134. McDonald, G.T., et al., *Inhibition of phosphatidylinositol 3-kinase promotes tumor cell resistance to chemotherapeutic agents via a mechanism involving delay in cell cycle progression.* Experimental Cell Research, 2010. **316**(19): p. 3197-3206.
135. Flinn, I., et al., *Evidence of clinical activity in a phase I study of CAL-101, an oral p110d isoform-selective inhibitor of phosphatidylinositol 3-kinase, in patients with relapsed or refractory B-Cell malignancies.* ASH Abstract, 2009.
136. van der Heijden, M.S. and R. Bernards, *Inhibition of the PI3K Pathway: Hope We Can Believe in?* Clinical Cancer Research, 2010. **16**(12): p. 3094-3099.
137. Chandarlapaty, S., et al., *AKT Inhibition Relieves Feedback Suppression of Receptor Tyrosine Kinase Expression and Activity.* Cancer Cell, 2011. **19**(1): p. 58-71.
138. Okuzumi, T., et al., *Inhibitor hijacking of Akt activation.* Nat Chem Biol, 2009. **5**(7): p. 484-493.
139. Andersen, J.N., et al., *Pathway-Based Identification of Biomarkers for Targeted Therapeutics: Personalized Oncology with PI3K Pathway Inhibitors.* Science Translational Medicine, 2010. **2**(43): p. 43ra55.
140. Wysocki, V.H., et al., *Mass spectrometry of peptides and proteins.* Methods, 2005. **35**(3): p. 211-222.
141. Cañas, B., et al., *Trends in sample preparation for classical and second generation proteomics.* Journal of Chromatography A, 2007. **1153**(1-2): p. 235-258.
142. Wisniewski, J.R., et al., *Universal sample preparation method for proteome analysis.* Nature Methods, 2009. **6**(5): p. 359-362.
143. Kellie, J.F., et al., *The emerging process of Top Down mass spectrometry for protein analysis: biomarkers, protein-therapeutics, and achieving high throughput.* Molecular BioSystems, 2010. **6**(9): p. 1532-1539.
144. Liu, J. and L. Konermann, *Protein-Protein Binding Affinities in Solution Determined by Electrospray Mass Spectrometry.* Journal of the American Society for Mass Spectrometry, 2011. **22**(3): p. 408-417.
145. Fenn, J.B., et al., *Electrospray ionization for mass spectrometry of large biomolecules.* Science, 1989. **246**(4926): p. 64-71.
146. Karas, M. and F. Hillenkamp, *Laser desorption ionization of proteins with molecular masses exceeding 10,000 daltons.* Analytical Chemistry, 1988. **60**(20): p. 2299-2301.
147. Ong, S.-E. and M. Mann, *Mass spectrometry-based proteomics turns quantitative.* Nat Chem Biol, 2005. **1**(5): p. 252-262.

148. Manning, B.D., et al., *Identification of the Tuberous Sclerosis Complex-2 Tumor Suppressor Gene Product Tuberin as a Target of the Phosphoinositide 3-Kinase/Akt Pathway.* Molecular Cell, 2002. **10**(1): p. 151-162.
149. McDonald, P.C., et al., *Rictor and Integrin-Linked Kinase Interact and Regulate Akt Phosphorylation and Cancer Cell Survival.* Cancer Res, 2008. **68**(6): p. 1618-1624.
150. Hunt, D.F., et al., *Protein sequencing by tandem mass spectrometry.* Proceedings of the National Academy of Sciences, 1986. **83**(17): p. 6233-6237.
151. Paizs, B. and S. Suhai, *Fragmentation pathways of protonated peptides.* Mass Spectrometry Reviews, 2005. **24**(4): p. 508-548.
152. Boersema, P.J., S. Mohammed, and A.J.R. Heck, *Phosphopeptide fragmentation and analysis by mass spectrometry.* Journal of Mass Spectrometry, 2009. **44**(6): p. 861-878.
153. Nagaraj, N., et al., *Feasibility of Large-Scale Phosphoproteomics with Higher Energy Collisional Dissociation Fragmentation.* Journal of Proteome Research, 2010. **9**(12): p. 6786-6794.
154. Roepstorff, P. and J. Fohlman, *Proposal for a common nomenclature for sequence ions in mass spectra of peptides.* Biomed Mass Spectrom. 1984 Nov;11(11):601., 1984. **11**: p. 601.
155. Meyer-Arendt, K., et al., *IsoformResolver: A Peptide-Centric Algorithm for Protein Inference.* Journal of Proteome Research, 2011. **10**(7): p. 3060-3075.
156. Perkins, D.N., et al., *Probability-based protein identification by searching sequence databases using mass spectrometry data.* Electrophoresis, 1999. **20**(18): p. 3551-3567.
157. Michalski, A., J. Cox, and M. Mann, *More than 100,000 Detectable Peptide Species Elute in Single Shotgun Proteomics Runs but the Majority is Inaccessible to Data-Dependent LCâˆ'MS/MS.* Journal of Proteome Research, 2011. **10**(4): p. 1785-1793.
158. Alcolea, M.P., O. Kleiner, and P.R. Cutillas, *Increased Confidence in Large-Scale Phosphoproteomics Data by Complementary Mass Spectrometric Techniques and Matching of Phosphopeptide Data Sets.* Journal of Proteome Research, 2009. **8**(8): p. 3808-3815.
159. Cutillas, P.R. and B. Vanhaesebroeck, *Quantitative Profile of Five Murine Core Proteomes Using Label-free Functional Proteomics.* Molecular & Cellular Proteomics, 2007. **6**(9): p. 1560-1573.
160. Rikova, K., et al., *Global Survey of Phosphotyrosine Signaling Identifies Oncogenic Kinases in Lung Cancer.* Cell, 2007. **131**(6): p. 1190-1203.
161. Forner, F., et al., *Proteome Differences between Brown and White Fat Mitochondria Reveal Specialized Metabolic Functions.* Cell Metabolism, 2009. **10**(4): p. 324-335.
162. Gygi, S.P., et al., *Quantitative analysis of complex protein mixtures using isotope-coded affinity tags.* Nat Biotech, 1999. **17**(10): p. 994-999.
163. Ross, P.L., et al., *Multiplexed Protein Quantitation in Saccharomyces cerevisiae Using Amine-reactive Isobaric Tagging Reagents.* Molecular & Cellular Proteomics, 2004. **3**(12): p. 1154-1169.
164. Ow, S.Y., et al., *iTRAQ Underestimation in Simple and Complex Mixtures: "The Good, the Bad and the Ugly".* Journal of Proteome Research, 2009. **8**(11): p. 5347-5355.
165. Thingholm, T.E., et al., *Undesirable Charge-Enhancement of Isobaric Tagged Phosphopeptides Leads to Reduced Identification Efficiency.* Journal of Proteome Research, 2010. **9**(8): p. 4045-4052.
166. Ong, S.-E., et al., *Stable Isotope Labeling by Amino Acids in Cell Culture, SILAC, as a Simple and Accurate Approach to Expression Proteomics.* Mol Cell Proteomics, 2002. **1**(5): p. 376-386.
167. Kruger, M., et al., *SILAC Mouse for Quantitative Proteomics Uncovers Kindlin-3 as an Essential Factor for Red Blood Cell Function.* Cell, 2008. **134**(2): p. 353-364.
168. Geiger, T., et al., *Use of stable isotope labeling by amino acids in cell culture as a spike-in standard in quantitative proteomics.* Nat. Protocols, 2011. **6**(2): p. 147-157.

169. Monetti, M., et al., *Large-scale phosphosite quantification in tissues by a spike-in SILAC method.* Nat Meth, 2011. **8**(8): p. 655-658.
170. Geiger, T., et al., *Super-SILAC mix for quantitative proteomics of human tumor tissue.* Nature Methods 2010. **7**: p. 383 - 385.
171. Zhu, W., J.W. Smith, and C.-M. Huang, *Mass Spectrometry-Based Label-Free Quantitative Proteomics.* Journal of Biomedicine and Biotechnology, 2010. **2010**.
172. Lu, P., et al., *Absolute protein expression profiling estimates the relative contributions of transcriptional and translational regulation.* Nat Biotech, 2007. **25**(1): p. 117-124.
173. Lange, V., et al., *Targeted Quantitative Analysis of Streptococcus pyogenes Virulence Factors by Multiple Reaction Monitoring.* Mol Cell Proteomics, 2008. **7**(8): p. 1489-1500.
174. Lengqvist, J., et al., *Robustness and accuracy of high speed LC-MS separations for global peptide quantitation and biomarker discovery.* Journal of Chromatography B, 2009. **877**(13): p. 1306-1316.
175. Old, W.M., et al., *Comparison of Label-free Methods for Quantifying Human Proteins by Shotgun Proteomics.* Mol Cell Proteomics, 2005. **4**(10): p. 1487-1502.
176. Yang, F., et al., *Applying a Targeted Label-Free Approach Using LC-MS AMT Tags to Evaluate Changes in Protein Phosphorylation Following Phosphatase Inhibition.* Journal of Proteome Research, 2007. **6**(11): p. 4489-4497.
177. Wang, Y.-T., et al., *An Informatics-assisted Label-free Quantitation Strategy that Depicts Phosphoproteomic Profiles in Lung Cancer Cell Invasion.* Journal of Proteome Research, 2010. **9**(11): p. 5582-5597.
178. Han, C.-L., et al., *An Informatics-assisted Label-free Approach for Personalized Tissue Membrane Proteomics: Case Study on Colorectal Cancer.* Molecular & Cellular Proteomics, 2011. **10**(4).
179. Casado, P. and P.R. Cutillas, *A Self-validating Quantitative Mass Spectrometry Method for Assessing the Accuracy of High-content Phosphoproteomic Experiments.* Mol Cell Proteomics, 2011. **10**(1).
180. Silva, J.C., et al., *Absolute Quantification of Proteins by LCMSE.* Molecular & Cellular Proteomics, 2006. **5**(1): p. 144-156.
181. Grossmann, J., et al., *Implementation and evaluation of relative and absolute quantification in shotgun proteomics with label-free methods.* Journal of Proteomics, 2010. **73**(9): p. 1740-1746.
182. Malmstrom, J., et al., *Proteome-wide cellular protein concentrations of the human pathogen Leptospira interrogans.* Nature, 2009. **460**(7256): p. 762-765.
183. Pratt, J.M., et al., *Multiplexed absolute quantification for proteomics using concatenated signature peptides encoded by QconCAT genes.* Nat. Protocols, 2006. **1**(2): p. 1029-1043.
184. Brownridge, P., et al., *Global absolute quantification of a proteome: Challenges in the deployment of a QconCAT strategy.* Proteomics, 2011. **11**(15): p. 2957-2970.
185. Schwanhausser, B., et al., *Global quantification of mammalian gene expression control.* Nature, 2011. **473**(7347): p. 337-342.
186. Fields, S. and O.-k. Song, *A novel genetic system to detect protein–protein interactions.* Nature, 1989. **340**(6230): p. 245-246.
187. Figeys, D., *Mapping the human protein interactome.* Cell Res, 2008. **18**(7): p. 716-724.
188. Venkatesan, K., et al., *An empirical framework for binary interactome mapping.* Nat Meth, 2009. **6**(1): p. 83-90.
189. Rual, J.-F., et al., *Towards a proteome-scale map of the human protein-protein interaction network.* Nature, 2005. **437**(7062): p. 1173-1178.
190. Vidal, M., Michael E. Cusick, and A.-L. Barabasi, *Interactome Networks and Human Disease.* Cell, 2011. **144**(6): p. 986-998.

191. Gavin, A.C., et al., *Proteome survey reveals modularity of the yeast cell machinery.* Nature, 2006. **440**(7084): p. 631-6.
192. Guerrero, C., et al., *An Integrated Mass Spectrometry-based Proteomic Approach: Quantitative Analysis of Tandem Affinity-purified in vivo Cross-linked Protein Complexes (qtax) to Decipher the 26 s Proteasome-interacting Network.* Mol Cell Proteomics, 2006. **5**(2): p. 366-378.
193. Trinkle-Mulcahy, L., et al., *Identifying specific protein interaction partners using quantitative mass spectrometry and bead proteomes.* J. Cell Biol., 2008. **183**(2): p. 223-239.
194. Musso, G.A., Z. Zhang, and A. Emili, *Experimental and Computational Procedures for the Assessment of Protein Complexes on a Genome-wide Scale.* Chemical Reviews, 2007. **107**(8): p. 3585-3600.
195. Beitz, E., et al., *Determinants of AQP6 trafficking to intracellular sites versus the plasma membrane in transfected mammalian cells.* Biol. Cell, 2006. **98**(2): p. 101-109.
196. Puig, O., et al., *The Tandem Affinity Purification (TAP) Method: A General Procedure of Protein Complex Purification.* Methods, 2001. **24**(3): p. 218-229.
197. Rees, J.S., et al., *In Vivo Analysis of Proteomes and Interactomes Using Parallel Affinity Capture (iPAC) Coupled to Mass Spectrometry.* Molecular & Cellular Proteomics, 2011. **10**(6).
198. Blagoev, B., et al., *A proteomics strategy to elucidate functional protein-protein interactions applied to EGF signaling.* Nat Biotech, 2003. **21**(3): p. 315-318.
199. Seebacher, J. and A.-C. Gavin, *SnapShot: Protein-Protein Interaction Networks.* Cell, 2011. **144**(6): p. 1000-1000.e1.
200. Cohen, P., *The role of protein phosphorylation in human health and disease.* European Journal of Biochemistry, 2001. **268**(19): p. 5001-5010.
201. Manning, G., et al., *The Protein Kinase Complement of the Human Genome.* Science, 2002. **298**(5600): p. 1912-1934.
202. Ubersax, J.A. and J.E. Ferrell Jr, *Mechanisms of specificity in protein phosphorylation.* Nature Reviews Molecular Cell Biology, 2007. **8**(7): p. 530-541.
203. Olsen, J.V., et al., *Global, In Vivo, and Site-Specific Phosphorylation Dynamics in Signaling Networks.* Cell, 2006. **127**(3): p. 635-648.
204. Cutillas, P.R. and J.F. Timms, *Approaches and Applications of Quantitative LC-MS for Proteomics and Activitomics* Methods in Molecular Biology, 2010. **658**(1): p. 3 - 17.
205. Cutillas, P.R. and C. Jorgensen, *Biological signalling activity measurements using mass spectrometry.* Biochemical Journal, 2011. **434**(2): p. 189-199.
206. Barford, D., A.K. Das, and M.-P. Egloff, *The Structure and Mechanism of Protein Phosphatases: Insights into Catalysis and Regulation.* Annual Review of Biophysics and Biomolecular Structure, 1998. **27**(1): p. 133-164.
207. Thingholm, T.E., et al., *TiO2-Based Phosphoproteomic Analysis of the Plasma Membrane and the Effects of Phosphatase Inhibitor Treatment.* Journal of Proteome Research, 2008. **7**(8): p. 3304-3313.
208. Reinders, J. and A. Sickmann, *State-of-the-art in phosphoproteomics.* Proteomics, 2005. **5**(16): p. 4052-4061.
209. Molina, H., et al., *Global proteomic profiling of phosphopeptides using electron transfer dissociation tandem mass spectrometry.* Proceedings of the National Academy of Sciences, 2007. **104**(7): p. 2199-2204.
210. Miliotis, T., et al., *Analysis of regulatory phosphorylation sites in ZAP-70 by capillary high-performance liquid chromatography coupled to electrospray ionization or matrix-assisted laser desorption ionization time-of-flight mass spectrometry.* Journal of Chromatography B: Biomedical Sciences and Applications, 2001. **752**(2): p. 323-334.

211. Gaberc-Porekar, V. and V. Menart, *Perspectives of immobilized-metal affinity chromatography.* Journal of Biochemical and Biophysical Methods, 2001. **49**(1-3): p. 335-360.
212. Muszynska, G., et al., *Model studies on iron(III) ion affinity chromatography: II. Interaction of immobilized iron(III) ions with phosphorylated amino acids, peptides and proteins.* Journal of Chromatography A, 1992. **604**(1): p. 19-28.
213. Li, S. and C. Dass, *Iron(III)-Immobilized Metal Ion Affinity Chromatography and Mass Spectrometry for the Purification and Characterization of Synthetic Phosphopeptides.* Analytical Biochemistry, 1999. **270**(1): p. 9-14.
214. Neville, D.C.A., et al., *Evidence for phosphorylation of serine 753 in CFTR using a novel metal-ion affinity resin and matrix-assisted laser desorption mass spectrometry.* Protein Science, 1997. **6**(11): p. 2436-2445.
215. Anguenot, R., S. Yelle, and B. Nguyen-Quoc, *Purification of Tomato Sucrose Synthase Phosphorylated Isoforms by Fe(III)-Immobilized Metal Affinity Chromatography.* Archives of Biochemistry and Biophysics, 1999. **365**(1): p. 163-169.
216. Posewitz, M.C. and P. Tempst, *Immobilized Gallium(III) Affinity Chromatography of Phosphopeptides.* Analytical Chemistry, 1999. **71**(14): p. 2883-2892.
217. Stensballe, A., S. Andersen, and O.N. Jensen, *Characterization of phosphoproteins from electrophoretic gels by nanoscale Fe(III) affinity chromatography with off-line mass spectrometry analysis.* Proteomics, 2001. **1**(2): p. 207-222.
218. Hart, S.R., et al., *Factors governing the solubilization of phosphopeptides retained on ferric NTA IMAC beads and their analysis by MALDI TOFMS.* Journal of the American Society for Mass Spectrometry, 2002. **13**(9): p. 1042-1051.
219. Ficarro, S.B., et al., *Phosphoproteome analysis by mass spectrometry and its application to Saccharomyces cerevisiae.* Nature Biotechnology, 2002. **20**(3): p. 301-305.
220. Ye, J., et al., *Optimized IMAC-IMAC Protocol for Phosphopeptide Recovery from Complex Biological Samples.* Journal of Proteome Research, 2010. **9**(7): p. 3561-3573.
221. Tsai, C.-F., et al., *Immobilized Metal Affinity Chromatography Revisited: pH/Acid Control toward High Selectivity in Phosphoproteomics.* Journal of Proteome Research, 2008. **7**(9): p. 4058-4069.
222. Thingholm, T.E., et al., *SIMAC (Sequential Elution from IMAC), a Phosphoproteomics Strategy for the Rapid Separation of Monophosphorylated from Multiply Phosphorylated Peptides.* Molecular & Cellular Proteomics, 2008. **7**(4): p. 661-671.
223. Aryal, U.K. and A.R.S. Ross, *Enrichment and analysis of phosphopeptides under different experimental conditions using titanium dioxide affinity chromatography and mass spectrometry.* Rapid Communications in Mass Spectrometry, 2009. **24**(2): p. 219-231.
224. Pinkse, M.W.H., et al., *Selective Isolation at the Femtomole Level of Phosphopeptides from Proteolytic Digests Using 2D-NanoLC-ESI-MS/MS and Titanium Oxide Precolumns.* Analytical Chemistry, 2004. **76**(14): p. 3935-3943.
225. Choudhary, C., et al., *Mislocalized Activation of Oncogenic RTKs Switches Downstream Signaling Outcomes.* Molecular Cell, 2009. **36**(2): p. 326-339.
226. Wu, J., et al., *Integrating titania enrichment, iTRAQ labeling, and Orbitrap CID-HCD for global identification and quantitative analysis of phosphopeptides.* Proteomics, 2010. **10**(11): p. 2224-2234.
227. Gates, M.B., K.B. Tomer, and L.J. Deterding, *Comparison of Metal and Metal Oxide Media for Phosphopeptide Enrichment Prior to Mass Spectrometric Analyses.* Journal of the American Society for Mass Spectrometry, 2010. **21**(10): p. 1649-1659.
228. Larsen, M.R., et al., *Highly Selective Enrichment of Phosphorylated Peptides from Peptide Mixtures Using Titanium Dioxide Microcolumns.* Molecular & Cellular Proteomics, 2005. **4**(7): p. 873-886.

229. Thingholm, T.E. and M.R. Larsen, *The Use of Titanium Dioxide Micro-Columns to Selectively Isolate Phosphopeptides from Proteolytic Digests*, in *Phospho-Proteomics*, J.M. Walker, Editor. 2009, Humana Press. p. 57-66.
230. Eriksson, A., et al., *Optimized Protocol for On-Target Phosphopeptide Enrichment Prior to Matrix-Assisted Laser Desorption-Ionization Mass Spectrometry Using Mesoporous Titanium Dioxide.* Analytical Chemistry, 2010. **82**(11): p. 4577-4583.
231. Zarei, M., et al., *Comparison of ERLIC-TiO2, HILIC-TiO2, and SCX-TiO2 for Global Phosphoproteomics Approaches.* Journal of Proteome Research, 2011. **10**(8): p. 3474-3483.
232. Montoya, A., et al., *Characterization of a TiO2 enrichment method for label-free quantitative phosphoproteomics.* Methods, 2011. 54(4): p. 370-378.
233. Gronborg, M., et al., *A Mass Spectrometry-based Proteomic Approach for Identification of Serine/Threonine-phosphorylated Proteins by Enrichment with Phospho-specific Antibodies.* Molecular & Cellular Proteomics, 2002. **1**(7): p. 517-527.
234. Zhang, G. and T.A. Neubert, *Use of detergents to increase selectivity of immunoprecipitation of tyrosine phosphorylated peptides prior to identification by MALDI quadrupole-TOF MS.* Proteomics, 2006. **6**(2): p. 571-578.
235. Pandey, A., et al., *Analysis of receptor signaling pathways by mass spectrometry: Identification of Vav-2 as a substrate of the epidermal and platelet-derived growth factor receptors.* Proceedings of the National Academy of Sciences of the United States of America, 2000. **97**(1): p. 179-184.
236. Blagoev, B., et al., *Temporal analysis of phosphotyrosine-dependent signaling networks by quantitative proteomics.* Nature Biotechnology, 2004. **22**(9): p. 1139-1145.
237. Cutillas, P.R., et al., *Quantification of Gel-separated Proteins and Their Phosphorylation Sites by LC-MS Using Unlabeled Internal Standards: Analysis of Phosphoprotein Dynamics in a B Cell Lymphoma Cell Line.* Molecular & Cellular Proteomics, 2005. **4**(8): p. 1038-1051.
238. Rush, J., et al., *Immunoaffinity profiling of tyrosine phosphorylation in cancer cells.* Nature Biotechnology, 2005. **23**(1): p. 94-101.
239. Adamczyk, M., J.C. Gebler, and J. Wu, *Selective analysis of phosphopeptides within a protein mixture by chemical modification, reversible biotinylation and mass spectrometry.* Rapid Communications in Mass Spectrometry, 2001. **15**(16): p. 1481-1488.
240. Weckwerth, W., L. Willmitzer, and O. Fiehn, *Comparative quantification and identification of phosphoproteins using stable isotope labeling and liquid chromatography/mass spectrometry.* Rapid Communications in Mass Spectrometry, 2000. **14**(18): p. 1677-1681.
241. Beausoleil, S.A., et al., *Large-scale characterization of HeLa cell nuclear phosphoproteins.* Proceedings of the National Academy of Sciences of the United States of America, 2004. **101**(33): p. 12130-12135.
242. Dai, J., et al., *Protein Phosphorylation and Expression Profiling by Yin-Yang Multidimensional Liquid Chromatography (Yin-Yang MDLC) Mass Spectrometry.* Journal of Proteome Research, 2006. **6**(1): p. 250-262.
243. Nie, S., et al., *Comprehensive Profiling of Phosphopeptides Based on Anion Exchange Followed by Flow-Through Enrichment with Titanium Dioxide (AFET).* Journal of Proteome Research, 2010. **9**(9): p. 4585-4594.
244. Han, G., et al., *Large-scale phosphoproteome analysis of human liver tissue by enrichment and fractionation of phosphopeptides with strong anion exchange chromatography.* Proteomics, 2008. **8**(7): p. 1346-1361.
245. McNulty, D.E. and R.S. Annan, *Hydrophilic Interaction Chromatography Reduces the Complexity of the Phosphoproteome and Improves Global Phosphopeptide Isolation and Detection.* Molecular & Cellular Proteomics, 2008. **7**(5): p. 971-980.
246. Gruhler, A., et al., *Quantitative Phosphoproteomics Applied to the Yeast Pheromone Signaling Pathway.* Molecular & Cellular Proteomics, 2005. **4**(3): p. 310-327.

247. Lim, K.B. and D.B. Kassel, *Phosphopeptides enrichment using on-line two-dimensional strong cation exchange followed by reversed-phase liquid chromatography/mass spectrometry.* Analytical Biochemistry, 2006. **354**(2): p. 213-219.
248. Gilar, M., et al., *Orthogonality of Separation in Two-Dimensional Liquid Chromatography.* Analytical Chemistry, 2005. **77**(19): p. 6426-6434.
249. Motoyama, A., et al., *Anion and Cation Mixed-Bed Ion Exchange for Enhanced Multidimensional Separations of Peptides and Phosphopeptides.* Analytical Chemistry, 2007. **79**(10): p. 3623-3634.
250. Alcolea, M.P. and P.R. Cutillas, *In-Depth Analysis of Protein Phosphorylation by Multidimensional Ion Exchange Chromatography and Mass Spectrometry* Methods in Molecular Biology, 2010. **658**: p. 111-126.
251. Salomon, A.R., et al., *Profiling of tyrosine phosphorylation pathways in human cells using mass spectrometry.* Proceedings of the National Academy of Sciences of the United States of America, 2003. **100**(2): p. 443-448.
252. Ahn, Y.H., et al., *Dynamic identification of phosphopeptides using immobilized metal ion affinity chromatography enrichment, subsequent partial β-elimination/chemical tagging and matrix-assisted laser desorption/ionization mass spectrometric analysis.* Rapid Communications in Mass Spectrometry, 2004. **18**(20): p. 2495-2501.
253. Steen, H., B. Küster, and M. Mann, *Quadrupole time-of-flight versus triple-quadrupole mass spectrometry for the determination of phosphopeptides by precursor ion scanning.* Journal of Mass Spectrometry, 2001. **36**(7): p. 782-790.
254. Schroeder, M.J., et al., *A Neutral Loss Activation Method for Improved Phosphopeptide Sequence Analysis by Quadrupole Ion Trap Mass Spectrometry.* Analytical Chemistry, 2004. **76**(13): p. 3590-3598.
255. Chi, A., et al., *Analysis of phosphorylation sites on proteins from Saccharomyces cerevisiae by electron transfer dissociation (ETD) mass spectrometry.* Proceedings of the National Academy of Sciences, 2007. **104**(7): p. 2193-2198.
256. Liao, P.C., et al., *An Approach to Locate Phosphorylation Sites in a Phosphoprotein: Mass Mapping by Combining Specific Enzymatic Degradation with Matrix-Assisted Laser Desorption/Ionization Mass Spectrometry.* Analytical Biochemistry, 1994. **219**(1): p. 9-20.
257. Gehrig, P.M., et al., *Phosphorylated serine and threonine residues promote site-specific fragmentation of singly charged, arginine-containing peptide ions.* Rapid Communications in Mass Spectrometry, 2009. **23**(10): p. 1435-1445.
258. Palumbo, A.M. and G.E. Reid, *Evaluation of Gas-Phase Rearrangement and Competing Fragmentation Reactions on Protein Phosphorylation Site Assignment Using Collision Induced Dissociation-MS/MS and MS3.* Analytical Chemistry, 2008. **80**(24): p. 9735-9747.
259. Beausoleil, S.A., et al., *A probability-based approach for high-throughput protein phosphorylation analysis and site localization.* Nat Biotech, 2006. **24**(10): p. 1285-1292.
260. Savitski, M.M., et al., *Confident Phosphorylation Site Localization Using the Mascot Delta Score.* Molecular & Cellular Proteomics, 2011. **10**(2).
261. Gao, J., et al., *Musite, a Tool for Global Prediction of General and Kinase-specific Phosphorylation Sites.* Molecular & Cellular Proteomics, 2010. **9**(12): p. 2586-2600.
262. Siepen, J.A., et al., *Prediction of missed cleavage sites in tryptic peptides aids protein identification in proteomics.* Journal of Proteome Research, 2007. **6**(1): p. 399-408.
263. Jones, S. and J.M. Thornton, *Principles of protein-protein interactions.* Proc Natl Acad Sci, 1996. **93**(1): p. 13-20.
264. Uetz, P., et al., *A comprehensive analysis of protein-protein interactions in Saccharomyces cerevisiae.* Nature, 2000. **403**(6770): p. 623-627.
265. von Kriegsheim, A., et al., *Cell fate decisions are specified by the dynamic ERK interactome.* Nat Cell Biol, 2009. **11**(12): p. 1458-1464.

266. Brazil, D.P., J. Park, and B.A. Hemmings, *PKB Binding Proteins: Getting in on the Akt.* Cell, 2002. **111**(3): p. 293-303.
267. Kim, D.-H., et al., *mTOR Interacts with Raptor to Form a Nutrient-Sensitive Complex that Signals to the Cell Growth Machinery.* Cell, 2002. **110**(2): p. 163-175.
268. Sarbassov, D.D., et al., *Rictor, a Novel Binding Partner of mTOR, Defines a Rapamycin-Insensitive and Raptor-Independent Pathway that Regulates the Cytoskeleton.* Current Biology, 2004. **14**(14): p. 1296-1302.
269. Chaussade, C., et al., *Evidence for functional redundancy of class IA PI3K isoforms in insulin signalling.* Biochem J, 2007. **404**(3): p. 449-458.
270. Cutillas, P.R., et al., *Ultrasensitive and absolute quantification of the phosphoinositide 3-kinase/Akt signal transduction pathway by mass spectrometry.* PNAS, 2006. **103**(24): p. 8959-8964.
271. Alcolea, M.P. and P.R. Cutillas, *Quantification of Protein Kinase Activities by LC-MS.* Methods in Molecular Biology, 2010. **658**(6): p. 325-337.
272. Knebel, A., N. Morrice, and P. Cohen, *A novel method to identify protein kinase substrates: eEF2 kinase is phosphorylated and inhibited by SAPK4/p38[delta].* EMBO J, 2001. **20**(16): p. 4360-4369.
273. Cartlidge, R.A., et al., *The tRNA methylase METTL1 is phosphorylated and inactivated by PKB and RSK in vitro and in cells.* EMBO J, 2005. **24**(9): p. 1696-1705.
274. Lu, X. and H. Zhu, *Tube-Gel Digestion: A Novel Proteomic Approach for High Throughput Analysis of Membrane Proteins.* Mol Cell Proteomics, 2005. **4**(12): p. 1948-1958.
275. Morris, H.R., et al., *A novel geometry mass spectrometer, the Q-TOF, for low-femtomole/attomole-range biopolymer sequencing.* J Protein Chem, 1997. **16**(5): p. 469-79.
276. Schwartz, J.C., M.W. Senko, and J.E.P. Syka, *A two-dimensional quadrupole ion trap mass spectrometer.* Journal of the American Society for Mass Spectrometry, 2002. **13**(6): p. 659-669.
277. Makarov, A., *Electrostatic axially harmonic orbital trapping: a high-performance technique of mass analysis.* Anal Chem, 2000. **72**(6): p. 1156-62.
278. Myers, M.P., et al., *The lipid phosphatase activity of PTEN is critical for its tumor supressor function.* Proc Natl Acad Sci, 1998. **95**(23): p. 13513-13518.
279. Kodaki, T., et al., *The activation of phosphatidylinositol 3-kinase by Ras.* Curr Biol, 1994. **4**(9): p. 798-806.
280. Gupta, N., et al., *The SH2 Domain-containing Inositol 5'-phosphatase (SHIP) Recruits the p85 Subunit of Phosphoinositide 3-Kinase during FcgammaRIIb1Inhibition of B Cell Receptor Signaling.* Journal of Biological Chemistry, 1999. **274**(11): p. 7489-7494.
281. Perez, O.D., et al., *Activation of the PKB/AKT Pathway by ICAM-2.* Immunity, 2002. **16**(1): p. 51-65.
282. Vogel, L.B. and D.J. Fujita, *The SH3 domain of p56lck is involved in binding to phosphatidylinositol 3'-kinase from T lymphocytes.* Mol Cell Biol, 1993. **13**(12): p. 7408-7417.
283. Rabinovsky, R., et al., *p85 Associates with Unphosphorylated PTEN and the PTEN-Associated Complex.* Mol Cell Biol, 2009. **29**(19): p. 5377-5388.
284. Dengjel, J., I. Kratchmarova, and B. Blagoev, *Mapping protein-protein interactions by quantitative proteomics.* Methods Mol Biol, 2010. **658**: p. 267-78.
285. Franco, S.J. and A. Huttenlocher, *Regulating cell migration: calpains make the cut.* J Cell Sci, 2005. **118**(17): p. 3829-3838.
286. Bertoli, C., et al., *Calpain small-1 modulates Akt/FoxO3A signaling and apoptosis through PP2A.* Oncogene, 2008. **28**(5): p. 721-733.
287. Katsube, M., et al., *Calpain-mediated regulation of the distinct signaling pathways and cell migration in human neutrophils.* J Leukoc Biol, 2008. **84**(1): p. 255-263.

288. Noma, H., et al., *Calpain inhibition induces activation of the distinct signalling pathways and cell migration in human monocytes.* Immunology, 2009. **128**(1 Suppl): p. e487-96.
289. Perrin, B.J. and A. Huttenlocher, *Calpain.* Int J Biochem Cell Biol, 2002. **34**(7): p. 722-725.
290. Demarchi, F. and C. Schneider, *The Calpain System as a Modulator of Stress/Damage Response.* Cell Cycle, 2007. **6**(2): p. 136 - 138.
291. Sorimachi, H., S. Hata, and Y. Ono, *Expanding members and the roles of the calpain superfamily and their genetically modified animals.* Experimental Animals, 2010. **59**(5): p. 549- 566.
292. Carragher, N.O. and M.C. Frame, *Calpain: a role in cell transformation and migration.* Int J Biochem Cell Biol, 2002. **34**(12): p. 1539-1543.
293. Goll, D.E., et al., *The Calpain System.* Physiol Rev, 2003. **83**(3): p. 731-801.
294. Goll, D.E., et al., *The Calpain System.* Physiological Reviews, 2003. **83**(3): p. 731-801.
295. Thompson, V. and D. Goll, *Purification of mu-calpain, m-calpain, and calpastatin from animal tissues.* Methods Mol Biol, 2000. **144**: p. 3 - 16.
296. Chou, J.S., et al., *m-Calpain activation in vitro does not require autolysis or subunit dissociation.* Biochimica et Biophysica Acta (BBA) - Proteins & Proteomics, 2011. **1814**(7): p. 864-872.
297. Leloup, L., et al., *m-calpain Activation Is Regulated by Its Membrane Localization and by Its Binding to Phosphatidylinositol 4,5-Bisphosphate.* J Biol Chem, 2010. **285**(43): p. 33549-33566.
298. Shao, H., et al., *Spatial Localization of m-Calpain to the Plasma Membrane by Phosphoinositide Biphosphate Binding during Epidermal Growth Factor Receptor-Mediated Activation.* Mol. Cell. Biol., 2006. **26**(14): p. 5481-5496.
299. Stifanese, R., et al., *Role of the calpain-calpastatin system in the density-dependent growth arrest.* Archives of Biochemistry and Biophysics, 2008. **479**(2): p. 145-152.
300. Azam, M., et al., *Disruption of the Mouse {micro}-Calpain Gene Reveals an Essential Role in Platelet Function.* Mol. Cell. Biol., 2001. **21**(6): p. 2213-2220.
301. Arthur, J.S.C., et al., *Disruption of the Murine Calpain Small Subunit Gene, Capn4: Calpain Is Essential for Embryonic Development but Not for Cell Growth and Division.* Mol. Cell. Biol., 2000. **20**(12): p. 4474-4481.
302. Zimmerman, U.-J.P., et al., *The Calpain Small Subunit Gene Is Essential: Its Inactivation Results in Embryonic Lethality.* IUBMB Life, 2000. **50**(1): p. 63-68.
303. Dutt, P., et al., *m-Calpain is required for preimplantation embryonic development in mice.* BMC Developmental Biology, 2006. **6**(1): p. 3.
304. Wang, K.K.W., et al., *Development and Therapeutic Potential of Calpain Inhibitors*, in *Advances in Pharmacology*. 1996, Academic Press. p. 117-152.
305. Tan, Y., et al., *Ubiquitous Calpains Promote Both Apoptosis and Survival Signals in Response to Different Cell Death Stimuli.* J Biol Chem, 2006. **281**(26): p. 17689-17698.
306. Dourdin, N., et al., *Reduced Cell Migration and Disruption of the Actin Cytoskeleton in Calpain-deficient Embryonic Fibroblasts.* J Biol Chem, 2001. **276**(51): p. 48382-48388.
307. Kabeya, Y., et al., *LC3, a mammalian homologue of yeast Apg8p, is localized in autophagosome membranes after processing.* EMBO J, 2000. **19**(21): p. 5720-5728.
308. Gao, T., F. Furnari, and A.C. Newton, *PHLPP: A Phosphatase that Directly Dephosphorylates Akt, Promotes Apoptosis, and Suppresses Tumor Growth.* Molecular Cell, 2005. **18**(1): p. 13-24.
309. Datta, S.R., et al., *Akt Phosphorylation of BAD Couples Survival Signals to the Cell-Intrinsic Death Machinery.* Cell, 1997. **91**(2): p. 231-241.
310. Kovacina, K.S., et al., *Identification of a Proline-rich Akt Substrate as a 14-3-3 Binding Partner.* Journal of Biological Chemistry, 2003. **278**(12): p. 10189-10194.

311. Cross, D.A.E., et al., *Inhibition of glycogen synthase kinase-3 by insulin mediated by protein kinase B.* Nature, 1995. **378**(6559): p. 785-789.
312. Inoki, K., et al., *TSC2 is phosphorylated and inhibited by Akt and suppresses mTOR signalling.* Nat Cell Biol, 2002. **4**(9): p. 648-657.
313. Lim, Y.P., *Mining the Tumor Phosphoproteome for Cancer Markers.* Clinical Cancer Research, 2005. **11**(9): p. 3163-3169.
314. Kohn, A.D., et al., *Construction and Characterization of a Conditionally Active Version of the Serine/Threonine Kinase Akt.* Journal of Biological Chemistry, 1998. **273**(19): p. 11937-11943.
315. Porstmann, T., et al., *PKB//Akt induces transcription of enzymes involved in cholesterol and fatty acid biosynthesis via activation of SREBP.* Oncogene, 2005. **24**(43): p. 6465-6481.
316. Schmidt, M., S. Hovelmann, and T.L. Beckers, *A novel form of constitutively active farnesylated Akt1 prevents mammary epithelial cells from anoikis and suppresses chemotherapy-induced apoptosis.* Br J Cancer, 2002. **87**(8): p. 924-932.
317. Millward, T.A., S. Zolnierowicz, and B.A. Hemmings, *Regulation of protein kinase cascades by protein phosphatase 2A.* Trends in Biochemical Sciences, 1999. **24**(5): p. 186-191.
318. Sittampalam, G.S., S.D. Kahl, and W.P. Janzen, *High-throughput screening: advances in assay technologies.* Current Opinion in Chemical Biology, 1997. **1**(3): p. 384-391.
319. Jia, Y., et al., *Current in vitro kinase assay technologies: the quest for a universal format.* Curr Drug Discov Tech, 2008. **5**(5): p. 59 - 69.
320. Yu, Y., et al., *A site-specific, multiplexed kinase activity assay using stable-isotope dilution and high-resolution mass spectrometry.* Proceedings of the National Academy of Sciences, 2009. **106**(28): p. 11606-11611.
321. Kubota, K., et al., *Sensitive multiplexed analysis of kinase activities and activity-based kinase identification.* Nat Biotech, 2009. **27**(10): p. 933-940.
322. Jacobs, D., et al., *Multiple docking sites on substrate proteins form a modular system that mediates recognition by ERK MAP kinase.* Genes & Development, 1999. **13**(2): p. 163-175.
323. Lee, T., et al., *Docking Motif Interactions in MAP Kinases Revealed by Hydrogen Exchange Mass Spectrometry.* Molecular Cell, 2004. **14**(1): p. 43-55.
324. Miller, M.L., et al., *Linear Motif Atlas for Phosphorylation-Dependent Signaling.* Sci. Signal., 2008. **1**(35): p. ra2-.
325. Leevers, S.J., B. Vanhaesebroeck, and M.D. Waterfield, *Signalling through phosphoinositide 3-kinases: the lipids take centre stage.* Curr Opin Cell Biol, 1999. **11**(2): p. 219-225.
326. Hyun, S., et al., *Conserved MicroRNA miR-8/miR-200 and Its Target USH/FOG2 Control Growth by Regulating PI3K.* Cell, 2009. **139**(6): p. 1096-1108.
327. Dixon, M.J., et al., *A Screen for Novel Phosphoinositide 3-kinase Effector Proteins.* Molecular & Cellular Proteomics, 2011. **10**(4).
328. Ritzenthaler, J.D., S. Han, and J. Roman, *Stimulation of lung carcinoma cell growth by fibronectin-integrin signalling.* Molecular BioSystems, 2008. **4**(12).
329. Ivaska, J., et al., *Novel functions of vimentin in cell adhesion, migration, and signaling.* Experimental Cell Research, 2007. **313**(10): p. 2050-2062.
330. Raser, K.J., A. Posner, and K.K.W. Wang, *Casein Zymography: A Method to Study u-Calpain, M-Calpain, and Their Inhibitory Agents.* Archives of Biochemistry and Biophysics, 1995. **319**(1): p. 211-216.
331. Storr, S.J., et al., *The calpain system and cancer.* Nat Rev Cancer, 2011. **11**(5): p. 364-374.
332. duVerle, D.A., et al., *Calpain Cleavage Prediction Using Multiple Kernel Learning.* PLoS One, 2011. **6**(5): p. e19035.
333. Liu, Z., et al., *GPS-CCD: A Novel Computational Program for the Prediction of Calpain Cleavage Sites.* PLoS One, 2011. **6**(4): p. e19001.
334. Clark, J., et al., *Quantification of PtdInsP3 molecular species in cells and tissues by mass spectrometry.* Nat Meth, 2011. **8**(3): p. 267-272.

335. Smith, I.J. and S.L. Dodd, *Calpain activation causes a proteasome-dependent increase in protein degradation and inhibits the Akt signalling pathway in rat diaphragm muscle.* Experimental Physiology, 2007. **92**(3): p. 561-573.
336. Kourtis, N. and N. Tavernarakis, *Autophagy and cell death in model organisms.* Cell Death Differ, 2008. **16**(1): p. 21-30.
337. Yang, Z. and D.J. Klionsky, *Eaten alive: a history of macroautophagy.* Nat Cell Biol, 2010. **12**(9): p. 814-822.
338. Demarchi, F., et al., *Calpain is required for macroautophagy in mammalian cells.* The Journal of Cell Biology, 2006. **175**(4): p. 595-605.
339. Yousefi, S., et al., *Calpain-mediated cleavage of Atg5 switches autophagy to apoptosis.* Nat Cell Biol, 2006. **8**(10): p. 1124-1132.
340. Williams, A., et al., *Novel targets for Huntington's disease in an mTOR-independent autophagy pathway.* Nat Chem Biol, 2008. **4**(5): p. 295-305.
341. Yuan, T.L., et al., *Cell-to-Cell Variability in PI3K Protein Level Regulates PI3K-AKT Pathway Activity in Cell Populations.* Current Biology, 2011. **21**(3): p. 173-183.
342. Xu, C., B. Bailly-Maitre, and J.C. Reed, *Endoplasmic reticulum stress: cell life and death decisions.* The Journal of Clinical Investigation, 2005. **115**(10): p. 2656-2664.
343. Dejeans, N., et al., *Endoplasmic reticulum calcium release potentiates the ER stress and cell death caused by an oxidative stress in MCF-7 cells.* Biochemical Pharmacology, 2010. **79**(9): p. 1221-1230.
344. Wullschleger, S., R. Loewith, and M.N. Hall, *TOR Signaling in Growth and Metabolism.* Cell, 2006. **124**(3): p. 471-484.
345. Zatz, M. and A. Starling, *Calpains and Disease.* New England Journal of Medicine, 2005. **352**(23): p. 2413-2423.
346. Saez, M.E., et al., *The therapeutic potential of the calpain family: new aspects.* Drug Discovery Today, 2006. **11**(19-20): p. 917-923.
347. Carragher, N.O., B.D. Fonseca, and M.C. Frane, *Calpain activity is generally elevated during transformation but has oncogene-specific biological functions.* Neoplasia, 2004. **6**(1): p. 53 - 73.
348. Salehin, D., et al., *Immunohistochemical analysis for expression of calpain 1, calpain 2 and calpastatin in endometrial cancer.* Anticancer Research, 2010. **30**(7): p. 2837 - 2843.
349. Reichrath, J., et al., *Different expression patterns of calpain isozymes 1 and 2 (CAPN1 and 2) in squamous cell carcinomas (SCC) and basal cell carcinomas (BCC) of human skin.* The Journal of Pathology, 2003. **199**(4): p. 509-516.
350. Liu, Y., et al., *Deficient brain insulin signalling pathway in Alzheimer's disease and diabetes.* The Journal of Pathology, 2011. **225**(1): p. 54-62.
351. Kobe, B.t., et al., *Substrate specificity of protein kinases and computational prediction of substrates.* Biochimica et Biophysica Acta (BBA) - Proteins & Proteomics, 2005. **1754**(1-2): p. 200-209.
352. Vincent, E.E., et al., *Akt phosphorylation on Thr308 but not on Ser473 correlates with Akt protein kinase activity in human non-small cell lung cancer.* Br J Cancer, 2011. **104**(11): p. 1755-1761.
353. Kuhn, I., et al., *Identification of AKT-regulated genes in inducible MERAkt cells.* Physiol Genomics, 2001. **7**(2): p. 105 - 114.
354. Rochefort, H., et al., *Steroidal and nonsteroidal antiestrogens in breast cancer cells in culture.* J Steroid Biochem, 1984. **20**(1): p. 105 - 110.
355. Pilat, M., J. Christman, and S. Brooks, *Characterization of the estrogen receptor transfected MCF10A breast cell line 139B6.* Breast Cancer Res Treat., 1996. **37**(3): p. 253 - 266.
356. Cohen, P. and A. Knebel, *KESTREL: a powerful method for identifying the physiological substrates of protein kinases.* Biochem J, 2006. **393**(1): p. 1-6.

357. Songyang, Z., et al., *Use of an oriented peptide library to determine the optimal substrates of protein kinases.* Current Biology, 1994. **4**(11): p. 973-982.
358. Reimer, U., U. Reineke, and J. Schneider-Mergener, *Peptide arrays: from macro to micro.* Current Opinion in Biotechnology, 2002. **13**(4): p. 315-320.
359. MacBeath, G. and S. Schreiber, *Printing proteins as microarrays for high-throughput function determination.* Science, 2000. **289**(5485): p. 1760 - 1763.
360. Meng, L., et al., *Protein kinase substrate identification on functional protein arrays.* BMC Biotechnology, 2008. **8**(1): p. 22.
361. Mok, J., H. Im, and M. Snyder, *Global identification of protein kinase substrates by protein microarray analysis.* Nat. Protocols, 2009. **4**(12): p. 1820-1827.
362. Ferrari, E., et al., *Identification of New Substrates of the Protein-tyrosine Phosphatase PTP1B by Bayesian Integration of Proteome Evidence.* Journal of Biological Chemistry, 2011. **286**(6): p. 4173-4185.
363. Koch, A. and S. Hauf, *Strategies for the identification of kinase substrates using analog-sensitive kinases.* European Journal of Cell Biology, 2010. **89**(2-3): p. 184-193.
364. Bishop, A.C., O. Buzko, and K.M. Shokat, *Magic bullets for protein kinases.* Trends in Cell Biology, 2001. **11**(4): p. 167-172.
365. Zhang, C., et al., *A second-site suppressor strategy for chemical genetic analysis of diverse protein kinases.* Nat Meth, 2005. **2**(6): p. 435-441.
366. Amano, M., et al., *A Proteomic Approach for Comprehensively Screening Substrates of Protein Kinases Such as Rho-Kinase.* PLoS One, 2010. **5**(1): p. e8704.
367. Ataullakhanov, F. and V. Vitvitsky, *What determines the intracellular ATP concentration.* Biosci Rep. 2002 Oct-Dec;22(5-6):501-11., 2002. **5**(6): p. 501 - 511.
368. Ozalp, V.C., et al., *Time-resolved Measurements of Intracellular ATP in the Yeast Saccharomyces cerevisiae using a New Type of Nanobiosensor.* Journal of Biological Chemistry, 2010. **285**(48): p. 37579-37588.
369. Imamura, H., et al., *Visualization of ATP levels inside single living cells with fluorescence resonance energy transfer-based genetically encoded indicators.* Proceedings of the National Academy of Sciences, 2009. **106**(37): p. 15651-15656.
370. Fitz, J.G., *Regulation of Cellular ATP Release.* Trans Am Clin Climatol Assoc, 2007. **118**: p. 199 - 208.
371. Reshkin, S.J., et al., *Phosphoinositide 3-Kinase Is Involved in the Tumor-specific Activation of Human Breast Cancer Cell Na+/H+Exchange, Motility, and Invasion Induced by Serum Deprivation.* Journal of Biological Chemistry, 2000. **275**(8): p. 5361-5369.
372. Larance, M., et al., *Global Phosphoproteomics Identifies a Major Role for AKT and 14-3-3 in Regulating EDC3.* Molecular & Cellular Proteomics, 2010. **9**(4): p. 682-694.
373. Moritz, A., et al., *Akt-RSK-S6 Kinase Signaling Networks Activated by Oncogenic Receptor Tyrosine Kinases.* Sci. Signal., 2011. **3**(136): p. ra64-.

Appendix 1

Summary of AP-MS screen results (Chapter 3).

		Experiment 1				Experiment 2				Experiment 3				Summary (across 3 Experiments)					
Protein Accession Number	Protein Description	Mascot Score	No. of Peptides	Mean Peak Intensity (Starved)	Mean Peak Intensity (Stimulated)	Mascot Score	No. of Peptides	Mean Peak Intensity (Starved)	Mean Peak Intensity (Stimulated)	Mascot Score	No. of Peptides	Mean Peak Intensity (Starved)	Mean Peak Intensity (Stimulated)	Mean Peak Intensity (Starved)	Mean Peak Intensity (Stimulated)	Mean Fold	Mean Log2 Fold	SD	p - value (Students t-test)
IPI00108939	Gapdhs glyceraldehyde-3-phosphate dehydrogenase, spermatogenic	99	3	1.2	0.8	270	6	1.1	0.9	239	5	0.9	1.1	1.1	0.9	1.1	0.2	0.4	0.517
IPI00110658	Hba-a2;Hba-a1 Putative uncharacterized protein	57	3	0.3	1.7	328	4	0.8	1.2	142	4	0.8	1.2	0.7	1.3	0.5	-1.0	1.0	0.160
IPI00110753	Tuba1a Tubulin alpha-1A chain	301	3	0.6	1.4	1039	3	0.2	1.8	417	3	0.8	1.2	0.5	1.5	0.3	-1.6	1.6	0.122
IPI00110827	Acta1 Actin, alpha skeletal muscle	532	3	0.9	1.1	218	3	0.9	1.1	493	3	1.0	1.0	0.9	1.1	0.9	-0.2	0.2	0.241
IPI00110850	Actb Actin, cytoplasmic 1	697	35	1.0	1.0	201	6	1.1	0.9	138	6	1.1	0.9	1.1	0.9	1.2	0.2	0.2	0.230
IPI00112947	Krt19 Keratin, type I cytoskeletal 19	66	4	1.3	0.7	871	13	1.1	0.9	239	3	1.0	1.0	1.1	0.9	1.3	0.3	0.5	0.347
IPI00116277	Cct4 T-complex protein 1 subunit delta	126	13	1.2	0.8	1447	7	1.3	0.7	265	17	0.1	1.9	0.9	1.1	0.8	-0.4	2.5	0.732
IPI00116281	Cct6a T-complex protein 1 subunit zeta	304	16	1.2	0.8	779	16	1.3	0.7	621	17	1.5	0.5	1.3	0.7	2.0	1.0	0.4	0.040
IPI00116753	Etfa Electron transfer flavoprotein subunit alpha, mitochondrial	54	9	1.0	1.0	1274	18	1.5	0.5	856	15	1.3	0.7	1.3	0.7	1.7	0.8	0.7	0.190
IPI00117042	Gfap Isoform 1 of Glial fibrillary acidic protein	107	3	0.9	1.1	558	4	0.8	1.2	274	5	0.5	1.5	0.7	1.3	0.6	-0.8	0.6	0.135
IPI00117063	Fus RNA-binding protein FUS	155	8	0.7	1.3	346	7	0.9	1.1	314	7	1.0	1.0	0.8	1.2	0.7	-0.5	0.4	0.160
IPI00117159	**Pik3r2 Phosphatidylinositol 3-kinase regulatory subunit beta**	**1082**	**46**	**1.1**	**0.9**	**1336**	**25**	**0.9**	**1.1**	**383**	**9**	**1.0**	**1.0**	**1.0**	**1.0**	**1.0**	**0.0**	**0.2**	**0.951**
IPI00117348	Tuba1b Tubulin alpha-1B chain	311	13	0.8	1.2	632	5	0.8	1.2	369	5	0.5	1.5	0.7	1.3	0.5	-0.9	0.6	0.091
IPI00117352	Tubb5 Tubulin beta-5 chain	209	10	0.9	1.1	1038	15	1.2	0.8	116	18	1.3	0.7	1.1	0.9	1.3	0.3	0.5	0.365
IPI00121440	Etfb Electron transfer flavoprotein subunit beta	83	3	1.0	1.0	318	6	1.7	0.3	219	5	1.6	0.4	1.4	0.6	2.6	1.4	1.3	0.168
IPI00121788	Prdx1 Peroxiredoxin-1	99	10	0.7	1.3	42	3	0.9	1.1	73	3	0.9	1.1	0.8	1.2	0.7	-0.4	0.5	0.250

IPI00123494	Psmd2 26S proteasome non-ATPase regulatory subunit 2	46	5	0.7	1.3	51	4	1.4	0.6	72	5	1.1	0.9	1.0	1.0	1.1	0.1	1.0	0.822
IPI00123501	Hnrnpul1 Isoform 1 of Heterogeneous nuclear ribonucleoprotein U-like protein 1	437	39	0.9	1.1	808	15	0.7	1.3	167	19	0.8	1.2	0.8	1.2	0.7	-0.5	0.2	0.041
IPI00124499	Krt79 Keratin, type II cytoskeletal 79	122	5	1.1	0.9	1223	6	0.8	1.2	190	5	1.3	0.7	1.0	1.0	1.1	0.1	0.7	0.753
IPI00129240	Vtn Vitronectin	107	3	1.3	0.7	58	3	0.4	1.6	92	4	0.5	1.5	0.7	1.3	0.6	-0.8	1.6	0.447
IPI00129526	Hsp90b1 Endoplasmin	404	34	0.8	1.2	296	3	1.0	1.0	125	3	0.9	1.1	0.9	1.1	0.8	-0.3	0.3	0.274
IPI00130381	Bat3 Large proline-rich protein BAT3	187	14	1.1	0.9	661	13	0.5	1.5	326	14	0.5	1.5	0.7	1.3	0.5	-1.0	1.1	0.254
IPI00130992	**Capns1 Calpain small subunit 1**	**121**	**8**	**1.6**	**0.4**	**182**	**7**	**1.4**	**0.6**	**132**	**6**	**1.4**	**0.6**	**1.5**	**0.5**	**2.7**	**1.4**	**0.3**	**0.010**
IPI00131091	C4b Complement C4-B	61	4	1.0	1.0	179	4	1.1	0.9	66	4	1.2	0.8	1.1	0.9	1.3	0.3	0.2	0.120
IPI00131695	Alb Serum albumin	83	3	1.1	0.9	1168	6	0.9	1.1	136	5	0.8	1.2	0.9	1.1	0.8	-0.3	0.4	0.363
IPI00133208	Hspa1l;ENSMUSG00000073415;Hspa1a Heat shock 70 kDa protein 1L	101	3	1.2	0.8	671	3	0.5	1.5	95	3	0.6	1.4	0.8	1.2	0.6	-0.7	1.1	0.364
IPI00134599	Rps3 40S ribosomal protein S3	116	9	0.9	1.1	143	5	1.2	0.8	140	6	1.2	0.8	1.1	0.9	1.3	0.3	0.5	0.378
IPI00136110	**Pik3cb Phosphatidylinositol-4,5-bisphosphate 3-kinase catalytic subunit beta isoform**	**107**	**7**	**0.7**	**1.3**	**415**	**13**	**1.0**	**1.0**	**262**	**11**	**0.8**	**1.2**	**0.8**	**1.2**	**0.7**	**-0.5**	**0.5**	**0.239**
IPI00139301	Krt5 Keratin, type II cytoskeletal 5	160	9	1.1	0.9	121	14	0.9	1.1	327	11	0.8	1.2	0.9	1.1	0.9	-0.2	0.5	0.561
IPI00154054	Acat1 Acetyl-CoA acetyltransferase, mitochondrial	76	6	1.0	1.0	76	3	1.3	0.7	83	4	1.2	0.8	1.2	0.8	1.4	0.4	0.3	0.143
IPI00169463	Tubb2c Tubulin beta-2C chain	139	3	0.9	1.1	674	11	1.4	0.6	82	3	1.3	0.7	1.2	0.8	1.5	0.6	0.7	0.271
IPI00172221	Dnm1l Isoform 2 of Dynamin-1-like protein	71	3	1.2	0.8	70	15	0.8	1.2	41	3	0.9	1.1	1.0	1.0	0.9	-0.1	0.6	0.797
IPI00221528	Actbl2 Beta-actin-like protein 2	216	3	1.3	0.7	45	4	0.7	1.3	112	4	0.7	1.3	0.9	1.1	0.8	-0.3	1.1	0.707
IPI00222228	4732456N10Rik Putative uncharacterized protein	91	3	1.1	0.9	854	6	1.0	1.0	142	4	0.8	1.2	1.0	1.0	1.0	-0.1	0.5	0.869
IPI00225378	Krt15 Keratin 15, isoform CRA_a	40	3	1.0	1.0	940	13	0.8	1.2	161	3	0.9	1.1	0.9	1.1	0.8	-0.3	0.3	0.252
IPI00226073	Hnrnpf Isoform 1 of Heterogeneous nuclear ribonucleoprotein F	171	3	1.0	1.0	88	4	0.8	1.2	157	4	0.8	1.2	0.9	1.1	0.7	-0.4	0.4	0.174
IPI00227140	Krt14 Keratin, type I cytoskeletal 14	64	3	0.9	1.1	1115	8	0.6	1.4	223	7	1.0	1.0	0.8	1.2	0.7	-0.5	0.6	0.277
IPI00227299	**Vim Vimentin**	**107**	**11**	**0.5**	**1.5**	**340**	**4**	**0.0**	**2.0**	**218**	**4**	**0.3**	**1.7**	**0.3**	**1.7**	**0.2**	**-2.6**	**2**	**0.031**
IPI00229080	Hsp90ab1 MCG18238	570	39	0.9	1.1	920	15	0.8	1.2	132	19	0.8	1.2	0.8	1.2	0.7	-0.5	0.1	0.013

IPI00230365	Krt17 Keratin, type I cytoskeletal 17	56	6	1.2	0.8	1375	8	0.9	1.1	408	9	1.0	1.0	1.0	1.0	1.0	0.0	0.5	0.950
IPI00263878	**Pik3r1 Phosphatidylinositol 3-kinase regulatory subunit alpha**	**520**	**37**	**1.0**	**1.0**	**1427**	**31**	**1.0**	**1.0**	**850**	**19**	**1.0**	**1.0**	**1.0**	**1.0**	**1.0**	**0.0**	**0.1**	**0.663**
IPI00273646	100040053 Glyceraldehyde-3-phosphate dehydrogenase	530	35	1.1	0.9	1506	15	1.5	0.5	294	18	1.5	0.5	1.3	0.7	2.0	1.0	0.7	0.127
IPI00307837	Eef1a1 Elongation factor 1-alpha 1	175	13	0.9	1.1	243	7	1.1	0.9	49	5	1.0	1.0	1.0	1.0	1.0	0.0	0.3	0.821
IPI00309224	**Pik3ca Phosphatidylinositol-4,5-bisphosphate 3-kinase catalytic subunit alpha isoform**	**100**	**8**	**0.7**	**1.3**	**831**	**23**	**1.0**	**1.0**	**319**	**11**	**1.0**	**1.0**	**0.9**	**1.1**	**0.8**	**-0.3**	**0.6**	**0.445**
IPI00311175	Tuba8 Tubulin alpha-8 chain	135	3	0.8	0.9	649	13	0.7	1.3	226	3	1.0	1.0	0.8	1.1	0.8	-0.4	0.6	0.371
IPI00314950	Rplp0 60S acidic ribosomal protein P0	205	8	1.1	0.9	68	7	1.0	1.0	58	4	0.8	1.2	1.0	1.0	1.0	0.0	0.4	0.865
IPI00317590	Rps18 40S ribosomal protein S18	178	8	1.0	1.0	68	3	1.0	1.0	114	5	0.8	1.0	0.9	1.0	0.9	-0.1	0.2	0.500
IPI00317740	Gnb2l1 Guanine nucleotide-binding protein subunit beta-2-like 1	64	7	1.0	1.0	155	4	1.5	0.5	52	3	0.9	1.1	1.1	0.9	1.3	0.4	0.9	0.557
IPI00319992	Hspa5 78 kDa glucose-regulated protein	825	39	1.0	1.0	2603	39	2.0	2.0	1199	41	2.2	1.8	1.8	1.6	1.1	0.2	0.2	0.385
IPI00319994	Ldha L-lactate dehydrogenase A chain	302	17	1.1	0.9	119	3	0.9	1.1	62	5	0.9	1.1	1.0	1.0	0.9	-0.1	0.4	0.567
IPI00322867	Itih1 Itih1 protein	58	5	1.1	0.9	65	3	0.7	1.3	47	5	0.9	1.1	0.9	1.1	0.8	-0.3	0.7	0.571
IPI00323357	Hspa8 Heat shock cognate 71 kDa protein	171	34	0.9	1.1	2673	35	1.0	1.0	1316	36	1.0	1.0	1.0	1.0	0.9	-0.1	0.1	0.177
IPI00330480	- 35 kDa protein	51	3	1.1	0.9	1240	30	0.8	1.2	240	12	1.1	0.9	1.0	1.0	1.0	0.1	0.5	0.853
IPI00330804	Hsp90aa1 Heat shock protein HSP 90-alpha	514	13	0.8	1.2	571	24	1.3	0.7	40	4	1.1	0.9	1.1	0.9	1.2	0.2	0.6	0.592
IPI00331174	Cct7 T-complex protein 1 subunit eta	52	7	0.8	1.2	52	5	1.0	1.0	102	4	0.9	1.1	0.9	1.1	0.8	-0.3	0.2	0.097
IPI00346834	Krt76 Keratin, type II cytoskeletal 2 oral	43	3	1.0	1.0	991	34	1.0	1.0	57	4	1.0	1.0	1.0	1.0	1.0	0.0	0.1	0.818
IPI00348328	Krt78 keratin Kb40	57	4	0.8	1.2	1551	44	1.1	0.9	255	12	1.1	0.9	1.0	1.0	1.0	0.0	0.5	0.943
IPI00352163	**Fn1 Putative uncharacterized protein**	**52**	**14**	**0.4**	**1.6**	**329**	**15**	**0.6**	**1.4**	**192**	**14**	**0.4**	**1.6**	**0.5**	**1.5**	**0.3**	**-1.8**	**0**	**0.007**
IPI00406377	Krt7 Keratin, type II cytoskeletal 7	44	3	0.6	1.4	787	33	0.7	1.3	111	9	1.1	0.9	0.8	1.2	0.6	-0.6	0.8	0.277
IPI00420312	Krt4 Keratin, type II cytoskeletal 4	81	3	0.9	1.1	607	34	0.9	1.1	42	4	0.9	1.1	0.9	1.1	0.8	-0.4	0.0	0.001
IPI00420363	Ddx5 Probable ATP-dependent RNA helicase DDX5	71	8	1.0	1.0	128	6	1.0	1.0	57	6	0.8	1.2	0.9	1.1	0.9	-0.2	0.3	0.485
IPI00420970	Krt74 Keratin, type II cytoskeletal 74	95	3	0.9	1.1	1204	23	1.0	1.0	241	3	1.1	0.9	1.0	1.0	1.0	0.0	0.2	0.904

IPI00459493	Tcp1 Isoform 1 of T-complex protein 1 subunit alpha B	229	13	1.1	0.9	1419	30	1.5	0.5	326	13	1.5	0.5	1.3	0.7	2.0	1.0	0.6	0.100
IPI00462140	Krt77 Keratin, type II cytoskeletal 1b	122	3	1.2	0.8	1208	27	1.1	0.9	446	5	1.1	0.9	1.1	0.9	1.3	0.4	0.2	0.060
IPI00463573	Eif3l Eukaryotic translation initiation factor 3 subunit L	61	6	0.9	1.1	116	4	1.1	0.9	211	4	1.0	1.0	1.0	1.0	1.0	0.0	0.3	0.849
IPI00468696	Krt42 Keratin, type I cytoskeletal 42	63	4	0.7	1.3	1036	45	1.0	1.0	175	5	1.1	0.9	0.9	1.1	0.9	-0.2	0.6	0.641
IPI00468956	Krt71 Keratin, type II cytoskeletal 71	114	3	1.3	0.7	1208	43	0.9	1.1	215	3	0.8	1.2	1.0	1.0	1.0	0.0	0.7	0.976
IPI00471341	Ubl4 Ubiquitin-like protein 4A	47	3	1.2	0.8	125	4	1.0	1.0	53	3	0.9	1.1	1.0	1.0	1.0	0.0	0.4	0.919
IPI00473667	Tuba3b;Tuba3a Putative uncharacterized protein	100	4	1.1	0.9	324	11	1.5	0.5	57	3	1.3	0.7	1.3	0.7	1.8	0.8	0.6	0.120
IPI00551206	C4a sex-limited protein	72	4	1.1	0.9	179	7	0.5	1.5	82	4	0.7	1.3	0.8	1.2	0.6	-0.7	1.0	0.358
IPI00555131	Hbb-y;LOC100044141 Hemoglobin subunit epsilon-Y2	43	3	0.9	1.1	638	33	1.3	0.7	47	3	1.2	0.8	1.1	0.9	1.3	0.4	0.6	0.316
IPI00622240	Krt2 Keratin, type II cytoskeletal 2 epidermal	87	3	1.0	1.0	1104	17	0.9	1.1	94	10	0.9	1.1	0.9	1.1	0.9	-0.2	0.2	0.279
IPI00625729	Krt1 Keratin, type II cytoskeletal 1	121	7	1.2	0.8	2349	28	0.9	1.1	425	10	0.9	1.1	1.0	1.0	1.0	0.0	0.5	0.900
IPI00626132	Hsd17b10 Hydroxysteroid (17-beta) dehydrogenase 10	44	7	1.1	0.9	40	5	1.1	0.9	51	4	1.0	1.0	1.1	0.9	1.2	0.2	0.2	0.169
IPI00751677	640374 similar to Glyceraldehyde-3-phosphate dehydrogenase	318	6	1.3	0.7	1101	43	0.7	1.3	78	3	0.6	1.4	0.9	1.1	0.8	-0.3	1.1	0.635
IPI00755181	Krt10 keratin complex 1, acidic, gene 10	188	9	1.0	1.0	2935	42	1.1	0.9	442	10	1.2	0.8	1.1	0.9	1.2	0.3	0.3	0.221
IPI00830803	Fbln2 fibulin 2 isoform b	155	7	0.7	1.3	233	6	0.8	1.5	132	6	0.8	1.5	0.8	1.4	0.5	-0.9	0.0	0.005
IPI00875096	Krt2 71 kDa protein	79	6	1.0	1.0	1104	36	1.1	0.9	350	16	1.1	0.9	1.1	0.9	1.2	0.3	0.2	0.099
IPI00880839	Hspa9 heat shock protein 9	55	10	0.8	1.2	3312	36	1.3	0.7	668	34	1.3	0.7	1.1	0.9	1.3	0.4	0.8	0.463
IPI00896727	Cand1 Cullin-associated NEDD8-dissociated protein 1	76	7	1.0	1.0	144	6	1.1	0.9	87	6	1.2	0.8	1.1	0.9	1.3	0.4	0.4	0.217
IPI00911185	Ighg;Igh-1a;Igh-1b Igh protein	40	3	1.2	0.8	50	3	0.8	1.2	47	4	1.0	1.0	1.0	1.0	1.0	-0.1	0.6	0.866

Appendix 2

Summary of phosphorylation events found to be dependent on Akt by phosphoproteomic analysis of MCF10A myrAktER cells (Chapter 5.3.).

Accesion Number	Phosphopeptide Identification	Mean Peptide Intensity 18 h EtOH	Mean Peptide Intensity 1 h 4-OHT	Mean Peptide Intensity 48 h 4-OHT	Fold 1 h 4-OHT:18 h EtOH	Fold 48 h 4-OHT:18 h EtOH	t-test p-value (18 h EtOH vs. 1 h 4-OHT)	t-test p-value (18 h EtOH vs. 48 h 4-OHT)	Known Akt Substrate
HS90A_HUMAN	HSP90AA1 p-S264 (z= 3)	24.8	43.1	59.4	1.7	2.4	0.081	<0.001	
MACF1_HUMAN	MACF1 p-T213 (z= 2)	15.0	87.3	61.3	5.8	4.1	0.000	<0.001	
ZO3_HUMAN	TJP3 p-S113 (z= 4)	28.9	79.9	61.9	2.8	2.1	0.002	<0.001	
IF4G1_HUMAN	EIF4G1 p-S1233 (z= 2)	16.1	73.1	69.5	4.5	4.3	0.000	<0.001	
CLMN_HUMAN	CLMN p-S302 (z= 3)	22.7	51.3	61.2	2.3	2.7	0.050	<0.001	
E41L1_HUMAN	EPB41L1 p-S579 (z= 3)	29.3	69.5	55.7	2.4	1.9	0.001	<0.001	
PALLD_HUMAN	PALLD p-S894 (z= 2)	24.9	80.8	66.9	3.2	2.7	0.000	<0.001	*
DC1L1_HUMAN	DYNC1LI1 p-S517 (z= 2)	24.4	64.4	45.6	2.6	1.9	0.000	<0.001	
HDGF_HUMAN	HDGF p-S166 (z= 2)	26.4	79.2	77.7	3.0	2.9	0.000	<0.001	
FARP1_HUMAN	FARP1 p-T25 (z= 2)	8.5	47.5	47.4	5.6	5.6	0.004	<0.001	
RS6_HUMAN	RPS6 p-S237 p-S241 (z= 2)	18.9	73.9	57.1	3.9	3.0	0.000	<0.001	*
ZBT7A_HUMAN	ZBTB7A p-S550 (z= 3)	25.1	64.9	46.3	2.6	1.8	0.001	<0.001	
LMO7_HUMAN	LMO7 p-S1511 (z= 3)	30.8	65.9	64.1	2.1	2.1	0.010	<0.001	
CALX_HUMAN	CANX p-S584 (z= 3)	31.2	75.4	61.4	2.4	2.0	0.000	<0.001	
USO1_HUMAN	USO1 p-S943 (z= 4)	28.7	63.1	68.2	2.2	2.4	0.002	<0.001	
RTKN_HUMAN	RTKN p-S521 (z= 3)	25.6	65.0	63.7	2.5	2.5	0.002	<0.001	
FAS_HUMAN	FASN p-T2205 (z= 2)	11.6	38.2	54.8	3.3	4.7	0.000	<0.001	
RS16_HUMAN	RS16 p-Y116 (z= 2)	28.8	74.4	70.7	2.6	2.5	0.000	<0.001	
TR150_HUMAN	THRAP3 p-S683 (z= 2)	28.8	74.4	70.7	2.6	2.5	0.000	<0.001	
SRC8_HUMAN	CTTN p-S419 (z= 2)	23.4	40.3	57.7	1.7	2.5	0.016	<0.001	
LAD1_HUMAN	LAD1 p-S39 (z= 2)	33.3	72.9	71.5	2.2	2.1	0.000	<0.001	
CC64B_HUMAN	CCDC64B p-S268 (z= 2)	25.7	52.4	63.8	2.0	2.5	0.000	<0.001	
CI142_HUMAN	C9orf142 p-S149 (z= 2)	16.2	76.9	51.2	4.8	3.2	0.000	<0.001	
T132A_HUMAN	TMEM132A p-S530 (z= 3)	24.8	81.0	58.8	3.3	2.4	0.000	<0.001	
AHNK_HUMAN	AHNAK p-S136 (z= 3)	20.9	74.8	61.8	3.6	3.0	0.000	<0.001	
FAK1_HUMAN	PTK2 p-S911 (z= 2)	18.1	69.3	57.8	3.8	3.2	0.000	<0.001	
SL9A1_HUMAN	SLC9A1 p-S704 (z= 2)	25.1	51.5	69.5	2.1	2.8	0.008	<0.001	
TRAD1_HUMAN	TRAFD1 p-S416 (z= 3)	30.1	62.4	61.8	2.1	2.1	0.011	<0.001	
TPIS_HUMAN	TPI1 p-S22 (z= 3)	25.8	68.9	52.5	2.7	2.0	0.001	<0.001	
HSPB1_HUMAN	HSPB1 p-S83 (z= 2)	16.9	88.3	58.5	5.2	3.5	0.000	<0.001	
HTSF1_HUMAN	HTATSF1 p-S580 (z= 3)	19.0	48.7	50.2	2.6	2.6	0.009	<0.001	
B2L14_HUMAN	B2L14 p-S153 (z= 2)	5.4	41.6	48.8	7.8	9.1	0.000	<0.001	
FA63A_HUMAN	FAM63A p-S442 (z= 2)	5.4	41.6	48.8	7.7	9.1	0.000	<0.001	
TMM40_HUMAN	TMEM40 p-S142 (z= 3)	24.9	72.2	70.4	2.9	2.8	0.000	<0.001	
CHSP1_HUMAN	CARHSP1 p-S42 (z= 2)	32.8	67.3	76.5	2.1	2.3	0.002	<0.001	*
AKTS1_HUMAN	AKT1S1 p-T247 (z= 2)	31.3	73.0	73.9	2.3	2.4	0.000	<0.001	*

LIMA1_HUMAN	LIMA1 p-S491 (z= 3)	29.6	69.5	61.1	2.3	2.1	0.001	<0.001	
ABCF1_HUMAN	ABCF1 p-S110 (z= 3)	37.5	76.4	71.5	2.0	1.9	0.000	<0.001	
PGK1_HUMAN	PGK1 p-S204 (z= 3)	27.8	57.2	51.6	2.1	1.9	0.004	0.001	
KAPCA_HUMAN	PRKACA p-T203 (z= 3)	15.4	70.7	63.3	4.6	4.1	0.001	0.001	
HS90A_HUMAN	HSP90AA1 p-S253 (z= 4)	16.3	47.7	69.4	2.9	4.3	0.001	0.001	
MK01_HUMAN	MAPK1 p-Y188 (z= 3)	17.7	59.6	45.2	3.4	2.6	0.000	0.001	
MK01_HUMAN	MAPK1 p-T186 (z= 3)	17.6	59.5	44.9	3.4	2.5	0.000	0.001	
MAP4_HUMAN	MAP4 p-S637 (z= 3)	17.1	42.0	53.3	2.5	3.1	0.001	0.001	
NDRG1_HUMAN	NDRG1 p-S331 (z= 2)	16.0	54.8	59.0	3.4	3.7	0.000	0.001	
RD23B_HUMAN	RAD23B p-S161 (z= 3)	9.4	61.5	34.5	6.5	3.7	0.000	0.001	
SRRM2_HUMAN	SRRM2 p-S324 (z= 4)	21.6	59.6	68.5	2.8	3.2	0.000	0.001	
NP1L4_HUMAN	NAP1L4 p-S126 (z= 3)	19.4	39.0	47.7	2.0	2.5	0.000	0.001	
F1142_HUMAN	FAM114A2 p-S147 (z= 3)	13.2	31.1	58.0	2.4	4.4	0.049	0.001	
AHNK_HUMAN	AHNAK p-S512 (z= 2) + oxidation	18.4	38.3	53.7	2.1	2.9	0.020	0.001	
AHNK_HUMAN	AHNAK p-S512 (z= 2)	29.2	82.1	59.4	2.8	2.0	0.000	0.001	
ICAL_HUMAN	CAST p-S365 (z= 3)	22.1	69.4	63.7	3.1	2.9	0.000	0.001	
LAD1_HUMAN	LAD1 p-S357 (z= 3)	30.7	80.6	56.4	2.6	1.8	0.000	0.001	
TFP11_HUMAN	TFIP11 p-S99 (z= 3)	19.9	56.0	42.0	2.8	2.1	0.003	0.001	
NUFP2_HUMAN	NUFIP2 p-S630 (z= 3)	23.4	45.3	56.6	1.9	2.4	0.001	0.001	
NIBL1_HUMAN	FAM129B p-S634 (z= 3)	2.7	48.7	35.4	18.0	13.1	0.000	0.002	
RFIP1_HUMAN	RAB11FIP1 p-S436 (z= 2)	6.3	67.9	34.2	10.8	5.5	0.000	0.002	
ZRAB2_HUMAN	ZRANB2 p-S121 (z= 3)	29.9	54.7	61.0	1.8	2.0	0.000	0.002	
HNRPC_HUMAN	HNRNPC p-S261 (z= 3)	26.2	56.5	48.8	2.2	1.9	0.002	0.002	
KPCD_HUMAN	PRKCD p-S665 (z= 2) + oxidation	30.7	23.5	63.2	0.8	2.1	0.669	0.002	
HS90A_HUMAN	HSP90AA1 p-S253 (z= 3)	21.1	45.2	72.0	2.1	3.4	0.035	0.002	
ZO2_HUMAN	TJP2 p-S131 (z= 3)	32.3	71.9	58.8	2.2	1.8	0.004	0.002	
NUBPL_HUMAN	NUBPL p-S75 (z= 2)	22.0	77.2	50.1	3.5	2.3	0.000	0.002	
1433E_HUMAN	YWHAE p-S211 (z= 2)	24.1	39.5	50.3	1.6	2.1	0.055	0.002	
NIBL1_HUMAN	FAM129B p-S634 (z= 3)	12.5	33.6	45.4	2.7	3.6	0.001	0.002	
DC1L1_HUMAN	DYNC1LI1 p-S208 (z= 3)	27.0	59.5	49.2	2.2	1.8	0.010	0.002	
MAP4_HUMAN	MAP4 p-T522 (z= 3)	20.6	49.4	62.7	2.4	3.0	0.000	0.003	
MAP4_HUMAN	MAP4 p-S281 (z= 3) + oxidation	18.4	43.2	60.6	2.4	3.3	0.024	0.003	
SEPT2_HUMAN	SEPT2 p-S219 (z= 4)	25.7	55.6	58.7	2.2	2.3	0.021	0.003	
AK1C1_HUMAN	AKR1C1 p-S233 (z= 3)	10.2	43.9	53.6	4.3	5.3	0.000	0.003	
RICS_HUMAN	RICS p-S872 (z= 2)	34.6	79.7	67.2	2.3	1.9	0.001	0.003	
AHNK_HUMAN	AHNAK p-S3427 (z= 3)	4.2	62.0	34.2	14.7	8.1	0.000	0.003	
SRC8_HUMAN	CTTN p-T402 p-S406 (z= 3)	37.2	74.7	69.9	2.0	1.9	0.000	0.003	
PNCB_HUMAN	NAPRT1 p-S538 (z= 2)	15.3	80.7	57.8	5.3	3.8	0.000	0.003	
DPOD3_HUMAN	POLD3 p-S308 (z= 3)	20.6	63.2	48.4	3.1	2.3	0.001	0.004	
PKP2_HUMAN	PKP2 p-S330 (z= 3)	19.8	57.6	57.5	2.9	2.9	0.001	0.004	
MAVS_HUMAN	MAVS p-S223 (z= 2)	40.1	85.1	72.8	2.1	1.8	0.001	0.004	
HNRPC_HUMAN	HNRNPC p-S261 (z= 4) + oxidation	15.3	17.7	42.5	1.2	2.8	0.689	0.004	
SYNE2_HUMAN	SYNE2 p-S6362 (z= 3)	21.1	54.6	38.2	2.6	1.8	0.004	0.004	
TACC1_HUMAN	TACC1 p-S277 (z= 3)	15.6	41.0	50.7	2.6	3.2	0.002	0.004	
RD23B_HUMAN	RAD23B p-S161 (z= 3)	18.8	42.6	48.1	2.3	2.6	0.002	0.004	
CALX_HUMAN	CANX p-S565 (z= 4)	15.5	53.9	41.4	3.5	2.7	0.001	0.004	
TPIS_HUMAN	TPI1 p-S22 (z= 2)	27.4	66.5	49.5	2.4	1.8	0.005	0.004	
EF1D_HUMAN	EEF1D p-S163 (z= 3)	23.9	50.1	38.1	2.1	1.6	0.002	0.004	
PLAK_HUMAN	JUP p-S666 (z= 2)	13.0	47.0	34.1	3.6	2.6	0.009	0.005	
HNRPK_HUMAN	HNRNPK p-T119 (z= 4)	18.7	33.1	51.1	1.8	2.7	0.137	0.005	
STK3_HUMAN	STK3 p-S317 (z= 3) + oxidation	6.2	19.8	35.7	3.2	5.8	0.014	0.005	

RS3_HUMAN	RPS3 p-T222 (z= 2)	16.9	36.2	46.4	2.1	2.7	0.014	0.005	
PLEC1_HUMAN	PLEC1 p-S4407 (z= 3)	15.5	50.4	50.9	3.2	3.3	0.000	0.005	
K1522_HUMAN	KIAA1522 p-S930 (z= 3)	13.0	26.2	42.0	2.0	3.2	0.003	0.005	
CALX_HUMAN	CANX p-S555 (z= 3)	36.9	75.6	65.4	2.1	1.8	0.000	0.005	
IF4B_HUMAN	EIF4B p-S94 (z= 3)	20.5	36.7	56.0	1.8	2.7	0.255	0.005	*
DAP1_HUMAN	DAP p-S52 (z= 3)	12.8	29.0	45.4	2.3	3.5	0.011	0.005	
PDCD4_HUMAN	PDCD4 p-S77 (z= 2)	31.3	63.0	53.7	2.0	1.7	0.003	0.005	*
NPM_HUMAN	NPM1 p-S71 (z= 3)	1.3	24.1	24.5	18.6	18.9	0.066	0.005	
CCD86_HUMAN	CCDC86 p-S19 (z= 2)	15.9	45.7	51.8	2.9	3.3	0.028	0.006	
TB182_HUMAN	TNKS1BP1 p-S430 (z= 3)	26.1	54.4	56.2	2.1	2.2	0.000	0.006	
SRRM1_HUMAN	SRRM1 p-S606 p-S608 (z= 2)	25.3	83.9	52.1	3.3	2.1	0.000	0.006	
AKAP8_HUMAN	AKAP8 p-S340 (z= 3)	28.1	73.8	68.1	2.6	2.4	0.000	0.006	
DNJC5_HUMAN	DNAJC5 p-S11 (z= 3)	21.0	34.3	46.2	1.6	2.2	0.127	0.006	
STAT3_HUMAN	STAT3 p-S728 (z= 3)	22.0	49.8	38.9	2.3	1.8	0.013	0.006	
H1BP3_HUMAN	HS1BP3 p-S195 (z= 2)	19.2	50.2	36.3	2.6	1.9	0.014	0.007	
UBP7_HUMAN	USP7 p-S19 (z= 3) + oxidation	23.7	34.0	53.7	1.4	2.3	0.403	0.007	
STRN3_HUMAN	STRN3 p-S230 (z= 2)	32.1	55.6	64.7	1.7	2.0	0.006	0.007	
ABCF1_HUMAN	ABCF1 p-T109 (z= 3)	26.1	58.7	45.4	2.2	1.7	0.006	0.007	
HNRPK_HUMAN	HNRNPK p-T119 (z= 5)	17.5	29.1	47.9	1.7	2.7	0.216	0.008	
BA2L1_HUMAN	BAT2L1 p-S389 (z= 2)	26.2	56.9	45.5	2.2	1.7	0.041	0.008	
NUMB_HUMAN	NUMB p-S426 (z= 3)	17.7	42.4	54.2	2.4	3.1	0.038	0.008	
SYAP1_HUMAN	SYAP1 p-S270 (z= 3)	27.7	46.8	58.2	1.7	2.1	0.059	0.009	
COPE_HUMAN	COPE p-S100 (z= 2)	17.8	36.1	49.2	2.0	2.8	0.001	0.009	
1433Z_HUMAN	YWHAZ p-S208 (z= 2)	16.5	29.7	40.4	1.8	2.5	0.172	0.009	
PGRC2_HUMAN	PGRMC2 p-T212 (z= 4)	6.7	39.4	37.5	5.8	5.6	0.027	0.009	
SCRIB_HUMAN	SCRIB p-S836 (z= 3) + oxidation	21.3	17.9	47.1	0.8	2.2	0.422	0.009	
PPIL4_HUMAN	PPIL4 p-S179 (z= 4)	20.2	34.2	46.1	1.7	2.3	0.148	0.009	
RBM14_HUMAN	RBM14 p-T207 (z= 2)	31.2	75.3	48.2	2.4	1.5	0.001	0.009	
PKHA6_HUMAN	PLEKHA6 p-T780 (z= 3)	25.4	51.2	53.1	2.0	2.1	0.002	0.009	
HSF1_HUMAN	HSF1 p-S321 (z= 3)	22.3	43.5	52.6	1.9	2.4	0.126	0.010	
HNRPK_HUMAN	HNRNPK p-T119 (z= 3)	17.9	30.1	46.0	1.7	2.6	0.166	0.010	
NRDC_HUMAN	NRD1 p-S95 (z= 3)	15.0	58.2	52.4	3.9	3.5	0.001	0.011	
MACOI_HUMAN	TMEM57 p-S332 (z= 2)	20.0	63.1	35.3	3.2	1.8	0.000	0.011	
YAP1_HUMAN	YAP1 p-T64 (z= 2) + oxidation	21.2	15.0	44.2	0.7	2.1	0.560	0.011	*
MK03_HUMAN	MAPK3 p-T203 p-Y205 (z= 3)	24.7	75.9	58.1	3.1	2.3	0.000	0.011	
EIF3C_HUMAN	EIF3C p-S40 (z= 3)	7.7	64.2	36.4	8.4	4.8	0.000	0.011	
MYH10_HUMAN	MYH10 p-S1957 (z= 3)	13.0	64.2	54.7	4.9	4.2	0.000	0.011	
NRG2_HUMAN	NRG2 p-Y288 (z= 2)	11.5	24.1	42.7	2.1	3.7	0.001	0.012	
STAM2_HUMAN	STAM2 p-Y362 (z= 2)	11.5	24.1	42.7	2.1	3.7	0.001	0.012	
EF1D_HUMAN	EEF1D p-S163 (z= 4)	17.2	53.3	43.3	3.1	2.5	0.000	0.012	
MFF_HUMAN	MFF p-T139 (z= 4)	12.8	44.5	40.0	3.5	3.1	0.038	0.012	
SCRIB_HUMAN	SCRIB p-S1449 (z= 2)	16.9	36.2	43.9	2.1	2.6	0.014	0.012	
LMO7_HUMAN	LMO7 p-S989 (z= 3)	21.9	38.6	52.5	1.8	2.4	0.061	0.012	
ESYT2_HUMAN	ESYT2 p-S759 (z= 2)	26.4	61.3	48.3	2.3	1.8	0.027	0.012	
MAP4_HUMAN	MAP4 p-T283 (z= 3)	26.9	59.8	50.9	2.2	1.9	0.001	0.012	
BCLF1_HUMAN	BCLAF1 p-S386 (z= 3)	16.8	28.4	47.5	1.7	2.8	0.005	0.013	
SF3A1_HUMAN	SF3A1 p-S330 (z= 3) + oxidation	11.9	13.1	37.0	1.1	3.1	0.701	0.013	
HS90A_HUMAN	HSP90AA1 p-S264 (z= 3)	10.9	35.2	39.9	3.2	3.7	0.009	0.013	
MACC1_HUMAN	MACC1 p-S75 (z= 3)	28.5	43.7	58.8	1.5	2.1	0.236	0.014	
ICAL_HUMAN	CAST p-S365 (z= 2)	15.7	45.1	40.4	2.9	2.6	0.008	0.014	
THUM1_HUMAN	THUMPD1 p-S87 p-S89 (z= 4)	16.3	61.5	49.9	3.8	3.1	0.001	0.014	

STIP1_HUMAN	STIP1 p-S17 (z= 2)	8.5	29.7	44.2	3.5	5.2	0.041	0.014	
VNRL4_HUMAN	VNRL4 p-T91 (z= 2)	11.5	34.9	48.6	3.0	4.2	0.001	0.015	
SCRIB_HUMAN	SCRIB p-S836 (z= 3)	23.9	54.3	39.2	2.3	1.6	0.011	0.016	
TCEA1_HUMAN	TCEA1 p-S101 (z= 3)	7.8	35.7	23.6	4.6	3.0	0.023	0.017	
ITPR1_HUMAN	ITPR1 p-T277 (z= 2)	20.6	58.1	52.0	2.8	2.5	0.001	0.017	*
PGRC1_HUMAN	PGRMC1 p-S182 (z= 3)	16.5	38.9	47.1	2.4	2.9	0.003	0.017	
DC1L2_HUMAN	DYNC1LI2 p-S206 (z= 3)	7.2	23.1	38.0	3.2	5.3	0.054	0.017	
ASAP2_HUMAN	ASAP2 p-S702 (z= 3)	16.6	53.2	52.9	3.2	3.2	0.000	0.018	
MAP4_HUMAN	MAP4 p-S508 (z= 2)	29.1	62.5	51.9	2.1	1.8	0.011	0.018	
EPN1_HUMAN	EPN1 p-S411 (z= 2)	31.0	70.7	68.9	2.3	2.2	0.008	0.019	
XPC_HUMAN	XPC p-S95 (z= 3)	26.1	59.8	44.0	2.3	1.7	0.009	0.019	
EPIPL_HUMAN	EPPK1 p-S2692 (z= 3)	23.4	47.8	47.2	2.0	2.0	0.000	0.019	
DSG2_HUMAN	DSG2 p-S681 (z= 2)	22.9	50.0	45.9	2.2	2.0	0.046	0.019	
EIF3C_HUMAN	EIF3C p-S40 (z= 2)	18.1	55.8	34.8	3.1	1.9	0.001	0.019	
SRRM2_HUMAN	SRRM2 p-S1180 (z= 2)	26.1	73.1	43.8	2.8	1.7	0.001	0.019	
TMX1_HUMAN	TMX1 p-S248 (z= 3)	21.0	16.9	51.1	0.8	2.4	0.580	0.020	
EF1D_HUMAN	EEF1D p-S163 (z= 3)	29.2	56.9	69.0	2.0	2.4	0.052	0.020	
AHNK_HUMAN	AHNAK p-S136 (z= 2)	27.7	68.7	58.3	2.5	2.1	0.002	0.021	
ALPK3_HUMAN	ALPK3 p-S295 (z= 2)	33.1	79.0	58.2	2.4	1.8	0.000	0.021	
CAV1_HUMAN	CAV1 p-S38 (z= 2)	33.1	79.0	58.2	2.4	1.8	0.000	0.021	
MK01_HUMAN	MAPK1 p-T186 p-Y188 (z= 3)	28.6	72.3	53.5	2.5	1.9	0.003	0.021	
K2C5_HUMAN	KRT5 p-S22 (z= 2)	34.9	76.0	61.8	2.2	1.8	0.000	0.022	
TEBP_HUMAN	PTGES3 p-S114 (z= 3) + oxidation	7.2	27.7	42.2	3.8	5.9	0.186	0.023	
STK10_HUMAN	STK10 p-S439 (z= 2)	11.9	77.7	33.0	6.5	2.8	0.000	0.023	
GPN1_HUMAN	GPN1 p-S315 (z= 3)	10.0	65.7	46.4	6.6	4.6	0.000	0.023	
ASML_HUMAN	ASMTL p-S240 (z= 3)	24.7	60.0	48.6	2.4	2.0	0.007	0.023	
SLTM_HUMAN	SLTM p-S554 (z= 3)	12.7	48.8	41.3	3.8	3.2	0.004	0.024	
SRRM1_HUMAN	SRRM1 p-S261 (z= 3)	21.9	35.0	49.7	1.6	2.3	0.097	0.025	
STK39_HUMAN	STK39 p-S388 (z= 2)	25.0	62.2	57.9	2.5	2.3	0.025	0.025	
DSG2_HUMAN	DSG2 p-S681 (z= 3)	20.1	52.8	54.3	2.6	2.7	0.026	0.026	
YAP1_HUMAN	YAP1 p-S110 (z= 3)	10.8	51.8	29.3	4.8	2.7	0.003	0.026	*
NPM_HUMAN	NPM1 p-S71 (z= 3) + oxidation	23.3	25.2	59.9	1.1	2.6	0.897	0.026	
TB182_HUMAN	TNKS1BP1 p-S1477 (z= 3)	17.9	24.8	39.6	1.4	2.2	0.352	0.026	
HDGF_HUMAN	HDGF p-S134 (z= 3)	34.0	59.8	71.3	1.8	2.1	0.060	0.029	
ZYX_HUMAN	ZYX p-S143 (z= 3)	0.8	19.9	23.5	25.0	29.6	0.128	0.029	*
AHNK_HUMAN	AHNAK p-S94 (z= 3)	31.6	70.9	45.5	2.2	1.4	0.003	0.029	
LAD1_HUMAN	LAD1 p-T20 (z= 3)	19.7	38.6	54.8	2.0	2.8	0.154	0.029	
PPIL4_HUMAN	PPIL4 p-S179 (z= 3)	16.4	22.7	37.5	1.4	2.3	0.317	0.029	
S6A15_HUMAN	SLC6A15 p-S676 (z= 3)	16.7	52.0	44.0	3.1	2.6	0.000	0.030	
KLC3_HUMAN	KLC3 p-S467 (z= 2)	23.4	47.7	44.4	2.0	1.9	0.000	0.030	
NCRP1_HUMAN	NCCRP1 p-S29 (z= 3) + oxidation	8.8	8.4	32.3	1.0	3.7	0.882	0.032	
SRC8_HUMAN	CTTN p-T402 p-Y422 (z= 3)	25.1	48.1	54.4	1.9	2.2	0.023	0.032	
OSBP1_HUMAN	OSBP p-S352 (z= 3) + oxidation	32.0	42.3	68.0	1.3	2.1	0.539	0.032	
NIBL1_HUMAN	FAM129B p-S629 p-T639 (z= 3)	21.4	52.7	52.0	2.5	2.4	0.061	0.032	
HTSF1_HUMAN	HTATSF1 p-S677 (z= 3)	9.2	14.0	39.9	1.5	4.3	0.153	0.032	
PROM2_HUMAN	PROM2 p-S816 p-S819 (z= 3)	23.0	45.5	53.7	2.0	2.3	0.072	0.034	
MY18A_HUMAN	MYO18A p-S1971 (z= 3)	24.8	53.5	39.1	2.2	1.6	0.071	0.034	
HNRPC_HUMAN	HNRNPC p-S254 p-S261 (z= 4)	25.2	72.2	55.8	2.9	2.2	0.001	0.035	
LRRF1_HUMAN	LRRFIP1 p-S125 (z= 3)	26.1	39.5	54.2	1.5	2.1	0.051	0.035	
DDB2_HUMAN	DDB2 p-S27 (z= 3)	26.3	54.0	50.8	2.1	1.9	0.004	0.035	
PGRC1_HUMAN	PGRMC1 p-S58 (z= 3)	24.6	61.3	59.1	2.5	2.4	0.001	0.036	

NCK1_HUMAN	NCK1 p-S90 (z= 3)	15.7	31.0	44.7	2.0	2.8	0.002	0.036	
TOIP1_HUMAN	TOR1AIP1 p-T221 (z= 3)	25.7	48.6	54.6	1.9	2.1	0.025	0.036	
HNRL2_HUMAN	HNRNPUL2 p-S162 (z= 3)	24.5	51.5	37.6	2.1	1.5	0.010	0.037	
ARFG2_HUMAN	ARFGAP2 p-S202 (z= 4)	13.0	22.4	42.4	1.7	3.3	0.354	0.039	
HNRPU_HUMAN	HNRNPU p-S272 (z= 5)	13.3	28.4	27.2	2.1	2.0	0.135	0.039	
AHNK_HUMAN	AHNAK p-T5795 (z= 3)	11.3	21.5	32.2	1.9	2.8	0.038	0.039	
MY18A_HUMAN	MYO18A p-S73 (z= 3)	27.0	59.5	45.5	2.2	1.7	0.009	0.039	
NOB1_HUMAN	NOB1 p-S202 (z= 2)	25.3	62.7	47.8	2.5	1.9	0.000	0.040	
ATX2L_HUMAN	ATXN2L p-S112 (z= 3)	29.7	61.0	52.2	2.1	1.8	0.006	0.040	
EF1B_HUMAN	EEF1B2 p-S107 (z= 4)	14.2	28.0	37.3	2.0	2.6	0.043	0.041	
NPM_HUMAN	NPM1 p-T76 (z= 4) + oxidation	8.0	11.7	39.6	1.5	5.0	0.599	0.041	
UBP20_HUMAN	USP20 p-S135 (z= 3)	28.4	62.2	51.7	2.2	1.8	0.000	0.042	
DC1L2_HUMAN	DYNC1LI2 p-S206 (z= 4)	3.4	11.3	28.9	3.3	8.6	0.073	0.044	
LAD1_HUMAN	LAD1 p-S65 (z= 4)	3.6	23.7	36.4	6.6	10.1	0.045	0.044	
HTSF1_HUMAN	HTATSF1 p-S643 (z= 2)	11.3	16.8	35.4	1.5	3.1	0.078	0.046	
CTNB1_HUMAN	CTNNB1 p-S553 (z= 3) + oxidation	21.2	48.2	36.4	2.3	1.7	0.038	0.046	*
HNRPK_HUMAN	HNRNPK p-S117 (z= 4)	5.7	28.0	21.8	4.9	3.8	0.085	0.046	
HPBP1_HUMAN	HSPBP1 p-S355 (z= 2)	27.8	66.8	54.5	2.4	2.0	0.001	0.046	
HNRPC_HUMAN	HNRNPC p-S261 (z= 4)	20.4	50.7	55.7	2.5	2.7	0.001	0.047	
TXLNA_HUMAN	TXLNA p-S515 (z= 3)	23.9	60.9	39.2	2.5	1.6	0.001	0.047	
NPM_HUMAN	NPM1 p-S126 (z= 4)	18.9	48.0	45.4	2.5	2.4	0.001	0.048	
SSRP1_HUMAN	SSRP1 p-S445 (z= 3) + oxidation	8.6	13.1	34.2	1.5	4.0	0.336	0.048	
CTNB1_HUMAN	CTNNB1 p-T557 (z= 3)	28.0	64.7	44.5	2.3	1.6	0.000	0.048	*
TPIS_HUMAN	TPI1 p-S22 (z= 3)	18.5	47.5	36.8	2.6	2.0	0.001	0.055	
LARP1_HUMAN	LARP1 p-S767 p-Y778 (z= 2)	25.3	74.3	56.6	2.9	2.2	0.004	0.055	
CTNB1_HUMAN	CTNNB1 p-S192 (z= 2)	19.7	57.3	52.4	2.9	2.7	0.002	0.057	*
FA40A_HUMAN	FAM40A p-S336 (z= 3)	23.3	54.1	42.9	2.3	1.8	0.003	0.057	
DOCK8_HUMAN	DOCK8 p-S905 (z= 3)	33.3	70.5	52.1	2.1	1.6	0.001	0.058	
SON_HUMAN	SON p-S1557 (z= 3) + oxidation	15.5	21.0	38.1	1.4	2.5	0.002	0.059	
ASAP2_HUMAN	ASAP2 p-S702 (z= 2)	36.4	74.4	59.5	2.0	1.6	0.000	0.061	
NPM_HUMAN	NPM1 p-S126 (z= 3)	16.0	56.0	41.1	3.5	2.6	0.000	0.066	
SFR15_HUMAN	SFRS15 p-S155 (z= 4)	20.3	48.5	40.0	2.4	2.0	0.004	0.067	
DDX54_HUMAN	DDX54 p-S783 (z= 2)	3.4	11.7	34.2	3.4	10.0	0.003	0.081	
NIBL1_HUMAN	FAM129B p-S629 p-S634 (z= 3)	6.4	42.8	28.8	6.7	4.5	0.003	0.101	
ACACA_HUMAN	ACACA p-S30 (z= 3)	27.2	69.2	49.9	2.5	1.8	0.001	0.105	
HS90B_HUMAN	HSP90AB1 p-S256 (z= 2)	3.7	7.1	32.8	1.9	8.8	0.003	0.106	
DNJC1_HUMAN	DNAJC1 p-S480 p-S481 (z= 3)	38.2	78.4	57.6	2.1	1.5	0.003	0.111	
EHD2_HUMAN	EHD2 p-S439 (z= 3)	24.2	63.2	53.9	2.6	2.2	0.001	0.151	
PRCC_HUMAN	PRCC p-T262 (z= 3)	27.7	74.8	51.4	2.7	1.9	0.001	0.153	
FMNL2_HUMAN	FMNL2 p-S172 (z= 2)	26.3	57.6	40.2	2.2	1.5	0.004	0.165	
ZRAB2_HUMAN	ZRANB2 p-S154 (z= 2)	13.5	4.4	33.6	0.3	2.5	0.005	0.167	
CTND1_HUMAN	CTNND1 p-S350 p-S353 (z= 2)	26.6	66.8	44.6	2.5	1.7	0.003	0.171	
NUCL_HUMAN	NCL p-T70 (z= 2)	15.5	52.9	21.9	3.4	1.4	0.004	0.182	
SNTB2_HUMAN	SNTB2 p-S111 (z= 3)	27.4	59.6	37.1	2.2	1.4	0.001	0.234	
HNRPC_HUMAN	HNRNPC p-S254 p-S261 (z= 3)	28.0	62.0	39.0	2.2	1.4	0.001	0.249	
UBR4_HUMAN	UBR4 p-S2720 (z= 2)	42.5	85.9	55.3	2.0	1.3	0.000	0.260	
ARHG6_HUMAN	ARHGEF6 p-S489 (z= 2)	37.5	75.7	42.8	2.0	1.1	0.001	0.304	
PR38A_HUMAN	PRPF38A p-S194 p-S195 (z= 3)	30.8	70.2	40.4	2.3	1.3	0.000	0.406	
TP53B_HUMAN	TP53BP1 p-S1363 (z= 2)	23.9	58.3	24.7	2.4	1.0	0.002	0.849	

Appendix 3

Summary of phosphorylation events found to be dependent on Akt1 by an *in vitro* reaction followed by phosphoproteomic analysis in MCF10A cells (Chapter 5.4.1.).

Accession Number	Peptide	Modification	Mean Peptide Intensity 0 µg Akt1	Mean Peptide Intensity 2 µg Akt1	Mean Peptide Intensity 10 µg Akt1	Fold 10 µg Akt1:0µg Akt1	Known Akt Substrate
AKT1_HUMAN	SGSPSDNSGAEEMEVSLAKPK	Phospho (ST)	0.4	16.8	100.0	225.3	
AKT1_HUMAN	SGSPSDNSGAEEMEVSLAKPK	Oxidation (M); Phospho (ST)	0.8	10.9	100.0	132.9	
AKTS1_HUMAN	LNTSDFQK	Phospho (ST)	0.9	17.1	100.0	113.8	*
AKT1_HUMAN	SGSPSDNSGAEEMEVSLAKPK	3 Phospho (ST)	0.9	29.5	100.0	106.5	
GOGA4_HUMAN	TSSFTEQLDEGTPNR	Phospho (ST)	1.8	39.9	100.0	55.0	
AKT1_HUMAN	SGSPSDNSGAEEMEVSLAKPK	2 Phospho (ST)	2.8	20.5	100.0	36.0	
AHNK_HUMAN	SNSFSDER	Phospho (ST)	3.6	32.6	100.0	28.0	
AKT1_HUMAN	RPHFPQFSYSASGTA	Phospho (ST)	3.9	20.2	100.0	25.8	
PURB_HUMAN	RGGGSGGGEESEGEEVDED	Phospho (ST)	4.1	71.0	100.0	24.6	
HS90B_HUMAN	IEDVGSDEEDDSGKDK	Phospho (ST)	5.0	75.5	99.8	19.9	
APIP_HUMAN	DISGPSPSK	Phospho (ST)	6.1	70.2	96.2	15.8	
ITFG3_HUMAN	SQENLGNPSK	Phospho (ST)	7.3	58.8	100.0	13.7	
WAC_HUMAN	QQGHEPVSPR	Gln->pyro-Glu (N-term Q); Phospho (ST)	8.8	88.0	100.0	11.4	
CALX_HUMAN	SDAEEDGGTVSQEEEDR	Phospho (ST)	9.6	94.1	97.1	10.2	
PLEC1_HUMAN	SSSVGSSSSYPISPAVSR	Phospho (ST)	10.2	30.7	100.0	9.8	
RBM26_HUMAN	LNHSPPQSSSR	Phospho (ST)	10.6	62.8	100.0	9.4	
TCOF_HUMAN	LGAGEGGEASVSPEK	Phospho (ST)	9.4	100.0	87.9	9.4	
MAML3_HUMAN	SPLNGDQQNGACDGNFSPTSK	Phospho (ST)	8.6	82.6	77.9	9.0	
IF4G1_HUMAN	AASLTEDR	Phospho (ST)	9.9	82.7	88.0	8.9	
APBA1_HUMAN	SNSQENVEASHPSQDGK	Phospho (ST)	12.1	56.9	100.0	8.2	
PLEC1_HUMAN	SDEGQLSPATR	Phospho (ST)	11.8	93.3	95.7	8.1	
NUCKS_HUMAN	EEDEEPESPPEK	Phospho (ST)	12.3	97.7	99.2	8.0	
HS90B_HUMAN	EISDDEAEEEK	Phospho (ST)	12.8	87.7	100.0	7.8	
DENR_HUMAN	LTVENSPK	Phospho (ST)	13.4	74.9	100.0	7.4	
TCF20_HUMAN	LNASPAAR	Phospho (ST)	13.9	17.5	100.0	7.2	
HS90B_HUMAN	IEDVGSDEEDDSGKDK	Phospho (ST)	11.7	100.0	82.8	7.1	
LA_HUMAN	FASDDEHDEHDENGATGPVK	Phospho (ST)	15.3	81.6	100.0	6.6	
MARCS_HUMAN	VNGDASPAAAESGAK	Phospho (ST)	16.2	88.2	100.0	6.2	

TBCD4_HUMAN	LGSVDSFER	Phospho (ST)	16.9	30.1	100.0	5.9	*
HS90B_HUMAN	EISDDEAEEEKGEK	Phospho (ST)	16.9	87.2	96.2	5.7	
TACC2_HUMAN	VQNSPPVGR	Phospho (ST)	17.7	87.1	100.0	5.7	
SRRM1_HUMAN	AASPSPQSVR	Phospho (ST)	17.8	76.1	100.0	5.6	
HTSF1_HUMAN	VLDEEGSER	Phospho (ST)	16.8	100.0	94.2	5.6	
SRRM1_HUMAN	RRTPSPPPR	2 Phospho (ST)	11.9	100.0	66.4	5.6	
HS90B_HUMAN	IEDVGSDEEDDSGK	Phospho (ST)	18.7	95.7	99.1	5.3	
ACLY_HUMAN	TASFSESR	Phospho (ST)	18.7	85.0	98.7	5.3	
NUCKS_HUMAN	EEDEEPESPPEKK	Phospho (ST)	17.8	100.0	91.7	5.2	
CD44_HUMAN	KPSGLNGEASK	Phospho (ST)	19.5	54.9	100.0	5.1	
SC31A_HUMAN	AQGEPVAGHESPK	Phospho (ST)	19.6	62.6	100.0	5.1	
NUCKS_HUMAN	TPSPKEEDEEPESPPEKK	Phospho (ST)	12.3	32.5	62.3	5.1	
MP2K2_HUMAN	LNQPGTPTR	Phospho (ST)	20.2	86.5	100.0	5.0	
HS90B_HUMAN	EKEISDDEAEEEK	Phospho (ST)	16.5	89.1	81.6	4.9	
HIRP3_HUMAN	EVSDSEAGGGPQGER	Phospho (ST)	20.4	70.1	100.0	4.9	
PAXI_HUMAN	ISASSATR	Phospho (ST)	21.4	74.9	100.0	4.7	
MCM2_HUMAN	TDALTSSPGR	Phospho (ST)	22.3	87.5	100.0	4.5	
MARCS_HUMAN	AEDGATPSPSNETPK	Phospho (ST)	22.5	79.6	100.0	4.4	
S10AB_HUMAN	ISSPTETER	Phospho (ST)	23.5	51.0	100.0	4.3	
SIRT1_HUMAN	SPGEPGGAAPER	Phospho (ST)	23.5	86.8	100.0	4.3	
MELT_HUMAN	DRSLPR	Phospho (ST)	23.6	79.0	100.0	4.2	
ZEP2_HUMAN	RDLSPR	Phospho (ST)	23.6	79.0	100.0	4.2	
ZO3_HUMAN	TISEPDEQR	Phospho (ST)	23.9	85.6	100.0	4.2	
CALX_HUMAN	QKSDAEEDGGTVSQEEEDR	Gln->pyro-Glu (N-term Q); 2 Phospho (ST)	24.4	92.3	99.6	4.1	
TGON2_HUMAN	DSPSKSSAEAQTPEDTPNK	Phospho (ST)	24.8	86.7	100.0	4.0	
LRRF1_HUMAN	EILHNTEK	Phospho (ST)	25.0	47.4	100.0	4.0	
BCLF1_HUMAN	QKSPEIHR	Gln->pyro-Glu (N-term Q); Phospho (ST)	25.1	69.9	100.0	4.0	
SMRC2_HUMAN	SPSPSPTPEAK	Phospho (ST)	25.2	46.5	100.0	4.0	
LAP2B_HUMAN	AKTPVTLK	Phospho (ST)	25.6	95.6	98.2	3.8	
TCOF_HUMAN	KLSGDQPAAR	Phospho (ST)	26.3	87.2	100.0	3.8	
TCOF_HUMAN	KLSGDQPAAR	Phospho (ST)	26.3	87.2	100.0	3.8	
CX026_HUMAN	GADSGEEKEEGINR	Phospho (ST)	23.7	89.9	89.4	3.8	
EPIPL_HUMAN	AEAEAGSPRPDPR	Phospho (ST)	26.0	91.9	92.5	3.6	
WRIP1_HUMAN	RPAAAAAAGSASPR	Phospho (ST)	29.2	83.2	100.0	3.4	
SHRPN_HUMAN	SPGNLTER	Phospho (ST)	27.0	88.5	91.7	3.4	
PSA3_HUMAN	ESLKEEDESDDDNM	Phospho (ST)	27.9	95.0	92.2	3.3	
REPS1_HUMAN	SSSLDMNR	Phospho (ST)	31.0	85.5	100.0	3.2	
YBOX1_HUMAN	NEGSESAPEGQAQQR	Phospho (ST)	32.5	28.2	100.0	3.1	*
SRRM1_HUMAN	APQTSSSPPPVR	Phospho (ST)	33.6	80.5	100.0	3.0	
E41L1_HUMAN	DEDGESGGQRSEAEEGEVR	Phospho (ST)	29.4	100.0	84.5	2.9	
APIP_HUMAN	DISGPSPSKK	Phospho (ST)	35.4	67.8	100.0	2.8	

KC1E_HUMAN	IQPAGNTSPR	Phospho (ST)	35.9	57.1	100.0	2.8	
CDN1B_HUMAN	VSNGSPSLER	Phospho (ST)	36.4	87.3	100.0	2.7	
HSPB1_HUMAN	QLSSGVSEIR	Phospho (ST)	39.1	39.2	100.0	2.6	
LRC47_HUMAN	EEGSLSDTEADAVSGQLPDPTTNPSAGK	Phospho (ST)	35.1	85.6	88.6	2.5	
CI078_HUMAN	VGDTEKPEPERSPPNR	Phospho (ST)	41.0	83.0	100.0	2.4	
VINC_HUMAN	GQGSSPVAMQK	Phospho (ST)	16.2	100.0	39.4	2.4	
NMT1_HUMAN	GGLSPANDTGAK	Phospho (ST)	37.4	100.0	89.0	2.4	
SSRP1_HUMAN	EFVSSDESSSGENK	Phospho (ST)	40.3	84.8	94.6	2.4	
F86C1_HUMAN	DSSDSELLR	Phospho (ST)	39.5	76.5	92.1	2.3	
TB182_HUMAN	ASPEPPGPESSSR	Phospho (ST)	42.9	74.3	100.0	2.3	
CTND1_HUMAN	VGGSSVDLHR	Phospho (ST)	42.9	74.6	100.0	2.3	
MRP_HUMAN	AAATPESQEPQAK	Phospho (ST)	43.9	39.5	100.0	2.3	
TPIS_HUMAN	QSLGELIGTLNAAK	Phospho (ST)	44.2	37.8	100.0	2.3	
HDGR2_HUMAN	ADSDGAKPEPVAMAR	Phospho (ST)	44.6	61.1	100.0	2.2	
T22D4_HUMAN	NGSPPPGAPSSR	Phospho (ST)	46.9	36.2	100.0	2.1	
SET_HUMAN	RQSPLPPQK	Phospho (ST)	47.3	81.0	100.0	2.1	
TRI16_HUMAN	ETEEQDSDSAEQGDPAGEGK	Phospho (ST)	49.4	33.4	100.0	2.0	

Appendix 4

Summary of phosphorylation events found to be dependent on Akt1 by an *in vitro* reaction followed by phosphoproteomic analysis in MCF10A cells (Chapter 5.4.2.).

		- Akt1					+ Akt1						
Accession Number	Phosphopepide Identification	Mean Peptide Intensity 0 µM ATP	Mean Peptide Intensity 10 µM ATP	Mean Peptide Intensity 50 µM ATP	Mean Peptide Intensity 100 µM ATP	Mean Peptide Intensity 500 µM ATP	Mean Peptide Intensity 0 µM ATP	Mean Peptide Intensity 10 µM ATP	Mean Peptide Intensity 50 µM ATP	Mean Peptide Intensity 100 µM ATP	Mean Peptide Intensity 500 µM ATP	Fold 100 +/-	Known Akt Substrate
NUCKS_HUMAN	NUCKS1 p-S59 p-S62 (z= 2)	1.0	1.2	0.5	0.0	2.2	17.0	52.3	13.9	32.6	16.7	697.4	
MOL1A_HUMAN	MOBKL1A p-T36 (z= 2)	0.0	0.0	1.3	0.2	0.0	0.0	25.5	59.9	76.5	95.3	509.7	
AKTS1_HUMAN	AKT1S1 p-T247 (z= 2)	0.0	0.8	0.6	0.1	0.4	0.0	7.6	24.3	44.2	92.6	469.1	*
LMNA_HUMAN	LMNA p-S637 (z= 2)	0.0	0.0	0.0	0.2	0.0	50.1	93.6	93.8	76.8	84.6	365.3	*
NSUN2_HUMAN	NSUN2 p-S752 (z= 3)	0.0	0.0	0.0	0.3	0.0	0.0	94.7	91.3	98.7	0.0	330.1	
AKT1_HUMAN	AKT1 p-S125 (z= 2)	1.9	1.1	0.0	0.2	0.6	90.6	69.2	56.6	48.9	45.3	292.5	
NUCL_HUMAN	NCL p-S146 p-S154 (z= 3)	0.0	0.0	0.0	0.2	0.0	9.9	81.3	45.7	41.0	26.4	240.1	
IF2B_HUMAN	EIF2S2 p-T32 (z= 3)	0.0	0.0	2.2	0.4	5.1	0.0	46.7	74.0	85.0	91.6	222.8	
HNRPU_HUMAN	HNRNPU p-S60 (z= 3) + oxidation	0.0	0.0	0.0	0.4	0.0	0.0	23.7	43.7	77.2	92.8	215.9	
ENPL_HUMAN	HSP90B1 p-S65 (z= 2)	0.0	0.0	0.0	0.3	0.0	45.6	48.1	62.9	60.2	99.3	214.5	
TXLNA_HUMAN	TXLNA p-S516 (z= 2)	17.0	18.0	12.6	0.3	11.8	74.1	48.0	42.8	51.6	53.4	171.5	
SRRM2_HUMAN	SRRM2 p-S2045 p-S2047 (z= 2)	0.0	0.0	0.0	0.3	71.8	0.0	50.0	0.0	39.6	94.4	156.5	
SGIP1_HUMAN	SGIP1 p-S161 (z= 2)	0.0	0.0	0.0	0.4	1.4	97.6	67.4	60.3	59.7	71.4	150.4	
HDGR2_HUMAN	HDGFRP2 p-T608 (z= 4)	0.0	0.0	0.0	0.6	0.0	0.0	20.6	43.9	76.9	86.3	134.9	
NEK9_HUMAN	NEK9 p-S945 (z= 3)	0.0	0.0	0.0	0.6	0.0	46.9	66.5	66.1	80.0	91.3	127.3	
MYH9_HUMAN	MYH9 p-S1944 (z= 2)	0.0	0.0	5.6	0.6	0.0	40.0	70.0	71.2	63.3	49.1	112.3	
HS90A_HUMAN	HSP90AA1 p-S232 (z= 2)	0.0	3.3	1.6	0.7	2.4	40.9	63.6	46.3	79.5	65.6	110.8	
RLA0L_HUMAN	ZRANB2 p-S308 (z= 2) + oxidation	0.0	0.0	0.0	0.9	44.9	7.1	53.4	72.7	94.9	74.9	107.9	
RERE_HUMAN	RERE p-S657 (z= 2)	0.0	0.0	0.0	1.1	0.0	36.6	52.3	43.7	95.1	83.6	86.9	
HDGF_HUMAN	HDGF p-S133 p-S134 (z= 3)	0.0	12.9	5.5	0.6	8.7	38.7	98.9	71.1	54.7	52.8	84.9	
KPCD_HUMAN	PRKCD p-S665 (z= 2)	0.0	0.0	0.0	0.6	1.2	82.9	91.5	85.7	48.6	32.4	84.7	
ODPAT_HUMAN	PDHA2 p-S292 (z= 3)	0.0	0.0	0.0	0.9	0.0	33.2	73.2	80.4	71.9	84.4	83.6	
BCKD_HUMAN	BCKDK p-T33 (z= 3) + oxidation	15.3	20.7	39.6	1.0	9.9	46.1	57.9	54.5	79.2	87.3	83.3	
LR16A_HUMAN	LRRC16A p-S969 (z= 2)	9.5	19.7	22.2	0.7	23.9	88.1	46.4	75.3	60.1	63.4	80.4	
VPS4B_HUMAN	VPS4B p-S103 (z= 2)	0.0	0.0	0.0	1.0	0.0	30.6	50.0	20.2	76.1	39.1	75.3	
ARD1A_HUMAN	ARD1A p-S187 (z= 2)	0.0	0.0	0.0	1.2	0.0	44.3	52.7	40.1	87.4	72.0	75.3	
G3P_HUMAN	GAPDH p-T185 (z= 3) + oxidation	0.0	0.0	0.0	0.4	0.0	24.4	68.6	11.0	28.5	27.8	71.8	
TFAM_HUMAN	TFAM p-S125 (z= 2)	0.0	0.0	0.0	1.0	0.0	76.7	51.2	68.2	69.0	97.5	70.3	
RMTL1_HUMAN	RNMTL1 p-S64 (z= 2)	0.0	0.0	0.0	1.0	12.1	0.0	17.2	40.8	66.6	86.6	63.9	

I2BP2_HUMAN	IRF2BP2 p-S461 (z= 2) + oxidation	22.9	12.1	9.0	1.3	15.2	47.9	37.9	26.9	83.6	79.2	63.9	
K1C18_HUMAN	KRT18 p-S399 (z= 2)	0.0	0.0	0.0	1.4	0.0	0.0	28.0	64.9	84.6	87.4	60.9	
STX4_HUMAN	STX4 p-S16 (z= 2)	0.0	0.0	0.0	0.7	0.0	12.9	53.1	14.0	44.6	22.4	60.3	
CD44_HUMAN	CD44 p-S698 (z= 2)	0.0	0.0	0.0	0.9	0.0	16.3	39.2	33.9	51.6	50.0	58.7	
NEK9_HUMAN	NEK9 p-S945 (z= 3) + oxidation	0.0	0.0	0.0	1.4	0.0	10.2	36.4	77.5	72.0	83.9	50.6	
IF2B_HUMAN	EIF2S2 p-T32 p-T37 (z= 3)	0.0	0.0	0.0	1.3	0.0	0.0	8.2	57.3	63.1	98.9	50.2	
I2BP1_HUMAN	IRF2BP1 p-S385 (z= 2)	22.4	11.7	0.0	1.2	7.7	83.9	50.8	49.8	55.8	64.5	47.5	
CTR9_HUMAN	CTR9 p-S942 (z= 2)	0.0	0.0	0.0	1.7	0.0	50.0	14.1	39.9	80.4	64.8	47.0	
CHRC1_HUMAN	CHRAC1 p-S125 (z= 3)	0.0	0.0	0.0	1.5	0.0	46.0	45.4	50.0	69.0	89.9	46.8	
AKT1_HUMAN	AKT1 p-S125 (z= 3)	3.2	2.4	1.7	1.5	2.8	99.4	83.2	75.1	60.9	54.4	41.7	
RS6_HUMAN	RPS6 p-S237 (z= 2)	0.0	8.9	15.2	0.9	28.0	7.4	9.6	43.0	35.7	94.0	37.9	*
RL17_HUMAN	RPL17 p-S6 (z= 2)	0.0	0.0	0.0	2.5	0.0	17.1	55.7	72.8	91.4	93.9	36.2	
NEK9_HUMAN	NEK9 p-S856 p-S869 (z= 3)	0.0	0.0	0.0	2.2	0.0	0.0	44.7	76.3	76.7	87.1	35.6	
RBGP1_HUMAN	RABGAP1 p-S43 (z= 2)	27.5	13.8	26.7	1.5	33.1	79.7	60.1	62.6	52.5	63.0	34.3	
VPS4B_HUMAN	VPS4B p-S103 (z= 2)	0.0	0.0	0.0	1.2	0.0	26.0	69.1	32.5	38.3	21.9	32.1	
YBOX1_HUMAN	YBX1 p-T272 (z= 3)	0.0	0.0	0.0	1.5	0.0	0.0	29.8	44.0	48.5	88.8	32.0	*
CALX_HUMAN	CANX p-S75 (z= 2)	0.0	0.0	0.0	2.2	0.0	0.0	12.2	3.1	66.4	50.0	30.7	
IF2B_HUMAN	EIF2S2 p-T37 (z= 3)	0.0	0.0	1.0	2.0	3.2	1.4	38.9	75.0	52.9	82.8	26.6	
AN32B_HUMAN	ANP32B p-T245 (z= 2)	0.0	0.0	0.0	2.3	42.9	21.3	77.3	64.6	59.8	41.9	25.6	
HUWE1_HUMAN	HUWE1 p-T656 (z= 2)	0.0	2.5	5.4	3.9	3.1	78.3	69.6	94.8	89.6	68.1	23.0	
NUCKS_HUMAN	NUCKS1 p-S62 (z= 2)	9.7	11.3	6.8	2.4	7.9	48.1	60.5	34.4	54.5	40.2	23.0	
CD11A_HUMAN	CDK11A p-S48 (z= 2)	0.0	9.0	0.0	3.6	14.6	0.0	41.3	55.2	81.4	92.7	22.9	
AKT1_HUMAN	AKT1 p-S123 p-S127 (z= 2)	0.0	0.0	0.0	2.4	0.0	42.2	96.4	73.1	50.1	50.8	20.9	
AKT1_HUMAN	AKT1 p-S125 (z= 3) + oxidation	0.0	0.0	0.0	4.5	1.9	86.1	78.3	64.5	94.7	73.7	20.9	
FKB15_HUMAN	FKBP15 p-S961 (z= 3)	18.0	22.1	5.4	4.3	4.9	93.8	69.3	77.9	79.4	79.2	18.5	
HNRL2_HUMAN	HNRNPUL2 p-S186 (z= 3)	0.0	0.0	0.0	4.1	0.0	50.0	40.7	29.9	67.6	55.4	16.3	
MCM2_HUMAN	MCM2 p-S42 (z= 2)	17.0	9.6	13.1	5.3	10.0	90.7	75.3	69.9	82.4	82.6	15.4	
SRRM2_HUMAN	SRRM2 p-S1500 (z= 2)	13.6	32.7	47.0	1.5	54.8	0.0	35.0	16.6	23.0	49.3	15.0	
HNRPD_HUMAN	HNRNPD p-S191 (z= 2)	0.0	50.0	0.0	1.8	82.2	0.0	37.7	0.0	25.5	0.0	14.5	
LIPB1_HUMAN	PPFIBP1 p-S795 (z= 2)	24.9	29.0	22.8	6.1	7.8	95.0	69.5	69.8	83.3	82.7	13.8	
EF1B_HUMAN	EEF1B2 p-S107 (z= 4)	0.0	3.9	3.9	2.8	8.7	96.1	79.1	55.5	38.2	43.1	13.5	
G3P_HUMAN	GAPDH p-T185 (z= 3)	0.0	0.5	0.6	0.6	3.4	36.5	60.7	3.9	7.6	3.6	13.4	
NUCKS_HUMAN	NUCKS1 p-S59 (z= 3)	6.0	4.1	3.7	4.0	9.7	47.3	59.1	34.7	51.5	36.9	12.8	
GYS1_HUMAN	GYS1 p-S654 (z= 3)	27.1	8.7	8.8	5.5	13.3	59.1	56.4	63.8	70.5	56.3	12.8	
TBB2C_HUMAN	TUBB2C p-S96 (z= 3)	17.6	0.0	4.4	7.3	10.1	9.5	62.4	27.6	85.0	82.9	11.6	
PGAM1_HUMAN	PGAM1 p-S15 (z= 2)	13.1	11.6	9.2	5.5	19.7	84.8	67.3	58.0	62.6	56.8	11.5	
CIP4_HUMAN	TRIP10 p-S297 (z= 2)	0.0	4.9	9.4	4.8	0.0	82.5	48.3	47.4	55.2	51.9	11.4	
SRRM1_HUMAN	SRRM1 p-S753 (z= 2)	0.0	0.0	0.0	6.4	14.5	22.9	29.0	39.5	71.8	88.2	11.2	
SRRM2_HUMAN	SRRM2 p-S1926 p-T1928 (z= 2)	7.7	4.7	4.6	7.2	18.6	36.0	61.1	59.9	80.7	80.4	11.2	
CC124_HUMAN	CCDC124 p-S142 (z= 2)	0.0	0.0	0.0	5.1	13.1	0.0	11.7	27.8	56.2	92.8	11.0	
SLU7_HUMAN	SLU7 p-S216 (z= 2)	7.5	0.0	0.0	8.5	12.9	55.0	47.6	40.9	84.1	71.9	9.9	
HNRPU_HUMAN	HNRNPU p-S60 (z= 3)	0.0	1.1	4.0	5.3	6.4	0.3	35.0	72.8	46.7	85.9	8.8	
HS90A_HUMAN	HSP90AA1 p-S232 (z= 3)	0.0	0.0	0.0	5.6	20.8	49.5	79.3	54.9	46.1	38.6	8.2	

CQ100_HUMAN	C17orf100 p-S55 (z= 2)	60.1	86.3	14.0	2.3	21.7	42.7	15.3	1.7	18.4	91.6	8.1	
HSF1_HUMAN	HSF1 p-S315 (z= 3)	0.0	0.0	16.4	9.1	20.2	78.0	0.0	33.7	69.7	14.3	7.7	
IWS1_HUMAN	IWS1 p-S238 (z= 3)	37.0	37.1	25.4	9.3	17.3	96.4	79.1	67.1	70.6	53.4	7.6	
CALX_HUMAN	CANX p-S584 (z= 2)	18.8	20.6	13.3	9.4	16.8	87.5	66.1	62.8	70.9	76.4	7.5	
MK01_HUMAN	MAPK1 p-Y188 (z= 3)	9.5	10.4	11.3	10.2	14.7	82.9	77.8	87.4	75.8	76.2	7.5	
MK01_HUMAN	MAPK1 p-T186 (z= 3)	9.5	10.4	11.3	10.2	14.7	82.9	77.8	87.4	75.8	76.2	7.5	
HNRPD_HUMAN	HNRNPD p-S83 (z= 3)	26.9	11.6	21.5	11.2	29.9	63.0	76.8	74.4	82.5	92.1	7.4	
RS17_HUMAN	RPS17 p-S116 (z= 2) + oxidation	0.0	7.1	22.0	11.1	23.6	5.6	43.2	60.0	81.3	71.0	7.3	
SSH3_HUMAN	SSH3 p-S650 (z= 2)	0.0	0.0	0.0	13.7	0.0	23.2	58.8	63.8	98.5	85.3	7.2	
TRI16_HUMAN	TRIM16 p-S61 (z= 2)	7.1	0.0	0.0	9.9	24.9	50.0	86.8	79.3	70.3	66.9	7.1	
RRBP1_HUMAN	RRBP1 p-S979 (z= 2)	0.0	0.0	0.0	11.1	0.0	0.0	29.0	57.2	78.6	89.8	7.1	
FRIH_HUMAN	FTH1 p-S180 (z= 3)	23.4	13.6	17.8	4.9	23.5	50.0	53.1	29.4	34.1	20.5	7.0	
TCOF_HUMAN	TCOF1 p-S1411 (z= 2)	14.9	14.6	5.3	11.7	5.9	26.0	30.9	55.0	80.3	94.0	6.9	
PGRC1_HUMAN	PGRMC1 p-S182 (z= 3)	11.8	11.3	11.2	8.5	7.8	91.5	82.4	69.3	57.9	60.9	6.8	
PGRC1_HUMAN	PGRMC1 p-Y181 (z= 3)	11.8	11.3	11.2	8.5	7.8	91.5	82.4	69.3	57.9	60.9	6.8	
CALX_HUMAN	CANX p-S555 (z= 3)	9.8	12.6	16.9	12.0	13.6	99.9	83.1	76.7	81.3	88.7	6.8	
IWS1_HUMAN	IWS1 p-S399 (z= 2)	0.0	12.1	12.4	9.6	23.2	92.2	87.2	71.4	64.5	51.7	6.7	
SRRM1_HUMAN	SRRM1 p-S563 (z= 2)	52.0	13.5	12.3	2.6	0.0	62.0	35.3	22.6	16.7	0.0	6.4	
DAP1_HUMAN	DAP p-S52 (z= 3)	15.0	4.6	10.1	10.7	8.5	84.7	76.2	51.0	66.5	41.5	6.2	
KPCD_HUMAN	PRKCD p-S507 (z= 2)	34.3	27.2	27.4	10.9	14.3	84.1	72.0	77.8	66.2	37.3	6.1	
BCLF1_HUMAN	BCLAF1 p-S649 (z= 2)	23.1	21.5	35.8	13.1	19.5	48.8	59.8	76.4	76.9	93.2	5.9	
IWS1_HUMAN	IWS1 p-S514 (z= 2)	12.7	11.0	8.1	10.5	15.4	52.3	85.0	61.2	61.6	61.8	5.9	
CTR9_HUMAN	CTR9 p-S942 (z= 3)	0.0	0.0	0.0	15.5	29.8	50.0	57.1	71.8	90.7	73.3	5.9	
HS90B_HUMAN	HSP90AB1 p-S262 (z= 3)	0.0	6.1	17.6	13.0	41.7	76.5	97.0	82.9	73.0	66.9	5.6	
HSP74_HUMAN	HSPA4 p-S648 (z= 2)	4.7	3.9	3.1	2.8	3.9	4.3	9.3	4.3	15.3	51.3	5.5	
NP1L4_HUMAN	NAP1L4 p-S126 (z= 3)	31.4	39.1	27.3	13.1	27.9	94.1	80.8	78.1	70.4	58.6	5.4	
TIF1B_HUMAN	TRIM28 p-S51 (z= 3)	30.2	17.2	7.4	9.2	5.9	88.5	82.5	70.2	49.5	53.5	5.4	
HS90B_HUMAN	HSP90AB1 p-S227 (z= 2)	10.5	0.0	0.0	11.8	24.9	71.1	90.5	79.1	62.5	50.1	5.3	
SRRM1_HUMAN	SRRM1 p-S798 (z= 2)	89.3	8.8	32.7	7.0	0.0	62.4	40.2	19.4	36.4	27.7	5.2	
MP2K2_HUMAN	MAP2K2 p-T395 (z= 2)	9.6	8.4	8.4	7.1	11.2	5.5	64.1	0.0	37.0	50.0	5.2	
PSD3_HUMAN	PSD3 p-S339 (z= 2)	15.7	21.8	10.4	13.7	0.0	90.4	90.6	88.8	70.6	48.8	5.2	
TB182_HUMAN	TNKS1BP1 p-S1025 (z= 3)	16.3	0.0	11.7	10.9	13.8	90.4	66.5	74.7	55.5	60.3	5.1	
CALX_HUMAN	CANX p-S584 (z= 3)	23.9	23.6	18.6	15.5	27.4	85.9	72.7	70.4	77.0	84.8	5.0	
LEO1_HUMAN	LEO1 p-S172 (z= 2)	0.0	0.0	0.0	10.7	0.0	66.9	77.3	65.6	52.9	45.2	5.0	
CX026_HUMAN	CXorf26 p-S198 (z= 3)	71.2	32.2	46.0	15.7	36.7	96.0	76.7	86.2	75.2	65.3	4.8	
SNX9_HUMAN	SNX9 p-S182 (z= 3)	71.2	32.2	46.0	15.7	36.7	96.0	76.7	86.2	75.2	65.3	4.8	
TBA1A_HUMAN	TUBA1A p-S49 (z= 2)	0.0	0.0	8.7	17.1	17.8	55.2	74.8	66.3	81.9	97.7	4.8	
SMAP_HUMAN	SMAP p-S16 (z= 3)	44.1	47.5	34.5	13.8	33.0	92.1	83.2	76.0	63.2	69.1	4.6	
MARCS_HUMAN	MARCKS p-S146 (z= 2)	40.4	19.8	36.4	13.6	28.3	84.5	79.2	58.7	61.6	61.3	4.5	
TCOF_HUMAN	TCOF1 p-S1351 (z= 2)	19.5	0.0	13.6	18.5	31.1	55.9	47.7	55.4	82.9	79.3	4.5	
COPB2_HUMAN	COPB2 p-T870 (z= 3)	26.4	74.1	63.6	17.5	19.8	34.2	78.6	73.4	77.7	84.9	4.4	
HDGF_HUMAN	HDGF p-S133 p-S134 (z= 2)	15.9	26.8	12.8	11.0	17.6	61.5	96.6	71.9	48.2	45.7	4.4	
SRRM1_HUMAN	SRRM1 p-S770 p-S776 (z= 3)	10.3	0.0	0.0	11.8	29.1	23.3	90.3	74.8	51.5	46.2	4.4	

DPOD3_HUMAN	POLD3 p-S308 (z= 2)	0.0	36.2	39.6	20.2	46.6	8.2	61.8	71.7	88.0	86.0	4.4	
LA_HUMAN	SSB p-S367 (z= 4)	31.5	49.4	53.7	22.3	52.4	85.2	83.5	77.4	96.4	85.7	4.3	
AGM1_HUMAN	PGM3 p-S65 (z= 2)	5.5	5.0	8.4	11.7	15.1	84.6	58.7	45.7	50.5	51.1	4.3	
CHSP1_HUMAN	CARHSP1 p-S53 (z= 2)	30.0	29.1	19.4	14.3	35.7	38.2	29.3	37.8	61.0	87.4	4.3	*
SSH3_HUMAN	SSH3 p-S38 (z= 2)	6.3	17.0	43.3	17.0	57.3	20.8	37.1	57.5	71.8	99.7	4.2	
RSLBA_HUMAN	RSLBA p-S42 (z= 2) + oxidation	6.3	17.0	43.3	17.0	57.3	20.8	37.1	57.5	71.8	99.7	4.2	
HSPB1_HUMAN	HSPB1 p-S83 (z= 2)	11.1	19.8	29.1	19.0	69.9	14.1	21.4	41.7	79.0	94.1	4.2	
G3BP1_HUMAN	G3BP1 p-S233 (z= 2)	50.3	46.4	40.6	13.9	24.7	96.0	67.5	47.9	57.6	52.0	4.2	
CX026_HUMAN	CXorf26 p-S198 (z= 2)	53.8	16.4	32.0	17.5	33.5	88.4	81.0	79.4	72.6	63.7	4.2	
RSRC2_HUMAN	RSRC2 p-S31 (z= 2)	36.7	56.2	40.4	16.0	37.8	80.3	60.2	47.8	65.8	68.4	4.1	
ANK1_HUMAN	ANK1 p-T15 (z= 2)	2.2	3.0	11.5	10.1	34.9	10.6	14.9	35.5	40.4	94.6	4.0	
BCLF1_HUMAN	BCLAF1 p-S178 (z= 2)	49.8	59.9	43.5	18.1	32.5	87.0	65.2	65.8	71.3	71.5	3.9	
E41L1_HUMAN	EPB41L1 p-S651 (z= 2)	0.0	28.9	6.9	18.0	28.4	15.2	58.0	97.9	70.6	62.6	3.9	
SRRM1_HUMAN	SRRM1 p-S697 (z= 2)	52.1	44.5	59.0	22.6	65.4	87.1	64.5	77.1	88.6	93.2	3.9	
CTR9_HUMAN	CTR9 p-T976 (z= 2)	12.4	5.1	3.5	18.9	61.6	36.2	86.5	89.4	73.4	69.0	3.9	
NP1L4_HUMAN	NAP1L4 p-S126 (z= 3)	29.0	0.0	31.9	8.6	0.0	88.5	73.7	22.6	33.1	71.2	3.9	
SRRM1_HUMAN	SRRM1 p-S598 (z= 2)	50.9	73.5	46.6	13.7	35.7	71.8	47.5	50.5	51.7	59.5	3.8	
HDGF_HUMAN	HDGF p-S166 (z= 3)	48.1	55.7	49.8	19.6	44.8	94.1	61.9	56.0	73.6	69.5	3.7	
NIBL1_HUMAN	FAM129B p-S653 (z= 3)	0.0	0.0	6.1	2.2	100.0	0.0	0.0	10.0	8.1	12.2	3.7	
MYL9_HUMAN	MYL9 p-S21 (z= 2) + oxidation	67.5	52.1	61.2	20.7	34.1	83.1	52.0	54.3	77.3	79.1	3.7	
IWS1_HUMAN	IWS1 p-S514 (z= 3)	15.4	7.1	12.3	16.6	24.8	50.0	80.7	62.7	61.5	58.0	3.7	
ZC3HF_HUMAN	ZC3H15 p-S382 (z= 2)	0.0	0.0	43.6	21.7	40.0	0.0	15.9	34.2	80.4	93.5	3.7	
PDPK1_HUMAN	PDPK1 p-S242 (z= 2)	74.4	66.1	54.1	17.4	37.5	95.3	91.4	74.2	64.4	82.4	3.7	
PEBP1_HUMAN	PEBP1 p-S53 (z= 2)	73.7	74.4	52.0	17.5	35.4	91.1	76.6	80.1	64.1	73.5	3.7	
RFIP1_HUMAN	RAB11FIP1 p-S235 (z= 3)	0.0	0.0	0.0	23.8	0.0	0.0	0.0	50.0	87.2	0.0	3.7	
MARK2_HUMAN	MARK2 p-S572 (z= 2)	0.0	22.9	28.2	21.4	14.7	0.0	36.9	61.2	77.1	91.1	3.6	
E41L1_HUMAN	EPB41L1 p-S668 (z= 2)	2.3	1.9	1.5	21.3	3.5	14.6	8.4	58.7	76.6	88.5	3.6	
GFPT1_HUMAN	GFPT1 p-S262 (z= 2)	37.3	40.1	41.2	23.4	30.1	90.0	94.1	81.2	83.3	77.9	3.6	
SRRM1_HUMAN	SRRM1 p-S739 (z= 2)	44.0	29.6	54.5	24.4	55.9	58.5	74.3	78.6	86.5	90.4	3.5	
I2BP2_HUMAN	IRF2BP2 p-S361 (z= 3)	81.2	87.0	87.9	21.9	47.1	79.7	52.7	57.6	77.7	76.0	3.5	
SOX9_HUMAN	SOX9 p-S217 (z= 4)	88.8	82.0	36.8	20.5	63.4	24.3	66.9	56.9	72.2	50.0	3.5	
YBOX1_HUMAN	YBX1 p-S175 (z= 2)	0.0	0.0	0.0	23.5	66.8	15.5	57.8	84.8	79.6	86.2	3.4	*
GRLF1_HUMAN	GRLF1 p-S976 (z= 3)	47.6	46.5	34.2	19.3	12.0	95.8	66.5	57.6	64.9	54.2	3.4	
HUWE1_HUMAN	HUWE1 p-S1908 (z= 2)	28.4	25.2	20.2	13.9	21.7	83.6	59.6	62.1	46.8	53.8	3.4	
DCAF5_HUMAN	DCAF5 p-S629 (z= 2)	78.0	65.2	48.4	14.6	45.2	93.4	59.4	44.1	48.5	24.1	3.3	
SFRS7_HUMAN	SFRS7 p-S193 (z= 2)	22.5	40.1	37.0	28.5	68.0	34.4	84.4	95.0	94.4	81.2	3.3	
TTL12_HUMAN	TTLL12 p-S17 (z= 3)	90.6	79.4	37.5	27.0	61.7	83.4	93.4	81.4	88.3	39.6	3.3	
H90B2_HUMAN	HSP90AB2P p-S178 (z= 3)	7.1	3.5	12.7	21.7	65.8	59.7	97.0	87.2	70.7	62.5	3.3	
DC1L2_HUMAN	DYNC1LI2 p-S195 (z= 2)	42.7	51.3	27.5	16.5	45.0	93.9	91.1	77.1	53.6	55.5	3.3	
WAC_HUMAN	WAC p-S512 (z= 3)	56.7	49.8	40.6	20.0	26.5	73.7	47.9	55.4	64.4	76.8	3.2	
AHNK_HUMAN	AHNAK p-S5732 (z= 2)	42.6	72.5	25.2	10.6	23.2	63.4	41.2	30.6	33.9	36.3	3.2	
LMNA_HUMAN	LMNA p-S393 (z= 2)	25.1	20.3	38.4	25.8	32.0	45.7	71.4	74.4	82.0	93.8	3.2	*
AHNK_HUMAN	AHNAK p-S217 (z= 2)	79.4	73.0	77.6	29.2	63.4	99.4	73.2	77.1	92.8	92.0	3.2	

PARVA_HUMAN	PARVA p-T37 (z= 2)	0.0	0.0	0.0	21.0	8.5	0.0	8.3	46.5	66.9	92.1	3.2	
PHYD1_HUMAN	PHYD1 p-T126 (z= 2)	0.0	0.0	0.0	21.0	8.5	0.0	8.3	46.5	66.9	92.1	3.2	
DOCK3_HUMAN	DOCK3 p-S837 (z= 2)	0.0	0.0	0.0	21.0	8.5	0.0	8.3	46.5	66.9	92.1	3.2	
IQGA1_HUMAN	IQGA1 p-S815 (z= 2)	0.0	0.0	0.0	21.0	8.5	0.0	8.3	46.5	66.9	92.1	3.2	
G3P_HUMAN	GAPDH p-S84 (z= 2)	68.5	33.6	34.5	19.5	35.5	99.7	64.1	26.8	61.7	66.6	3.2	
HDGF_HUMAN	HDGF p-S166 (z= 2)	33.1	28.2	20.7	24.1	46.9	93.2	78.2	70.2	75.9	64.6	3.2	
ATX2L_HUMAN	ATX2L p-S410 (z= 2)	33.1	28.2	20.7	24.1	46.9	93.2	78.2	70.2	75.9	64.6	3.2	
AKAP3_HUMAN	AKAP3 p-S206 (z= 2)	33.1	28.2	20.7	24.1	46.9	93.2	78.2	70.2	75.9	64.6	3.2	
IF2B_HUMAN	EIF2S2 p-T34 (z= 3) + oxidation	0.0	0.0	0.0	28.5	0.0	0.0	34.4	50.5	89.4	86.7	3.1	
MCM2_HUMAN	MCM2 p-S28 (z= 2)	57.3	56.5	49.3	20.3	50.0	90.5	59.6	55.4	63.6	67.2	3.1	
SRRM1_HUMAN	SRRM1 p-S739 p-S741 (z= 2)	6.8	4.9	0.0	17.4	17.4	51.6	65.8	54.9	53.8	51.2	3.1	
RHG12_HUMAN	ARHGAP12 p-S241 (z= 3)	20.0	47.2	22.3	26.0	64.2	91.7	75.6	80.7	80.3	71.1	3.1	
LRRF2_HUMAN	LRRFIP2 p-S329 (z= 2)	42.9	40.5	32.1	15.7	18.0	94.2	51.6	48.6	48.3	49.0	3.1	
TLE3_HUMAN	TLE3 p-S204 (z= 2)	58.8	43.0	28.0	18.4	34.8	95.9	67.3	60.3	56.7	52.0	3.1	
SPTB2_HUMAN	SPTBN1 p-S2103 (z= 2)	90.7	68.0	76.5	25.6	62.6	70.6	49.4	68.9	78.6	85.1	3.1	
RS17_HUMAN	RPS17 p-S114 (z= 2)	3.1	17.2	28.1	27.5	55.7	4.2	53.6	66.3	84.2	62.0	3.1	
PAXI_HUMAN	PXN p-S534 (z= 3)	88.6	98.4	70.7	18.1	41.5	70.7	20.6	38.8	55.5	47.1	3.1	
HDGF_HUMAN	HDGF p-S133 p-S134 (z= 3)	24.4	28.4	15.3	17.9	27.5	60.3	98.3	72.9	54.2	49.0	3.0	
TCAL3_HUMAN	TCEAL3 p-S122 (z= 2)	82.8	62.6	79.1	21.4	55.9	70.2	70.6	55.2	64.5	58.2	3.0	
AKT1_HUMAN	AKT1 p-S125 (z= 2) + oxidation	0.0	0.0	0.0	28.7	0.0	71.7	99.3	76.7	84.7	76.3	3.0	
PYRG1_HUMAN	CTPS p-S576 (z= 3)	26.5	39.2	30.4	15.2	9.9	98.1	69.1	50.6	43.0	42.2	2.8	
ADIP_HUMAN	SSX2IP p-T7 (z= 3)	0.0	0.0	0.0	28.9	0.0	47.3	17.7	50.0	81.6	71.0	2.8	
APIP_HUMAN	APIP p-S88 (z= 2)	52.8	16.2	24.5	31.0	73.0	54.7	69.0	64.1	87.5	79.3	2.8	
NIBL1_HUMAN	FAM129B p-S679 (z= 2)	64.6	57.0	49.0	22.4	35.8	98.4	76.8	59.6	63.0	61.2	2.8	
FA40A_HUMAN	FAM40A p-S336 (z= 2)	12.0	4.8	11.2	13.9	1.7	91.8	59.4	72.9	38.8	82.3	2.8	
RSRC2_HUMAN	RSRC2 p-S33 (z= 2)	55.1	60.4	55.1	28.6	48.6	96.8	66.4	69.8	79.1	78.9	2.8	
ZEP2_HUMAN	HIVEP2 p-S2131 (z= 2)	13.5	5.7	0.0	30.0	38.1	55.9	62.4	65.0	81.9	77.8	2.7	
MELT_HUMAN	VEPH1 p-S784 (z= 2)	13.5	5.7	0.0	30.0	38.1	55.9	62.4	65.0	81.9	77.8	2.7	
HSPB1_HUMAN	HSPB1 p-S84 (z= 2)	6.1	8.0	17.8	15.2	57.4	10.3	13.9	33.1	41.4	90.5	2.7	
NP1L4_HUMAN	NAP1L4 p-S126 (z= 3)	49.4	37.3	39.2	21.8	49.5	82.8	86.0	80.1	59.3	60.6	2.7	
COHA1_HUMAN	COL17A1 p-S149 (z= 2)	5.8	0.0	0.0	18.6	72.4	8.2	25.7	23.7	50.4	60.4	2.7	
HMGA1_HUMAN	HMGA1 p-S100 p-S103 (z= 3)	0.0	0.0	7.6	26.6	6.4	0.0	73.7	93.2	72.2	52.6	2.7	
CHD4_HUMAN	CHD4 p-S1536 (z= 2)	50.0	27.1	32.3	28.6	56.9	51.6	68.3	76.7	77.3	93.8	2.7	
SRRM1_HUMAN	SRRM1 p-S432 (z= 2)	27.8	17.6	26.3	25.3	78.0	20.4	35.0	63.1	68.1	92.4	2.7	
MYL9_HUMAN	MYL9 p-T20 p-S21 (z= 2)	4.6	6.8	17.0	15.4	31.7	36.0	27.6	98.4	40.8	47.6	2.7	
HSF1_HUMAN	HSF1 p-S304 (z= 2)	53.7	73.7	49.6	11.5	24.3	43.7	29.3	25.4	30.5	33.9	2.6	
SRRM1_HUMAN	SRRM1 p-S561 (z= 2)	8.9	0.0	0.0	3.8	0.0	62.0	20.0	0.0	10.2	0.0	2.6	
F10A1_HUMAN	ST13 p-S77 p-S80 (z= 4)	15.8	14.2	18.4	15.0	22.4	50.6	50.0	69.1	39.4	43.4	2.6	
F10A4_HUMAN	FAM10A4 p-S73 (z= 4) + oxidation	15.8	14.2	18.4	15.0	22.4	50.6	50.0	69.1	39.4	43.4	2.6	
BL1S3_HUMAN	BLOC1S3 p-S28 (z= 2)	20.4	24.4	0.0	16.5	0.0	90.8	54.1	34.9	43.0	27.1	2.6	
SPTA2_HUMAN	SPTAN1 p-S1218 (z= 2)	41.1	36.4	37.3	23.8	41.7	87.2	63.2	63.6	61.8	63.5	2.6	
SRF_HUMAN	SRF p-S225 (z= 3)	89.8	64.9	67.8	28.9	38.0	91.2	64.3	67.4	74.6	82.8	2.6	
RLA2_HUMAN	RPLP2 p-S106 (z= 2) + oxidation	5.1	21.7	23.3	30.1	53.4	15.9	68.0	74.9	77.5	95.7	2.6	

NDRG1_HUMAN	NDRG1 p-S331 (z= 2)	40.7	46.2	30.0	22.1	49.5	38.0	27.9	35.7	56.4	87.5	2.6	
KPCD_HUMAN	PRKCD p-S646 (z= 2)	42.6	64.1	40.9	18.6	38.0	80.9	60.6	62.8	47.5	46.0	2.6	
HDGF_HUMAN	HDGF p-S134 (z= 3)	68.0	74.6	59.0	24.1	48.6	91.3	61.4	51.6	61.4	62.6	2.5	
BRAF_HUMAN	BRAF p-S366 (z= 3)	51.7	61.9	52.6	26.8	29.8	74.7	55.1	50.8	67.1	21.5	2.5	*
HDGF_HUMAN	HDGF p-S134 (z= 3)	85.3	57.5	55.4	27.1	61.5	72.0	63.7	66.5	67.7	58.5	2.5	
ABCF1_HUMAN	ABCF1 p-S110 (z= 3)	14.7	69.1	64.2	37.3	91.2	12.6	67.3	84.3	92.9	72.4	2.5	
RBM39_HUMAN	RBM39 p-S137 (z= 3)	68.9	77.2	59.6	25.8	40.5	84.2	60.8	65.2	63.9	67.3	2.5	
RS17_HUMAN	RPS17 p-S116 (z= 3)	5.8	15.3	28.7	32.4	71.7	4.6	46.8	60.9	79.0	50.1	2.4	
ICAL_HUMAN	CAST p-S244 (z= 3)	49.4	35.8	35.1	23.6	29.3	91.5	71.5	52.8	57.5	38.9	2.4	
TB22A_HUMAN	TBC1D22A p-S133 (z= 4)	65.3	0.0	0.0	14.7	93.3	35.3	46.1	0.0	35.6	38.6	2.4	
MRP_HUMAN	MARCKSL1 p-S23 (z= 2)	98.2	87.3	87.6	18.4	75.5	63.1	44.1	37.9	44.4	44.4	2.4	
BAT3_HUMAN	BAT3 p-S114 (z= 4)	95.7	80.7	66.0	27.7	56.3	71.2	58.8	56.6	66.8	54.6	2.4	
OSBP1_HUMAN	OSBP p-S194 (z= 3)	14.1	34.0	19.3	21.6	34.9	89.9	87.7	67.6	52.0	49.3	2.4	
ILF3_HUMAN	ILF3 p-S383 (z= 3)	48.2	12.3	27.5	20.0	64.9	60.5	67.5	58.4	47.7	45.1	2.4	*
OGFR_HUMAN	OGFR p-S316 (z= 3)	67.5	40.3	44.0	30.2	38.7	85.9	61.5	57.5	71.4	66.7	2.4	
CJ047_HUMAN	C10orf47 p-S180 (z= 2)	71.6	84.4	69.8	24.6	43.3	79.0	46.7	47.2	58.1	61.2	2.4	
EMID1_HUMAN	EMID1 p-T81 p-Y82 (z= 2)	72.8	55.2	90.6	30.0	86.7	85.9	50.3	62.4	70.1	94.6	2.3	
BRAF_HUMAN	BRAF p-S730 (z= 2)	76.6	71.8	55.3	24.8	68.5	89.4	73.4	59.3	57.9	51.5	2.3	*
SRRM1_HUMAN	SRRM1 p-S617 (z= 2)	36.7	53.9	67.4	31.2	89.0	45.7	62.7	63.4	72.6	63.8	2.3	
AHNK_HUMAN	AHNAK p-S5732 (z= 2)	62.9	67.5	49.4	27.8	43.6	89.4	63.0	55.7	64.5	67.2	2.3	
NU214_HUMAN	NUP214 p-S431 (z= 2)	43.6	62.8	14.3	28.2	0.0	94.6	53.9	57.5	65.5	47.3	2.3	
HTSF1_HUMAN	HTATSF1 p-S580 (z= 2)	0.0	0.0	0.0	32.8	5.1	17.3	56.4	22.7	76.0	38.5	2.3	
HEG1_HUMAN	HEG1 p-T1083 (z= 2)	93.4	43.2	86.8	15.6	30.2	34.2	56.8	62.5	36.1	37.3	2.3	
ANK3_HUMAN	ANK3 p-S1406 (z= 2)	45.9	37.4	46.3	36.7	57.3	58.9	86.6	81.7	84.8	90.4	2.3	
PHC3_HUMAN	PHC3 p-S264 (z= 2)	21.3	20.6	21.1	30.1	66.7	46.4	45.0	39.4	69.1	76.4	2.3	
CDR2L_HUMAN	CDR2L p-S180 (z= 3)	43.1	45.6	37.8	30.7	42.6	71.6	50.3	44.6	70.3	64.2	2.3	
SRRM2_HUMAN	SRRM2 p-S2582 (z= 2)	60.3	68.9	78.5	16.4	39.9	39.9	24.4	29.8	37.4	36.6	2.3	
SFRS2_HUMAN	SFRS2 p-S27 (z= 2)	36.1	2.6	16.1	38.6	84.6	50.0	74.4	82.8	87.1	61.3	2.3	
SCRIB_HUMAN	SCRIB p-S1310 (z= 3)	97.5	78.8	60.6	30.1	59.2	81.3	80.0	82.4	67.7	65.1	2.3	
SFRS2_HUMAN	SFRS2 p-S190 p-S192 (z= 2)	2.2	7.2	4.3	15.4	69.6	19.5	63.6	48.8	34.4	35.2	2.2	
RBM27_HUMAN	RBM27 p-S121 (z= 2)	34.0	9.0	13.0	20.6	47.1	56.5	40.0	32.3	45.4	31.1	2.2	
SRRM1_HUMAN	SRRM1 p-S875 (z= 2)	10.5	56.8	56.8	39.2	98.3	4.6	63.6	78.3	85.8	84.2	2.2	
LRRF1_HUMAN	LRRFIP1 p-S117 (z= 2)	0.0	25.4	57.6	30.3	80.3	2.2	47.1	72.3	65.8	97.7	2.2	
CG055_HUMAN	CG055 p-Y30 (z= 2)	82.2	81.3	77.9	32.9	69.0	81.1	61.5	60.6	71.1	81.3	2.2	
HTSF1_HUMAN	HTATSF1 p-S454 (z= 3)	72.7	79.7	66.4	28.4	35.1	87.1	51.6	48.5	61.4	67.0	2.2	
NUCKS_HUMAN	NUCKS1 p-S205 p-S215 (z= 3)	45.1	50.4	35.0	25.5	57.7	75.9	88.1	68.6	54.9	57.3	2.2	
KAP2_HUMAN	PRKAR2A p-S100 (z= 2)	51.7	82.8	59.5	19.7	33.0	65.5	48.5	41.7	42.3	50.8	2.1	
CALX_HUMAN	CANX p-S555 (z= 2)	0.0	0.0	0.0	41.9	19.7	74.1	91.1	91.2	89.4	82.6	2.1	
DC1L2_HUMAN	DYNC1LI2 p-S195 (z= 3)	58.4	66.1	42.7	22.7	44.1	92.8	83.4	69.7	48.3	48.1	2.1	
ZO3_HUMAN	TJP3 p-S361 (z= 2)	0.0	13.4	47.1	37.6	91.0	4.0	56.6	70.7	78.3	83.4	2.1	
NDKB_HUMAN	NME2 p-T95 (z= 2)	38.1	34.8	36.3	14.2	31.2	78.9	40.2	37.8	29.4	28.4	2.1	
NPM_HUMAN	NPM1 p-S138 (z= 2)	0.0	9.2	9.0	19.8	36.7	8.1	27.0	55.1	40.9	85.9	2.1	
CNTP4_HUMAN	CNTNAP4 p-S521 (z= 2)	0.0	9.2	9.0	19.8	36.7	8.1	27.0	55.1	40.9	85.9	2.1	

ICAL_HUMAN	CAST p-S244 (z= 4)	83.2	71.5	46.3	28.5	53.9	59.2	79.8	64.1	58.7	46.3	2.1	
HS90A_HUMAN	HSP90AA1 p-S264 (z= 3)	21.4	15.2	14.8	30.2	37.8	71.8	93.2	86.8	62.1	55.0	2.1	
SRRM1_HUMAN	SRRM1 p-S714 (z= 3)	62.9	71.2	17.2	16.8	43.6	58.2	28.6	29.2	34.5	40.5	2.1	
ZNRF2_HUMAN	ZNRF2 p-S136 (z= 2)	61.8	42.8	42.1	22.9	64.4	31.6	42.2	38.8	46.5	43.7	2.0	
ZO3_HUMAN	TJP3 p-S165 (z= 2)	71.3	58.6	44.1	23.5	44.0	86.0	65.5	51.4	47.5	46.0	2.0	
TPIS_HUMAN	TPI1 p-S22 (z= 2)	95.7	76.3	98.1	24.7	39.8	68.1	51.3	43.0	49.8	54.1	2.0	
IF2P_HUMAN	EIF5B p-S138 (z= 3) + oxidation	18.1	42.6	41.3	43.3	66.1	45.9	89.9	73.1	87.2	67.7	2.0	
MMTA2_HUMAN	MMTAG2 p-T216 p-S221 (z= 3)	55.3	34.9	28.1	32.5	76.5	92.0	91.5	93.1	65.4	62.4	2.0	

Appendix 5

Summary of kinase activities identified in P31/Fuj and Kasumi-1 cells using GKAP (Chapter 6.3.).

		P31/Fuj				Kasumi-1				AUC	
Accession Number	Phosphopeptide Identification	Mean Normalized Peptide Intensity 0 µM ATP	Mean Normalized Peptide Intensity 10 µM ATP	Mean Normalized Peptide Intensity 50 µM ATP	Mean Normalized Peptide Intensity 500 µM ATP	Mean Normalized Peptide Intensity 0 µM ATP	Mean Normalized Peptide Intensity 10 µM ATP	Mean Normalized Peptide Intensity 50 µM ATP	Mean Normalized Peptide Intensity 500 µM ATP	P31/Fuj	Kasumi-1
ZCCHV_HUMAN	ZC3HAV1 p-S323 (z= 2)	0.01	2.78	35.49	95.89	0.01	0.13	0.27	0.28	134.16	0.70
RL29_HUMAN	RPL29 p-S143 (z= 2)	0.00	17.15	76.67	95.70	0.00	0.38	0.57	0.56	189.52	1.51
HNRPU_HUMAN	HNRNPU p-S60 (z= 3)	0.01	38.62	11.21	29.55	0.01	0.06	0.41	0.35	79.40	0.84
OSTP_HUMAN	SPP1 p-S312 (z= 2)	0.00	13.00	0.01	20.31	0.00	0.01	0.47	0.01	33.33	0.49
TR150_HUMAN	THRAP3 p-S212 (z= 2)	0.05	5.16	0.28	91.57	0.05	0.99	1.82	2.60	97.06	5.46
PHF6_HUMAN	PHF6 p-T359 (z= 2)	0.01	13.84	18.32	89.70	0.01	1.43	2.44	3.37	121.87	7.25
TAOK3_HUMAN	TAOK3 p-T317 (z= 2)	0.05	8.51	0.26	88.51	0.05	3.60	3.99	4.17	97.33	11.80
TFAM_HUMAN	TFAM p-S125 (z= 2)	0.07	28.14	35.15	54.85	0.07	3.02	9.06	9.73	118.21	21.88
HNRPM_HUMAN	HNRNPM p-S482 (z= 2)	4.14	15.00	43.84	77.07	4.14	9.97	12.15	9.10	140.06	35.35
PRS33_HUMAN	PRSS33 p-S100 (z= 2)	4.14	15.00	43.84	77.07	4.14	9.97	12.15	9.10	140.06	35.35
LIMA1_HUMAN	LIMA1 p-S727 (z= 2)	3.00	17.01	14.49	90.35	3.00	0.34	13.71	20.82	124.85	37.88
ACINU_HUMAN	ACIN1 p-T977 (z= 2)	2.66	6.23	18.58	94.60	2.66	6.29	14.13	18.57	122.07	41.66
HNRPU_HUMAN	HNRNPU p-S60 (z= 3) + oxidation	4.45	21.28	54.56	72.80	4.45	7.41	26.06	17.65	153.09	55.56
ENPL_HUMAN	HSP90B1 p-S65 (z= 2)	1.06	6.06	19.87	90.25	1.06	3.23	12.77	28.73	117.25	45.79
CC124_HUMAN	CCDC124 p-S142 (z= 2)	0.21	5.36	37.75	88.64	0.21	7.44	17.52	35.26	131.96	60.43
NOLC1_HUMAN	NOLC1 p-S644 (z= 2)	5.61	16.55	36.92	94.16	5.61	15.41	22.42	40.93	153.23	84.37
MYL9_HUMAN	MYL9 p-T20 (z= 2) + oxidation	13.34	26.61	73.83	29.08	13.34	8.31	43.37	29.87	142.85	94.89
RCN1_HUMAN	RCN1 p-T186 (z= 2)	1.19	3.50	10.07	97.45	1.19	9.07	23.02	46.21	112.20	79.49
TBA1A_HUMAN	TUBA1A p-T335 (z= 2)	2.22	2.69	21.63	99.58	2.22	6.33	25.86	56.68	126.13	91.09
ACINU_HUMAN	ACIN1 p-S329 (z= 2)	8.12	29.02	36.50	93.71	8.12	27.66	54.11	66.21	167.36	156.11
ZC3HF_HUMAN	ZC3H15 p-T349 (z= 2)	0.98	2.97	37.25	96.26	0.98	8.55	51.67	83.47	137.46	144.67
2A5D_HUMAN	PPP2R5D p-S599 (z= 2)	1.84	5.85	12.18	94.11	1.84	10.87	47.41	67.95	113.99	128.07

THOC4_HUMAN	THOC4 p-S9 (z= 2) + oxidation	0.00	1.05	14.91	72.84	0.00	18.97	19.92	65.46	88.80	104.35
CALX_HUMAN	CANX p-S555 p-T563 (z= 2)	5.65	14.85	20.28	12.23	5.65	45.67	26.37	14.29	53.00	91.98
PA2G4_HUMAN	PA2G4 p-T387 (z= 2)	0.44	4.17	56.45	35.89	0.44	36.34	47.89	97.23	96.94	181.89
TF2B_HUMAN	GTF2B p-S71 (z= 2)	9.28	6.26	30.82	49.62	9.28	7.46	97.55	67.40	95.99	181.69
HNRPK_HUMAN	HNRNPK p-S380 (z= 2)	10.88	13.56	29.38	39.19	10.88	13.28	81.60	92.53	93.01	198.29
ENPL_HUMAN	HSP90B1 p-S747 (z= 2)	0.55	0.33	1.36	62.28	0.55	4.39	36.57	98.94	64.52	140.45
CALR_HUMAN	CALR p-S70 (z= 2)	0.00	2.72	25.06	40.85	0.00	24.47	36.85	92.40	68.63	153.73
CBX3_HUMAN	CBX3 p-S177 (z= 2)	4.80	6.18	21.41	50.34	4.80	18.10	68.75	96.59	82.73	188.23
NONO_HUMAN	NONO p-T374 (z= 2)	0.28	0.67	4.02	44.60	0.28	18.68	55.16	99.03	49.57	173.16
CCAR1_HUMAN	CCAR1 p-S215 (z= 2)	0.00	0.00	9.50	21.59	0.00	16.73	81.01	90.98	31.10	188.73
RRBP1_HUMAN	RRBP1 p-S979 (z= 2)	0.00	0.17	1.99	16.49	0.00	20.48	54.27	95.68	18.65	170.43
LYRIC_HUMAN	MTDH p-S295 (z= 2)	0.00	0.02	0.13	0.24	0.00	32.49	72.05	98.03	0.38	202.57
TF2B_HUMAN	GTF2B p-S71 (z= 2) + oxidation	0.00	0.00	0.06	0.15	0.00	0.83	37.62	83.21	0.21	121.66
TRM6_HUMAN	TRMT6 p-T292 (z= 2)	0.00	0.01	0.02	0.12	0.00	46.58	92.83	76.68	0.15	216.09
OSTP_HUMAN	SPP1 p-S220 (z= 2)	0.01	25.52	0.04	16.24	0.01	0.01	0.49	0.01	41.81	0.52
ALS2_HUMAN	ALS2 p-S493 (z= 2)	0.32	18.36	1.80	46.71	0.32	0.17	0.27	0.23	67.18	0.99
HNRPM_HUMAN	HNRNPM p-S576 (z= 2)	1.10	20.46	54.26	42.60	1.10	1.04	1.20	1.76	118.41	5.09
STK4_HUMAN	STK4 p-T341 (z= 2)	0.50	35.75	9.51	16.27	0.50	0.79	0.79	0.80	62.02	2.88
NPTX1_HUMAN	NPTX1 p-S123 (z= 2) + oxidation	0.65	34.74	5.10	11.09	0.65	0.68	0.58	0.53	51.58	2.45
REPS1_HUMAN	REPS1 p-S563 (z= 2)	0.65	34.74	5.10	11.09	0.65	0.68	0.58	0.53	51.58	2.45
STK3_HUMAN	STK3 p-T175 (z= 2)	1.64	48.15	37.80	4.50	1.64	1.00	2.78	2.03	92.10	7.45
PRDM8_HUMAN	PRDM8 p-S376 (z= 2)	3.99	15.93	39.15	97.27	3.99	4.17	4.57	4.82	156.35	17.55
FA53B_HUMAN	FA53B p-T29 (z= 2)	4.39	14.94	73.36	10.20	4.39	5.57	5.07	3.88	102.90	18.91
ACLY_HUMAN	ACLY p-S456 (z= 2)	20.55	69.94	86.30	63.34	20.55	23.95	8.82	17.21	240.13	70.54
MST4_HUMAN	MST4 p-T173 (z= 2)	13.95	60.09	98.21	66.88	13.95	14.28	22.37	22.13	239.13	72.73
H90B2_HUMAN	HSP90AB2P p-S178 (z= 2)	13.32	46.45	56.13	56.42	13.32	19.42	9.07	14.36	172.33	56.17
MST4_HUMAN	MST4 p-T171 (z= 3)	14.50	47.08	40.16	72.26	14.50	4.19	32.58	12.74	174.00	64.01
SLU7_HUMAN	SLU7 p-S216 (z= 2)	24.49	72.13	55.92	61.29	24.49	21.04	14.02	20.35	213.83	79.90
NUCL_HUMAN	NCL p-S68 (z= 2)	13.56	37.42	27.26	29.02	13.56	11.77	8.38	8.13	107.26	41.85
HNRPM_HUMAN	HNRNPM p-S619 (z= 2) + oxidation	19.19	61.26	41.93	65.45	19.19	16.36	20.05	19.29	187.82	74.89
PDCD4_HUMAN	PDCD4 p-S458 (z= 2)	23.69	60.93	48.11	53.99	23.69	25.33	17.01	17.50	186.71	83.52
RBM14_HUMAN	RBM14 p-S621 (z= 2)	13.50	8.62	46.37	96.68	13.50	9.23	21.01	34.61	165.17	78.36
TIF1B_HUMAN	TRIM28 p-S502 (z= 2)	21.42	46.92	69.37	90.69	21.42	18.12	36.79	39.71	228.40	116.04
NEUG_HUMAN	NRGN p-S37 (z= 2)	29.22	34.54	73.58	69.43	29.22	29.66	25.78	21.08	206.78	105.74
ASPM_HUMAN	ASPM p-S1834 (z= 2)	29.22	34.54	73.58	69.43	29.22	29.66	25.78	21.08	206.78	105.74
CC106_HUMAN	CC106 p-S199 (z= 2)	29.22	34.54	73.58	69.43	29.22	29.66	25.78	21.08	206.78	105.74
NUCKS_HUMAN	NUCKS1 p-S182 (z= 2)	27.32	64.14	61.62	60.03	27.32	41.53	32.63	21.26	213.11	122.75
MP2K2_HUMAN	MAP2K2 p-T395 (z= 2)	32.42	73.42	72.17	69.75	32.42	46.46	36.21	30.19	247.76	145.27
BIN2_HUMAN	BIN2 p-T455 (z= 2)	34.95	67.70	70.92	73.47	34.95	46.76	51.75	39.25	247.04	172.71
SI1L3_HUMAN	SIPA1L3 p-S1502 (z= 2)	18.15	57.12	43.95	72.77	18.15	57.85	19.09	48.70	191.99	143.79
ZN319_HUMAN	ZNF319 p-S329 (z= 2)	18.15	57.12	43.95	72.77	18.15	57.85	19.09	48.70	191.99	143.79
TCEA3_HUMAN	TCEA3 p-S146 (z= 2)	18.15	57.12	43.95	72.77	18.15	57.85	19.09	48.70	191.99	143.79
KIT_HUMAN	KIT p-Y704 (z= 2)	16.90	17.71	39.65	76.87	16.90	21.38	25.56	34.63	151.13	98.48

TBA1A_HUMAN	TUBA1A p-S49 (z= 2)	41.34	63.43	83.86	96.51	41.34	32.47	80.30	88.23	285.13	242.33
YBOX1_HUMAN	YBX1 p-S314 (z= 2)	24.53	55.12	50.64	95.59	24.53	50.07	46.75	87.86	225.88	209.21
4EBP1_HUMAN	EIF4EBP1 p-S113 (z= 2)	2.24	3.61	0.11	100.00	2.24	4.20	19.67	26.94	105.96	53.06
SNUT1_HUMAN	SART1 p-T431 (z= 2)	3.52	15.67	0.21	94.10	3.52	24.80	52.24	83.04	113.49	163.60
KCC2G_HUMAN	CAMK2G p-S312 (z= 2)	2.79	60.45	0.09	2.40	2.79	27.86	53.45	28.63	65.73	112.71
HTSF1_HUMAN	HTATSF1 p-S617 (z= 2)	12.29	38.93	19.83	31.06	12.29	72.77	42.53	50.66	102.11	178.24
ZCCHV_HUMAN	ZC3HAV1 p-S285 (z= 2)	14.27	16.98	25.55	58.44	14.27	33.84	78.07	98.36	115.24	224.53
ZCH18_HUMAN	ZC3H18 p-S47 (z= 2)	10.88	15.94	12.22	17.93	10.88	43.74	33.74	43.97	56.97	132.33
IF2P_HUMAN	EIF5B p-S67 (z= 2)	15.18	15.43	10.90	28.19	15.18	23.05	69.50	95.58	69.71	203.30
THOC4_HUMAN	THOC4 p-S9 (z= 2)	2.21	9.09	0.15	41.07	2.21	7.56	78.46	68.34	52.52	156.57
YBOX1_HUMAN	YBX1 p-S175 (z= 2)	10.85	12.75	5.73	10.11	10.85	51.42	50.00	70.19	39.45	182.46
U520_HUMAN	SNRNP200 p-S226 (z= 2) + oxidation	0.79	1.18	1.34	1.60	0.79	19.42	6.21	2.14	4.91	28.56
TBB2A_HUMAN	TUBB2A p-T73 (z= 2)	4.29	10.33	0.04	8.92	4.29	5.95	56.70	80.80	23.59	147.74
KIF4A_HUMAN	KIF4A p-S1039 (z= 2)	0.95	0.82	5.38	0.79	0.95	8.37	30.74	26.41	7.95	66.47
PERM_HUMAN	MPO p-T176 (z= 2)	1.83	0.03	0.17	0.03	1.83	9.95	37.67	93.80	2.06	143.25

Appendix 6

Summary of kinase activities identified in MCF10A cells stimulated with EGF and treated with the inhibitors LY294002 or UO126 (Chapter 6.4.).

	- EGF					+ EGF					+ EGF + LY294002					+ EGF + UO126							
	µM ATP																						
Phosphopeptide Identification	Mean Normalized Peptide Intensity 0	Mean Normalized Peptide Intensity 10	Mean Normalized Peptide Intensity 50	Mean Normalized Peptide Intensity 100	Mean Normalized Peptide Intensity 500	Mean Normalized Peptide Intensity 0	Mean Normalized Peptide Intensity 10	Mean Normalized Peptide Intensity 50	Mean Normalized Peptide Intensity 100	Mean Normalized Peptide Intensity 500	Mean Normalized Peptide Intensity 0	Mean Normalized Peptide Intensity 10	Mean Normalized Peptide Intensity 50	Mean Normalized Peptide Intensity 100	Mean Normalized Peptide Intensity 500	Mean Normalized Peptide Intensity 0	Mean Normalized Peptide Intensity 10	Mean Normalized Peptide Intensity 50	Mean Normalized Peptide Intensity 100	Mean Normalized Peptide Intensity 500	Kinase Activity + EGF	Kinase Activity + EGF +LY294002	Kinase Activity + EGF + UO126
YBX1 p-S314 (z= 2)	0	0	0	0	0	0	94	100	74	92	0	0	0	0	0	0	0	0	0	0	1	1	1
FAM129B p-S680 p-S684 (z= 2)	25	18	49	41	32	25	30	38	39	53	25	75	45	33	99	37	66	35	61	100	0	0	0
FAM129B p-S680 p-S684 (z= 3)	9	9	31	36	17	9	20	31	26	34	9	71	40	33	100	9	38	19	27	52	0	0	0
EIF4G1 p-S1210 (z= 2)	5	1	2	1	1	5	100	41	18	15	5	2	0	1	0	5	3	2	2	0	1	1	1
FAM40A p-S336 (z= 2)	18	32	36	31	26	18	100	86	68	54	18	14	9	11	8	23	44	38	37	21	1	1	0
FASN p-T2205 (z= 2)	47	64	74	68	61	47	92	100	99	70	47	51	46	50	35	58	86	82	83	38	0	1	0
SEC16A p-S1906 (z= 2)	24	33	45	37	26	24	82	79	77	100	24	28	17	13	23	37	50	36	46	50	0	1	0
MARCKS p-S146 (z= 2)	32	30	24	31	21	32	100	93	97	60	32	25	28	30	19	16	20	21	22	13	1	1	1
HDGFRP2 p-S609 (z= 3)	15	10	24	17	30	15	63	64	72	100	15	13	24	10	27	8	27	45	24	38	1	1	0
CANX p-S584 (z= 2)	13	6	4	2	1	13	100	99	40	35	13	21	5	13	3	13	59	42	49	13	1	1	0
CANX p-S584 (z= 3)	4	6	4	2	1	4	86	100	35	26	4	34	8	21	4	4	97	69	80	23	0	1	0
ARHGAP29 p-S356 (z= 2)	0	4	31	6	100	0	0	0	0	0	0	0	0	0	1	0	23	65	19	75	0	1	0
HUWE1 p-S1396 (z= 2)	27	22	19	18	12	27	100	100	81	57	27	25	16	22	13	12	23	22	22	8	1	1	1
NADL2 p-Y282 (z= 3)	16	21	31	20	16	16	100	97	97	50	16	48	25	39	20	6	44	33	37	19	1	1	1
EDC3 p-T61 (z= 2)	2	17	12	12	6	2	10	55	62	31	2	84	74	100	47	0	5	5	6	3	1	0	1
HDGF p-S166 (z= 2)	46	14	18	11	10	46	100	36	29	23	46	13	5	9	4	40	23	18	19	3	1	1	0
NSUN2 p-S744 p-S752 (z= 3)	0	3	29	17	14	0	17	41	40	76	0	21	3	5	14	0	87	48	74	100	0	1	0
NSUN2 p-S744 (z= 3)	0	3	23	5	3	0	15	33	43	83	0	1	0	0	0	0	59	25	41	100	0	1	0
PGM1 p-T116 (z= 2)	0	2	27	1	4	0	80	64	55	98	0	32	0	1	5	0	62	33	34	100	1	1	0
PGM1 p-S118 (z= 3)	0	1	4	1	1	0	51	53	40	46	0	16	1	2	4	0	67	43	46	100	0	1	0
TMPO p-T209 (z= 2)	88	30	37	33	6	88	9	4	100	86	88	57	17	25	11	26	7	9	9	3	0	1	1
LRRFIP1 p-S769 (z= 2)	2	22	50	26	44	2	7	6	5	4	2	2	1	1	1	43	100	74	89	61	0	1	0
C19orf21 p-S395 (z= 2)	21	76	74	44	54	21	70	100	100	86	21	24	24	22	20	30	39	33	32	36	0	1	1
RNF20 p-S139 (z= 2)	36	51	68	100	61	36	94	92	78	60	36	30	24	27	21	63	94	75	88	65	0	1	0
DBNL p-S270 (z= 2)	20	0	0	0	0	20	1	12	1	30	20	6	28	5	100	0	0	0	0	0	0	0	1
DOCK5 p-S1757 (z= 2)	2	4	4	4	3	2	3	4	3	4	2	65	93	70	100	2	2	3	4	4	0	0	1
EXOSC9 p-S307 (z= 2)	23	24	26	27	20	23	94	100	73	52	23	23	18	18	13	15	38	29	32	16	1	1	1
SRRM1 p-S697 (z= 2)	23	36	29	30	19	23	83	94	100	76	23	32	29	28	22	10	27	33	31	21	1	1	1
TRIP10 p-S297 (z= 2)	0	38	62	32	38	0	35	33	35	35	0	9	6	6	6	0	100	81	97	67	0	1	0
TRIP10 p-S297 (z= 3)	0	16	29	18	15	0	73	75	100	73	0	0	0	0	0	2	35	29	32	28	1	1	1
SSH3 p-S88 (z= 3)	0	0	0	0	0	0	1	1	1	1	0	0	0	0	0	0	98	82	100	75	0	1	0
UBAC1 p-S99 (z= 2)	9	22	18	23	14	9	97	96	100	72	9	24	45	31	37	3	15	17	15	10	1	0	1
FLNA p-S2153 (z= 2)	1	46	66	56	61	1	23	19	28	23	1	8	9	6	8	4	94	100	96	66	0	1	0
FLNA p-S2153 (z= 3)	0	52	74	76	63	0	18	18	22	17	0	10	10	8	10	1	93	100	91	68	0	1	0
FLNB p-S2108 (z= 2)	62	27	28	30	26	62	100	72	81	64	62	24	30	20	26	47	28	40	33	31	1	1	0
CANX p-S75 (z= 2)	0	0	4	0	18	0	1	32	5	100	0	0	0	0	0	0	2	15	1	36	1	1	1
PSMD2 p-S17 (z= 3)	0	0	0	0	0	0	16	51	92	100	0	47	34	19	52	0	53	41	61	83	1	0	0
SEC31A p-S800 (z= 2)	1	13	12	8	7	1	71	52	35	23	1	88	78	100	70	0	15	17	15	9	0	0	1

SRRM2 p-T1004 (z= 2)	41	32	35	34	23	41	91	74	100	56	41	22	21	22	16	30	43	50	39	19	1	1	0
ZC3H18 p-S47 (z= 2)	2	3	4	2	3	2	100	51	58	37	2	2	1	1	0	2	5	5	4	3	1	1	1
CAD p-S1860 (z= 2)	18	60	58	65	66	18	100	82	83	57	18	19	17	19	14	42	74	77	77	38	0	1	0
API5 p-S463 (z= 2)	0	0	0	0	0	0	43	34	75	100	0	1	1	1	0	0	0	0	0	0	1	1	1
XPO6 p-S8 (z= 2)	0	31	11	55	58	0	0	33	17	30	0	26	100	24	51	0	8	12	4	33	0	0	0
STMN1 p-S17 p-S26 (z= 2)	12	1	6	12	5	12	48	74	80	81	12	100	82	81	82	12	60	66	77	62	1	0	0
STMN1 p-S17 (z= 2)	7	5	7	5	5	7	100	84	87	73	7	7	4	4	3	7	42	45	44	20	1	1	0
ZC3HAV1 p-S285 (z= 2)	22	12	43	2	22	22	100	98	48	82	22	22	3	5	3	33	65	78	55	57	1	1	0
IRF2BP1 p-S385 (z= 2)	0	2	1	2	1	0	2	2	4	2	0	74	100	65	40	0	1	1	1	1	0	0	1
IRF2BPL p-S548 (z= 2)	2	19	13	22	11	2	88	99	100	63	2	9	16	14	11	1	12	9	10	9	1	1	1
TNKS1BP1 p-S673 (z= 2)	12	30	25	26	18	12	87	100	100	72	12	21	20	21	14	9	22	26	24	14	1	1	1
DFFA p-S316 (z= 2)	21	30	25	30	21	21	100	78	78	48	21	16	17	17	12	16	23	27	26	13	1	1	1
PKN2 p-S584 (z= 2)	46	35	72	39	52	46	53	63	48	53	46	42	22	32	23	100	100	89	73	47	0	1	0
WDPCP p-S20 (z= 2)	2	12	9	12	7	2	100	89	100	49	2	9	8	8	5	2	13	17	18	10	1	1	1
CHMP2B p-S200 (z= 2)	49	7	10	6	5	49	100	91	52	36	49	14	5	9	4	49	36	24	28	4	1	1	0
RSL1D1 p-S362 (z= 2)	20	38	34	32	30	20	67	73	100	71	20	19	42	40	27	31	46	62	46	36	1	0	0
MYL9 p-T20 (z= 2) + oxidation	18	1	11	1	5	18	85	86	37	100	18	3	0	0	0	18	23	20	14	24	1	1	1
MYL9 p-S21 (z= 3) + oxidation	9	0	34	0	2	9	89	100	34	92	9	4	0	0	0	9	29	26	15	33	1	1	1
MYL9 p-T20 (z= 2)	0	0	0	0	0	0	0	0	0	0	0	0	0	0	0	0	43	48	21	100	0	1	0
MYL9 p-S21 (z= 3)	0	0	0	0	0	0	0	0	0	1	0	0	0	0	0	0	36	42	19	100	0	1	0
SPPL2A p-T203 (z= 2)	0	32	27	23	17	0	100	40	84	56	0	19	13	11	6	1	25	30	27	12	0	1	0
AHNAK2 p-S295 (z= 3)	5	75	67	67	24	5	100	95	99	57	5	83	56	70	37	1	74	59	62	51	0	0	0
RRBP1 p-S979 (z= 2)	0	0	0	0	0	0	54	100	31	66	0	0	0	0	0	0	18	38	18	33	1	1	0
EEF1B2 p-S107 (z= 2)	30	0	9	12	7	30	27	38	100	61	30	41	33	36	20	30	77	70	78	56	1	1	0
TGBR3 p-S323 (z= 2)	3	100	82	95	75	3	39	41	42	28	3	9	8	12	7	14	74	75	85	59	0	1	0
RPS3 p-T222 (z= 2)	24	98	75	68	61	24	93	100	95	71	24	31	34	32	24	36	63	51	59	44	0	1	0
RAPGEFL1 p-S257 (z= 2)	100	14	13	13	31	100	35	36	22	41	100	40	42	34	46	96	16	17	14	30	1	0	0
DYNC1LI2 p-S195 (z= 2)	0	0	0	0	0	0	0	0	0	0	0	0	0	0	0	0	100	98	100	58	0	1	0
HUWE1 p-S2363 (z= 2)	2	15	12	17	5	2	35	39	41	14	2	64	85	100	53	0	13	9	13	6	0	0	1
ERGIC3 p-S117 (z= 2)	36	68	58	61	40	36	88	80	100	41	36	38	36	39	30	33	52	43	51	28	0	0	0
RSRC2 p-S18 (z= 2)	0	98	100	79	69	0	1	0	1	0	0	0	0	0	0	0	90	88	100	55	0	1	0
AHNAK p-S178 (z= 2)	33	74	47	60	39	33	95	96	100	48	33	49	48	54	31	27	34	28	35	24	1	0	0
APIP p-S90 (z= 2)	5	27	27	31	19	5	90	59	100	61	5	37	33	33	22	2	25	28	29	19	1	0	1
APIP p-S90 (z= 2)	16	58	47	49	22	16	23	19	100	62	16	44	36	24	19	4	33	43	41	26	0	0	0
CHSTD p-S313 (z= 2)	4	78	71	62	56	4	52	48	52	36	4	84	96	100	74	0	66	67	74	41	0	0	0
HSP90AA1 p-S232 (z= 2)	0	35	48	82	54	0	1	1	2	1	0	1	1	0	0	0	78	90	100	72	0	1	0
SAMD9L p-T1038 (z= 3)	4	25	17	25	23	4	100	92	51	45	4	19	38	34	17	3	18	16	12	12	1	0	1
EPB41L1 p-S651 (z= 2)	19	14	30	35	20	19	69	77	100	59	19	26	23	31	19	15	36	31	33	25	1	1	1
HTATSF1 p-S580 (z= 2)	1	38	43	59	34	1	30	10	100	50	1	64	53	40	24	1	71	83	77	50	0	0	0
TNKS1BP1 p-S1332 (z= 2)	2	3	12	6	16	2	30	54	30	100	2	1	3	1	10	1	12	18	12	26	1	1	1
CDK11A p-S272 (z= 2)	13	1	12	17	8	13	39	43	100	50	13	14	17	14	14	13	49	42	49	38	1	1	0
RGS3 p-S807 (z= 2)	36	100	84	97	54	36	88	79	81	50	36	26	33	35	24	51	82	70	87	44	0	1	0
HARS2 p-S68 (z= 2)	4	78	71	62	56	4	52	48	52	36	4	84	96	100	74	0	66	67	74	41	0	0	0
CTTNBP2NL p-S489 (z= 2)	27	81	65	66	47	27	100	89	91	54	27	29	25	28	15	41	57	53	63	30	0	1	0
MAP4 p-S281 (z= 2) + oxidation	42	25	30	29	23	42	100	85	76	59	42	12	9	11	5	67	25	22	26	18	1	1	1
MAP4 p-S281 (z= 2)	13	29	23	23	14	13	67	59	65	45	13	77	66	100	62	0	21	19	22	16	1	0	1
MAP4 p-T283 (z= 3)	4	22	18	14	9	4	29	32	28	15	4	86	78	100	58	0	16	13	12	11	0	0	1
MAP4 p-S508 (z= 2)	5	7	9	2	3	5	27	23	24	19	5	100	27	42	21	0	14	12	15	7	1	0	1
ARFGAP2 p-S369 (z= 2)	8	2	32	6	55	8	9	44	8	88	8	5	28	6	47	5	16	48	10	100	0	0	0
EAF1 p-S166 (z= 3)	1	51	86	41	32	1	36	36	43	24	1	19	10	16	8	1	98	94	100	63	0	1	0
TJP2 p-S987 (z= 2)	3	54	100	76	50	3	66	68	99	97	3	38	30	21	35	3	99	58	92	87	0	1	0
VCL p-S291 (z= 2)	20	12	26	8	12	20	100	95	87	66	20	24	4	10	5	20	56	54	50	26	1	1	0
EPS8L1 p-S183 (z= 2)	1	13	12	11	7	1	47	53	79	55	1	27	33	29	20	1	90	90	100	67	1	1	0
TRMT6 p-S289 (z= 2)	2	29	78	17	49	2	59	97	50	82	2	31	27	28	46	0	74	100	63	77	0	0	0
SLK p-S778 (z= 2)	60	15	15	17	12	60	93	100	95	32	60	15	13	15	10	39	19	16	17	10	1	1	1
VATF p-S105 (z= 2)	7	50	19	9	23	7	20	26	5	16	7	100	97	63	84	7	27	58	22	23	0	0	0
UNC45A p-S494 (z= 2)	7	50	19	9	23	7	20	26	5	16	7	100	97	63	84	7	27	58	22	23	0	0	0
COPE p-S100 (z= 2)	0	3	3	2	2	0	85	100	96	51	0	16	10	15	6	0	7	4	5	4	1	1	1
TOP2B p-S1359 (z= 2)	7	50	19	9	23	7	20	26	5	16	7	100	97	63	84	7	27	58	22	23	0	0	0
PAK4 p-S105 (z= 2)	0	40	37	56	18	0	23	13	100	62	0	42	30	26	19	0	13	21	23	20	0	0	0
LASP1 p-S147 (z= 2)	0	1	1	1	0	0	6	11	100	61	0	1	1	1	1	0	43	48	34	26	0	1	0
ZC3H15 p-S352 (z= 2)	1	0	1	0	2	1	32	84	28	96	1	9	24	7	53	1	22	43	19	100	1	0	0
MAP4 p-T522 (z= 2)	30	31	31	29	16	30	74	72	100	68	30	29	41	30	25	23	24	21	27	23	1	0	1
MAP4 p-T522 (z= 3)	18	35	38	36	15	18	80	82	100	59	18	49	74	47	42	10	24	22	23	25	1	0	1

PTGES3 p-S114 (z= 2)	12	0	2	2	2	12	21	25	34	22	12	28	7	13	6	12	97	78	100	52	0	1	0
ANK1 p-S16 (z= 2)	100	14	13	13	31	100	35	36	22	41	100	40	42	34	46	96	16	17	14	30	1	0	0
TUBB2C p-T137 (z= 3)	0	0	0	0	0	0	0	0	0	100	0	1	0	0	0	0	0	0	0	1	0	1	0
TUBB4Q p-T137 (z= 3)	0	0	0	0	0	0	0	0	0	100	0	1	0	0	0	0	0	0	0	1	0	1	0
ZKSCAN1 p-S14 (z= 2)	29	23	18	17	13	29	100	75	85	49	29	21	18	21	12	16	19	19	19	11	1	1	1
PRKAR1A p-S84 (z= 2)	13	64	100	86	57	13	57	55	70	52	13	15	14	13	14	41	76	59	82	73	0	1	0
SNRNP200 p-S226 (z= 2)	16	31	45	48	28	16	47	63	74	44	16	91	60	100	63	1	75	60	70	42	0	0	0
NUCKS1 p-S215 (z= 2)	0	44	58	75	53	0	0	0	0	0	0	0	0	0	0	17	72	83	100	57	0	1	0
NUCKS1 p-S215 (z= 2)	0	17	16	17	11	0	58	56	100	57	0	0	0	0	0	0	3	2	3	2	1	1	1
NUCKS1 p-S215 (z= 3)	0	18	21	21	13	0	64	65	100	50	0	27	18	27	17	0	24	23	28	18	1	1	1
HSP90B1 p-S65 (z= 2)	0	1	11	1	33	0	11	29	12	100	0	1	4	1	10	0	6	17	6	40	1	1	0
GOLGA4 p-S267 (z= 2)	20	31	49	38	31	20	75	63	68	43	20	18	9	13	8	42	100	82	84	45	0	1	0
ZRANB2 p-S121 (z= 2)	23	23	49	66	42	23	36	43	62	29	23	18	15	22	14	57	97	83	100	56	0	1	0
SEC62 p-T159 (z= 2)	0	2	3	4	1	0	17	7	100	80	0	65	43	50	32	0	20	26	26	23	0	0	0
YY1 p-S119 (z= 2)	24	14	22	23	16	24	100	86	97	49	24	21	16	19	9	21	35	25	33	13	1	1	1
GSTP1 p-S44 (z= 2)	34	8	13	2	11	34	100	50	63	36	34	8	2	4	3	37	33	24	33	16	1	1	0
NAP1L4 p-S126 (z= 3)	7	0	1	0	0	7	100	34	23	20	7	7	0	0	0	7	43	22	21	9	1	1	0
PGRMC1 p-S182 (z= 3)	2	9	15	6	6	2	51	52	55	30	2	100	23	57	31	0	19	16	23	10	1	0	1
TTC21A p-S271 (z= 3) + oxidation	3	31	22	20	19	3	92	100	70	30	3	26	28	31	15	0	27	20	21	13	1	0	1
FOXK2 p-S399 (z= 2)	27	15	21	19	16	27	92	83	100	73	27	15	21	20	18	15	15	9	14	9	1	1	1
KTN1 p-S78 (z= 2)	8	5	8	1	5	8	91	77	89	88	8	24	4	8	3	8	100	98	91	51	1	1	0
HSP90AB1 p-S227 (z= 2)	0	51	57	100	57	0	19	21	40	19	0	11	20	16	14	12	85	90	90	61	0	1	0
HSP90AB1 p-S227 (z= 2)	0	34	45	61	46	0	61	57	100	48	0	1	2	2	1	2	57	56	67	45	0	1	0
HSP90AB1 p-S227 (z= 3)	0	51	74	100	77	0	3	4	6	3	0	1	1	1	1	0	88	78	86	68	0	1	0
HSP90AB1 p-S227 (z= 2)	0	57	75	100	73	0	2	2	3	2	0	0	0	0	0	7	81	73	88	62	0	1	0
EIF5B p-S67 (z= 2)	0	2	9	2	10	0	49	69	39	100	0	6	11	5	23	0	11	25	14	33	1	1	1
SHC1 p-S427 (z= 2)	5	0	0	0	0	5	51	48	52	51	5	26	7	13	7	5	100	73	76	56	1	1	0
SHC1 p-Y428 (z= 2)	5	0	0	0	1	5	51	48	52	51	5	26	7	13	7	5	100	73	76	56	1	1	0
SRRM2 p-S1321 (z= 2)	33	25	22	19	13	33	100	68	65	36	33	17	14	15	8	18	21	20	19	11	1	1	1
RFC1 p-S191 (z= 2)	1	38	96	15	53	1	74	94	62	64	1	45	29	31	36	0	100	99	95	78	0	1	0
UBR3 p-S1422 (z= 2)	10	19	19	12	11	10	100	73	62	40	10	13	4	8	3	11	32	19	24	11	1	1	1
BAG6 p-S974 (z= 2)	17	51	54	53	40	17	95	75	81	49	17	100	84	100	57	1	66	48	62	29	0	0	0
SRRM2 p-S1330 (z= 2)	49	31	40	27	19	49	83	69	100	57	49	26	35	36	16	43	34	35	41	20	0	0	0
GEMIN5 p-S779 (z= 2)	8	15	35	17	23	8	28	24	39	25	8	10	4	6	3	29	100	70	76	48	0	1	0
TCEA1 p-S101 (z= 2)	26	47	40	51	36	26	96	81	100	58	26	29	36	36	25	20	44	40	46	28	1	1	1
ARHGEF1 p-S787 (z= 2)	0	0	0	0	0	0	0	0	0	1	0	3	4	3	5	0	0	84	55	100	0	1	0
ESYT2 p-S759 (z= 2)	2	31	68	36	28	2	22	36	48	50	2	13	7	5	15	2	69	46	62	100	0	1	0
TFAM p-S125 (z= 2)	0	2	6	1	9	0	23	46	24	100	0	1	9	2	11	0	2	6	2	11	1	1	1
RSRC2 p-S33 (z= 2)	29	24	23	21	13	29	94	95	100	55	29	38	19	30	18	13	25	23	26	11	1	1	1
ZNF185 p-S469 (z= 2)	3	29	21	37	20	3	50	56	100	39	3	16	34	36	19	2	24	24	21	24	1	0	0
HSP90AA1 p-S264 (z= 2)	15	25	36	49	38	15	54	43	73	47	15	22	16	21	15	23	100	66	79	52	0	1	0
HSP90AA1 p-S264 (z= 3)	5	27	38	54	38	5	71	58	84	46	5	32	22	28	22	7	100	61	73	52	0	1	0
HSP90AA1 p-S264 (z= 3)	1	4	6	4	3	1	40	51	100	60	1	14	12	14	13	1	42	29	41	31	1	1	0
PSMA3 p-S251 (z= 2) + oxidation	0	29	45	56	30	0	1	0	1	0	0	0	0	0	0	10	88	78	100	69	0	1	0
PSMA3 p-S251 (z= 2)	0	1	1	1	1	0	2	2	3	1	0	91	61	100	60	0	2	1	2	1	0	0	1
TLE3 p-S204 (z= 2)	22	36	29	32	22	22	91	100	100	59	22	24	23	34	19	15	34	32	38	20	1	1	1
STMN1 p-S39 (z= 2)	48	65	76	55	36	48	83	83	100	73	48	44	47	43	39	49	49	41	51	38	0	0	0
LARP1 p-S522 (z= 2)	1	10	8	9	3	1	16	21	100	56	1	70	47	48	30	1	21	18	18	7	0	0	1
BCLAF1 p-T495 (z= 2)	1	38	30	43	11	1	12	8	91	51	1	100	51	57	36	0	13	13	16	11	0	0	1
SCAF8 p-S618 (z= 2)	29	36	35	38	27	29	100	82	62	39	29	25	18	21	14	29	43	35	40	19	1	1	0
ATXN2L p-S595 (z= 2)	25	22	23	9	12	25	80	69	79	48	25	100	59	68	38	1	31	32	38	21	1	0	1
HSP90AA1 p-S232 (z= 2)	0	2	3	6	4	0	13	10	100	51	0	43	64	42	36	0	41	47	44	40	0	0	0
HIRIP3 p-S371 (z= 2)	0	29	26	33	15	0	91	88	100	49	0	0	0	0	0	0	29	23	32	12	1	1	1
CDK11A p-S578 (z= 2)	1	19	15	13	8	1	27	46	47	17	1	100	71	98	52	0	6	6	8	5	0	0	1
EPRS p-T889 (z= 2)	7	40	66	73	48	7	42	43	48	42	7	11	10	11	10	29	100	70	83	64	0	1	0
SSB p-S367 (z= 3)	0	45	65	41	23	0	0	0	0	0	0	0	0	0	1	0	77	62	84	100	0	1	0
CLNS1A p-S103 (z= 3)	8	0	4	0	0	8	49	37	69	46	8	48	2	13	2	8	100	63	94	63	1	1	0
ACACA p-S30 (z= 2)	10	9	32	21	15	10	62	58	100	70	10	8	5	5	3	14	59	48	51	48	0	1	0
RRAS2 p-S187 (z= 2)	5	63	100	47	50	5	21	20	31	24	5	7	4	5	3	36	69	73	91	61	0	1	0
RAB9A p-S72 p-Y78 (z= 2)	0	0	1	5	9	0	3	8	9	4	0	31	100	62	58	0	0	0	0	1	0	0	1
N4BP1 p-S289 (z= 2)	0	30	29	38	22	0	100	80	72	46	0	1	1	1	1	0	32	29	31	22	1	1	1
MYO18A p-S141 (z= 2)	34	76	77	60	71	34	100	98	93	72	34	17	17	17	17	58	68	56	56	53	0	1	0
GTF3C1 p-S1380 (z= 2)	1	27	21	28	20	1	88	93	100	57	1	25	24	30	16	0	20	21	20	15	1	1	1
PDCD4 p-S458 (z= 2)	100	2	4	3	2	100	81	46	25	47	100	36	9	16	9	100	12	12	6	2	1	0	1
EPB41L1 p-T687 (z= 2)	40	36	39	37	26	40	76	76	100	58	40	37	29	31	23	6	23	23	30	20	0	1	1

CXorf26 p-S198 (z= 2)	0	16	16	16	12	0	34	36	54	33	0	95	80	100	65	0	22	18	24	15	0	0	1
MYH9 p-S1944 (z= 2)	0	45	40	83	36	0	6	7	19	8	0	71	100	83	58	0	33	38	44	31	0	0	0
PPP1R7 p-S13 (z= 2)	0	0	0	0	0	0	0	0	0	0	0	39	28	17	100	0	0	0	0	0	0	0	1
PGRMC1 p-S58 (z= 2)	6	2	44	37	37	6	26	21	37	33	6	12	10	9	15	10	77	74	100	78	0	1	0
YAP1 p-S62 (z= 2) + oxidation	13	2	17	11	12	13	15	15	100	84	13	9	3	1	4	13	49	26	28	73	0	1	0
YAP1 p-S62 (z= 2)	0	0	0	0	0	0	2	0	29	100	0	1	0	0	0	0	17	7	39	99	0	1	0
DAB2IP p-S979 (z= 2)	3	24	25	20	16	3	96	85	100	46	3	29	30	34	17	1	14	14	16	9	1	1	1
PDCD4 p-S77 (z= 2)	44	1	0	10	3	44	20	68	10	67	44	20	58	16	100	46	0	1	0	5	1	0	1
MARCKSL1 p-S23 (z= 2)	12	30	26	28	18	12	100	85	99	67	12	31	20	27	14	6	28	22	27	15	1	1	1
MARCKS p-S28 (z= 2)	1	72	68	40	36	1	42	39	54	44	1	42	30	36	28	1	91	77	100	75	0	1	0
MARCKS p-S102 (z= 2)	49	40	40	45	26	49	32	32	41	33	49	57	73	100	78	41	26	27	36	20	0	0	1
GSK3A p-Y280 (z= 2)	33	42	56	28	24	33	100	79	71	63	33	27	11	18	11	48	89	69	78	23	0	1	0
SPTBN1 p-S2139 (z= 2)	26	28	40	18	20	26	89	79	100	65	26	25	12	17	8	29	50	47	53	30	0	1	0
CSRP1 p-S193 (z= 2)	17	18	28	22	14	17	75	77	100	65	17	17	20	20	11	21	24	29	30	13	1	1	1
PYGO2 p-T303 (z= 2)	22	20	18	18	11	22	75	79	100	53	22	19	19	23	17	8	13	14	13	8	1	1	1
NMT1 p-S48 (z= 2)	27	46	36	24	21	27	98	76	100	64	27	27	32	40	23	14	21	30	25	15	1	1	1
KRT15 p-S23 p-S35 (z= 2)	13	0	4	1	8	13	5	30	15	100	13	2	7	3	17	13	3	8	5	30	1	1	1
KRT15 p-S35 (z= 2)	90	5	12	5	12	90	51	72	57	100	90	6	9	6	11	90	13	15	13	17	1	1	1
KRT15 p-S35 (z= 3)	76	12	28	9	23	76	53	100	74	100	76	11	20	12	20	70	24	24	14	30	1	1	1
AHNAK p-S5732 (z= 2)	19	49	29	25	17	19	79	80	100	44	19	27	27	36	22	10	13	11	13	7	1	1	1
KRT5 p-S575 (z= 2)	15	11	43	10	44	15	33	79	32	100	15	9	11	6	21	20	32	48	26	60	0	1	0
TPD52L2 p-S22 (z= 2)	2	0	1	0	0	2	14	9	10	9	2	4	0	0	0	2	100	74	85	51	0	1	0
MCM2 p-S140 (z= 2)	3	4	64	27	22	3	73	78	100	60	3	47	32	38	24	1	71	57	92	51	0	1	0
CALR p-S70 (z= 2)	0	12	53	12	22	0	10	14	28	100	0	0	0	0	0	0	18	47	20	20	0	1	0
LARP1 p-S547 (z= 2)	8	14	42	24	20	8	44	35	100	100	8	13	5	3	10	10	57	38	36	59	0	1	0
MCM2 p-S28 (z= 2)	53	10	14	5	5	53	100	58	55	39	53	16	4	9	4	53	35	29	31	3	1	1	0
SNTB2 p-S111 (z= 2)	10	54	48	48	39	10	98	87	100	65	10	19	19	21	15	12	41	47	47	31	0	1	0
CD2BP2 p-S195 (z= 2)	0	5	6	11	3	0	33	33	100	96	0	67	52	47	38	0	20	34	33	37	1	0	0
NPM1 p-S244 (z= 2)	7	16	21	16	20	7	60	100	57	78	7	15	23	20	31	3	13	24	12	25	1	1	1
HSPB1 p-S16 (z= 2)	100	23	30	38	34	100	11	12	14	10	100	52	94	80	73	62	20	20	18	29	0	0	1
VCL p-S347 (z= 2)	1	1	1	1	1	1	8	6	6	3	1	10	5	9	5	1	99	71	100	25	0	1	0
TMEM40 p-S138 (z= 2)	7	62	60	100	62	7	27	32	43	20	7	8	14	15	9	21	58	42	58	45	0	1	0
LRRFIP1 p-S121 (z= 2)	8	64	66	92	65	8	66	58	100	57	8	14	28	25	22	14	84	70	81	67	0	1	0
HN1L p-S70 (z= 2)	7	29	50	11	69	7	47	65	47	89	7	11	21	7	33	7	51	52	41	100	0	1	0
HUWE1 p-S1908 (z= 2)	39	51	63	61	43	39	95	100	83	63	39	34	20	30	20	55	96	62	72	38	0	1	0
NRD1 p-S95 (z= 2)	3	100	82	95	75	3	39	41	42	28	3	9	8	12	7	14	74	75	85	59	0	1	0
FAM83H p-S937 (z= 2)	29	22	20	15	15	29	98	85	100	69	29	15	14	18	12	18	19	18	20	13	1	1	1
TJAP1 p-S301 (z= 2)	45	8	15	3	7	45	100	88	96	84	45	29	6	11	6	45	45	45	56	32	1	1	0
KIAA1522 p-S405 (z= 2)	16	52	54	38	39	16	100	83	77	47	16	19	12	17	10	26	62	53	65	37	0	1	0
FAM83H p-S882 (z= 2)	7	19	16	16	10	7	69	68	100	53	7	13	13	15	7	7	27	30	30	19	1	1	1
FAM83H p-S893 (z= 2)	10	65	55	52	40	10	100	90	89	61	10	18	16	20	12	14	63	61	66	39	0	1	0
CDK12 p-S424 (z= 2)	29	34	52	18	21	29	100	87	71	73	29	22	6	9	4	39	58	43	58	26	0	1	0
FAM83H p-S915 (z= 2)	6	20	20	19	13	6	58	67	100	59	6	10	12	11	9	5	15	15	16	13	1	1	1
EWSR1 p-S511 (z= 2)	1	43	47	44	43	1	55	89	100	79	1	7	17	13	19	2	24	35	31	43	0	1	0
ARFGEF2 p-S277 (z= 2)	24	50	49	53	42	24	100	94	86	61	24	33	32	37	30	24	80	44	50	29	0	1	0
EGFR p-Y1198 (z= 2)	0	0	0	0	0	0	0	0	0	0	0	0	0	0	0	0	95	100	90	23	0	1	0
LCP1 p-S6 (z= 2)	0	0	0	0	0	0	0	0	0	0	0	100	39	77	35	0	0	0	0	0	0	0	1
REPS1 p-S144 (z= 2)	0	10	12	8	8	0	100	93	76	56	0	29	31	40	28	0	15	18	18	13	1	0	1
HNRNPK p-S380 (z= 2)	17	5	47	13	44	17	12	33	22	82	17	6	6	2	21	36	28	55	23	100	0	1	0
SMN1 p-S29 (z= 2)	16	10	17	20	11	16	64	55	100	51	16	17	19	24	18	14	38	27	38	17	1	1	1
HDGFRP2 p-T135 (z= 2)	37	52	73	33	32	37	100	94	96	76	37	40	17	30	18	9	94	89	98	62	0	1	0
ABLIM1 p-S707 (z= 2)	14	14	9	13	9	14	47	29	57	27	14	40	99	100	61	1	10	5	6	5	0	0	1
PRPSAP2 p-S228 (z= 2)	0	0	0	0	0	0	54	34	100	54	0	1	0	1	1	0	1	1	1	1	1	1	1
FCHO2 p-S395 (z= 2)	0	1	1	0	0	0	0	0	1	0	0	100	51	47	28	0	1	1	1	0	0	0	1
TP53I11 p-S15 (z= 2)	7	48	67	33	46	7	71	69	100	82	7	27	26	42	25	4	45	36	40	38	0	1	0
MAPK14 p-T181 (z= 2)	0	0	58	0	67	0	1	2	1	4	0	1	1	1	1	1	24	44	29	100	0	1	0
MAPK14 p-Y183 (z= 2)	0	1	58	0	68	0	1	2	1	4	0	1	1	1	1	1	25	44	29	100	0	1	0
USP11 p-S537 (z= 2)	0	32	28	29	22	0	84	88	100	74	0	0	0	0	0	0	21	24	23	17	1	1	1
FTH1 p-S180 (z= 2)	1	26	36	32	12	1	10	9	100	51	1	48	21	34	16	0	53	34	45	25	0	0	0
PALLD p-S894 (z= 2)	16	9	8	9	5	16	19	20	18	22	16	94	100	92	75	9	6	5	5	2	0	0	1
HSP90AB1 p-S256 (z= 2)	1	48	58	94	56	1	39	36	60	32	1	7	8	8	6	9	100	97	94	62	0	1	0
HSP90AB1 p-S256 (z= 2)	0	78	75	82	65	0	39	40	49	30	0	2	2	3	2	8	90	97	100	65	0	1	0
HSP90AB1 p-S256 (z= 3)	0	59	68	76	55	0	89	97	100	57	0	10	11	14	9	0	74	75	75	56	0	1	0
HSP90AB1 p-S262 (z= 3)	0	24	22	16	8	0	68	81	100	91	0	11	7	8	8	0	36	24	37	35	1	1	1
SLC9A1 p-S704 (z= 2)	29	26	21	14	17	29	59	65	58	46	29	82	100	83	74	29	35	29	38	27	1	0	1

TACC2 p-S2535 (z= 2)	1	2	12	0	16	1	26	70	22	100	1	1	1	0	4	1	12	19	10	21	1	1	1
PDLIM4 p-S113 (z= 2)	7	100	30	15	15	7	47	42	19	28	7	14	6	7	6	5	34	30	37	16	0	1	0
PDLIM4 p-S113 (z= 3)	2	20	30	12	13	2	100	91	97	61	2	23	8	14	8	1	30	28	32	11	1	1	1
RC3H2 p-T454 (z= 2)	19	35	35	19	16	19	100	97	87	64	19	36	16	29	12	9	25	23	24	7	1	1	1
AKAP9 p-T921 (z= 2)	5	71	67	61	47	5	84	78	100	36	5	51	65	76	41	2	48	52	55	28	0	0	0
PPP1R13L p-S359 (z= 2)	0	0	0	0	0	0	0	1	0	7	0	0	1	0	5	0	0	12	0	100	0	0	0
CLIP1 p-S349 (z= 2)	4	8	9	4	5	4	97	100	89	62	4	10	4	8	3	4	19	17	24	11	1	1	1
PSME3 p-T24 (z= 2)	0	0	2	0	0	0	0	0	4	11	0	0	0	0	0	0	77	62	37	100	0	1	0
SEPT2 p-S219 (z= 2)	2	2	39	14	25	2	25	22	35	24	2	5	4	5	3	5	100	69	94	81	0	1	0
SEPT2 p-S219 (z= 3)	32	57	73	52	38	32	67	64	90	70	32	33	30	36	24	37	100	67	64	87	0	1	0
XRN2 p-S500 p-S502 (z= 2)	0	0	0	0	0	0	38	65	100	36	0	0	0	0	0	0	0	0	0	0	1	1	1
BCLAF1 p-S178 (z= 2)	4	33	30	15	15	4	100	94	86	70	4	87	42	62	38	0	40	35	36	15	1	0	1
IRF2BP1 p-S385 (z= 2)	0	1	1	1	1	0	62	45	100	68	0	1	0	0	0	0	0	0	0	0	1	1	1
IRF2BPL p-S548 (z= 2)	8	8	10	6	6	8	100	82	96	68	8	4	2	3	2	8	4	4	5	2	1	1	1
MAP4 p-S637 (z= 2)	20	18	30	2	17	20	100	80	67	69	20	32	2	7	4	12	31	34	34	21	1	1	0
TJAP1 p-S546 (z= 2)	46	74	66	60	46	46	87	100	98	80	46	24	26	20	26	56	64	60	67	41	0	1	0
RPLP2 p-S103 p-S106 (z= 2)	29	0	0	1	0	29	16	26	72	56	29	70	17	34	23	29	27	58	80	100	0	1	0
RPLP2 p-S103 (z= 2) + oxidation	100	0	0	1	0	100	25	46	99	67	100	31	30	42	21	100	23	22	40	31	1	0	1
RPLP2 p-S106 (z= 2) + oxidation	72	0	3	4	4	72	63	100	96	66	72	15	16	22	7	72	20	15	21	11	1	1	1
RPLP2 p-S106 (z= 2)	10	0	3	2	1	10	21	26	37	29	10	22	10	15	11	10	98	81	100	68	0	1	0
TCEA1 p-S101 (z= 2)	0	0	0	0	0	0	1	1	1	1	0	1	1	1	1	0	85	90	100	55	0	1	0
SRRM1 p-T873 (z= 2)	42	35	51	4	24	42	84	97	63	49	42	34	7	13	8	42	77	77	100	47	0	1	0
PPAP p-S97 (z= 2)	5	58	52	43	47	5	70	67	100	60	5	37	44	49	32	2	26	32	28	20	0	0	1
MYH9 p-S1944 (z= 2)	0	64	61	65	39	0	12	13	52	33	0	29	18	18	12	0	84	100	100	68	0	1	0
MYH9 p-S1944 (z= 3)	0	32	35	37	20	0	25	29	100	58	0	50	33	35	23	0	51	54	45	37	0	0	0
WARS p-S468 (z= 2)	22	29	37	23	19	22	100	98	88	55	22	21	24	35	10	22	37	45	53	11	1	1	0
EBAG9 p-S37 (z= 2)	21	51	75	57	31	21	46	63	100	87	21	12	18	11	11	37	52	55	59	67	0	1	0
EBAG9 p-S37 (z= 3)	6	35	52	43	23	6	58	72	100	77	6	10	12	8	9	5	40	30	32	39	0	1	0
TCOF1 p-S1351 (z= 2)	11	66	65	33	27	11	44	31	73	57	11	100	60	39	27	1	60	73	85	27	0	0	0
EEF1D p-S163 (z= 3)	4	0	8	0	2	4	45	39	56	48	4	21	0	1	0	4	100	69	75	38	1	1	0
EHBP1 p-S1059 (z= 2)	1	5	3	4	3	1	6	7	7	6	1	84	100	97	87	0	3	3	3	2	0	0	1
CD44 p-S698 (z= 2)	3	79	61	56	44	3	38	32	100	56	3	70	82	54	47	1	58	70	55	40	0	0	0
IRF2BP2 p-S361 (z= 2)	0	0	0	0	0	0	55	67	100	94	0	0	0	0	0	0	1	0	1	1	1	1	1
DYNC1LI1 p-S517 (z= 2)	30	30	57	17	24	30	55	46	50	40	30	100	34	62	24	15	65	53	65	40	0	0	0
TPI1 p-S22 (z= 2)	100	3	8	0	0	100	87	34	29	31	100	2	0	0	0	100	34	24	24	1	1	1	0
TPI1 p-S22 (z= 3)	82	4	10	0	0	82	100	49	32	33	82	3	0	0	0	82	42	28	26	0	1	1	0
NSFL1C p-S115 (z= 2)	5	2	14	1	2	5	100	76	80	63	5	9	0	1	0	5	60	53	42	15	1	1	0
CBFA2T2 p-T400 p-T402 (z= 2)	6	26	15	30	24	6	88	100	36	46	6	10	20	9	14	3	9	18	9	10	1	1	1
TMX1 p-S248 (z= 3)	0	3	3	2	2	0	71	90	100	61	0	5	2	4	1	0	4	3	4	2	1	1	1
RPLP2 p-S87 (z= 3)	1	0	1	0	0	1	0	9	9	35	1	0	1	1	100	1	4	4	1	24	0	0	1
SORBS3 p-S531 (z= 2)	32	34	53	18	22	32	100	74	68	71	32	20	5	8	4	57	40	29	35	13	0	1	0
TACC2 p-S2318 p-S2322 (z= 3)	18	14	90	25	16	18	50	80	84	100	18	80	18	18	49	18	20	10	13	25	0	1	1
CCDC6 p-S241 p-S245 (z= 2)	93	11	25	13	16	93	100	100	94	92	93	31	12	17	14	93	53	49	50	16	1	1	0
TNKS1BP1 p-S495 (z= 3)	6	1	9	0	1	6	48	9	56	28	6	2	0	0	0	6	90	35	45	100	0	1	0
TRAFD1 p-S416 (z= 2)	23	43	46	36	28	23	100	84	81	59	23	19	9	15	8	41	51	48	62	29	0	1	0
HTATSF1 p-S703 (z= 2)	0	0	0	0	0	0	4	3	100	62	0	0	0	0	0	0	0	0	0	0	1	1	1
MLLT4 p-S1800 (z= 2)	69	4	13	0	5	69	71	80	48	100	69	42	36	32	63	69	60	43	51	10	1	0	0
TCOF1 p-S1379 (z= 2)	19	35	28	35	21	19	95	83	100	50	19	26	23	34	19	13	37	31	34	19	1	1	1
EIF3A p-S883 (z= 2)	1	0	99	0	94	1	0	0	0	8	1	0	0	0	0	1	0	100	0	0	0	1	0
SEMA4B p-S826 (z= 2)	8	9	10	8	5	8	81	70	49	43	8	33	15	21	13	8	99	89	100	36	0	1	0
AHNAK p-S136 (z= 2)	7	1	1	1	0	7	20	19	21	21	7	100	93	94	94	7	10	4	3	1	0	0	1
AHNAK p-S136 (z= 3)	3	8	5	6	3	3	30	31	27	23	3	100	86	91	90	3	0	3	0	3	0	0	1
KRT18 p-S400 (z= 2)	0	1	1	0	0	0	0	2	0	100	0	0	0	0	0	0	1	7	0	25	0	1	0
KRT18 p-S402 (z= 3)	0	0	2	1	0	0	0	0	0	3	0	2	0	0	0	0	16	34	4	100	0	1	0
FAM186B p-S817 (z= 2)	16	62	59	55	47	16	100	69	84	52	16	26	27	19	15	12	42	49	44	37	0	1	0
SLIRP p-T102 (z= 2)	1	79	78	100	65	1	92	81	84	45	1	44	49	48	34	14	78	96	98	64	0	0	0
SLIRP p-S103 (z= 2)	0	7	6	8	4	0	50	25	100	63	0	1	2	1	1	0	3	4	4	3	1	1	1
AHNAK p-S217 (z= 2)	19	72	51	46	29	19	100	99	100	54	19	15	17	18	16	22	33	32	37	20	0	1	1
DAB2IP p-S703 (z= 2)	7	100	78	92	66	7	26	25	27	19	7	20	23	28	17	27	56	57	61	41	0	1	0
EPB41L1 p-S541 (z= 2)	26	43	33	42	27	26	77	100	83	72	26	47	66	51	52	17	23	28	23	25	1	0	1
CTTN p-S419 (z= 2)	60	54	50	29	31	60	100	100	83	52	60	44	27	36	20	48	38	37	44	29	0	1	0
HNRNPU p-S60 (z= 3) + oxidation	1	0	2	0	0	1	40	65	24	100	1	2	0	0	0	1	23	21	19	34	1	1	0

HNRNPU p-S60 (z= 3)	0	0	0	0	0	0	0	0	0	0	0	0	0	0	0	0	53	44	37	100	0	1	0
CLCA p-S106 (z= 2)	76	16	14	14	28	76	22	23	13	26	76	26	29	23	33	100	12	15	12	26	0	0	0
ALDOA p-S47 (z= 2)	60	24	27	23	22	60	100	85	78	51	60	25	14	17	12	53	49	30	35	14	1	1	1
MYH15 p-Y728 (z= 2)	22	29	37	23	19	22	100	98	88	55	22	21	24	35	10	22	37	45	53	11	1	1	0
FAM91A1 p-S672 (z= 2)	0	30	39	51	16	0	3	4	100	69	0	53	34	31	27	0	20	24	18	22	0	0	0
MIPEP p-S326 (z= 2)	30	25	26	20	42	30	79	86	56	100	30	48	33	46	51	13	23	17	16	24	1	0	1
STK10 p-T953 (z= 2)	54	0	1	0	0	54	100	90	59	74	54	86	39	52	41	54	1	0	0	1	1	0	1
WRNIP1 p-S76 (z= 2)	1	23	19	24	20	1	88	100	82	53	1	19	27	21	17	0	17	18	16	12	1	1	1
TCOF1 p-S1351 (z= 2)	0	1	1	1	0	0	14	16	100	59	0	1	2	1	1	0	31	44	44	43	0	1	0
KRT17 p-S33 (z= 2)	74	28	21	17	13	74	100	72	64	48	74	22	13	17	9	45	24	24	23	11	1	1	1
LMNA p-S391 p-S393 (z= 2)	5	17	17	42	11	5	64	81	100	61	5	23	9	18	11	4	23	26	28	21	1	1	1
LMNA p-S391 (z= 2)	26	26	23	14	9	26	100	90	93	65	26	40	16	21	13	26	39	48	48	16	1	1	0
SCAMP3 p-S77 (z= 2)	1	18	16	14	11	1	100	87	79	52	1	20	22	24	16	0	8	9	9	5	1	1	1
BCL2L12 p-S243 (z= 2)	21	39	40	36	23	21	98	100	59	34	21	35	24	29	15	12	34	38	37	12	1	1	0
MTDH p-S296 (z= 2)	0	17	74	18	48	0	34	55	19	67	0	17	20	7	28	0	63	100	44	44	0	1	0
CTNNB1 p-S676 (z= 2)	2	3	8	1	2	2	100	77	60	80	2	7	1	1	0	2	32	41	31	9	1	1	0
ITA2 p-T829 (z= 2)	0	12	5	17	11	0	12	18	7	5	0	39	100	81	64	0	1	2	2	1	0	0	1
SHAN1 p-T947 (z= 2)	8	33	36	34	25	8	87	89	100	55	8	17	19	21	15	4	21	21	22	16	1	1	1
WDR44 p-S162 (z= 2)	19	21	25	12	13	19	73	55	100	75	19	6	4	5	4	19	34	28	31	17	1	1	0
WDR44 p-T164 (z= 3)	12	31	33	19	18	12	87	70	100	74	12	8	6	6	5	21	58	45	48	29	1	1	0
LEO1 p-S631 (z= 2)	2	42	38	54	31	2	82	76	100	53	2	5	5	6	4	7	51	49	46	31	1	1	0
CBX3 p-S177 (z= 2)	38	0	14	0	4	38	93	100	20	96	38	4	0	0	0	38	35	49	24	10	1	1	0
ANXA1 p-S6 (z= 2)	33	94	66	100	56	33	67	77	59	39	33	50	54	46	36	29	68	63	64	40	0	0	0
SAMM50 p-T4 (z= 2)	34	5	5	5	2	34	100	75	41	28	34	10	6	6	5	34	23	21	25	7	1	1	0
PRDM5 p-Y6 (z= 3) + oxidation	3	30	22	31	21	3	34	53	31	9	3	48	98	100	100	1	25	25	14	14	0	0	1
AN36A p-S1814 (z= 2) + oxidation	5	19	25	24	21	5	59	60	100	49	5	4	4	6	3	12	20	18	21	14	1	1	1
LIX1 p-S205 (z= 2) + oxidation	19	23	23	14	13	19	100	70	86	54	19	20	12	21	10	11	34	29	31	19	1	1	1
MAP3K7 p-S390 (z= 2)	6	13	20	10	10	6	42	36	34	20	6	100	57	81	55	0	30	24	23	5	0	0	1
BAD p-S119 (z= 2)	9	32	35	33	31	9	51	45	57	29	9	61	91	100	46	0	69	56	68	23	0	0	0
ERCC5 p-S385 (z= 2)	34	12	13	3	8	34	88	87	100	61	34	21	6	11	5	34	40	27	38	9	1	1	1
ADRB2 p-S408 (z= 2)	0	0	0	0	0	0	100	6	0	0	0	0	6	19	4	0	0	0	0	0	0	0	1
HNRNPD p-S83 (z= 2)	0	56	58	100	33	0	1	1	2	1	0	3	3	3	2	0	67	65	62	37	0	1	0
YBX1 p-S177 (z= 2)	1	76	71	100	61	1	40	37	68	42	1	4	8	8	6	6	78	68	81	61	0	1	0
SH3PXD2A p-S1003 (z= 2)	53	14	40	18	43	53	22	36	19	60	53	5	10	8	10	100	30	40	19	50	0	1	0
TAGLN2 p-S164 (z= 2)	56	23	43	14	40	56	88	93	100	82	56	59	55	54	43	20	86	64	85	41	1	0	0
EIF5B p-S215 (z= 2)	3	14	16	13	10	3	56	59	92	74	3	37	33	43	30	3	86	69	100	65	1	1	0
EIF5B p-S215 (z= 3)	1	23	28	27	18	1	52	72	84	59	1	81	72	100	64	0	33	27	37	26	1	0	1
LSR p-S644 (z= 2)	19	35	35	19	16	19	100	97	87	64	19	36	16	29	12	9	25	23	24	7	1	1	1
SEC22B p-S138 (z= 2)	72	35	43	23	30	72	73	67	100	77	72	50	43	58	38	61	39	31	38	29	0	0	1
PTPN12 p-S436 (z= 2)	25	42	50	43	36	25	65	58	55	62	25	80	56	100	74	12	76	64	62	52	0	0	0
FCHO2 p-S404 (z= 2)	18	17	21	27	14	18	38	41	100	34	18	12	26	26	8	10	12	11	13	7	0	0	1
LAD1 p-S39 (z= 2)	64	0	0	0	2	64	11	33	13	100	64	22	32	20	80	64	0	0	0	2	1	0	1
FKBP5 p-S14 (z= 2)	13	44	47	31	31	13	44	42	52	30	13	15	8	15	8	36	100	61	78	34	0	1	0
PLCG1 p-Y784 (z= 2)	0	0	0	0	0	0	0	0	0	2	0	12	21	4	100	0	0	1	0	2	0	0	1
BROMI p-T816 p-Y818 (z= 3)	0	59	68	76	55	0	89	97	100	57	0	10	11	14	9	0	74	75	75	56	0	1	0
SNX13 p-S337 (z= 2)	1	46	37	32	23	1	100	89	83	48	1	22	19	20	12	0	34	28	29	21	1	1	1
MEPCE p-S153 (z= 2)	24	30	21	54	17	24	26	39	34	100	24	22	30	20	41	26	16	19	17	15	0	0	1
SCRIB p-S1221 (z= 2)	11	69	87	48	34	11	48	50	66	34	11	21	11	17	9	27	100	83	96	43	0	1	0
XRN2 p-S679 (z= 2)	4	56	46	44	37	4	82	88	100	56	4	12	24	23	15	8	35	45	52	24	0	1	0
PTK2B p-S376 (z= 2)	0	7	21	2	6	0	64	67	75	98	0	33	2	3	7	0	72	42	55	100	1	1	0
GRLF1 p-S590 (z= 2)	2	2	0	1	0	2	4	4	5	5	2	84	88	100	89	2	6	1	0	1	0	0	1
SGPP1 p-S113 (z= 2)	3	85	71	100	98	3	34	33	49	29	3	7	11	10	8	13	52	46	52	37	0	1	0
XRN2 p-S449 (z= 2)	31	24	19	18	15	31	71	66	100	73	31	27	23	33	19	31	41	42	52	30	1	1	0
ANKRD17 p-S2060 (z= 2)	26	58	67	34	31	26	78	56	100	57	26	27	26	36	21	24	64	61	66	34	0	1	0
MARK2 p-S487 (z= 2)	6	29	23	22	19	6	48	53	100	57	6	11	13	15	5	5	20	19	19	13	1	1	1
SSBP3 p-S348 (z= 2)	13	55	63	57	38	13	21	19	27	15	13	4	3	4	2	100	79	50	76	53	0	1	0
STK11IP p-S773 (z= 2)	1	30	29	24	20	1	56	57	100	54	1	11	9	13	8	0	22	25	26	18	0	1	1
NUCKS1 p-S59 p-S62 (z= 2)	0	9	23	42	20	0	1	1	2	1	0	0	0	0	0	0	96	78	100	50	0	1	0
HN1 p-S88 (z= 2)	3	42	33	53	42	3	41	48	100	36	3	17	44	38	21	4	40	36	43	41	0	0	0
CDK12 p-S1083 (z= 2)	22	56	60	67	48	22	74	66	100	84	22	22	26	27	18	35	47	46	49	36	0	1	0
DOCK5 p-S1835 (z= 2)	16	25	35	35	25	16	69	62	100	47	16	13	17	15	10	24	60	40	55	29	0	1	0
FAM122B p-T53 (z= 2)	27	31	30	26	18	27	86	90	100	71	27	66	62	66	62	3	23	23	26	15	1	0	1
SPAG9 p-S333 (z= 2)	0	38	38	33	25	0	100	73	86	39	0	11	8	10	6	0	44	44	51	28	0	1	0

YAP1 p-T111 (z= 2)	20	75	60	84	42	20	100	92	79	56	20	17	18	18	14	33	63	56	66	34	0	1	0
MAP3K12 p-S350 (z= 2)	0	89	44	100	41	0	50	41	90	94	0	1	1	0	0	0	42	86	38	20	0	1	0
SRPK1 p-S312 (z= 2)	6	81	79	67	49	6	44	50	28	27	6	9	8	8	6	47	100	94	78	36	0	1	0
MACF1 p-S1861 (z= 2)	26	35	28	35	23	26	100	94	65	52	26	16	17	13	10	33	40	38	35	17	1	1	0
PCBP1 p-S174 (z= 2)	6	0	0	0	0	6	33	11	2	21	6	5	0	0	0	6	100	37	47	29	0	1	0
PCBP2 p-S174 (z= 2)	5	0	2	0	0	5	51	22	6	26	5	7	0	0	0	5	100	54	57	47	0	1	0
CANX p-S555 p-S565 (z= 3)	0	1	17	7	5	0	19	27	100	52	0	48	17	24	12	0	65	35	59	65	0	1	0
CANX p-S555 p-S565 (z= 2)	1	5	22	39	30	1	29	47	64	45	1	1	1	1	1	61	95	100	88	58	0	1	0
CANX p-S555 (z= 2)	1	3	3	3	3	1	83	87	100	65	1	1	1	1	1	1	2	2	2	1	1	1	1
CANX p-T563 (z= 3)	1	19	18	20	16	1	71	100	77	35	1	4	3	5	3	4	39	39	24	20	1	1	0
CANX p-S555 (z= 3)	0	20	55	12	17	0	2	2	8	4	0	2	1	2	1	0	89	41	96	100	0	1	0
CANX p-T563 p-S565 (z= 3)	1	18	19	10	7	1	24	43	32	34	1	100	30	64	33	0	38	28	38	25	1	0	0
BCLAF1 p-S649 (z= 2)	0	1	1	0	0	0	3	2	1	1	0	82	81	100	83	0	1	1	1	0	0	0	1
MYH10 p-S1957 (z= 2)	20	7	15	10	9	20	93	87	100	57	20	15	9	10	4	20	33	41	33	21	1	1	1
ENSA p-S85 (z= 2)	6	46	45	36	40	6	35	13	25	19	6	100	72	57	30	2	48	34	44	26	0	0	0
SYNRG p-S753 (z= 2)	29	14	15	19	19	29	84	85	82	100	29	37	45	30	47	15	16	17	15	25	1	0	1
HSPB1 p-S83 (z= 2)	76	16	14	14	28	76	22	23	13	26	76	26	29	23	33	100	12	15	12	26	0	0	0
HSPB1 p-S83 (z= 2)	100	3	10	1	5	100	10	5	5	14	100	28	2	13	7	47	11	6	12	5	0	0	0
MMP28 p-T88 (z= 2)	34	5	5	5	2	34	100	75	41	28	34	10	6	6	5	34	23	21	25	7	1	1	0
CAPR2 p-T545 (z= 2)	0	35	40	100	30	0	18	12	95	63	0	44	62	49	41	0	9	11	14	16	0	0	1
EIF3C p-S40 (z= 2)	21	37	27	34	21	21	89	100	77	49	21	19	23	18	14	22	24	26	28	19	1	1	1
EIF3C p-S40 (z= 3)	0	0	0	0	0	0	0	0	0	0	0	67	34	100	51	0	0	0	0	0	0	0	1
PEA15 p-S117 (z= 2)	33	94	66	100	56	33	67	77	59	39	33	50	54	46	36	29	68	63	64	40	0	0	0
KIAA1671 p-T1523 (z= 2)	0	35	40	100	30	0	18	12	95	63	0	44	62	49	41	0	9	11	14	16	0	0	1
RBM14 p-T207 (z= 2)	26	27	21	28	15	26	60	89	75	100	26	20	32	16	29	27	20	19	19	18	1	1	1
SFRS18 p-S212 (z= 2)	77	23	23	17	12	77	92	86	48	63	77	14	6	4	5	100	37	27	31	11	1	1	0
CDK12 p-S304 p-Y306 (z= 2)	8	12	23	26	14	8	62	71	100	61	8	38	34	46	33	3	24	24	31	19	1	0	1
TPI1 p-S22 (z= 2)	2	10	16	8	9	2	82	75	81	100	2	5	2	1	2	2	20	26	20	20	1	1	1
TPI1 p-S22 (z= 2)	1	10	29	5	5	1	37	35	100	73	1	4	3	3	3	1	42	29	36	34	0	1	0
UTRN p-S834 (z= 2)	5	71	67	61	47	5	84	78	100	36	5	51	65	76	41	2	48	52	55	28	0	0	0
SET p-S8 (z= 2)	6	77	54	100	48	6	0	0	61	46	6	61	45	38	31	3	51	61	52	40	0	0	0
CLASP1 p-T652 (z= 2)	14	29	22	34	21	14	52	100	97	61	14	28	47	29	42	7	17	18	20	16	1	0	1
GL54D p-T154 p-S155 (z= 2)	6	26	15	30	24	6	88	100	36	46	6	10	20	9	14	3	9	18	9	10	1	1	1
STK10 p-S439 (z= 2)	9	19	13	14	11	9	100	83	52	44	9	3	2	3	1	20	17	16	14	5	1	1	1
EPPK1 p-S2717 (z= 2)	51	30	35	22	36	51	63	84	57	100	51	16	11	8	15	73	44	52	55	51	1	1	0
FAM55D p-Y361 p-S365 (z= 3)	0	9	7	12	7	0	3	9	22	8	0	26	80	100	87	0	3	2	3	3	0	0	1
HDGF p-S166 (z= 2)	71	2	6	0	0	71	100	40	26	25	71	14	0	3	0	71	61	38	46	0	1	1	0
COPE p-S100 (z= 2)	23	25	41	6	17	23	100	75	46	36	23	24	2	9	4	18	48	39	60	10	0	1	0
ZNF185 p-S466 (z= 2)	55	19	23	9	11	55	94	63	100	50	55	33	14	26	18	26	31	26	27	15	1	1	1
TNKS1BP1 p-S430 (z= 2)	39	40	70	30	38	39	78	64	100	63	39	23	12	13	11	24	93	70	81	48	0	1	0
TNKS1BP1 p-S430 (z= 3)	12	45	69	31	36	12	92	78	100	42	12	24	12	23	16	2	92	65	72	45	0	1	0
MARCKS p-S160 (z= 2)	88	9	36	2	4	88	96	100	37	77	88	12	1	4	2	88	54	70	54	6	1	1	0
TMEM40 p-S138 (z= 2)	9	14	15	11	8	9	73	66	88	58	9	28	26	31	16	9	95	80	100	42	1	1	0
TMEM40 p-S138 (z= 3)	0	2	3	2	1	0	16	17	18	10	0	16	13	16	9	0	100	82	87	48	0	1	0
LRRFIP1 p-S121 (z= 2)	3	19	22	21	16	3	90	73	100	69	3	8	10	10	8	3	33	25	27	19	1	1	1
LRRFIP1 p-S125 (z= 3)	1	23	32	33	20	1	92	85	100	65	1	25	30	36	29	0	40	29	31	25	1	1	1
LRRFIP2 p-T332 (z= 3)	14	17	27	25	11	14	44	51	100	56	14	28	37	43	25	7	12	15	14	16	0	0	1
NRD1 p-S97 (z= 2)	17	11	19	6	4	17	100	73	57	47	17	29	7	17	7	17	86	66	99	15	1	1	0
EI2BA p-S106 (z= 2)	0	0	0	0	0	0	100	95	62	94	0	0	0	0	0	0	3	3	3	2	1	1	1
FAM83H p-S1004 (z= 2)	19	23	23	14	13	19	100	70	86	54	19	20	12	21	10	11	34	29	31	19	1	1	1
ZC3H3 p-S570 (z= 2)	0	0	0	0	0	0	100	95	62	94	0	0	0	0	0	0	3	3	3	2	1	1	1
RPS6 p-S237 (z= 2)	0	0	0	0	0	0	100	95	62	94	0	0	0	0	0	0	3	3	3	2	1	1	1
RPS6 p-S237 (z= 2)	0	0	0	0	0	0	100	95	62	94	0	0	0	0	0	0	3	3	3	2	1	1	1
RUNDC3A p-S140 p-T144 (z= 2)	4	59	20	100	39	4	13	40	38	17	4	9	76	32	46	3	4	7	7	5	0	0	1
HN1 p-S88 (z= 2)	27	20	28	12	18	27	100	80	92	60	27	31	16	25	13	20	45	36	41	20	1	1	1
HN1 p-S89 (z= 3)	16	21	31	20	16	16	100	97	97	50	16	48	25	39	20	6	44	33	37	19	1	1	1
SPTBN1 p-S2103 (z= 2)	0	8	6	5	3	0	11	9	24	17	0	8	8	6	5	0	88	100	94	66	0	1	0
PPFIBP1 p-S795 (z= 2)	1	76	90	79	67	1	21	23	28	20	1	19	20	23	15	1	93	100	96	65	0	1	0
TNKS1BP1 p-S1546 (z= 2)	1	35	29	20	22	1	79	58	100	88	1	81	94	70	79	0	22	34	38	32	0	0	1
UPF3B p-S326 (z= 2)	3	29	23	29	56	3	18	23	33	38	3	43	70	66	100	1	10	12	12	52	0	0	0
CCD91 p-S382 (z= 2)	9	49	65	46	34	9	77	79	100	70	9	30	20	31	18	7	74	59	77	34	0	1	0
RCC1 p-S12 (z= 2)	0	0	0	0	0	0	100	88	91	65	0	24	15	18	11	0	0	0	0	0	1	1	1

QSOX2 p-S26 (z= 2)	0	48	37	57	25	0	68	76	100	57	0	25	28	24	14	0	11	20	18	13	1	1	1
FA47A p-S259 (z= 2)	0	0	0	0	0	0	100	95	62	94	0	0	0	0	0	0	3	3	3	2	1	1	1
CXorf56 p-T149 (z= 2)	4	21	17	16	12	4	100	89	74	53	4	17	20	17	17	0	16	17	19	10	1	1	1
SRRM1 p-S726 p-T728 (z= 3)	0	14	32	16	9	0	25	43	100	83	0	45	13	15	12	0	26	35	42	17	0	1	0
TNKS1BP1 p-S1667 (z= 2)	3	67	66	65	46	3	31	28	37	23	3	9	8	11	7	36	100	76	76	46	0	1	0
ARL6IP4 p-S272 (z= 2)	41	11	13	5	13	41	88	100	81	83	41	16	7	16	9	41	42	36	34	32	1	1	1
LBR p-S100 (z= 2)	13	13	22	6	6	13	11	2	88	100	13	54	13	19	12	13	41	51	55	17	0	1	0
SMAP p-S18 (z= 2)	43	2	10	0	2	43	100	69	91	64	43	23	0	4	0	43	44	25	41	21	1	1	1
SMAP p-S18 (z= 3)	23	4	19	0	4	23	90	70	100	52	23	33	0	5	0	23	60	33	52	31	1	1	0
SLC9A3R1 p-S292 (z= 2)	39	18	32	20	21	39	81	68	100	70	39	23	10	19	10	49	56	42	52	33	1	1	0
SRRM2 p-S877 (z= 2)	35	71	77	37	34	35	77	69	94	47	35	25	13	25	13	48	100	62	95	30	0	1	0
EPB41L1 p-S467 (z= 2)	0	24	31	38	29	0	47	24	100	39	0	12	14	9	6	1	40	45	45	30	0	1	0
HDGFRP2 p-S455 (z= 2)	2	0	1	1	1	2	3	4	2	3	2	50	67	66	100	0	0	0	1	1	0	0	1
ANKS1A p-S648 (z= 2)	18	13	15	12	7	18	70	76	100	50	18	12	9	13	7	18	32	22	23	13	1	1	1
CEP110 p-S2163 (z= 2)	29	57	32	57	91	29	80	100	25	65	29	55	67	38	63	25	24	37	20	38	0	0	1
SLC4A10 p-S239 (z= 2)	0	34	68	40	51	0	46	68	100	79	0	0	0	0	0	0	55	51	40	32	0	1	0
S4A8 p-S238 (z= 2)	0	34	68	40	51	0	46	68	100	79	0	0	0	0	0	0	55	51	40	32	0	1	0
SEPT9 p-S31 (z= 2)	75	18	29	12	15	75	99	86	100	80	75	25	12	17	10	75	44	39	50	33	1	1	1
CCNYL1 p-S345 (z= 2)	100	1	10	1	2	100	65	39	70	56	100	13	4	7	3	100	23	23	26	4	1	1	0
C10orf47 p-S44 (z= 2)	30	4	6	1	3	30	39	93	42	87	30	44	96	67	100	30	6	6	8	8	1	0	1
HNRNPUL2 p-S162 (z= 2)	9	16	15	15	10	9	73	63	100	24	9	11	10	11	7	10	18	16	18	10	1	1	1
CTNND1 p-S921 (z= 2) + oxidation	23	14	19	12	14	23	100	86	100	73	23	2	1	2	1	23	3	2	2	2	1	1	1
CTNND1 p-S921 (z= 2)	9	28	30	21	20	9	88	82	100	61	9	34	19	30	17	1	18	17	21	10	1	1	1
AGL p-Y970 p-S972 (z= 2)	0	71	66	100	70	0	0	0	0	0	0	0	0	0	0	5	67	71	75	38	0	1	0
TRIM28 p-S474 (z= 2)	24	61	82	66	56	24	22	22	24	15	24	97	100	94	76	3	68	71	92	45	0	0	0
ERBB2 p-S1055 (z= 2)	15	0	1	0	0	15	100	39	29	38	15	2	0	0	0	15	18	13	16	8	1	1	0
MORC1 p-S108 (z= 2)	4	21	17	16	12	4	100	89	74	53	4	18	20	17	17	0	16	17	19	10	1	1	1
MORC3 p-S109 (z= 2)	4	21	17	16	12	4	100	89	74	53	4	18	20	17	17	0	16	17	19	10	1	1	1
STMN1 p-S64 (z= 2)	6	46	45	36	40	6	35	13	25	19	6	100	72	57	30	2	48	34	44	26	0	0	0
ADCY5 p-S729 (z= 2)	7	50	19	9	23	7	20	26	5	16	7	100	97	63	84	7	27	58	17	23	0	0	0
MAP3K7 p-S440 (z= 2)	19	29	34	35	20	19	72	74	100	54	19	18	16	22	12	18	29	26	35	20	1	1	1
KRT7 p-S255 (z= 2)	11	10	40	27	27	11	42	54	100	97	11	12	18	9	21	11	23	33	24	43	0	1	0
KRT8 p-S254 (z= 2)	0	0	0	0	0	0	0	0	0	0	0	0	0	0	0	0	73	89	69	100	0	1	0
GSTA2 p-S213 (z= 2)	0	78	62	100	29	0	2	0	99	59	0	67	65	59	43	0	37	31	30	35	0	0	0
FHOD1 p-S368 (z= 2)	40	45	34	34	23	40	100	69	99	74	40	53	54	63	36	15	39	34	36	18	1	0	1
EIF4B p-S446 (z= 2)	11	49	65	81	55	11	38	30	72	31	11	15	23	19	14	34	100	78	81	51	0	1	0
C18orf34 p-S177 (z= 2)	0	78	62	100	29	0	2	0	99	59	0	67	65	59	43	0	37	31	30	35	0	0	0
ARHGEF10 p-S380 (z= 2)	0	0	3	0	79	0	0	0	0	4	0	0	0	0	1	0	3	1	1	100	0	1	0
RIPK2 p-S364 (z= 2)	1	0	1	0	4	1	27	39	19	100	1	2	1	0	3	1	12	16	9	29	1	1	1
AKT1S1 p-S184 (z= 2)	42	1	9	0	1	42	100	54	49	66	42	9	0	0	0	42	30	21	20	20	1	1	1
DOCK5 p-S1767 (z= 2)	22	42	58	28	31	22	100	99	86	58	22	85	31	51	26	1	83	64	83	29	0	0	0
SPTAN1 p-S1218 (z= 2)	32	53	68	32	37	32	100	82	100	51	32	26	20	22	13	40	95	65	75	28	0	1	0
CBX3 p-S96 (z= 2)	0	12	22	19	11	0	0	0	100	59	0	46	23	27	16	0	55	41	42	37	0	0	0
F1891 p-S21 (z= 2)	0	0	0	0	0	0	100	95	62	94	0	0	0	0	0	0	3	3	2	2	1	1	1
NEDD4L p-S449 (z= 2)	15	16	20	15	12	15	61	75	100	91	15	15	22	20	16	15	38	32	43	22	1	1	1
DNAJC5 p-S11 (z= 2)	1	17	62	22	28	1	13	17	59	31	1	1	1	0	1	13	100	72	56	74	0	1	0
DNAJC5 p-S11 (z= 3)	1	12	53	17	20	1	19	28	100	53	1	3	1	1	2	4	74	49	38	54	0	1	0
SLC38A1 p-S53 (z= 2)	5	58	52	43	47	5	70	67	100	60	5	37	44	49	32	2	26	32	28	20	0	0	1
KRT6A p-S61 (z= 2)	72	8	18	6	18	72	17	23	12	22	72	2	2	2	4	100	9	13	9	15	0	1	0
KRT5 p-S65 (z= 2)	93	24	50	11	28	93	78	74	41	56	93	11	3	5	5	100	48	51	35	34	0	1	0
TMPRSS15 p-S848 (z= 2)	7	28	36	27	34	7	67	100	75	83	7	9	10	9	10	5	29	31	23	32	1	1	1
FKBP4 p-S454 (z= 2)	0	0	0	0	0	0	0	38	31	100	0	0	0	0	0	0	0	0	0	0	1	1	1
SORBS3 p-S564 (z= 2)	12	31	55	18	25	12	92	69	100	76	12	32	17	27	20	17	47	39	51	37	0	1	0
TJP3 p-S334 (z= 2)	15	17	19	14	13	15	81	65	100	58	15	26	14	30	14	7	29	23	28	17	1	1	1
AIM1 p-S534 (z= 2)	15	64	64	78	49	15	60	47	100	60	15	58	66	65	61	14	54	48	55	38	0	0	0
LIMCH1 p-S719 (z= 2)	22	36	80	59	43	22	55	57	79	89	22	37	21	15	29	41	83	61	76	100	0	1	0
AHNAK p-S94 (z= 2)	51	89	77	84	47	51	100	88	67	46	51	50	44	48	40	50	60	52	64	30	0	0	0
ZNF532 p-S315 (z= 2)	27	44	47	56	45	27	62	64	100	47	27	16	21	24	21	30	52	51	61	31	0	1	0
SIRT1 p-S48 (z= 2)	4	16	16	15	10	4	68	59	100	56	4	27	19	26	15	4	46	44	52	28	1	1	0
TJP3 p-S165 (z= 2)	21	19	24	20	9	21	76	62	100	68	21	16	19	15	12	18	24	24	26	19	1	1	1
SRRM2 p-S2133 (z= 2)	22	68	88	66	62	22	62	64	78	65	22	100	83	77	75	2	89	83	93	74	0	0	0
NCOR2 p-S2270 (z= 2)	28	26	30	26	17	28	87	100	91	79	28	24	28	25	21	21	28	22	32	22	1	1	1
BICD2 p-S583 (z= 2)	16	47	55	47	35	16	100	84	81	51	16	21	17	22	13	15	40	36	39	26	0	1	0
DDB2 p-S27 (z= 2)	7	82	78	100	73	7	27	29	42	27	7	10	14	12	10	33	62	71	73	43	0	1	0
NSFL1C p-S115 (z= 2)	13	4	12	1	4	13	83	66	100	73	13	11	1	2	1	13	43	38	39	38	1	1	0

RCC1 p-S12 (z= 2)	13	42	30	33	27	13	63	70	100	58	13	16	23	26	19	12	21	23	23	20	1	1	1
SH3BP1 p-S551 (z= 2)	0	2	2	1	1	0	3	3	3	2	0	100	29	54	27	0	3	2	3	1	0	0	1
SSH3 p-S10 (z= 2)	28	20	42	25	22	28	99	98	95	100	28	20	6	6	8	57	91	46	62	49	1	1	0
MORC2 p-S616 (z= 2)	40	21	43	9	8	40	100	85	88	86	40	27	9	8	7	40	27	23	30	17	0	1	1
WDR4 p-S392 (z= 2)	1	13	11	16	9	1	4	3	7	5	1	95	100	72	71	0	9	14	12	11	0	0	1
FAM116A p-S471 (z= 2)	0	1	1	2	0	0	0	0	100	53	0	49	91	63	55	0	13	25	26	40	0	0	0
C15orf52 p-S202 (z= 2)	15	22	23	21	14	15	86	88	100	58	15	18	20	23	12	8	23	21	24	13	1	1	1
NCAPH2 p-S285 (z= 2)	19	33	29	25	20	19	100	75	88	52	19	25	22	22	15	11	23	23	27	16	1	1	1
SYMPK p-S1244 (z= 2)	12	92	100	81	61	12	90	82	100	57	12	61	57	55	50	2	85	72	80	48	0	0	0
TRIM29 p-S22 (z= 2)	30	29	24	25	15	30	76	86	100	58	30	28	24	29	23	13	20	21	20	13	1	1	1
KANK4 p-S974 (z= 2) + oxidation	4	59	20	100	39	4	13	40	38	17	4	9	76	32	46	3	4	7	7	5	0	0	1
CTTNBP2NL p-S569 (z= 2)	8	33	36	34	25	8	87	89	100	55	8	17	19	21	15	4	21	21	22	16	1	1	1
RHG32 p-T955 (z= 2)	5	71	67	61	47	5	84	78	100	36	5	51	65	76	41	2	48	52	55	28	0	0	0
PML p-S531 (z= 3)	3	11	46	6	15	3	56	58	54	75	3	75	11	15	19	3	100	65	79	100	0	1	0
C10orf18 p-S445 (z= 2)	0	45	39	38	22	0	100	100	99	74	0	8	9	11	7	0	23	21	28	16	1	1	1
SRRM2 p-S2450 (z= 2)	35	77	76	77	42	35	62	54	62	44	35	26	25	26	16	61	100	82	97	54	0	1	0
LSM14A p-S217 (z= 2)	2	16	15	10	6	2	50	55	73	62	2	23	23	23	21	2	100	76	86	62	1	1	0
LSM14A p-S217 (z= 3)	0	27	29	21	12	0	62	80	100	73	0	38	35	42	36	0	30	21	22	20	1	0	1
COBLL1 p-S519 (z= 2)	6	1	13	3	8	6	18	21	37	100	6	2	1	0	3	6	13	19	13	41	0	1	0
TNKS1BP1 p-S837 (z= 2)	58	29	46	41	34	58	27	27	47	23	58	83	68	100	63	48	42	35	47	41	0	0	0
CLASP1 p-S1197 (z= 2)	6	22	29	22	19	6	79	100	96	79	6	29	33	34	23	1	30	25	25	15	1	1	1
CD44 p-S707 (z= 2) + oxidation	5	19	25	24	21	5	59	60	100	49	5	4	4	6	3	12	20	18	21	14	1	1	1
CD44 p-S707 (z= 2)	3	87	99	86	59	3	67	67	100	52	3	47	61	83	49	0	66	59	73	37	0	0	0
CD44 p-S707 (z= 3)	1	89	100	93	56	1	52	58	84	33	1	55	76	97	52	0	70	60	59	41	0	0	0
ITFG3 p-S22 (z= 2)	5	28	27	33	25	5	66	62	100	43	5	10	12	15	9	7	25	24	28	19	1	1	1
MAF1 p-S76 (z= 2)	5	0	1	2	16	5	28	25	22	9	5	0	2	4	3	18	0	97	100	27	0	1	0
PPFIBP1 p-T603 (z= 2)	39	16	32	10	32	39	76	67	75	100	39	48	64	57	78	0	38	37	42	52	1	0	0
MAST3 p-S886 (z= 2)	37	17	25	23	38	37	10	53	63	100	37	12	54	28	70	14	8	10	8	24	1	0	1
TJP3 p-S606 (z= 2)	8	33	48	31	29	8	90	99	100	67	8	16	19	22	14	4	34	35	36	21	1	1	1
TJP1 p-S618 (z= 2)	6	22	26	23	16	6	100	92	97	49	6	23	25	27	16	1	16	15	21	8	1	1	1
KLC1 p-S522 (z= 2)	9	49	65	46	34	9	77	79	100	70	9	30	20	31	18	7	74	59	77	34	0	1	0
TMC6 p-S94 (z= 2)	43	3	10	3	4	43	33	79	100	60	43	36	11	22	9	43	32	43	56	11	1	1	0
ARHGAP9 p-T263 (z= 3)	0	7	6	10	6	0	3	9	22	8	0	26	80	100	87	0	2	2	2	3	0	0	1
SRRM2 p-S2045 p-S2047 (z= 2)	14	5	17	15	6	14	43	59	100	50	14	24	18	33	19	14	60	61	69	39	1	1	0
SRSF2 p-S190 p-S192 (z= 2)	4	30	49	54	19	4	12	15	100	59	4	26	15	17	14	4	42	48	62	39	0	1	0
SRRM2 p-S2033 p-T2035 (z= 2)	8	18	76	72	46	8	38	46	64	32	8	14	15	18	14	18	88	84	100	60	0	1	0
SGTA p-S306 (z= 2)	0	21	18	17	6	0	6	6	29	19	0	100	49	52	31	0	22	20	21	14	0	0	1
THRAP3 p-T565 (z= 2)	7	100	77	89	63	7	69	27	60	32	7	26	18	17	10	6	67	64	86	52	0	1	0
PHF20L1 p-S606 (z= 2)	4	51	29	74	49	4	65	60	37	27	4	48	100	43	55	0	17	38	21	16	0	0	1
RAB11FIP1 p-S436 (z= 2)	1	1	1	1	1	1	3	2	4	3	1	4	3	4	4	1	100	75	88	55	0	1	0
KCNT1 p-S94 (z= 2)	0	0	0	0	0	0	100	94	62	93	0	0	0	0	0	0	3	3	3	2	1	1	1
UBR5 p-S295 (z= 2)	15	7	3	5	2	15	100	67	18	14	15	6	4	4	3	3	3	5	3	1	1	1	1
LSM14A p-S184 (z= 2)	17	37	73	35	43	17	47	38	41	31	17	8	4	6	3	77	100	69	87	40	0	1	0
FAM83H p-S926 (z= 2)	15	14	20	15	9	15	56	60	100	52	15	14	13	15	12	15	25	25	27	17	1	1	1
SLC9A7 p-S694 (z= 2)	1	0	1	0	1	1	6	7	10	9	1	72	100	100	41	1	2	0	0	0	0	0	1
KIAA1614 p-S1000 p-S1003 (z= 2)	9	3	7	17	1	9	31	6	12	28	9	79	18	100	27	3	2	4	4	2	0	0	1
G3BP1 p-S233 (z= 2)	16	21	21	9	11	16	70	52	100	56	16	7	10	9	7	16	42	44	44	24	1	1	0
G3BP1 p-S232 (z= 3)	5	31	21	12	11	5	75	69	100	54	5	9	15	14	10	5	36	34	31	21	1	1	1
PHACTR4 p-S118 (z= 2)	21	12	13	8	5	21	100	76	74	42	21	10	8	11	6	21	32	20	26	11	1	1	1
BDP1 p-S93 (z= 2)	4	51	29	74	49	4	65	60	37	27	4	48	100	43	55	0	17	38	21	16	0	0	1
C2orf49 p-S92 (z= 2)	3	29	23	29	56	3	18	23	33	38	3	43	70	66	100	1	10	12	12	52	0	0	0
COG2 p-S106 (z= 2)	3	29	23	29	56	3	18	23	33	38	3	43	70	66	100	1	10	12	12	52	0	0	0
AIM1 p-T21 (z= 2)	18	18	25	15	14	18	59	64	68	60	18	90	74	100	74	18	15	12	14	9	1	0	1
PGM3 p-S65 (z= 3)	0	0	2	1	1	0	3	4	4	3	0	100	25	69	98	0	3	2	3	1	0	0	1
LSR p-S494 (z= 2)	17	11	13	8	8	17	64	79	100	65	17	17	14	17	9	17	23	22	23	14	1	1	1
ARFGEF1 p-S1570 (z= 2)	10	26	38	31	34	10	88	85	100	68	10	17	24	28	19	3	25	18	25	14	1	1	1
PTMS p-S6 (z= 2)	21	25	24	35	23	21	100	76	88	47	21	25	24	29	19	12	34	25	28	19	1	1	1
PI4KB p-S429 (z= 2)	2	67	89	56	47	2	56	52	92	65	2	57	54	55	43	1	99	91	100	67	0	0	0
PI4KB p-S429 (z= 3)	0	0	0	0	0	0	2	2	3	2	0	0	0	1	0	0	100	93	97	74	0	1	0
ADCY5 p-S156 (z= 2)	0	3	3	2	2	0	85	100	96	51	0	16	10	15	6	0	5	3	4	3	1	1	1
YBX1 p-S103 (z= 2)	10	0	0	1	1	10	5	16	7	42	10	57	58	47	100	10	18	5	8	5	0	0	1
LMNA p-S637 (z= 2)	28	39	61	23	33	28	68	87	100	94	28	17	13	14	18	46	57	50	52	36	0	1	0
NASP p-S245 (z= 2)	22	36	46	61	44	22	88	61	100	29	22	27	30	31	22	27	72	74	71	45	0	1	0

SRSF6 p-S315 p-S317 (z= 2)	2	12	15	15	5	2	19	23	100	83	2	25	12	16	13	2	9	10	14	9	0	0	1
KRT8 p-S25 (z= 2)	100	17	29	13	23	100	31	28	48	74	100	32	36	17	33	25	17	28	18	25	0	0	0
PA2G4 p-T387 (z= 2)	0	0	0	0	0	0	1	1	0	1	0	0	1	1	0	0	97	90	68	100	0	1	0
CSMD1 p-T412 p-S415 (z= 2)	1	63	38	39	84	1	19	22	24	25	1	31	100	56	88	0	13	12	10	43	0	0	1
MCM2 p-S42 (z= 2)	16	18	25	12	10	16	100	67	70	48	16	17	9	14	6	11	23	19	22	5	1	1	1
SMC4 p-S42 (z= 2)	13	14	20	4	11	13	100	68	98	56	13	16	4	10	3	14	48	34	34	20	1	1	1
CARHSP1 p-S53 (z= 2)	27	7	12	5	4	27	100	59	70	40	27	18	3	10	5	27	41	31	35	7	1	1	0
DHTKD1 p-S559 (z= 3)	0	7	6	10	6	0	3	9	22	8	0	26	80	100	87	0	2	2	2	3	0	0	1
TUBA1A p-T52 (z= 2)	1	9	36	21	72	1	25	48	44	100	1	6	18	8	24	2	37	59	36	87	0	1	0
KCNH1 p-S870 (z= 2)	0	1	1	1	0	0	1	1	100	57	0	44	36	38	26	0	20	24	28	24	0	0	0
MTOR p-S1167 (z= 2)	76	16	14	14	28	76	22	23	13	26	76	26	29	23	33	100	12	15	12	26	0	0	0
GON4L p-S2195 (z= 2)	0	32	28	29	22	0	84	88	100	74	0	0	0	0	0	0	21	24	23	17	1	1	1
CTNNA1 p-S642 (z= 2)	33	1	11	0	3	33	85	66	100	67	33	19	0	5	0	33	66	43	54	31	1	1	0
EEF1G p-T47 (z= 2)	1	62	100	73	74	1	5	6	7	4	1	2	3	3	2	9	55	52	62	41	0	1	0
NCF2 p-T234 (z= 2)	1	62	100	73	74	1	5	6	7	4	1	2	3	3	2	9	55	52	62	41	0	1	0
SYAP1 p-T249 (z= 2)	8	22	22	23	16	8	69	64	100	42	8	14	17	21	13	4	18	16	17	9	1	1	1
FAM21A p-S334 (z= 2)	7	22	24	21	21	7	74	81	100	56	7	20	15	18	11	6	37	30	35	25	1	1	1
RALBP1 p-S30 (z= 2)	17	42	40	43	34	17	83	72	100	55	17	24	26	34	19	14	43	42	43	26	0	1	0
CTTN p-T400 p-S406 (z= 2)	55	40	59	61	42	55	46	51	76	59	55	83	83	100	84	55	46	39	57	36	0	0	0
CTTN p-T402 (z= 2)	19	14	16	12	10	19	67	71	100	65	19	10	10	10	9	19	19	18	23	17	1	1	1
BRCA2 p-S1633 (z= 2)	1	19	11	21	15	1	12	12	13	5	1	50	100	90	67	0	4	5	6	4	0	0	1
CTNNB1 p-S553 (z= 2)	14	46	58	46	48	14	83	80	100	54	14	5	5	5	3	88	51	42	49	29	0	1	0
CTNNB1 p-S553 (z= 2)	4	84	100	66	64	4	41	39	52	32	4	24	20	23	18	2	60	80	78	48	0	1	0
CTNNB1 p-S553 (z= 3)	0	73	100	37	39	0	0	0	0	0	0	63	68	55	51	0	64	60	38	42	0	0	0
CIKS p-S404 (z= 2)	76	16	14	14	28	76	22	23	13	26	76	26	29	23	33	100	12	15	12	26	0	0	0
SRSF2 p-S27 (z= 2)	2	9	10	9	6	2	100	55	92	57	2	21	15	17	8	2	22	21	21	12	1	1	1
SRRM2 p-S2399 (z= 2)	37	82	95	52	53	37	100	80	99	67	37	27	18	24	14	56	82	76	88	52	0	1	0
GOLGA4 p-S41 (z= 2)	46	13	48	17	30	46	82	100	56	83	46	21	7	7	9	81	45	49	64	40	1	1	0
SNCA p-S88 p-T93 (z= 3)	0	9	10	7	6	0	19	19	25	12	0	75	52	100	57	0	8	7	9	6	0	0	1
RAD50 p-T825 (z= 2)	32	53	68	32	37	32	100	82	100	51	32	26	20	22	13	40	95	65	75	28	0	1	0
PNMA3 p-T117 (z= 2)	1	16	16	11	9	1	22	25	32	19	1	100	69	97	53	0	15	12	13	8	0	0	1
NASP p-S452 (z= 2)	0	2	2	3	1	0	24	16	100	91	0	63	26	30	21	0	0	0	0	0	1	0	1
RERE p-S657 (z= 2)	1	21	18	18	14	1	100	76	64	36	1	73	55	53	26	0	22	23	22	12	1	0	1
SLK p-S572 (z= 2)	0	23	51	93	52	0	1	1	1	1	0	1	1	1	1	0	92	92	100	69	0	1	0
GFPT1 p-S262 (z= 2)	16	44	52	35	36	16	79	78	100	51	16	29	24	29	17	18	51	51	53	34	0	1	0
GAB1 p-Y660 (z= 2)	1	0	0	0	0	1	6	6	7	4	1	100	71	96	53	1	0	33	38	19	0	0	1
CHTF18 p-S872 (z= 3)	2	10	49	3	12	2	8	8	11	12	2	3	0	0	1	12	78	38	53	100	0	1	0
ERC1 p-S16 (z= 2)	2	35	28	32	22	2	73	81	100	53	2	18	20	22	14	1	26	25	26	17	1	1	1
MICALL1 p-S579 (z= 2)	12	9	15	6	5	12	95	77	71	59	12	10	4	5	6	12	100	79	97	26	1	1	0
PPAN p-S360 (z= 2)	15	38	29	33	20	15	90	86	100	54	15	29	32	48	26	11	36	34	38	22	1	1	1
CTNND1 p-S269 (z= 2)	100	4	9	4	17	100	22	35	15	54	100	4	9	4	12	34	3	6	3	14	1	1	1
WDR44 p-S51 (z= 2)	21	16	14	14	10	21	100	92	93	51	21	18	18	21	13	21	34	27	31	14	1	1	1
MAP4 p-S1074 (z= 2)	2	8	18	9	15	2	32	51	36	100	2	4	5	3	10	2	9	12	8	23	1	1	1
MAP4 p-S1074 (z= 3)	0	3	6	3	4	0	36	66	40	100	0	2	3	2	6	0	19	30	18	56	1	1	0
AAK1 p-T621 p-S625 (z= 2)	33	15	6	18	9	33	49	50	100	65	33	11	7	15	10	33	5	31	26	14	1	1	0
KRT8 p-S44 (z= 2)	45	6	15	4	21	45	33	54	17	100	45	5	8	3	15	18	7	15	6	15	1	1	1
HTATSF1 p-S617 (z= 2)	2	6	5	6	4	2	99	86	100	56	2	3	2	3	1	2	4	4	4	2	1	1	1
RPTOR p-S864 (z= 2)	11	100	83	89	57	11	67	62	70	49	11	13	13	14	11	31	82	76	82	44	0	1	0
CCDC124 p-S142 (z= 2)	1	4	12	3	13	1	33	66	23	100	1	1	3	1	6	1	12	24	10	23	1	1	1
LIG1 p-S67 (z= 2)	32	12	39	1	10	32	100	92	75	54	32	26	0	6	1	32	72	56	58	26	1	1	0
CLASP2 p-S597 (z= 2)	16	61	94	57	36	16	70	51	97	100	16	11	13	7	14	22	93	83	76	67	0	1	0
CLASP1 p-S798 (z= 2)	10	5	23	3	9	10	34	42	87	100	10	2	1	0	1	10	20	23	14	26	0	1	0
AARS p-S834 (z= 2) + oxidation	0	4	2	4	1	0	1	5	15	3	0	12	100	84	47	0	0	0	0	0	0	0	1
MARCKS p-S47 (z= 2)	8	19	17	20	10	8	98	90	100	66	8	13	9	11	7	8	15	17	22	11	1	1	1
RRM2 p-S21 (z= 2)	33	3	34	1	4	33	100	78	63	65	33	11	0	0	2	33	51	15	27	33	1	1	0
SRRM2 p-S2582 (z= 2)	1	12	11	11	7	1	95	82	100	66	1	9	13	12	8	1	23	29	28	22	1	1	1
GOLGA4 p-S72 (z= 2)	29	12	10	8	8	29	87	91	100	90	29	10	11	10	7	29	17	16	14	11	1	1	1
FAM83H p-S648 (z= 2)	5	11	12	12	11	5	67	77	80	100	5	7	7	5	11	5	12	12	14	15	1	1	1
NACA p-S167 (z= 3)	21	10	21	12	12	21	87	62	100	78	21	33	11	18	12	21	64	42	57	46	1	1	0
USP24 p-S2048 (z= 2)	30	15	19	8	10	30	100	70	61	56	30	10	3	7	3	30	19	19	21	5	1	1	1
ASCC3 p-S2196 (z= 2)	0	10	19	4	22	0	90	96	75	100	0	11	14	10	13	0	27	31	26	16	1	1	1
IFI16 p-S154 (z= 2)	18	85	88	60	68	18	53	49	66	68	18	75	68	45	78	7	76	100	80	56	0	0	0
AKAP3 p-S206 (z= 2)	71	2	6	0	0	71	100	40	26	25	71	14	0	3	0	71	61	38	46	0	1	1	0

PRKACA p-S340 (z= 2)	0	43	41	62	39	0	58	69	100	41	0	14	20	19	14	2	15	23	25	18	0	1	1
TLE3 p-S264 p-S268 (z= 2)	11	21	28	31	19	11	54	72	100	69	11	24	25	27	19	10	40	37	44	26	1	1	0
JUP p-S666 (z= 2)	3	12	11	7	5	3	100	83	75	65	3	9	7	8	4	3	22	23	26	9	1	1	1
PCM1 p-S66 (z= 2)	39	30	30	17	11	39	100	93	92	60	39	48	25	38	24	39	78	78	97	20	1	1	0
NUCKS1 p-S20 (z= 2)	42	3	30	3	13	42	77	89	100	82	42	28	2	9	2	42	57	43	49	26	1	1	1
RIOK1 p-S23 (z= 2)	23	22	55	1	28	23	100	100	80	72	23	18	6	8	7	47	94	72	97	48	0	1	0
NCL p-S68 (z= 2)	88	30	37	33	6	88	9	4	100	86	88	57	17	25	11	26	7	9	9	3	0	1	1
PTPN11 p-Y585 (z= 2)	0	0	0	2	26	0	1	1	1	2	0	33	24	29	50	0	77	71	72	100	0	0	0
PAK2 p-S142 (z= 2)	41	26	36	20	14	41	100	78	76	48	41	24	9	15	6	42	33	28	34	11	1	1	1
AMN1 p-T28 (z= 2)	4	20	15	26	16	4	100	86	63	33	4	15	14	12	8	3	18	11	14	7	1	1	1
ZRANB2 p-S189 (z= 2)	34	47	52	59	34	34	66	90	100	53	34	25	19	28	17	51	71	62	62	29	0	1	0
SRRM1 p-S598 (z= 2)	10	26	20	19	14	10	77	100	94	65	10	14	15	17	12	4	12	16	16	9	1	1	1

Appendix 7

Investigation into the association between calpain and class IA PI3K in human DLD1 colorectal cancer cells.

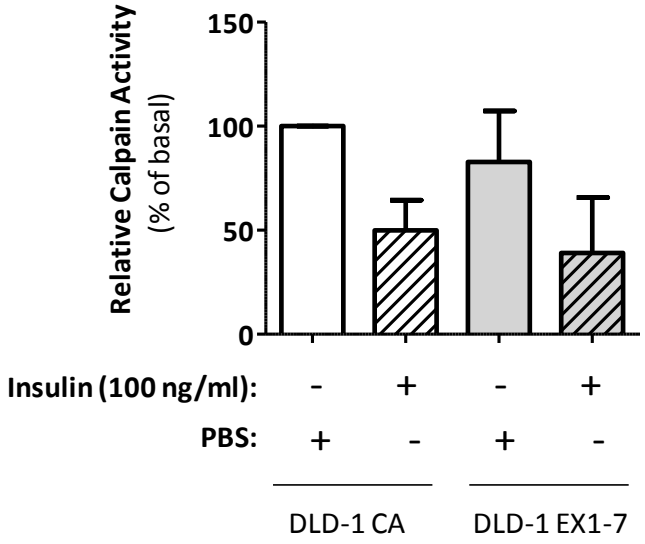

Figure A9.2. Active calpain heterodimers associate dynamically with Class IA PI3K in human DLD-1 colorectal cancer cells. The association between calpain and class IA PI3K was investigated in human DLD-1 colorectal cancer cells that expressed wild-type p110α (CA) or p110α with an activating mutation in exon 9 (EX1-7). PI3K p85 protein complexes (n = 2) were isolated by immunoprecipitation from both cell types after serum-starvation for 18 h (0.5% FBS) followed by stimulation with 100 ng/ml insulin for 10 min or treatment with PBS vehicle control for 10 min. The purified PI3K p85 protein complexes were then subjected to an *in vitro* protease assay for calpain activity. Data expressed as mean+/- SEM (n=2).